UHF RFID Reader Antenna Applications of Non-Conventional Radio-Frequency Materials

Prabakar Parthiban

A thesis submitted to

Auckland University of Technology

in fulfilment of the requirements for the degree of

Doctor of Philosophy

2020

School of Engineering, Computer and Mathematical Sciences,

Auckland University of Technology

New Zealand

Declaration

I, hereby declare that this submission is my own work and that, to the best of my knowledge and belief, it contains no material previously published or written by another person (except where explicitly defined in the acknowledgements), nor material which to a substantial extent has been submitted for the award of any other degree or diploma of a university or other institution of higher learning. Section 2.3 and contribution Chapters 4–12 of this thesis represent works that have either been published in or submitted to peer-reviewed journals or conferences. All co-authors have approved the inclusion of the joint work in this doctoral thesis.

________________________ 30 July 2020

Prabakar Parthiban Date

Chapter	Publication reference	Author %
Chapter 2	P. Parthiban, "Fixed UHF RFID Reader Antenna Design for Practical Applications: A Guide for Antenna Engineers with Examples," *IEEE Journal of Radio Frequency Identification*, vol. 3, no. 3, pp. 191-204, Sept. 2019.	PP: 100%
Chapter 4	P. Parthiban, B.-C. Seet and X. J. Li, "Recycled polyolefin as dielectric substrate for patch antennas," *IEEE Transactions on Dielectrics and Electrical Insulation*, vol. 26, no. 5, pp. 1720-1726, Oct. 2019.	PP: 85% BCS: 10% XJL: 5%
Chapter 5	P. Parthiban, B.-C. Seet and X. J. Li, "Scalable Near-Field Fed Far-Field RAIN RFID Reader Antenna for Retail Checkout Counters," *IEEE Journal of Radio Frequency Identification*, vol. 4, no. 1, pp. 24-37, March 2020. P. Parthiban, B.-C. Seet and X. J. Li, "Scalable Near-field fed Far-field UHF RFID Reader Antenna for Retail Checkout Counters," *2019 IEEE International Conference on RFID (RFID)*, Phoenix, AZ, USA, 2019, pp. 1-6.	PP: 85% BCS: 10% XJL: 5%

Chapter 6	P. Parthiban, B.-C. Seet and X. J. Li, "An Ultra-Rugged UHF RFID Reader Antenna: A New Design for Convention Center Loading Docks," *IEEE Antennas and Propagation Magazine*, vol. 62, no. 1, pp. 84-95, Feb. 2020	PP: 85% BCS: 10% XJL: 5%
Chapter 7	P. Parthiban, "Bandwidth enhancement for thin substrate UHF RFID patch antenna," *International Journal on Smart Sensing and Intelligent Systems*, vol. 12, no. 1, pp. 1-8, June 2019.	PP: 100%
Chapter 8	P. Parthiban, B.-C. Seet and X. J. Li, "Low-cost low-profile UHF RFID reader antenna with reconfigurable beams and polarizations," *2017 IEEE International Conference on RFID (RFID)*, Phoenix, AZ, 2017, pp. 81-87.	PP: 85% BCS: 10% XJL: 5%
Chapter 9	P. Parthiban, B.-C. Seet and X. J. Li, "3D Printed Circularly Polarized Concave Patch with Enhanced Bandwidth and Radiation Pattern," *submitted to a Journal*, 2020.	PP: 82% BCS: 15% XJL: 3%
Chapter 10	P. Parthiban, B.-C. Seet and X. J. Li, "Radiative Quadrature Hybrid Coupler for Near-Zone UHF RFID Applications," *2019 IEEE International Electromagnetics and Antenna Conference (IEMANTENNA)*, Vancouver, BC, Canada, 2019, pp. 001-007.	PP: 85% BCS: 10% XJL: 5%
Chapter 11	P. Parthiban, B.-C. Seet and X. J. Li, "Low-cost scalable UHF RFID reader antenna with no surface dead zones," *2016 IEEE Asia-Pacific Conference on Applied Electromagnetics (APACE)*, Langkawi, 2016, pp. 24-29.	PP: 85% BCS: 10% XJL: 5%
Chapter 12	P. Parthiban, B.-C. Seet and X. J. Li, "Display Frame UHF RFID Antenna for Museums," *2018 IEEE Asia-Pacific Conference on Antennas and Propagation (APCAP)*, Auckland, 2018, pp. 532-533.	PP: 85% BCS: 10% XJL: 5%

We, the undersigned, hereby agree to the percentages of participation to the chapters identified above.

_________________________ 30 June 2020

Prabakar Parthiban (PP) Date

_________________________ 30 June 2020

Associate Professor Dr. Boon-Chong Seet (BCS) Date

_________________________ 30 June 2020

Senior Lecturer Dr. Xue Jun Li (XJL) Date

Copyright Notice

Abstract

Antennas are complicated passive devices, found in transceivers which transform the electrical signals into electromagnetic radiation in the form of propagating radio waves. While there is a wide range of antennas, this thesis focuses on designing and fabricating low-cost patch antennas from non-conventional radio frequency (RF) materials. Patch antennas are low profile, planar antennas commonly used in cellular communications (mobile phone and base station antennas), point-to-point link communications (MIMO, SCADA, etc.), UHF radio frequency identification (RFID) systems and other radio frequencies (RF) products. Patch antennas are very common and attractive due to their form factor and cost. They are typically designed and manufactured using virgin dielectric substrate and conductive materials that are produced in well-controlled environments. These virgin RF materials, e.g. Rogers printed circuit boards (PCB), polyolefin like polyethylene, polypropylene, etc., exhibit both well-known and uniform electrical properties, which greatly aid in the design and manufacturing of high-performance RF products. Conventional RF materials are usually considered for high-frequency applications due to their consistent and predictable RF properties.

However, these conventional materials are expensive and are dumped as e-waste at the end of their products' lifespan. This research aims to design and fabricate a low cost yet robust patch antenna and array using commercially available non-conventional materials. Commercially available non-conventional materials include thermoplastic sheets, thermal insulation materials, recycled materials etc. They tend to lose their

virginity due to the manufacturing process and/or impurities being introduced. This leads to changes in the electrical properties of the materials, which inevitably impact the performance of the products manufactured using these materials. Designing patch antennas from such non-conventional materials requires an in-depth study of the materials and their electrical properties mainly its dielectric constant parameter as a patch antenna constitutes a metal radiating element as a patch and a ground plane, fairly larger than the size of a patch separated by a dielectric. Moreover, the electrical properties may or may not remain unchanged between different samples of the same material, or even between different regions of the same sample, due to the less stringent manufacturing processes of recycled materials, and this research aims to mitigate their impacts on products' performance through novel and innovative design and manufacturing techniques.

UHF RFID application is chosen to make reader antennas using non-conventional materials to meet the form, fit and functional requirements. Various antenna designs in different non-conventional RF substrates are designed at a low-cost. Wideband antenna design methodologies are adopted to handle the changes in resonant frequencies caused by changes in dielectric parameters of a non-conventional patch antenna and array. The outcome of this research potentially open doors in the telecommunication industry to manufacture robust, eco-friendly antennas from various forms of commercially available inexpensive raw, reground/recycled materials without compromising its performance through proper optimisation and compensation.

Acknowledgements

சரஸ்வதி நமஸ்துப்யம் வரதே காமரூபிணி, வித்யாரம்பம் கரிஷ்யாமி சித்திர் பவதுமே சதா.

sarasvatī namastubhyaṃ varade kāmarūpiṇī, vidyārambhaṃ kariṣyāmi siddhirbhavatu meh sadā.

A Sanskrit recitation to salute the ‘Hindu goddess of knowledge’ - the giver of boons and fulfiller of wishes.

Firstly, I would like to thank my primary supervisor Associate Professor Dr. Boon-Chong Seet for his motivation, encouragement, and support throughout the tenure of my PhD research. His guidance and mentoring assisted me in shaping my research career effectively. I would also like to thank my secondary supervisor Senior Lecturer Dr. Xuejun (Jack) Li for his valuable time and effort in eminent research guidance.

Secondly, I would like to thank the CEO and Director of Times-7 Research Ltd, Jos Kunnen for his continual support and encouragement towards my PhD. I would also like to thank to all my colleagues who supported me directly and indirectly.

Finally, I want to thank my family, who helped to accomplish my dreams with fewer inconveniences and disruption. Special mention to my wife ‘Sheela Rani’; son ‘Nathan’; ‘*the expected little one*’; father and mother – ‘Parthiban’ *and* ‘Premalatha’. An extended thanks to my brother ‘Soorya Prakash’; maternal uncle - aunt – ‘Dharmesh - Uma’; paternal uncles - aunts – ‘Arumugam - Kamaleswari’, ‘Sowndharapandiyan - PandiRani’ *and* ‘Ramakrishnan - PunithaKumari’; grandparents – ‘V.S. Sundaram - Sakunthala’; in-laws – ‘Soundarrajan - Rajeswari’, ‘Jayavel *and* Srividya’; cousins – ‘Buvana - Vidhyasagar’ ‘Chandravadhana - Rajesh’, ‘Siddeshwaran - Akalya’, ‘Senthil - Sharmila’ & ‘Mohana - Prasad’; and all other good-hearted friends and relatives.

This thesis is dedicated to my late grandmother, *Mahalakshmi*.

Contents

List of Figures

List of Tables

List of Acronyms and Symbols

Acronyms:

3-D	Three Dimensional
ABS	Acrylonitrile Butadiene Styrene
ADS	Advanced Design Systems
AIDC	Automatic Identification and Data Capture
ANSI	American National Standards Institute
AR	Axial-Ratio
ASTM	American Society of Testing and Materials
ATEX	ATmosphères EXplosibles
BBP	Benzyl Butyl Phthalate
BoM	Bill of Materials
cd	Cadmium

CE	Conformité Européenne
CEO	Chief Executive Officer
Cr VI	Hexavalent Chromium
DAS	Distributed Antenna Systems
DBP	Dibutyl Phthalate
DC	Direct Current
DEHP	Bis () 2-Ethylhexyl phthalate
D_F	Dissipation Factor
DIBP	Di-isobutyl Phthalate
D_k	Dielectric Constant
DSB-ASK	Double-Sideband Amplitude-Shift Keying
EIRP	Effective Isotropic Radiated Power
EM	Electromagnetic
EN	European codes
ERP	Effective Radiated Power
ESD	Electrostatic Discharge
ETSI	European Telecommunications Standards Institute
FBR	Front-to-Back Ratio
FCC	Federal Communications Commission
FF	Far Field
FHSS	Frequency Hop Spread Spectrum
FR-4	Flame Retardant glass reinforced epoxy laminate material

GHz	Giga Hertz
GPS	Global Positioning System
HDPE	High Density Polyethylene
HERO	Hazards of Electromagnetic Radiation of Ordnance
HF	High Frequency
HFSS	High Frequency Electromagnetic Field Simulation Software
Hg	Mercury
HPBW	Half-Power Beam-Width
Hz	Hertz
IEC	International Electrotechnical Commission
IECEx	International Electrotechnical commission – Explosives
IEEE	Institute of Electrical and Electronics Engineers
IoT	Internet of Things
IP	Ingress Protection
ISM	Industrial, Scientific and Medical
kHz	Kilo Hertz
LDPE	Low Density Polyethylene
LF	Low Frequency
LHCP	Left-Hand Circular polarization
MHz	Mega Hertz
MIL-STD	Military Standard
MIMO	Multiple Input Multiple Output

mm-Wave	Millimetre Wave
MoM	Method of Moments
MSRP	Maximum Suggested Retail Price
NF	Near Field
NFPA	National Fire Protection Association
pb	Lead
PBB	Polybrominated Biphenyls
PBDE	Polybrominated Diphenyl Ethers
PC	Poly Carbonate
PCB	Printed Circuit Board
PIFA	Planar Inverted ‘F’ Antenna
POS	Point of Sale
PP	Polypropylene
PPE	Polyphenylene Ether
PPS	Polyphenylene Sulfide
PR-ASK	Phase Reversal Amplitude-Shift Keying
PTFE	Poly Tetra Fluro Ethylene
PVC	Polyvinyl Chloride
Q-factor	Quality factor
RADAR	Radio Detection and Ranging
RAIN	Radio Frequency Identification
RED	Radio Equipment Directive

RF	Radio Frequency
RFID	Radio Frequency Identification
RH	Relative Humidity
RHCP	Right-Hand Circular Polarization
RoHS	Restrictions of Hazardous Substances
RSSI	Return Signal Strength Indicator
SCADA	Supervisory Control and Data Acquisition
SMA	Sub Miniature version A
SSB-ASK	Single-Sideband Amplitude-Shift Keying
TIA	Telecommunications Industry Association
TiO_2	Titania
TM	Transverse Magnetic
TNC	Threaded Neill-Concelman
UHF	Ultra-High Frequency
UL	Underwriters Laboratory
USD	United Stated Dollar
UV	Ultra-Violet
VESA	Video Electronics Standards Association
VNA	Vector Network Analyzer
VRMS	Voltage – Root Mean Square
VSWR	Voltage Standing Wave Ratio
Wi-Fi	Wireless Fidelity

WiMAX	Worldwide Interoperability for microwave access
WLAN	Wireless Local Area Network

Symbols:

Ω	Ohm (unit of resistance)
λ	Lambda (wavelength)
ε	Epsilon (permittivity)
δ	Delta (loss)
Δ	Delta (deviation)
Π	Pi
μ	Mu (micro)
E	Electric
H	Magnetic
j	j operator (imaginary number)

Chapter 1

Introduction

1.1 Motivation and scope

The primary motivation of this research is to design a patch antenna and array for UHF RFID applications from commercially available non-conventional radio-frequency materials. Antennas will have the following advantages when they are made from non-conventional radio-frequency materials:

a) Antenna's material cost (both conductor and dielectric) can be significantly reduced
b) Non-conventional materials being used for this research are commercially available, and thus there is no particular need in terms of manufacturing.

c) E-Wastes (from conventional RF substrate materials such as PCB electronics) will be minimised as the non-conventional materials are often recyclable. Some non-conventional materials are even made from recycled materials.
d) Common manufacturing techniques are employed, which would reduce the production costs involved in making antennas.
e) Antennas will have added advantages viz., chemical resistance, UV protection, mechanically robust, which are inherited from the non-conventional substrate.

The scope of this research is;

a) Non-conventional antenna's electrical properties are unknown as they are not manufactured for RF purposes. Thus, they will need to be researched to analyse their electrical properties.
b) Non-conventional material's electrical properties could vary between samples due to less stringent manufacturing process. The changes in the substrate's electrical properties may lead to changes in antenna's critical performance such as its resonant frequency. Thus, the antenna design will have to adapt to the changes.
c) Wideband patch antenna and array designs are researched to find it can withstand different nonconventional substrate's dielectric constant changes. Both conventional and non-conventional bandwidth enhancement techniques are researched.
d) Various UHF RFID application needs are analysed to design and manufacture antennas from nonconventional materials. Inherited substrate properties such as chemical resistance, impact resistance, flame retardancy, and so on can be used to create antennas that meet special usage requirements.

e) Research in non-conventional antennas involves fewer budgets as the study is based on inexpensive materials.

1.2 Contributions

This thesis has five significant novel contributions,

1. Dielectric constant estimation on commercially available virgin and recycled non-conventional radio-frequency substrate materials for patch antennas.
2. Novel UHF RFID patch antenna and array designs using commercially available virgin and recycled non-conventional substrate materials.
3. Conformal antenna designs for various UHF RFID applications.
4. Novel non-conventional bandwidth enhancement technique in thin substrate patch antenna is proposed.
5. Novel non-conventional substrate fabrication using bio-degradable materials is proposed.

The following is the list of publications generated during the period of this research;

Published journals articles:

1. P. Parthiban, "Fixed UHF RFID Reader Antenna Design for Practical Applications: A Guide for Antenna Engineers with Examples," *IEEE Journal of Radio Frequency Identification*, vol. 3, no. 3, pp. 191-204, 2019.
2. P. Parthiban, B.-C. Seet and X. J. Li, "Recycled polyolefin as dielectric substrate for patch antennas," *IEEE Transactions on Dielectrics and Electrical Insulation*, vol. 26, no. 5, pp. 1720-1726, 2019.

3. P. Parthiban, B.-C. Seet and X. J. Li, "An Ultra-Rugged UHF RFID Reader Antenna: A New Design for Convention Center Loading Docks," *IEEE Antenna and Propagation Magazine*, vol. 62, no. 1, pp. 84-95, 2020.
4. P. Parthiban, "Bandwidth enhancement for thin substrate UHF RFID patch antenna," *International Journal on Smart Sensing and Intelligent Systems*, vol. 12, no. 1, pp. 1-8, 2019.
5. P. Parthiban, B.-C. Seet and X. J. Li, "Scalable Near-field fed Far-field RAIN RFID Reader Antenna for Retail Checkout Counters," *IEEE Journal of Radio Frequency Identification*, vol. 4, no. 1, pp. 24-37, 2020.

Under submission:

1. P. Parthiban, B.-C. Seet and X. J. Li, "3D Printed Circularly Polarized Concave Patch with Enhanced Bandwidth and Radiation Pattern," *submitted to a Journal,* 2020.

Published conference papers:

1. P. Parthiban, B.-C. Seet and X. J. Li, "Scalable Near-field fed Far-field UHF RFID Reader Antenna for Retail Checkout Counters," *2019 IEEE International Conference on RFID (RFID)*, Phoenix, AZ, USA, 2019, pp. 1-6.
2. P. Parthiban, B.-C. Seet and X. J. Li, "Display Frame UHF RFID Antenna for Museums," *2018 IEEE Asia-Pacific Conference on Antennas and Propagation (APCAP)*, Auckland, 2018, pp. 532-533.
3. P. Parthiban, B.-C. Seet and X. J. Li, "Low-cost low-profile UHF RFID reader antenna with reconfigurable beams and polarizations," *2017 IEEE International Conference on RFID (RFID)*, Phoenix, AZ, 2017, pp. 81-87.
4. P. Parthiban, B.-C. Seet and X. J. Li, "Low-cost scalable UHF RFID reader antenna with no surface dead zones," *2016 IEEE Asia-Pacific Conference on Applied Electromagnetics (APACE)*, Langkawi, 2016, pp. 24-29.
5. P. Parthiban, B.-C. Seet and X. J. Li, "Radiative quadrature hybrid coupler for near-zone UHF RFID applications," *2019 IEEE International Electromagnetics and Antenna Conference*, Vancouver, Canada, 2019.

1.3 Thesis structure

This thesis follows a manuscript structure, commonly known as publication-style thesis. This format is typically more concise than a traditional monograph style thesis and hence each chapter looks like a stand-alone research article. Yet, each chapter has a strong connection to the research topic and has answered research questions such as the rationale and significance of using a non-conventional material for patch antennas, finding non-conventional substrate's properties that has an impact in antennas' performance and finding ways to design antennas that can handle those impacts. Manuscripts that are published or submitted for publication in peer-reviewed journals (mentioned in section 1.2) are included in this thesis as stand-alone chapters. This thesis also consists of a few peer-reviewed conference papers presented in reputed IEEE conferences.

There are thirteen chapters including 'introduction' and 'conclusion' chapters but excluding the 'references' section. The 'introduction' chapter, chapter 1 outlines the motivation and scope of this thesis and its contributions. It also unveils the structure of the thesis. The 'background' chapter, chapter 2 discusses patch antenna, arrays, and its applications including UHF RFID. Requirements for a practical reader antenna and its design methodology is also presented in this chapter. It is followed by the 'Literature review' chapter, chapter 3 where existing works with conventional and non-conventional materials are reviewed. It reveals the gaps in present state-of-the-art that the thesis will fulfil. Chapter 4 – 12 are original contributions which consist of direct inclusion of the journal and conference papers except for the references which are listed at the end of the thesis under the 'reference' section. A 'prelude' section is included at the beginning of each chapter. 'Prelude' provides a synopsis of the chapter and its significance in relation to the thesis topic. Prelude also provides the connection between chapters. Chapter 13 summarizes the contribution chapters and presents the limitations of the current work. This chapter then concludes the thesis and discusses the directions for future research. The Reference section consists of a ‘full reference list’ for the entire thesis, as well as separate ‘reference list’ for each contribution chapter (Chapters 4−12).

Chapter 2

Background

2.1 Patch antennas

A transmitting antenna converts electrical signals into electromagnetic (EM) waves, and vice-versa for a receiving antenna [1]. The same antenna can be used for both transmission and reception as antennas follow the principle of reciprocity [2]. Figure.2.1 shows a classification of different antennas types. This thesis focuses on patch antennas (a.k.a. microstrip antennas), which consist of a metal radiating patch and a ground plane, separated by a dielectric substrate (Figure.2.2) [3].

The radiating patch can be of any geometry viz., rectangle, circle, square, ellipse, triangle or a circular ring [4]. Patch antennas can either be probe fed through a coaxial cable/connector or fed by a transmission line like microstrip line/stripline, and tend to suffer from narrow bandwidth [5]. When electric field vector of the antenna rotates with circular motion in its direction of propagation, the wave pattern generated is known as circular polarization. When electric field vector stays in the same horizontal, vertical or slant plane, the resulting wave pattern is known as linear polarization. Patch antennas can be configured to polarize linearly or circularly without disturbing its planar nature. Multiple patch antennas can be used to form an array to obtain high gain and high directionality.

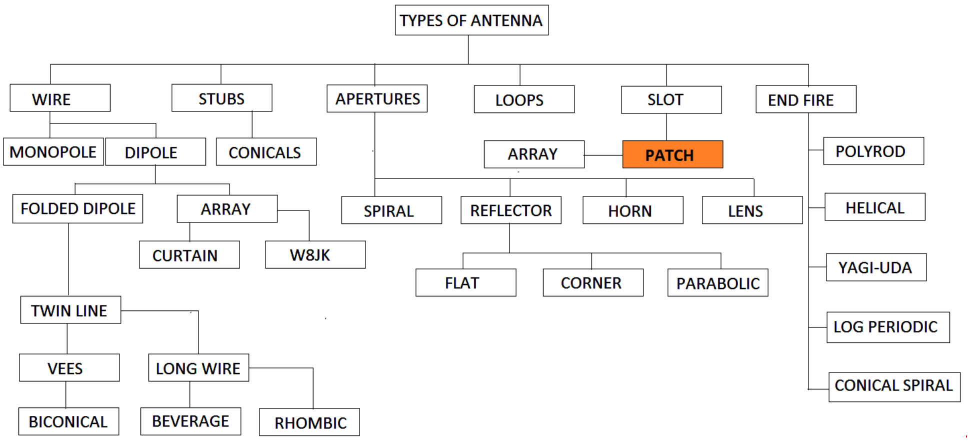

Figure.2.1. Classification of antennas

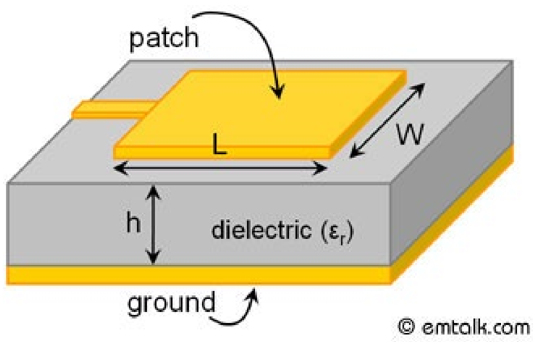

Figure.2.2. Typical structure of patch antenna

2.2 Patch antenna applications

Due to their planar nature and array-ability, patch antennas are predominantly used in areas such as mobile communication, satellite communication, GPS (global positioning system) applications, RFID (radio-frequency identification) applications, WiMax (worldwide interoperability for microwave access) applications, radar applications, rectenna applications, telemedicine applications, and so on.

In this thesis, RFID is chosen as the application of the patch antennas to be designed. As these antennas operate in the sub-GHz frequency range, the size of the antenna becomes enormously larger compared to a 2.4 GHz or mm-Wave antenna. Multiple RFID antennas are often distributed like DAS (distributed antenna systems). Thus, these large-sized distributed antenna systems (DAS) are required to have low material and fabrication cost. Besides, these antennas are necessary to fulfil other needs that are discussed in the following section.

2.3 UHF RFID Reader antennas

Automatic identification and data capture (AIDC) is an emerging technology that identifies objects, capture, and stores the object data directly into a server system without any human intervention. Radio Frequency Identification (RFID) is one of the AIDC technologies which is widely used in our day-to-day life. RFID systems can be classified into an active or passive system based on the tag's architecture. Tags are passive when they do not require a power supply, such as a battery to operate. Active tags consist of a battery and a transceiver built-in. Passive RFID systems are categorized based on their frequency of operation viz., the low frequency (LF) 125 - 134 kHz, the high frequency (HF) 13.56 MHz and ultra-high frequency (UHF) 860 to 960 MHz passive RFID systems. A typical UHF RFID system consists of an interrogator (also known as the reader), reader antenna, transponder (called a tag), software (reader firmware, middleware, and the application software), and other accessories such as coaxial cables for antenna connection, data cables, and power cables. The UHF RFID is advantageous over the LF and HF RFID systems because they have a greater tag detection range (more than 8 meters), faster data transfer rate, multiple tag detection (around 200 tags or more at a time) and lower tag costs.

The UHF RFID frequency of operation, the reader to tag communication technique and the maximum allowed effective radiated power (ERP) and the effective isotropic radiated power (EIRP) are region-specific and are specified by [6]. The two main frequency bands for UHF RFID are 902 - 928 MHz and 865 - 868 MHz. Countries like Canada adopts the full 902 - 928 MHz bandwidth for communication whereas countries like Israel (915 - 917 MHz) or Singapore (920 - 925 MHz) uses part of the 902 - 928 MHz spectrum for communication. The reader to tag communication technique can either be frequency-hopping spread-spectrum (FHSS) or listen-before-talk (LBT) or according to the European telecommunications standards institute (ETSI) - 302 208 standards. The communication techniques and the ERP/EIRP power mentioned above are different for different regions. The reader to tag modulation can either be double-sideband amplitude-shift keying (DSB-ASK), single-sideband amplitude-shift keying (SSB-ASK) or phase-reversal amplitude-shift keying (PR-ASK) modulation types [7]. The reader transmits an unmodulated carrier signal in fewer periods along with a modulated signal where the unmodulated signal is rectified to harvest the energy by the tag. The harvested DC energy powers the chip for data processing and back-scattering. The back-scatter modulation takes place by varying the front-end complex radio frequency (RF) input impedance of the chip [8]. The modulated signal contains the information of the tag/asset that is interpreted by the RFID reader through the software by liaising with the database.

Reader antennas in UHF RFID systems are critical unlike LF and HF RFID where an inductor coil is used for transmission and reception. Inductor coils create near-zone RF fields. The UHF RFID reader antennas can be both far-field and near-field radiators. The antenna's characteristics such as polarization, bandwidth, gain, voltage standing wave ratio (VSWR), beam-width, front-to-back ratio are vital and have a direct impact on the tag detection performance. During a practical UHF RFID system deployment, often reader antennas are not given enough importance compared to other system components such as the readers, tags or the software. Reader antenna installation is usually the final step in an RFID project implementation. The selection criteria for a reader antenna design is much more than the recommendations specified in [9]. It is rather application specific. A generic patch antenna or a dipole antenna would not satisfy all the RFID reader antenna requirements in an application.

2.3.1 Reader antenna applications and challenges

UHF RFID is being adopted by most of the industries viz., the primary sectors (raw materials), the secondary industries (manufacturing and production), the service industries (retail, healthcare, hospitality, transport and so on) and the intellectual service industries (information technology and other knowledge-based services). Fixed readers are preferred over handheld readers because the use of handheld readers involve human operators and consequently are subject to human errors. The following elaborates common UHF RFID fixed reader antenna applications and their challenges;

2.3.1.1 Point of sale (PoS) applications

Reader antennas are predominantly installed in point-of-sale counters and self-service kiosks in the retail or hospitality industries. In retail stores, RFID in point-of-sale and self-service kiosks are used for billing and purchasing the goods whereas, in hospitality industries, RFID in help-desk/reception is used for personal identification and services. Fixed UHF RFID enables fast and reliable billing, unlike traditional barcode-based operation [10]. Retail industry varies from small convenience stores to bigger supermarket chains. The point-of-sale counter and the self-service kiosks will not be the same across all the shops, and thus the antenna choice will also differ based on the antenna's physical parameters such as dimensions, antenna's radome material, fastening options, etc.

The assets in a retail store can be metals, high or low-density solids, liquids, frozen items, fabrics, and so on. Some of these assets posses' technical challenges in tag readability by the reader antenna. A liquid asset is difficult to be read by a far-field reader antenna as RF gets absorbed by liquids. Similarly, a near-field antenna may not have enough energy to read a stack of high-density solid assets. A far-field antenna operating at high power may find other stationary tags in the proximity leading to stray tag reads. Eliminating the stray reads is key for a robust retail RFID system.

2.3.1.2 Inventory management

Asset and inventory management in the industry is one of the primary reasons why UHF RFID became more popular as it can detect multiple tagged assets at greater distances at once. Inventory is managed in both front-end (stores, manufacturing plants and offices) and back-end premises (storage warehouses, procurement and delivery areas, disposal and recycling stations). Assets can either be stored in free form (in bins or tubs) or can be boxed (cardboard or plastic containers) in a back-end store. They may be arranged on racks or be palletized. Each asset can have a dedicated tag, and they can be grouped in a box to bear a master tag. The number of tags per shelf or pallet is humongous, and this becomes a challenge in reliable inventory management. In addition, a densely palletized asset may encounter the risk of tags not being read in the center of the package. A high gain antenna without breaching the power regulations is necessary to achieve the intended performance. Metal shelves and racks are not transparent for the RF fields, and thus multiple reader antenna deployments per shelf are essential. The reader antenna`s cost is an essential factor as tens and hundreds of them will have to be deployed. The reader antenna needs to be robust in its performance when it is located near metal shelves or racks.

Assets are segregated in front-end shops and are stored in different locations. In a tool shop, for instance, hand tools, power tools, and air tools are stored in different aisles in the front-end shop. Inventory on these segregated assets is relatively but may face other challenges such as RF field obstruction by humans (customers), false reads due to the environmental reflections and stray reads.

2.3.1.3 Shelving and cabinetry applications

Unlike the warehouse shelving asset management mentioned above, high-value assets such as pieces of jewellery, documents, shreds of evidence, museum pieces and artifacts require real-time inventory management. The RFID read accuracy has to be 100% as the industry cannot afford to lose any single asset. In addition to the read accuracy, the location information of the assets is vital as well. Localization of the assets can be achieved by grouping them in two different ways viz., a) shelf-based within the entire cabinetry b) sector-based within each shelf. This localization can only be achieved by deploying a dedicated reader antenna per shelf, that fills the RF energy in that shelf alone or multiple reader antennas within a shelf, with controlled radiation. The former requires an antenna whose beam is controlled and would not spill over to the other shelves, and the latter requires an antenna with limited surface dead zones and little to no back radiation for consistent retrieval of the information on assets' location.

2.3.1.4 Portal applications

A portal refers to a gateway where RFID reader antennas are deployed to track assets that traverse through. A portal can be an industrial portal, a retail portal or a door-way portal. Industrial portals can be as wide as a dock-door in a warehouse loading dock [11]. Heavy-duty trucks, forklifts, and vans travel through the industrial portal. The reader antenna's physical robustness to handle impacts and the ability to read tags accurately in a highly dense and RF reflective environment is a challenge. Retail portal, on the other hand, has different types of challenges viz., elimination of stray tag reads, the ability to read densely packed assets, antenna's aesthetics, and so on. Personnel tracking in small offices using a door-way portal has challenges associated with the human body attenuation. The human body absorbs the radio waves, and thus reliability in personnel tracking is affected. Door-way reader antennas must be aesthetically appealing and seamlessly installed to avoid any safety risks. Most common doorway frames are 80 to 100 mm wide, where a 10-inch square antenna becomes a safety hazard when installed without protection.

2.3.1.5 Race timing application

One of the most common uses of UHF RFID is race-timing. UHF RFID is preferred because of its ability to detect tags faster and at farther distances. Outdoor race timing events required water-resistant reader antennas to handle harsh environments. A race timing reader antenna can be installed overhead or pole mount on the sides, or the floor at the finish line [12]. Tags are located on the runners' bibs, or shoes and cyclists bear tags on their helmets or their bikes [13]. Installing ground antennas involves less infrastructure. A higher read accuracy can be achieved as the antennas are close to the tags (in the case of shoe or bike tags). Conversely, a rugged ground antenna is a requirement to handle the wear and tear caused by the runners and cyclists. The antenna may also have to withstand dirt, rain, varied ambient temperature and humidity, and other environmental impacts. When longer array antennas are installed on the ground to cover a larger finish line with less number of antennas, the antenna array must have an even power distribution along the length of the array at different heights to avoid dead zones. This is a challenge as array antennas tend to have maximum power in its center and droops in the edges.

2.3.1.6 Conveyor applications

Industry automation, airport baggage handling systems, supermarket checkout areas and many other industries rely on conveyors and are interested in tracking the assets that travel through those conveyors. Reader antennas can either be mounted over the conveyors (on top or on the sides) or under the conveyor belt to detect the tagged assets [14]. The under-belt approach is practical as it is seamless and requires less infrastructure. The collision of assets traveling on the conveyor with the reader antennas can also be prevented. The size of the reader antenna is critical when installing under the conveyor belt. The antenna must match the belt's width to have an even power distribution across the width and accurately track the assets traveling in the edge of the conveyor belt. The antenna's radome must be sufficiently strong enough to handle extreme wear and tear and offer low friction. The conveyor antennas must have a confined beam to avoid detecting unwanted assets in the near-by area. For instance, the reader antennas installed in an airport check-in area should not read the tags of baggage that are in the proximity of the passengers who are checking-in.

2.3.1.7 Pharmaceutical and medical applications

Asset tracking management in the pharmaceutical and medical industries are highly critical due to the nature of the products. Pharma assets can range from vaccines, drugs, and steroids, which requires a controlled temperature environment for storage and transportation [15]. Reader antennas installed in the fridges and freezers must be able to operate at extremely low temperatures for real-time asset management. The antennas may have to withstand condensation if there is any change in temperature and humidity. Medical industries can be broadly classified into medical devices or instruments manufacturers and users, such as hospitals and clinics. Medical instruments such as surgical instruments, cannula, and so on require regular monitoring for autoclaving, sterilization and maintenance. The instruments will be monitored throughout this cleaning process, and the reader antenna must meet the medical compliances. UHF RFID is also used in hospitals for general asset tracking and patient monitoring applications. Low-profile conformal reader antennas are health and safety compliant, preventing patients from bumping into the antennas. Chemically resistant radomes are necessary to guard the antennas against the cleaning reagents used in hospitals.

2.3.1.8 Vehicle tolling and vehicular applications

Passive UHF RFID gains interest in vehicle tolling applications where the reader antennas are installed in toll gates [16], checkpoints and car parks barricades. As the antennas are permanently installed outdoors, they will have to withstand the environmental changes and climates without trading off the performance. Challenges include varied temperature and humidity, long-term exposure to solar and UV radiation, wind, and rain. Powerful antennas are necessary for long-distance tag detection. The reader antennas installed in vehicles for mobile asset management such as freight and transport industries require an antenna that can handle vibrations and physical impacts.

2.3.2 Reader antenna design requirements

Each industry is unique, and its UHF RFID requirements are also different. In this section, the UHF RFID reader antenna design requirements are formulated by understanding the applications and their challenges in the previous section. The design requirements are classified into physical, environmental, electrical and RF requirements.

2.3.2.1 Physical requirements

Size:

The size of the antenna is a critical factor in a practical reader antenna. Smaller antennas are preferred in space-constrained applications whereas larger array antennas are necessary for powerful radiation that can read tags at greater distances. Antennas designed for standard dimensions are more attractive in practical implementations than a non-standard design. For example, a 10-12 inch or 300 mm square antenna is preferred for non-destructive installation in shelving applications because the standard depth of a shelf varies from 10 to 12 inches. Standard antenna dimensions enable modular array antenna realization. Low-profile and planar antennas are preferred as they utilize less hardware space [17].

Substrate material:

A practical reader antenna is susceptible to stress, strain, abrasion, and impact. The radome of the antenna is a protective cover that shields the antenna from the above mentioned physical influences. The radome will have to be indestructible and RF compatible. Plastics such as poly-tetra fluoro ethylene (PTFE), acrylonitrile butadiene styrene (ABS), poly-carbonate and fiber-glass are some of the commonly used RF compatible radomes. Radomes made from self-lubricating materials such as nylon, acetal and polyphenylene sulfide (PPS) offer very minimal friction and survive extreme wear and tear [18]. Certain types of planar antennas like microstrip patch antennas have a dielectric substrate as part of the design whose dielectric properties are critical for the antenna's RF performance [19]. Other properties of the substrate such as fire retardancy are also essential to meet the on-site health and safety requirements. Both radome and substrate material has a more significant impact on the antenna's cost. Material's availability, manufacturing techniques, and ease-of-manufacturing are some of the parameters that are directly proportional to the cost.

Feeding mechanism:

Planar antennas such as patch antennas can be probe fed using a cable or connector, or excited through strip lines, microstrip lines and co-planar waveguides which are in turn coaxial cable or connector fed. A cable-fed antenna is reliable during practical installations compared to a connector-fed antenna as they do not involve any in-between connection joints while routing the cable to connect with the RFID reader located in a different location. Cable's power losses, impedance and bend radiuses are some of the essential parameters to select a cable. Any damage to the cables in a cable-fed antenna will require replacement of the antenna while it is practical to replace just the cable alone in a connector-fed antenna. Strain relief is necessary for both cabled and connector fed antenna to relieve the mechanical stress and protect them. Strain relieves are often incorporated within the antenna structure or with the housing (radome).

Fastening or mounting:

Practical antenna deployment requires ease of mounting or fastening the antenna into existing structures such as walls, desktop, cabinets, shelves or on masts and poles. The planar flat panel antennas can have corner holes for mounting the antenna flush against one of the structures mentioned above. The antenna's performance will have to be optimized for the interference caused by the metal fastening screws or bolts. Pole or mast mounting is viable using commercial video electronics standards association (VESA) mounting brackets. The planar antennas should bear threaded rear studs that are compatible with the VESA standards. The VESA brackets will have a metal plate with pre-drilled holes through which the antenna's studs slot through. This will then be fastened with washers and nuts. The antenna's performance will have to be optimized for the impact of the bracket's metal plate.

Aesthetics:

Reader antennas deployed in customer-facing environments like a jewellery shop or a self-service supermarket kiosk requires aesthetically appealing and seamlessly installed antennas. The antennas used in health-care applications needs to be hazard-free and safe. Sharp-edged and protruding antennas pose serious safety risks in hospitals and clinics. The location of the cable or the connector's exit plays a vital role in the elegant installation. The cable routing can be hidden and made invisible with a rear connector or cabled antenna.

2.3.2.2 Environmental requirements

Temperature:

The storage and operating temperatures are the two essential temperature specifications that are essential for a practical reader antenna. Temperature changes affect the antenna's resonance, return loss and radiation parameters [20]. Antennas should not deform or get damaged internally when stored in warehouses or containers due to changing weather and different daytime or nighttime temperatures. Materials insusceptible to change in temperatures are required for designing a reader antenna. Operating temperatures of an antenna are the maximum and minimum temperatures at which the antenna can function effectively without deviating from its specifications significantly. Passive elements such as resistors, capacitors or any other components such as adhesives used as part of the antenna design are required to meet the operating temperature specifications. Antennas installed in pharmaceutical fridges and freezers have the requirement for low-temperature operation. The international electrotechnical commission (IEC) prepares and publishes the international standards for electrical and electronic related equipment. The IEC 60068-2-1 and IEC 60068-2-2 are the low and high-temperature standards used to assess the antenna's ability to perform under extreme cold and dry heat environmental conditions [21]. Tests are performed in controlled test chambers for up to 72 hours.

Humidity:

Humidity is a measure of the presence of water vapor in the atmosphere and has an impact on the antenna's performance [22]. Reader antennas installed in environments where the atmospheric humidity is not controlled will have detrimental effects inaccurate tag detection. Moreover, condensation occurs when the temperature changes along with the humidity. The dew or the water droplets inside an antenna considerably influence the antenna's performance. Thus, a robust antenna design is required to adopt the change in humidity. The antenna design should be in accordance with the specification prescribed by ETSI EN300019-2-4 to comply with the effect of humidity [23]. Humidity tests are performed in a controlled humidity chamber at a 95% relative humidity for at least 150 hours. Condensation in an antenna can be eliminated by ingress protecting the antenna, which is discussed in the following section.

Ingress protection:

The dust and water-resistant requirement for a practical reader antenna enable the antenna to outlast in various indoor and outdoor applications. IP rating defined by IEC 60529 [24]. classifies the degree of solid (dust) and liquid (water) ingress protection. The IP code is a two to a four-digit code where the first and second numeral corresponds to the product's level of protection against dust and water, respectively (refer to Table.2.1). The third and fourth letters are optional, and they are termed as the additional and supplementary letters (refer to Table.2.2).

Table.2.1. Ingress protection codes

1st Digit	Dust Protection level	2nd Digit	Water Protection level
0	Not protected	0	Not protected
1	Protected against 50 mm diameter solids	1	Protected against vertically falling water drops
2	Protected against 12.5 mm diameter solids and greater	2	15° tilted equipment protected against vertically falling water drops
3	Protected against 2.5 mm diameter solids and greater	3	Protected against water spray at any angle up to 60°
4	Protected against 1 mm diameter solids and greater	4	Protected against splashing water in any direction
5	Dust protected to some degree. Equipment's operation is unimpaired.	5	Protected against a 6.3mm nozzle water jet in any direction with
6	Dust tight. No ingress at all.	6	Protected against 12.5 mm water jet in any direction
		7	Equipment is immersed up to 1m water depth.
		8	Equipment is immersed up to 3m water depth

Table.2.2. Additional and supplementary letters

1st	Dust Protection level	2nd	Water Protection level
A	Protected against hand	f	Protection against oil ingress
B	Protected against finger	H	For high voltage equipment
C	Protected against a tool	M	Water test on the moving parts when in motion
D	Protected against a wire	S	Water test on the moving parts when they are stationary
		W	Protected for specified weather conditions

Almost all the industries require reader antennas to be IP rated to some extent. Monolithic printed antenna design can be IP rated without a radome. Antenna's IP rating is otherwise enabled by the radome's design A higher IP rating is achieved by using rubber gaskets or flexible silicone-based gaskets with the antenna's radome. Dust and water tightness around the connector or the cable is achieved by using O-ring and grommet gaskets. In a connector-fed antenna, the extension cable that connects the reader and the antenna is also required to be IP rated. It is important to perform both water jet and immersion testing as the physical pressure handled by the antenna will be different for both the cases. A typical outdoor antenna is IP65 and IP67 rated.

Vibration and impact resistance:

Reader antennas installed in vehicles such as trucks and vans undergo a range of vibration and impacts. Vibrations can cause disconnects within the antenna's architecture and may lead to malfunctioning. For instance, a disconnected antenna feed may change the antenna's input impedance leading to a poor VSWR (Voltage Standing Wave Ratio). Other physical structures such as the screws holding the antenna's radome intact are also vulnerable to the effects of vibration. This creates the vibrational resistant requirements for the reader antennas. A monolithic patch antenna design is less prone to damage compared to suspended patch antennas over air dielectric. Screws can be replaced with industrial adhesives to sandwich the layers of the antennas. Pressure sensitive adhesives have a greater vibration resistance due to its vibration damping properties [25]. Antenna radome can also be adhered to the antenna making the whole construction solid-state.

Impact or shock, on the other hand, are more prominent in industrial applications. Automated robotic arms, conveyor systems, and forklift operated warehouses are some of the applications where the reader antennas may experience physical impacts. A solid-state antenna with a hard radome can overcome these impacts. The IEC 60721-3-4 standard elaborates on the test requirements for both vibration and shock resistance [26]. Vibrational tests can either be sinusoidal or random. In sinusoidal vibration, the vibration frequency, displacement, and acceleration are specified for different axes and the test is performed for 3-5 sweep cycles. In random vibration tests, the test is carried on a defined frequency for a duration of 30 minutes in various axes. For shocks, the shock spectrum duration, acceleration, number of bumps and the direction of bumps are defined.

Flammability:

Indoor reader antennas need to comply with the building's fire and flammability requirements. When the antenna's substrate and radome are made from plastic, they must comply with the safety standards prescribed by the Underwriters Laboratory (UL) [28]. The UL-94 standard determines the plastic's propensity to either spread the flame or extinguish when subject to ignition. A 127 x 127 mm^2 sample is burnt to find out applicable flame-retardancy rating according to Table.2.3.

Table.2.3. UL flammability ratings

Type	Specimen Orientation	Extinguishing time	Test outcomes
5VA	Vertical	Within 60 seconds	Drips not allowed. Plaque specimen may not develop hole
5VB.	Vertical	Within 60 seconds	Drips not allowed. Plaque specimen may develop hole
V-0 V-1	Vertical Vertical	Within 10 seconds Within 30 seconds	Non-inflamed particles drips allowed Non-inflamed particles drips allowed
V-2	Vertical	Within 30 seconds	Drips of flaming particles allowed
HB	Horizontal	<76mm/min burning of <3mm thick specimen or burning stops before 100mm	

Solar radiation:

Permanently installed outdoor antennas are scorched by the sun especially in regions closer to the equator. The ultra-violet-A (UV-A) light is not absorbed by the earth's ozone layer. Certain types of plastic radomes cannot handle long-term UV-A solar exposure and can become brittle. A brittle outdoor antenna has a greater chance for dust or water ingress through the cracks. The internal antenna's performance is impaired when the ingress protection is compromised. UV inhibitor additives can be added to plastic radomes during the process of injection molding. The long-term solar radiation test can be accelerated in a laboratory by using various light sources for different testing scenarios.

Different exposure conditions can be simulated by using different UV lamps with corresponding irradiance levels, temperature, and light exposure timing. The ASTM G154 test standard describes the standards for accelerated weathering [27].

Salt mist:

Outdoor reader antennas can corrode over time especially those which are deployed in coastal regions. Corroded antenna parts such as the antenna's ground plane or the radiator can have adverse effects on the antenna's overall performance. The corroded antenna can also break over time leaving the antenna unusable and need to be replaced. Corrosion can be avoided by using highly corrosive-resistant metals or treating the metals through galvanization or anodization. The Salt mist test is defined by IEC 60068-2-11 standard [29]. The test is carried out in an enclosed chamber at a temperature of 35°C by a continuous indirect spray of salt water solution with a pH between 6.5 and 7.2. The salt water's spray rate is between 1.0 and 2.0 ml/80cm^2 per hour.

Wind survival:

Reader antennas mounted in masts for applications such as vehicle tolling is susceptible to the effects of winds. Antennas with the large surface area will be pushed away by the wind compared to smaller ones. Planar antennas such as patch antennas are less affected by the wind as they are often enclosed by a radome. Antennas like Yagi-Uda and log periodic consists of metal elements at fixed locations in relation to the operating wavelengths. When the position of these elements is disturbed by the force of the wind, the antenna's characteristics such as resonant frequency, radiation pattern, impedance matching, antenna gain are greatly altered. Heavy-duty mounting studs are also required to mount the antennas safely and will not pose any health and safety hazard. Wind load tests are specified by ANSI/TIA-222-G [30] and EN 1991-1-4 [31] in the USA region and Europe regions, respectively. The impact of wind speed and wind direction on antenna loading is tested by the wind tunnel tests viz., constant speed yaw sweeps and velocity sweeps, also known as the Reynolds number sweeps. During the constant speed yaw sweep, the wind load is measured in different yaw angles at incremental 10 or 5 degrees from 0° to 180° at a constant wind speed of 150 km/h. The speed of the wind is varied from 40 to 180 km/h during the velocity sweep tests.

2.3.2.3 Electrical requirements

Antenna detection circuitry:

The readers use two different antenna detection methods to ensure that an antenna is connected before the reader can start to transmit the energy through its RF ports. An open-circuited RF port offers maximum power reflection due to impedance mismatch that would damage the reader. When the port impedance is matched by connecting an antenna (load), the reflected power is minimized. Some RFID readers like Impinj Speedway r420 measures the reflected RF power in terms of VSWR to make sure that an antenna is connected to its RF ports. Other readers like the JADEK’s Thing-Magic M6e senses for a DC resistance across the center pin and the ground of the RF ports. The DC resistance that the reader’s algorithm is sensing is between 50 Ω and 10 kΩ [32]. For a reader antenna to be compatible with all the RFID readers in the market, the antenna must have a DC resistance across the center pin and the antenna’s ground, and a good VSWR specification. In some other readers, a 0 Ω DC resistance between the input and the ground is also accepted.

Electrostatic discharge (ESD) protection:

Electrostatic charges can be built on the antennas in applications where the assets are constantly moved over the antennas. For instance, in a point-of-sale application, static charges can get built on the antenna's surface when assets are moved over the antennas during billing. A simple event like picking up a common polyethylene bag can generate 20,000 volts of ESD at 20% relative humidity [33]. When the antenna is mounted underneath the counter's conveyor belt, the magnitude of the built static charges will even be greater as the conveyor belt now acts as a Van-de-Graff generator. If the antenna is not earthed properly then the static electricity can damage the RFID readers. Electrostatic charges building in a folded dipole antenna or a traveling-wave antenna is minimal as the ground is referenced to the radiator either directly or through a load resistance. In a patch antenna, the radiating element is isolated from the antenna's ground plane completely. The static charges built on the radiating element may leak through the cable and can damage the reader's transceiver system. If the radiating patch has a low DC resistance path between the radiator and the ground plane, then the electrostatic charges can get discharged through the RFID reader's earth connection. The DC resistance path can be created by having a short-circuiting via between the ground plane and the center of the patch in case of a half-wavelength patch antenna, where the patch antenna's voltage is 0 V theoretically. A quarter-wave short-circuiting stub may also be incorporated as part of the design at the antenna's input which will create a DC short for the ESD.

2.3.2.4 Radio Frequency (RF) requirements

Frequency of operation:

Resonant antennas are tuned for a range of frequencies and are called as the antenna's operating frequency. The antenna's operating frequency must complement with the RFID reader for efficient operation. Reader antennas can either be designed for the two main frequency bands viz., 865 - 868 MHz (ETSI) and 902 - 928 MHZ (FCC) or for a global 865 - 930 MHz frequencies. The FCC and ETSI UHF RFID frequencies are defined in FCC part 15.247 [34] and ETSI EN 302 208 V3.1.0 (2016-02) [35], respectively. Every country has its own regulatory standards for the UHF RFID frequency of operation. They either authorize the whole FCC or ETSI frequency band or a sub-band within those frequencies. For instance, the sub-band 915 - 917 MHz is the authorized frequencies in Israel while Chile is authorized to use the entire 902 - 928 MHz FCC frequency band.

Mode of operation:

A resonant antenna typically has two types of operating modes namely near-field and far-field operation [36]. In UHF RFID, the antenna's propagating far-field components are utilized to detect the tags at a greater distance. The near-field components are essential in tag detection at instances where the far-field components are incapable. For example, in liquid asset management, the near-field components are far more efficient than the far-field in tag detection as the far-field components are vulnerable to absorption by the liquids. Thus, the mode of operation is an important design parameter for a reader antenna design. When a reader antenna is designed for near-field operation, a uniform magnetic field distribution on the antenna's surface is vital to eliminate the null zones.

Reader antennas have to be specifically designed for near-field or far-field mode of operation.

Polarization:

The polarization of the reader antenna refers to the wave's polarization transmitted by the antenna [37]. A vertically polarized tag cannot be detected by a horizontally polarized reader antenna and vice-versa. Thus, the reader antenna's polarization should match the tag antenna for efficient tag detection. The tag's read distance can be greatly affected due to polarization mismatch. A circularly polarized reader antenna can detect tags in any orientation. Linearly polarized antennas can be used in applications like vehicle tolling where the tags on the vehicles are made to match the reader antenna's polarization and are fixed. In a shelving application, the tagged assets may not always be oriented in the same manner, leading to a mismatch between the reader antenna's and the tag's polarization. This problem can be overcome by using a circularly polarized reader antenna.

Gain and directivity:

An antenna's gain is the measure of maximum power transmission in a given direction [37]. An antenna's directivity is the measure of the directionality or the focusing-ability of its radiation [37]. The antenna's gain and directivity are essential parameters for reader antennas. They enable long-distance tag detection ability. A patch antenna is a type of low-profile planar directional antenna whose gain and directivity are dependent on the size of the ground plane, substrate's dielectric constant, loss tangent and the number of patches. A slot or a dipole antenna over a ground plane can also produce directional radiation. Their gain is also dependent on the factors like the size of the ground plane and the substrate's characteristics and the number of radiators, mentioned above. Other non-planar directional antenna's gain such as in a Yagi-Uda or an axial-mode helical antenna is dependent on the number of director elements and the number of helical turns present, respectively.

The antenna's impedance matching has an impact over the antenna's gain too. The reader antenna's gain must be the same for all the frequencies in the band of operation. This is essential because the signal that is transmitted by the RFID reader would hop between various frequency channels at different times due to the underlying frequency-hopping spread spectrum (FHSS) reader to a tag communication technique. An antenna with a narrow gain bandwidth (say 6 dBi at the center of the band and 4 dBi at towards edge) may lead to different tag read distances at different instances. The FCC frequencies have 50 frequency channels and it takes at least 60 seconds to successfully hop between all the frequencies. Narrow gain bandwidth leads to intermittent tag detection as it is practically impossible for some applications such as vehicle tolling, to continually read tags for 60 seconds.

VSWR:

The voltage standing wave ratio (VSWR) of an antenna is the function of the reflection coefficient of an antenna. The antenna's input impedance must match the UHF RFID reader's nominal impedance (50 Ω) to get a VSWR closer to 1 across the operating frequencies. When the antenna's input impedance is not adequately matched, the reflected power would be directed back to the reader's port to damage the reader's receiver. The antenna's VSWR bandwidth must be at least 4 MHz and 27 MHz for ETSI and FCC frequencies, respectively. The threshold used to determine the VSWR bandwidth varies from reader to reader. Impinj r420 readers have specified the antenna's return loss to be at least 10 dB (1.92 VSWR) while the Thing-Magic M6e requires 17 dB (1.33 VSWR) across the operational frequencies [32]. When the RFID readers use the VSWR parameter in their antenna detection algorithm, a poor VSWR reading at certain frequencies (during the frequency hopping) leads to continuous antenna connection and disconnection from the reader's port, enabling disruption in tag detection reliability.

Radiation pattern:

An antenna's radiation pattern (Figure.2.3) is a graphical representation of the antenna's radiated power in a three-dimensional space at far-field distances. Main lobe or the major lobe is where the antenna's radiation is maximum. The maximum directive gain of an antenna lies within the peak of the main lobe radiation [37].

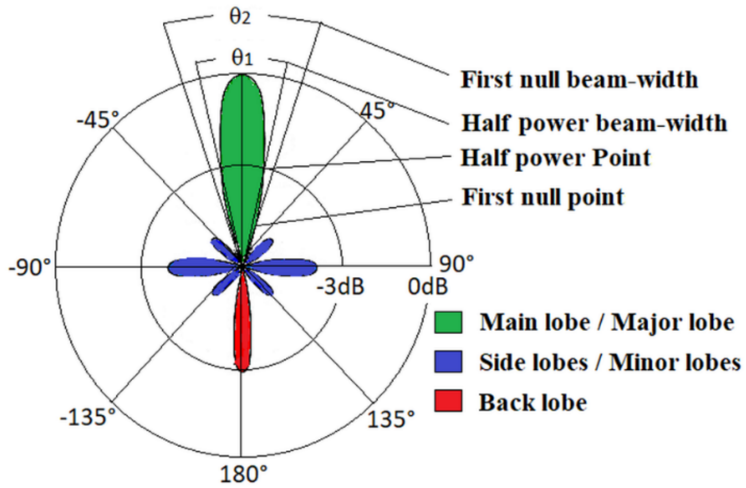

Figure.2.3. Radiation pattern of a directional antenna

A reader antenna's ability to detect tags in a given area is dependent on its far-field and near-field/Fresnel radiation. Detecting unwanted tags present in a given area is also dependent on the radiation parameters. Reader antennas designed for applications like warehouse inventory management must have a wider far-field and near-field radiation to cover a large area whereas the antenna used in a shelving/cabinetry application for asset localization requires a confined read zone. Sidelobe suppression is also essential for vehicle-tolling applications where intended zones are created using narrow main lobes.

Axial ratio:

Axial ratio (AR) is a parameter that is related to circularly polarized antennas. It is the ratio between the minor and the major axis of a polarization ellipse. The axial ratio in practical reader antennas is quoted in the magnitude difference between the orthogonal polarizations. A 0 dB AR means the orthogonal magnitudes of that antenna is equal. The axial ratio parameter is a requisite when the gain of a circularly polarized antenna is expressed in dBiC. A circularly polarized antenna with 6 dBiL (linear gain) and 0 dB AR can be expressed as 9 dBiC. Since the magnitude is equal in orthogonal directions, 3 dB can be added to the linear gain of the antenna [38]. dBiL to dBiC gain conversion can be made using the chart shown in Figure.2.4. Axial ratio is a key parameter for practical reader antennas used in applications where the tag's orientation is unpredictable. Axial ratio up to 2 dB is optimal and an AR beyond that will yield unreliable and intermittent tag detection. Axial ratio is also important for the effective radiated power (ERP) and the effective isotropic radiated power (EIRP) calculations to meet the regulatory requirements defined by local regulatory bodies.

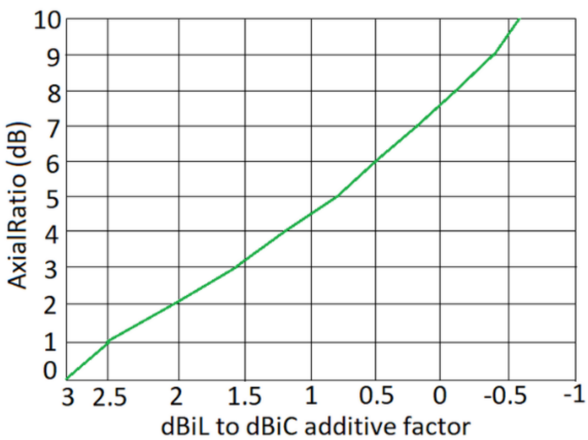

Figure.2.4. dBiL to dBiC additive factors for various axial ratios.

Maximum input power:

Maximum input power rating is the maximum allowable power that can be inputted into an antenna for transmission without damaging the antenna's components. The substrate and the passive components used in an antenna design are susceptible to detrimental effects when the input power exceeds than the rated power. A practical reader antenna's power may be increased to achieve a greater read distance or to detect tags in a dense environment such as palletized assets. High gain antennas fed with a higher reader power cannot comply with the ERP and EIRP based power regulations prescribed by the regional regulatory authorities. For instance, an antenna with a 6 dBi gain can only be provided with 1 W reader power when used in the USA region to comply with the 4 Watts EIRP regulation prescribed by the FCC regulatory authority [34]. An antenna with a 0 dBi gain can be provided up to 4 Watts reader power and can still meet the FCC's EIRP specification. Thus, the input power rating for high gain antennas is not critical compared to the antennas with a lower gain.

2.3.2.5 Other compliance and certification requirements

CE compliance:

Conformité Européenne (CE) is a certification mark indicating that a product that is sold within Europe meets the standards of safety, health, and environmental protection. Products can bear CE marking if the manufacturers declare the CE conformity through self-certification. There are a variety of CE directives among which the RED 2014/53/EU (radio equipment directive) [39] and the RoHS-3 2015/863 (restrictions of hazardous substances) [40] directives are relevant for a piece of RFID equipment. Antennas with one or more active components interacting with the RF signal are known as active antennas and those without any active components are called passive antennas. Active antennas are required to adhere to the RED norms. When the passive antennas are made available on its own, it is exempted from compliance. Passive antennas are subject to RED CE compliance if they are permanently attached to the RFID readers. The RoHS standards restrict the use of specific hazardous materials found in electrical and electronic products. Table.2.4 shows the restricted substances and their levels in parts per million (ppm).

Table.2.4. Restrictions of hazardous substances RoHS-3

Restricted Substances	ppm
Lead (pb)	< 1000
Mercury (Hg)	< 100
Cadmium (cd) Hexavalent Chromium (Cr VI)	< 100 < 1000
Polybrominated Biphenyls (PBB)	< 1000
Polybrominated Diphenyl Ethers (PBDE)	< 1000
Bis ()2-Ethylhexyl) phthalate (DEHP)	< 1000
Benzyl butyl phthalate (BBP)	< 1000
Dibutyl phthalate (DBP)	< 1000
Di-isobutyl phthalate (DIBP)	< 1000

Explosive standards and certification:

Explosions can be caused by electrical equipment in certain atmospheres and thus it is advisable to test the RFID equipment against the explosive standards. IECEx (IEC-60079 explosive standards) [41] and ATEX 2014/34/EU (ATmosphères EXplosibles) [42] are some of the explosive standards widely used around the globe. Explosive certified reader antennas and readers must be used in explosive hazardous applications such as oil refineries, mining industries, hospital operating rooms, pharmaceutical industries, chemical processing industries and in aircraft workshops.

HERO certification:

HERO stands for the hazard of electromagnetic radiation to ordnance. It is an

EMC/EMI (electromagnetic compatibility/ interference) compliance certification defined by the military standard MIL-STD-464 for electrical and electronic equipment used in seaborne, airborne, ground and space-defense environment [43]. The antennas can be HERO (Hazards of Electromagnetic Radiation of Ordnance) certified along with an RFID reader. HERO certified RFID system is preferred in military applications.

Plenum rating:

Plenum spaces are areas in a building that facilitates air circulation. When cables such as ethernet cat5e, RF coaxial cables are routed through these spaces, the cables must comply with the NFPA-90A (national fire protection association) standards [44]. The plenum rated cable's outer jackets are made from fire-retardant and low-smoke polyolefins. Reader antennas that are cable-fed must be plenum rated to comply with the building's regulations.

2.3.3 Reader antenna design methodology

The flow chart in Figure.2.5 illustrates the reader antenna design methodology. The RFID reader antenna's intended use case is analyzed, firstly. The second step is to analyze the reader antenna's design requirements viz., physical, environmental, electrical and RF requirements. The design specifications for the reader antenna is then formulated and the antenna is designed to meet the specifications. If the specifications are met, then the antenna is tested for RFID performance. If the specifications are not met, then the antenna design is tweaked to meet all the specifications.

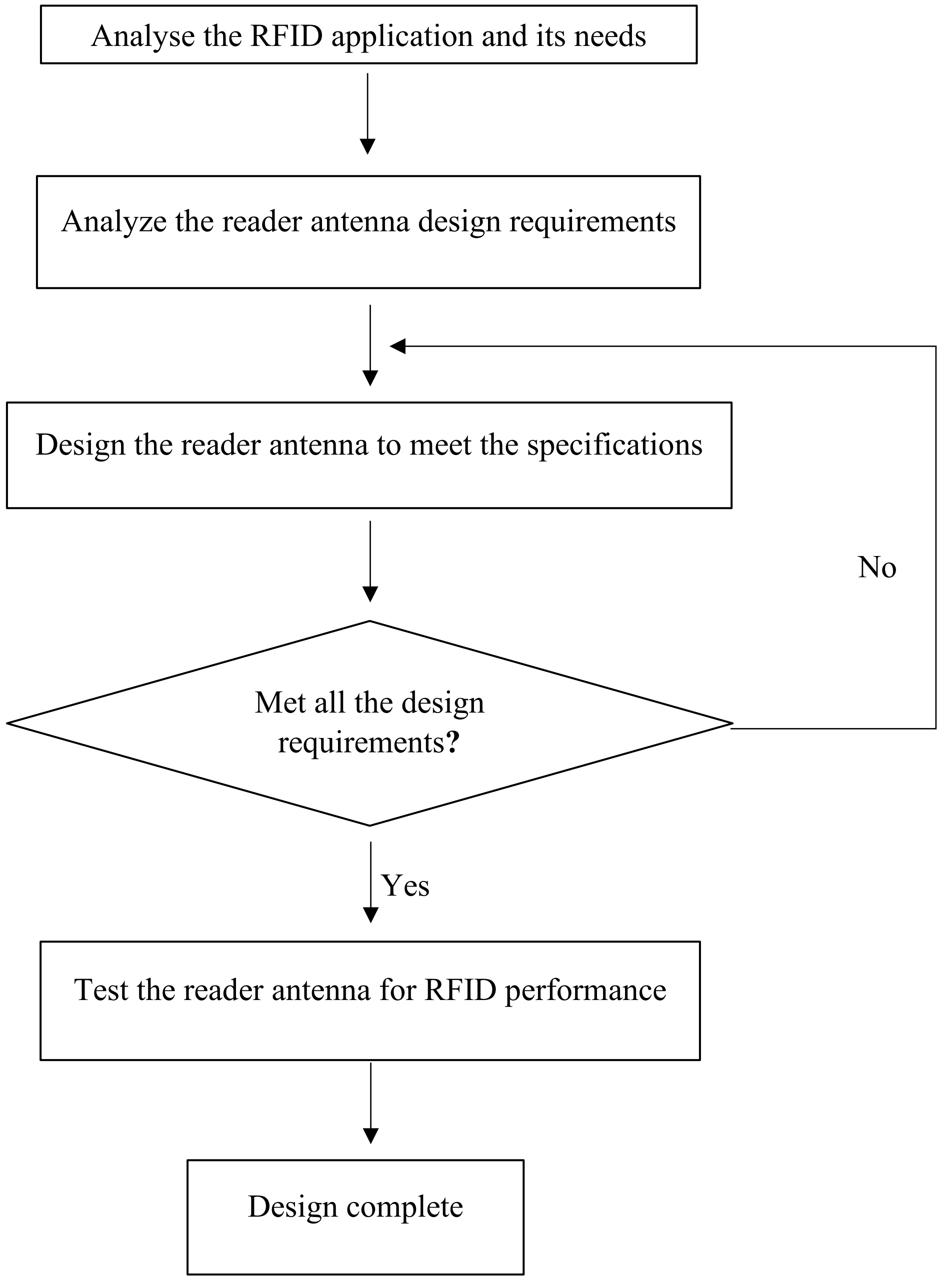

Figure.2.5. Reader antenna design methodology

2.4 Conclusion

Commercially available non-conventional RF materials can offer low-cost antennas with ease-of-manufacturability. Uncontrolled manufacturing of these materials results in variable dielectric properties such as dielectric constant and loss tangent.

Challenges with an unknown and variable dielectric constant are addressed in this research. The inherited properties of various non-conventional materials can contribute to fulfilling different physical and environmental requirements of a UHF RFID antenna design. A novel and innovative UHF RFID antenna design contribute towards the electrical and RF requirements. Non-conventional substrate's losses are tolerable as it is a trade-off between meeting the requirements and designing an efficient antenna.

Chapter 3

Literature Review

3.1 Introduction

Materials used in patch antennas can be broadly classified into conventional and non-conventional materials. Conventional materials are typically designed and manufactured using a virgin dielectric substrate that is produced in well-controlled environments. These virgin RF materials exhibit both well-known and uniform electrical properties, which greatly aid in the design and manufacturing of high-performance RF products. On the other hand, non-conventional materials are those which are predominantly used in applications other than RF design. Table.3.1 shows some of the commonly used conventional materials and non-conventional materials suitable for antenna design. The table also lists the proposed non-conventional materials for patch antenna array design.

Proposed non-conventional materials include recycled plastics, plastics used for construction and thermal insulation and other eco-friendly plastics that are biodegradable. Construction and insulator grade plastics may not be purely virgin and may contain impurities. Thus, they can also be categorized under recycled plastics. Biodegradable plastic materials can be both virgin or recycled. It has been widely accepted that recycling is the best way to manage plastic wastes. Recycling of plastics goes through sorting, shredding, washing, water treatment, drying and extrusion. These plastics can also be reinforced with glass or flax fibres, and a comparison between virgin and a recycled plastic showed equal stiffness. So, making antennas out of non-conventional materials which are recycled in most cases is definitely eco-friendly and cost-effective. Plastics are insulators that conduct some electrical energy at higher frequencies. As this proposal deals with antenna design in the ultra-high frequency range, the effectiveness of insulation has to be measured through 'Dielectric Constant (D_K)' and 'Dissipation Factor (D_F)' otherwise known as 'Loss Tangent (tanδ)'. Variables like additives, fillers, part thickness and even environmental conditions like moisture devastate the recycled plastic's D_K [45]. Polarizability of polymers defines the value of D_K and recycling could affect this property. [45] has proved that manufacturing tolerances with respect to resin flow and part thickness also impact the material's D_K. The addition of graphene during the process of injection moulding has dramatically impacted the D_K value as per [46]. The underlying cross-linked chain chemistry, relaxation and temperature explains the dielectric properties [47].

Table.3.1. Antenna substrate materials

Conventional materials	**Existing non-conventional materials**	**Proposed non-conventional materials**
1. Air	1. Cellulose (paper / cardboard)	1. Recycled Plastic
2. FR-4	2. Heterogeneous Substrate	2. Plastics used for construction
3. Taconic	3. Fabric	3. Thermal Insulation Materials
4. Rogers	4. Wood	4. Bio-degradable materials

3.2 Patch antennas on conventional substrates

Conventional substrates are those whose dielectric properties such as dielectric constant and loss tangent are non-varying. They could be either be naturally occurring or fabricated. Fabricated materials are manufactured in a controlled environment and have strict dielectric constant tolerances. The following are some of the commonly used conventional substrates in the literature.

3.2.1 Air

Air is a naturally occurring dielectric whose dielectric constant value is 1. A patch antenna can simply have an air gap between the radiator or a ground plane or can have air cavities introduced in a substrate. The antenna design shown in [48] has a patch antenna separated from the ground to introduce an air gap. This air gap acts as a substrate, and the patch is excited using an ‘L-shaped’ probe. An aperture is introduced foe efficient coupling and patch excitation. This configuration is renowned, and slight modifications to the patch’s shape and size, such as a ‘U-shaped’ patch proposed in [49] are also ubiquitous. Air cavities are also introduced by some authors in the literature such as [50] where the antenna is a stacked patch array. The stacked patches contain air cavities that are embedded within other conventional substrate layers. Air cavities are also introduced by recessing the ground plane (as shown in [51]) such that the patch has an air dielectric substrate, but the feed network operates on an alumina ceramic conventional substrate.

3.2.2 FR-4

FR-4 is a glass-reinforced laminate material. Epoxy resin is used to bind the woven fibreglass cloth. FR-4 substrates are flame resistant and are most commonly used in the printed circuit board. Its dielectric constant value is 4.4. There are different grades of FR-4 substrates with a different temperature rating. The dielectric constant value is also different between those grades. The dielectric constant is consistent with tight tolerances due to uncompromising manufacturing processes. There are a lot of patch antenna and array designs reported in the literature and among which [52] is a recent work in 5G beam-steering antenna. Although the substrate is lossy, low insertion losses are achieved by employing appropriate combinations of spatial filter unit cells. A dual-band reconfigurable patch antenna with defective ground structures reported in [53] uses FR-4 substrate for MIMO applications in 1 – 3 GHz range. Varactor diodes are used to achieve frequency reconfigurability. A suspended FR-4 patch antenna with an air gap, reported in [54] consists of two patches separated by the FR-4 substrate and are connected using two connecting pins. This stack is suspended over an air gap above the ground plane.

3.2.3 Taconic

Taconic or TLC Taconic are engineered laminates suitable for microwave applications. These substrates are low-loss and have low dielectric constant, unlike FR-4. Dielectric constant over a frequency range will be uniform and are suitable for multiband or wideband antenna designs. TLX-8 type Taconic substrate is used in [55] for a high gain dual-polarized ultra-wideband patch antenna array. The array is intended to use with chipless RFID applications. Electronic beam switching antenna is designed in

Taconic RF60A substrate reported in [56] has both patch and feed network created in the same substrate.

3.2.4 Rogers and RT-Duroid

Rogers Corporation has a family of microwave laminates (substrates with copper-clad) that are manufactured to have very precise dielectric constant across a wide frequency range. Rogers has a variety of laminates with various dielectric constant, loss tangent and temperature properties. MIMO antennas for smart 5G devices in [57] have used RT-5880 Rogers board whose dielectric constant is 2.2. An 8 X 8 antenna array is designed for 26 – 30 GHz 5G applications. High-gain broadband 60 GHz, planar patch antenna arrays, designed with and without air cavities in RT-5880 substrates in [58] have low insertion loss, wide bandwidth and symmetrical radiation pattern. Rogers' ULTRALAM liquid crystalline polymer material is used to design miniature dual-band antenna for implantable applications in [59].

RT-Duroid is another type of laminate offered by Rogers that is made from PTFE. They have low electrical losses, low moisture absorption and have a stable dielectric constant over a wide frequency range. An ultra-wideband antenna (3 – 11 GHz) is designed in RT-Duroid 6010LM substrate [60]. A coplanar waveguide is used to feed a rose-curve shaped monopole. A conductive polymer polyaninine (PANI) multi-wall carbon nanotubes (MWCNTs) is fabricated to use with RT-Duroid 5870 substrate for localisation and WLAN systems. The substrate's dielectric constant is 2.33, and the loss tangent is 0.0012. A 4 element ultra-wideband MIMO antenna is designed in RT-Duroid 5880 substrate for WiMax and WLAN applications in [62]. The antenna has enhanced isolation and dual-band rejection. The antenna is directly etched on the RT-Duroid laminate.

This thesis does not adopt any of these conventional substrate materials for research purposes. Instead, it focusses on using non-conventional materials for patch antenna and array designs that will have an acceptable performance.

3.3 Patch antennas on non-conventional substrates

Non-conventional substrates are those which are manufactured to be used as a patch antenna substrate. They are rather intended to be used for a different purpose. The following are some of the non-conventional materials that are used as a patch antenna substrate in the literature for various applications such as body-worn antennas, printed antennas, and so on.

3.3.1 Cellulose

Paper and cardboard are cellulose-based non-conventional materials. There are some existing works such as [68] where a three-dimensional patch antenna array is made on a cuboid cardboard box. Microstrip lines are used to feed the antenna array. The antenna is stub tuned for impedance matching, and the radiation pattern of the array does not combine but radiates in all the directions, three-dimensionally for UHF RFID tag detection. The substrate's dielectric constant evaluation is not performed. In addition, the work is only based on simulation and not on fabricated hardware. Two 2.45 GHz patch antennas are designed in low loss corrugated cardboard substrates are proposed in [64]. Dielectric constants are estimated by small perturbation method using resonant cavities as this method is accurate to measure very thin substrates. Inkjet printing technology is adopted using conductive silver ink on a thin fibrous cardboard substrate in [65 and 66]. Microstrip lines are printed and evaluated before fabricating a microstrip line patch antenna.

3.3.2 Heterogeneous

Heterogeneous substrates are a combination of several conventional or non-conventional substrates. The stack of substrate constitutes a new dielectric constant value. Patch antenna's performance is associated with the effective dielectric constant that is realized from the heterogeneous substrate stack. A substrate and superstrate grids are 3D printed in [67] using a material called 'Watershed XC 11122' by a process called additive stereolithography. The substrate grids are filled with an air dielectric, and thus the overall dielectric constant is measured to design a double-stack patch array. Similarly, [68] has reported a heterogeneous substrate made from a thermoplastic elastomer called 'Ninjaflex' and Acrylonitrile Butadiene Styrene (ABS). Different percentages of Ninjaflex and ABS are trialled, and their dielectric constant values are estimated. A patch antenna is designed, fabricated and tested for wearable applications. A flexible substrate is 3D printed from DM9760 material with airgaps forming a heterogeneous substrate in [69]. The patch antenna's bandwidth is increased by combining TM_{10} and TM_{01} modes. A heterogeneous substrate composed of Taconic RF-45 or FF-27 and T9ST substrates is proposed in [70]. The substrate's anisotropy and diamagnetism are analysed in this paper. The work reported in [71] is similar to [67] where the heterogeneous substrate is a combination of 3D printed substrate grid and air gaps.

3.3.3 Fabric

Fabric or textile substrates are one of the popular non-conventional material in present times for wearable antenna technology. Different types of fabrics with different dielectric properties were used as patch antenna substrates in the literature. A conventional felt substrate is used with copper polyester taffeta fabric conductors for a dual-mode single band microstrip antenna design in [72]. As the substrate is conventional with known dielectric constant, the substrate is not analysed for its properties before designing the antenna. A wearable patch antenna made from a cotton substrate is tested for two bend modes such as E-plane and H-plane for various bend radiuses from 35mm to 250mm in [73]. Virgin cotton's dielectric constant, 2.1, is used for analysis and the substrate is analysed only in dry condition to avoid losses. A stacked patch array configuration is shown in [74] with two flexible substrates viz., Kapton polymer for the bottom patch and SU-8 polymer whose dielectric constant values are 3.4 and 2.9, respectively. As the D_K values are known, the patch antenna design is relatively simple and easier. Polyethylene terephthalate (PET) substrate is used in [75] for a flexible 4 X 4 patch antenna array. The substrate's parameter is assumed to be unchanging, and thus the antenna design does not include any techniques that can handle the changes in the dielectric substrate's properties.

3.3.4 Wood

Works from [76-78] have used wood-based materials for patch antenna substrates. Wood is a naturally occurring material and it is treated to make different forms such as timber, plywood, fibrous wood, etc. Bamboo (Bambusa Vulgaris) is used as the substrate for patch antenna in [76]. The substrate properties are analysed to determine the dielectric constant as 2.2 loss tangent as 0.07. Authors in [77] used cork substrate that enables a bio-degradable antenna design for smart floor tiles. A copper-plated Tafetta electro-conducting textile material is used for the conductor layer. PVC substrate is used as the antenna's protective radome. The dielectric constant values are estimated for both cork as well as the PVC substrate. But their variances or stability are not analysed. Plywood substrate's suitability in microstrip patch antenna designs for satellite and earth exploration applications is analysed in [78].

This thesis does not use any of these substrates mentioned above but other commercially available substrates that are used for construction purposes. Proposed substrates are not manufactured in a controlled environment and thus have impurities in them. They may as well be recycled. These materials are used for low-cost and robust UHF RFID reader antenna designs. Fabrication of antennas on these substrates also require special techniques such as inkjet printing in the case of cellulose.

3.4 Patch antennas on other non-conventional substrates

3.4.1 Eco-friendly materials

Eco-friendly materials are harmless to the environment when they are dumped as e-waste. The materials may be bio-degradable or recyclable so that they are not dumped in the first place. Cellulose-based antennas reported in [79] and [80] are friendlier to the environment where the formerly used paper and the later used a cardboard substrate. The antenna designs are dipole and inverted-F, and thus their dependencies on the substrate's properties are minimal compared to a patch antenna and array design. Silver ink is to print the conductive layer in [79 and 80]. The feasibility of graphene printing is also studied in

[79]. A patch antenna designed using graphene on a conventional epoxy substrate is discussed in [81]. Authors claim that it is a possible low-cost, eco-friendly solution for antenna applications. Liquid epoxy resins un an uncured state is often toxic and not eco-friendly. The proposed substrate materials are not hazardous to the environment and are also recyclable, thus lessening e-wastes being dumped.

DRA antenna by [82] has an eco-design of dielectric resonator antenna where they have proposed 'swastika' geometry for the DRA instead of traditional rectangular or circular DRAs. Their paper claims that it is the first and foremost proposal that focuses more on the environmental perspective by choosing TMM10i, which is a ceramic thermoset polymer composite material from Rogers high-frequency laminates. The 'eco-design' in this paper is supported by two important advantages:

a) TMM10i substrate dielectric is nontoxic, less hazardous and easily recyclable;
b) The amount of substrate they have used is only about 6.48 cm^3 i.e., 52% less than a traditional rectangular DRA and thus they dump less waste into the environment, which is considered to be eco-friendly.

Their paper is distinguishable from my proposal as, a) they deal with DRA and not with patch antenna; b) their dielectric material is not a recycled material rather a conventional RF material (TMM10i) with superior RF properties at high frequencies.

3.4.2 Waste materials

Authors of [83] have proposed a single patch antenna design from wasted polyolefin as a substrate at 4GHz. A polyolefin is a group of major thermoplastics, and their idea is to use engineering plastic wastes such as old toys, wires, cable jackets, etc. This work is based on simulation, and it does not have any data from hardware measurements. Their design methodology has a 'material selection' task which failed to analyse a particular polyolefin waste rather they simply used a D_K value of 2.32 and a tanδ of 0.01 from the simulation which is most likely to be a virgin polyolefin's properties. In addition to this, the type of olefin is not disclosed, and thus the D_K values chosen are subject to uncertainty as D_K of the same type of polyolefin could even vary; for instance, HDPE has a D_K of 2.3 whereas LDPE has 2.2, both being the same 'ethylene' olefin. A single patch radiator is designed with simulation ports, but an array antenna with a coaxial cable/connector will be produced at the end of the proposed research. [83] has concluded that recycling of waste pipes and wire jackets can be a good idea to fabricate a patch antenna with no effort in pointing out the manufacturing process of turning a waste pipe into a sheet of the dielectric substrate and its impact over antenna's performance. This thesis is different from [83] because it uses commercially available non-conventional substrates (including recycled substrates) rather manufacturing it from plastic wastes. The dielectric constant is measured for every non-conventional substrate instead of a random value chosen in [83]'s simulation.

Authors in [84] have reutilised materials from construction debris to make a UHF RFID reader antenna. They used waste tins and cans for the conductor and recycled polyethylene products as the dielectric substrate for a driven patch, and the stacked patch uses air as dielectric. The dielectric material's electrical properties were not tested after recycling. Design assumed that the material is polyethylene. The conductor uses steel sheets which are flattened to become virgin ones. There is no evidence on a material study to confirm that the recycled polyethylene's properties are the same as a virgin polyethylene but used the virgin polyethylene's electrical parameters to come up with a patch antenna design. They use this stacked patch configuration, where the antenna response is a combination of the driven patch (PE dielectric) and the parasitic excited patch element (air dielectric). A stacked patch antenna's response is the combination of the driven patch's substrate and its superstrate – which is the substrate for the parasitic excited patch. Thus, the main parameters such as dielectric constant, resonant length, etc. are not absolute, rather they are effective. This thesis does not use a combination of a conventional and a non-conventional dielectric substrate (like a heterogeneous substrate stack). The material's properties in [84] are unknown, and no D_K estimation methodology is adopted. There is a vast difference between reutilizing materials and using recycled material, which is far more challenging with unknown and varying dielectric properties that are discussed in this thesis.

Other relevant research in terms of using non-conventional materials (multiple substrates or varying dielectric properties within a substrate) is not prevalent in patch antenna array design for UHF.

Prelude to Manuscript 1

This manuscript proposes and investigates the use of recycled polyolefin (high-density polyethylene and polypropylene) which is not specifically manufactured for RF applications and thus with unknown RF properties, as the dielectric substrate for high-performance UHF patch antennas. The substrate's dielectric constant is estimated by patch antenna's resonant frequency method. This method works by firstly designing a patch antenna based on an assumed dielectric constant value for the substrate, and then using the deviation of the measured patch antenna's resonant frequency to calculate the actual dielectric constant value. As a demonstrative application, a polarization-reconfigurable patch antenna with dual feeds is designed and fabricated using adhesive copper foil on recycled polyolefin substrate.

The patch is excited on its orthogonal points where TM_{01} and TM_{10} modes exist, to obtain multiple polarizations. A cross-shaped slot is added in the centre of the patch to enhance its operating bandwidth for the entire 902-928 MHz band. Simulated ports were located on the vertices lining along the center of patch to find the impedance at those locations. A quarter-wave transformer is used to match the input impedance to the load impedance, by inset feeding. Since the antenna was inset-fed through two orthogonal locations, a similar replica was used on the other half to maintain a D4 symmetry. Depending on the feed's magnitude and phase (controlled by the RFID transceiver), different types of linear and circular polarizations can be achieved. UHF RFID FCC band 902 – 928 MHz is chosen for the design. The point of resonance for both ports is centred at 915 MHz with -10 dB return loss bandwidth of 28 MHz. Port isolation is as low as -17 dB with peak linear and circular gain of 7.0 dBi, and 7 dBiC, respectively, observed in all polarizations. The antenna's radiation is symmetric with a half-power beam-width of ~80° in both azimuth and elevation planes. The antenna's longest and shortest axes are X-axis and Y-axis, respectively and the direction of propagation is Z-axis. Thus, XZ = Azimuth (H-plane) and YZ = Elevation (E-plane). The centre frequency 915 MHz is used to plot the radiation pattern. The plot does not vary across the operational bandwidth.

The resulting antenna not only performs well, but is also low-cost, lightweight, low moisture absorbent, mechanically sturdy, inexpensive and ecologically friendly arising from its use of recycled materials. The antenna inherits these properties from the substrate which are proven by the manufacturer. Moisture absorbency is majorly contributed by substrates of a patch antenna as metals or acrylic adhesives do not absorb moisture. Similarly, mechanical sturdy-ness is offered by the substrate and not generally offered by the metal layers. The same substrate can also be used as a radome to protect other parts of the antenna such as the metallic layers. There are many test methodologies for dielectric constant estimation viz., two microstrip lines and covered microstrip lines, etc. These are non-resonant methods and the estimation based on the patch antenna's resonance is chosen here because patch antennas are intended to be designed eventually. The estimated Er based on this method is more accurate when designing patch antennas from non-conventional substrate. Moreover, the estimated dielectric constant of a non-conventional substrate may vary between samples of the same type of material due to less-stringent manufacturing process. Thus, this research is not intended to accurately estimate the dielectric constant of a non-conventional substrate but to come up with a strategy to use this substrate in applications that demand low antenna costs. The strategy adopted in this research is to design a wideband antenna/array in non-conventional materials that can handle fluctuations in dielectric constant withing a range. The fabrication tolerance variation in this method can be addressed by coming up with a measurement jig where the patch antenna's top conductor, ground plane and the feeding methodology can be kept fixed and the substrate alone can be swapped to test various samples' dielectric constant – instead of fabricating patch antennas from different substrates. The feeding method should not be conductive as it will cause impedance mismatched and that leads to uncertainties in the Er estimation. But capacitively fed antenna can resonate patches with different dielectric substrates. Fabrication imperfections are worrisome for mm-wave and high-end of the microwave spectrum and are not a serious problem for Sub-GHz. As this research is focussed on designing patch antennas using non-conventional substrate materials where the need for loss-tangent is not demanding. Loss tangent values are helpful to evaluate the patch antenna's performance as its efficiency drops when the loss tangent increases and conversely the bandwidth increases when the loss tangent is increased. It is a known fact that non-conventional substrates are lossy and their dielectric constant fluctuates with-in a range compared to conventional substrates due to its less-stringent manufacturing process. Since the research is focussed on UHF RFID application which is generally not intended for long-distance communication, it is not absolutely necessary to precisely know the loss tangent of the substrate.

Chapter 4

Manuscript 1

Recycled polyolefin as dielectric substrate for patch antennas

4.1 Introduction

The conveyance of radio waves through air is achieved by antennas which convert between electrical signals and electromagnetic (EM) waves. At transmitter side, the antenna appears in the final stage, where the fed electrical signal is converted into EM wave. At receiver side, the antenna appears in the first stage, where the received EM wave is converted into electrical signal. The same antenna can be used for both transmission and reception as antennas follow the principle of reciprocity. The antenna is a resonant structure whose physical length depends upon its geometry. Patch antennas are planar antennas commonly found in portable ultra-high frequency (UHF) devices such as mobile phones, laptops and radio frequency identification (RFID) systems. Often also referred to as a microstrip antenna, the patch antenna has a radiating metallic patch and ground plane separated by a dielectric substrate [1]. The radiating patch can be of any geometry, with rectangle, square and circle being most common. Patch antennas can be probe fed through a coaxial cable and connector, or fed by a transmission line, e.g. microstrip line, which can make their fabrication less complex. Though patch antennas have many advantages, they suffer from narrow bandwidth due to their high Q-factor [2].

EM waves are composed of electric (E) and magnetic (H) field vectors. When the E-field vector rotates with a circular motion in its propagation direction, the EM wave is said to have a circular polarization. When the E-field or H-field vector movement is confined within a plane along its propagation direction, the EM wave is said to have a linear polarization. Patch antennas can be designed to exhibit linear or circular polarization without disturbing its planar nature. Commercial UHF patch antennas operating in the industrial, scientific, and medical (ISM) bands are typically constructed of costly high frequency materials specifically designed for RF applications.

This manuscript presents a novel design of an inexpensive and ecologically friendly polarization-reconfigurable UHF patch antenna using recycled polyolefin (a form of recycled plastic) as the dielectric substrate originally intended for many other industry applications. The antenna is designed for the 902–928 MHz band as it represents the median ISM band in the UHF range (300 MHz – 3 GHz). Other ISM bands in the UHF range are 433–435 MHz and 2.4–2.5 GHz.

4.2 Related works

Dielectric materials for RF applications can be broadly classified into conventional and non-conventional materials. Conventional dielectric materials are typically virgin materials with tailored dielectric properties manufactured in controlled environments to achieve high RF performance. Some of the conventional RF materials are air, FR-4, Rogers 4730, RT Duroid, and PTFE. The non-conventional materials are those manufactured for use in predominantly non-RF applications. Existing non-conventional dielectric substrate materials used for patch antennas include cellulose (cardboard and paper), fabric and wood. In [3] and [4], 2.45 GHz patch antennas were made on corrugated and fibrous cardboard substrates, respectively. The antennas were printed using conductive ink directly on the substrates. Corrugated and fibrous cardboard's dielectric properties are a combination of air's and cardboard itself (a virgin cellulose material). The authors in [5] used felt fabric for patch antenna design for body communication in 2.45 GHz. Fabrics are a common alternative substrate used in recent days for wearable antennas. Neither the corrugated cardboard nor the felt material is a recycled material unlike the proposed substrate.

The inhomogeneous substrates in [6] and [7] are a stack and array of virgin substrates, respectively, which collectively yield a dielectric property that is different from each of the source substrate. Since the dielectric properties of source substrates are known, the effective dielectric properties can be calculated. The amount of inhomogeneity within the substrate is predictable, unlike the recycled substrate studied in this manuscript. In [8], a composite of low-density polyethylene (LDPE) and Titania (TiO_2) material was used as a substrate of a patch antenna operating in X-band for satellite communication. This type of polyolefin is a blend rather than a mixture of unknown impurities found in recycled substrates. This graded substrate antenna design is based on the known properties of virgin LDPE and

Titania (TiO_2) unlike the recycled substrate herein whose gradient is variable and unpredictable. The difference between a recycled and reused substrate is worth noting. The underlying dielectric properties are altered in a recycled substrate whereas the substrate's properties remain unchanged when they are reused or reutilized.

In [9], a stacked patch antenna array for UHF RFID reader is made with materials from construction debris. Flatten tin and galvanized steel sheets are used as conductor, while reused polyethylene products and air are used as the dielectric for the driven patch, and stacked patch, respectively. The authors assumed the dielectric properties of virgin polyethylene for their patch antenna design. A stacked patch antenna array's resonance will be a combination of the driven and parasitic excited patch's response. This is different from the antenna design in this manuscript where a recycled substrate is used whose dielectric properties are altered.

4.3 Recycled Polyolefin Substrate

The plastic wastes are best managed by recycling, which involves the processes of sorting, shredding, water treatment, drying and extrusion. The recycled plastics can be reinforced with glass or flax fibers to achieve a stiffness comparable to virgin plastics. Even as insulators, plastics may conduct some electrical energy at higher frequencies. The effectiveness of a material's insulation can be measured through its dielectric constant (D_K) and dissipation factor (D_F). The latter is also known as loss tangent ($\tan \delta$). Additives, fillers, polarizability of polymers and environmental conditions can affect the D_K of the recycled plastic. Manufacturing tolerances with respect to resin flow and part thicknesses can also impact the material's D_K. Recycled polyolefin is predominantly used for industrial flooring, upholstery support, battery boxes, and many other industry applications. In this manuscript, recycled polyolefin (not reused virgin polyolefin as in [9]) is chosen as our antenna substrate due to its low-cost (Table.4.1) and wide availability.

Table.4.1. Proposed and traditional substrate materials' cost comparison.

Substrate Materials	**Cost (USD) per 90000 mm^2**
Rogers FR4	$28.91
Rogers RO4350B	$203.60
RT/duroid 5870	$339.02
Taconic TLC 32-31	$107.204
Taconic TLX-9-30	$72.117
RT/duroid 5880	$345.65
Uniboard-Eco	$6.480

4.3.1 Substrate Characterization

Recycled polyolefin is an engineered plastic sheet with closed cell foamed core and solid skin. The core is a combination of recycled high-density polyethylene (HDPE) and polypropylene (PP), and the outer skin is made from virgin HDPE (Figure.4.1). The material is available in 10, 12, 15, and 19 mm thickness and the thinnest one was chosen for this research. The trade name of this recycled polyolefin is 'Uniboard Eco' [10].

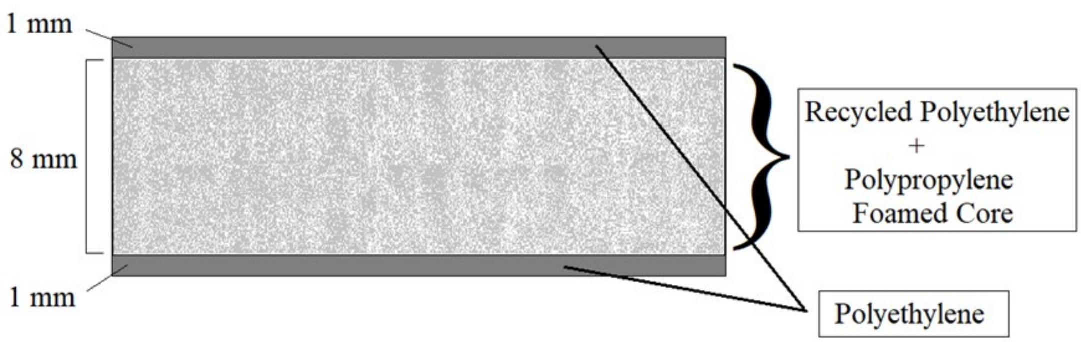

Figure.4.1. Cross-section view of recycled polyolefin substrate.

Unlike conventional substrates for UHF patch antennas such as Rogers RO4000 series and RT-Duroid, the recycled polyolefin is much lower in cost, while being UV resistant, chemically resistant, impact resistant, ecologically friendly, recyclable, very low moisture absorbent and highly durable. This material also exhibits greater structural strength than other low-cost substrates such as air-foam, and thus suit applications that require good load bearing properties, e.g. floor-mounted UHF RFID reader antennas to detect tagged assets on trolleys or carts that run over them.

4.3.2 Dielectric constant estimation

The dielectric properties of recycled polyolefin substrate can deviate from those of virgin ones due to the introduction of impurities during the recycling and manufacturing process. As this material is not originally intended for RF applications, its dielectric properties are not characterized by the manufacturer. Knowing the precise dielectric constant of the material is vital for a patch antenna design. The antenna's attributes such as resonant frequency, antenna gain, and impedance matching, are dependent on the dielectric constant parameter [11]. The dielectric constant of a material can be found by various means such as two-microstrip-line method, strip line method, and patch antenna's resonant method. Although these methods will yield similar results, the patch antenna's resonant method is chosen for the dielectric constant analysis as the substrate in question will be used for antennas, which are resonant structures [11]. This method works by firstly designing a patch antenna based on an assumed dielectric constant value for the substrate, and then using the deviation of the measured patch antenna's resonant frequency to calculate the actual dielectric constant value. The dielectric constant is initially assumed to be 2.375, which is that of a virgin HDPE substrate for frequencies close to our intended patch antenna's resonant frequency of 915 MHz.

The width of patch antenna is determined by [12]:

$$w = \left(\frac{v_0}{2f_r}\right)\left(\sqrt{\frac{2}{\varepsilon_r+1}}\right) \tag{1}$$

where, v_0 = free-space velocity of light

w = width of the patch

f_r = resonant frequency

ε_r = dielectric constant

Using the measured substrate's height (10 mm) and the calculated antenna's width, the effective dielectric constant can be found by [12]:

$$\varepsilon_{reff} = \frac{\varepsilon_r+1}{2} + \frac{\varepsilon_r+1}{2}\left(1+\frac{12h}{w}\right)^{-\left(\frac{1}{2}\right)} \qquad \frac{w}{h} > 1 \tag{2}$$

where, h = height of dielectric substrate (thickness)

ε_{reff} = effective dielectric constant

The patch antenna's electrical length is longer than its physical length as the fringe fields convolve further out during radiation [22]. The length extension is given by [12]:

$$\Delta L = 0.412h\left[\frac{(\varepsilon_{reff}+0.3)\left(\frac{w}{h}+0.264\right)}{(\varepsilon_{reff}-0.258)\left(\frac{w}{h}+0.8\right)}\right] \tag{3}$$

The patch's physical length can now be calculated using the extended length and effective dielectric constant as [12]:

$$L = \frac{v_0}{2f_r\sqrt{\varepsilon_{reff}}} - 2\Delta L \tag{5}$$

The patch antenna's dimensions for a 915 MHz resonant frequency (f_r) are shown in Table.4.2. The patch antenna is excited using a microstrip line. As most ISM products operate at a nominal characteristic impedance of 50 Ω, a 50 Ω microstrip line is designed to feed the patch antenna. The effective dielectric constant of the microstrip line (ε_{reff}) is calculated using the equation (6) for $\frac{W}{h} < 1$ and (7) for $\frac{W}{h} > 1$ [13]:

$$\varepsilon_{\text{reff}} = \left(\frac{\varepsilon_{r+1}}{2}\right)\left(\frac{\varepsilon_{r-1}}{2}\right)\left[\left(\frac{1}{\sqrt{1+\frac{12h}{W}}}\right) + 0.04\left(1 - \frac{W}{h}\right)\right] \tag{6}$$

$$\varepsilon_{\text{reff}} = \left(\frac{\varepsilon_{r+1}}{2}\right)\left(\frac{\varepsilon_{r-1}}{2}\right)\left[\left(\frac{1}{\sqrt{1+\frac{12h}{W}}}\right)\right] \tag{7}$$

Using the calculated ε_{eff}, the microstrip line's impedance (Z_0) can be calculated as [13]:

$$Z_0 = \left(\frac{120\pi}{2\sqrt{2}\pi\sqrt{\varepsilon_r+1}} \ln\left\{1 + \frac{4H}{W\prime}\left[\frac{14+\frac{8}{\varepsilon_{reff}}}{11}\frac{4H}{W\prime} + \sqrt{\left(\frac{14+\frac{8}{\varepsilon_{reff}}}{11}\right)^2\left(\frac{4H}{W\prime}\right)^2 + \left(\frac{1+\frac{1}{\varepsilon_{reff}}}{2}\right)\pi^2}\right]\right\}\right) \tag{8}$$

where, H = height of the substrate

$W' = W + \Delta W'$

W = width of the microstrip line

$$\Delta W' = \Delta W\left(\frac{1+\frac{1}{\varepsilon_{eff}}}{2}\right) \tag{9}$$

$$\Delta W = \frac{t}{\pi}\ln\left[\frac{4e}{\left(\frac{t}{H}\right)^2 + \left(\frac{\frac{1}{\pi}}{\left(\frac{W}{t}\right)+1.1}\right)^2}\right] \tag{10}$$

The 50 Ω impedance of a microstrip line operating at 915 MHz is 29.34 mm wide for a substrate thickness of 10 mm and dielectric constant of 2.375. This microstrip line was inset fed to the patch antenna. The inset depth was optimized at one third of patch antenna's length from the patch's edge for improved return loss [14]. The optimum inset feed length is 30 mm.

Table.4.2. Patch antenna dimensions

L	***w***	***h***	ε_r	f_r
100.8 mm	125.8 mm	10 mm	2.375	915 MHz

Figure.4.2 shows the patch antenna design with inset fed microstrip line on a 300 mm × 300 mm ground plane (90000 mm^2), which is larger than the wavelength for 915 MHz. The patch antenna is fabricated on a recycled polyolefin substrate using a 0.1 mm copper foil, and 0.2 mm tinned steel sheet, for the radiation patch, and ground plane, respectively. A SMA connector is used to feed the patch antenna.

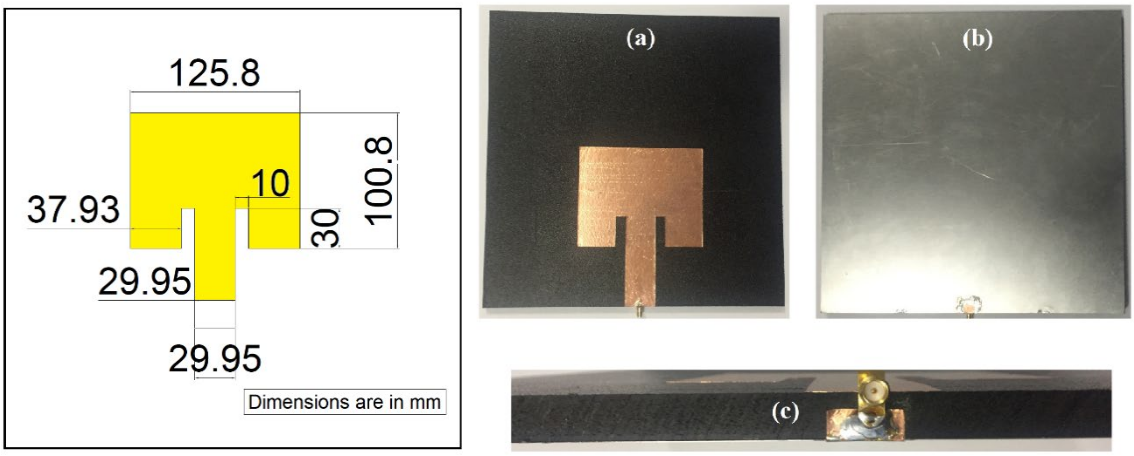

Figure.4.2. Dielectric constant measurement using patch antenna's resonance *Left:* Simple patch antenna design (dimensions in mm); *Right*: Fabricated patch antenna: (a) Front view showing radiation patch; (b) Rear view showing ground plane; and (c) Side view showing the connector and substrate.

Figure.4.3 shows the antenna resonated at 974.77 MHz instead of the desired 915 MHz with a return loss of –24.24 dB. Using (1)-(5) and resonant frequency of 974.77 MHz, the dielectric constant of recycled polyolefin substrate is found to be 2.06, or 0.315 lower than virgin polyethylene. This may be in part due to the impurities in recycled polyolefin material and in part due to air ($\varepsilon_r = 1$) in the closed cell core that lowers the effective ε_r of the recycled substrate material.

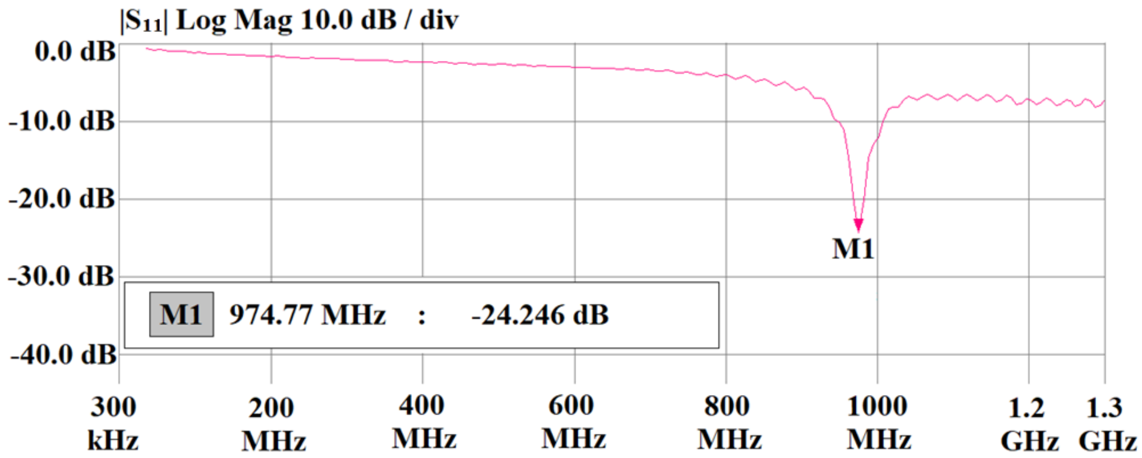

Figure.4.3. Resonance of fabricated patch antenna.

4.4 Multi-polarizable antenna design

This section discusses the design of an UHF RFID reader antenna using the recycled polyolefin substrate. The antenna is designed to operate in the center of ISM band for Region 2 (902-928 MHz), which is 915 MHz. The patch antenna designed for dielectric constant measurement in Section 3.2 is a simple linearly (vertically) polarized antenna with an inset feed. The antenna design discussed herein is a polarization-reconfigurable patch antenna with dual feeds and is fabricated on the same recycled polyolefin substrate. To achieve different polarizations, the patch must be driven on its orthogonal points, which can be either along the vertices or along the perpendicular bisectors intersecting the sides where TM_{01} and TM_{10} modes exist (Figure.4.4). Using equations (1)-(10), the patch antenna's physical resonant length, input impedances and microstrip line's widths are found. The square patch's length is 106 mm for 915 MHz. An 18 mm long cross-shaped slot is added in the center of the patch to enhance its operating bandwidth for the entire 902-928 MHz band [15]. The patch antenna is driven along the orthogonal vertices to achieve slant polarization when driven by either of the two ports. Simulated ports were located on the vertices lining along the center of patch to find the impedance at those locations. An impedance of 448 Ω was found at a location 35.87 mm along the diagonals, which is 23.3 mm away from the sides of the square.

A 149.6 Ω quarter-wave transformer was chosen to match the 50 Ω input impedance to the 448 Ω load impedance. The quarter-wave transformer is 64.5 mm long and 3.39 mm wide, which connects with a 32.14 mm wide and 10 mm long 50 Ω microstrip line where excitation takes place. Since the antenna was inset-fed through two orthogonal locations, a similar replica was used on the other half to maintain a D4 symmetry [16]. The ground plane's dimension is 300 × 300 mm which is longer than a wavelength in both directions. The sharp corners were chamfered to avoid reflections in the patch, which itself is located at the centre of the substrate.

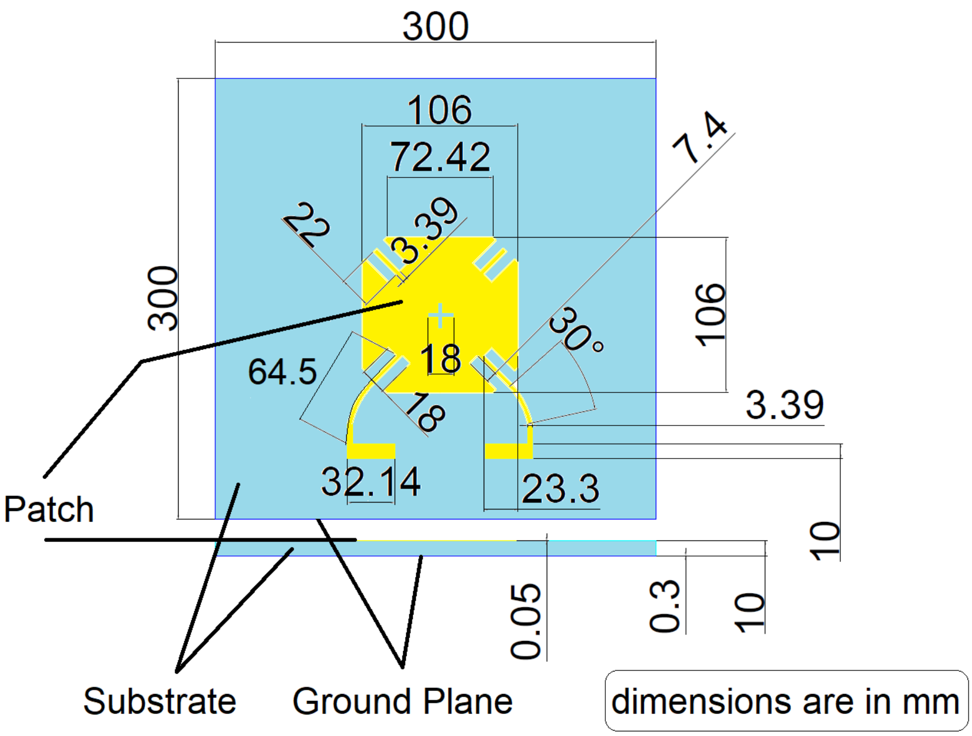

Figure.4.4. Polarization-reconfigurable patch antenna design.

4.5 Antenna analysis

4.5.1 Simulation

The antenna design was simulated in HFSS simulation software. The patch layers were defined as having 0.1 mm thick conductor (copper of conductivity 5.8×10^7 S/m) and 10 mm dielectric layer. The obtained dielectric constant value from Section 3.2 is used here. A radiation boundary was defined, and the simulation was swept between 800 MHz and 1000 MHz.

Table.4.3. Simulated $|S_{11}|$ and $|S_{21}|$ Results

Frequency (MHz)	Port 1		Port 2	
	$\|S_{11}\|$ (dB)	**$\|S_{21}\|$ (dB)**	**$\|S_{11}\|$ (dB)**	**$\|S_{21}\|$ (dB)**
902	-12.50	-18.0	-12.50	-18.0
915	-19.0	-17.5	-19.0	-17.5
928	-12.50	-18.5	-12.50	-18.5

The patch antenna resonated at 915 MHz (center frequency f_c) with a $|S_{11}|$ of -19.0 dB in both the ports. The port isolation $|S_{21}|$ at f_c was -17.5 dB for both ports. Table.4.3. Lists the $|S_{11}|$ and $|S_{21}|$ values for the low, mid and high operating frequencies. The antenna can be excited through port 1 or 2 as shown in Table 4 to realize different orientations of linear and circular polarizations. The magnitude and phase will be changed within the transmitter's settings. The simulated antenna has a peak gain of 7.5 dBi at 915 MHz when excited through either port. The azimuth and elevation half power beam-width (HPBW) was found to be 90°, and 85°, respectively for port 1, and 94° and 85°, respectively for port 2 (Figure 8). The maximum front-to-back ratio (FBR) was found to be −15.7 and −7.7 dB in azimuth, and elevated patterns, respectively. The circular polarization's axial ratio was 0.6 dB on the bore sight when both ports were excited 90° out-of-phase. The axial ratio is within 1.7 dB throughout the HPBW. A symmetric far-field beam (Figure 8) is plotted in azimuth and elevation plane for vertical linear polarization. The beam pattern remained similar for all other polarizations and orientations in Table.4.4.

Table.4.4. Polarization configurations

Polarization / Orientations	Port 1		Port 2	
	Mag	Phase	Mag	Phase
Linear: 45° slant	Hi†	n/a	Lo‡	n/a
Linear: - 45° slant	Lo	n/a	Hi	n/a
Linear: Vertical	Hi	0°	Hi	0°
Linear: Horizontal	Hi	0°	Hi	180°
Circular: RHCP	Hi	0°	Hi	90°
Circular: LHCP	Hi	0°	Hi	270°

† 7.07 Vrms with a 30 dBm transmitter
‡ 0 Vrms (i.e. transmitter is off)

4.5.2 Fabricated Hardware

The antenna was fabricated using a 0.1 mm thick copper foil. Figure.4.5(a) shows the top conductor layer with antenna pattern and Figure.4.5(b) shows the bottom conductor forming the ground plane. The copper foil is secured to the substrate using non-conductive acrylic based adhesive. TNC connectors are soldered from the back through the ground plane with the microstrip line in the top layer. The signal phase remains the same for both port excitations.

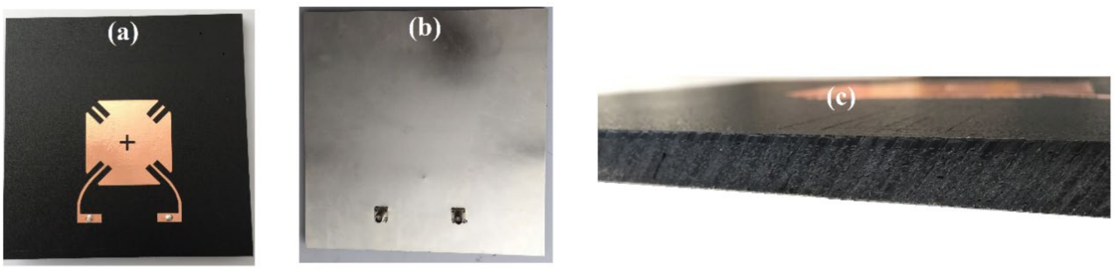

Figure.4.5. Fabricated multi-polarizable patch antenna design

(a) Front view showing the patch antenna; (b) Rear view showing the connector and the ground plane; and (c) Side view showing the substrate.

Figure.4.6 shows the measured antenna's resonance is between 902-928 MHz on both ports with minimum return loss $|S_{11}|$ of −11.30 dB at 902 MHz in both the ports. Port isolation $|S_{21}|$ is as low as −17.90 dB. A 28 MHz, 10 dB return loss bandwidth is observed. Table.4.5 lists the $|S_{11}|$ and $|S_{21}|$ values for the low, mid and high operating frequencies. The antenna's peak linear gain and circular gain in their respective orientations are 7 dBi and 7 dBiC, respectively (Figure.4.7). The minimum gain (6.5 dB and 6.5 dBiC) is noted only at the edge of the band (Table.4.6).

Table.4.5. Measured $|S_{11}|$ and $|S_{21}|$ results.

Frequency (MHz)	Port 1		Port 2	
	$\|S_{11}\|$ (dB)	$\|S_{21}\|$ (dB)	$\|S_{11}\|$ (dB)	$\|S_{21}\|$ (dB)
902	-11.30	-17.80	-11.30	-17.80
915	-19.0	-17.90	-20.5	-17.50
928	-13.60	-18.0	-13.60	-18.0

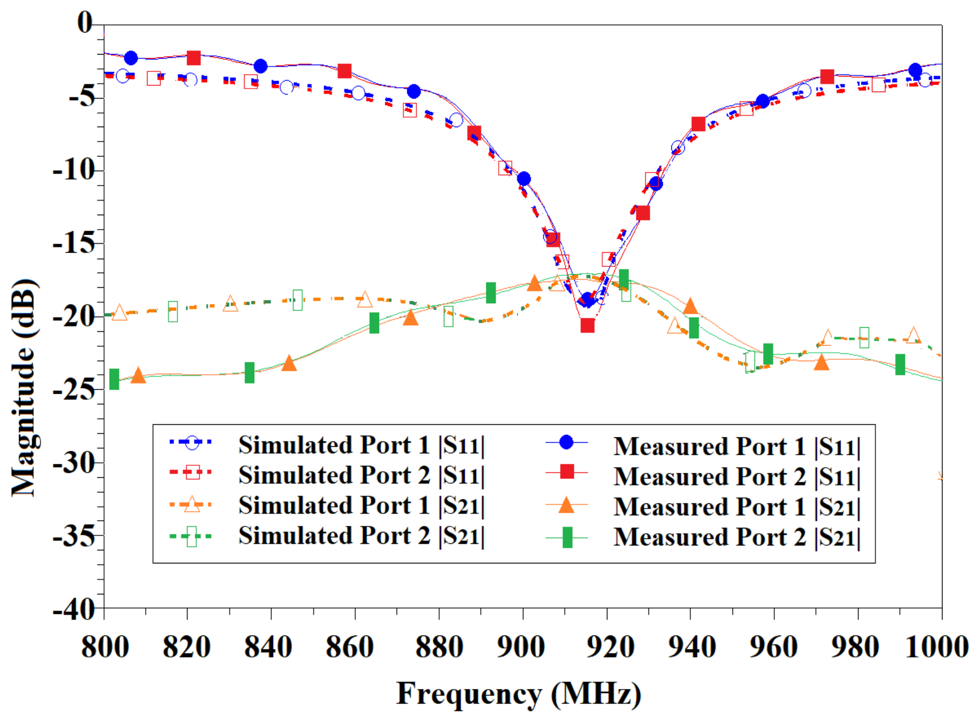

Figure.4.6. Simulated and measured return loss $|S_{11}|$ and isolation $|S_{21}|$.

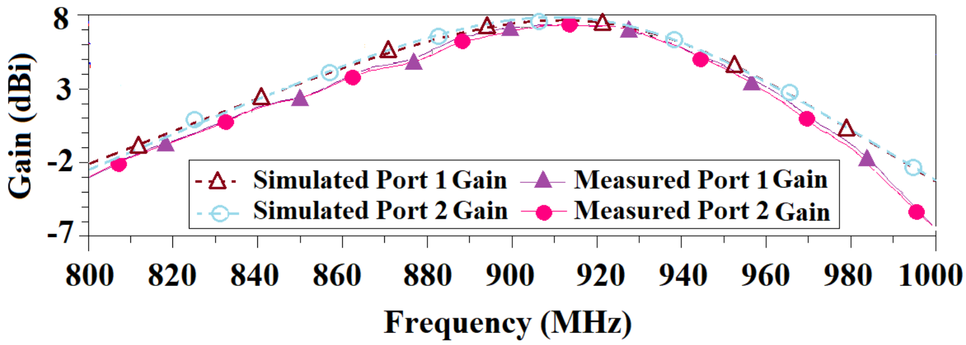

Figure.4.7. Simulated and measured gain for Port 1 and Port 2.

Table.4.6. Gain measurements.

Frequency (MHz)	Port 1 Gain (dBi)		Port 2 Gain (dBi)	
	Simulated	Measured	Simulated	Measured
902	7.0	6.5	7.0	6.5
915	7.5	7.0	7.5	7.0
928	7.0	6.5	7.0	6.5

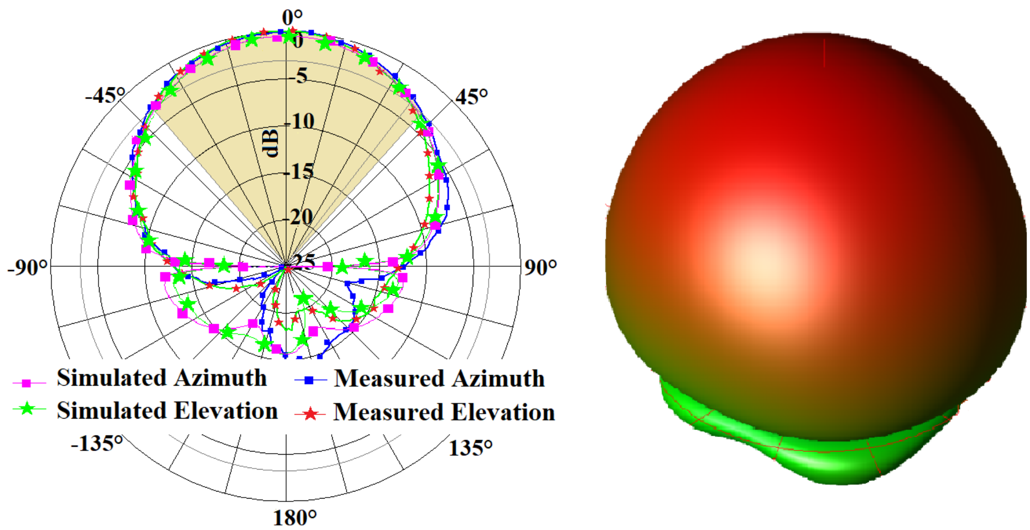

Figure.4.8. Simulated and measured 2D azimuth and elevation radiation pattern (Left), and Simulated 3D radiation pattern (Right)

Figure.4.8 shows the antenna's far-field pattern measured in both azimuth and elevation planes. The HPBW is symmetrical in both the planes and it is noted to be ~80° in both planes. The maximum FBR was found to be −15 dB and −18 dB in azimuth, and elevated patterns, respectively. The circular polarization's axial ratio was less than 2 dB across the band with a peak axial ratio of 0.9 dB, and it remains the same for both LHCP and RHCP polarizations. The antenna's 28 MHz 10 dB return loss bandwidth measured under linear slant 45° and linear slant -45° polarization remained the same for other antenna polarizations: vertical, horizontal, RHCP and LHCP. As the antenna's impedance matching is unaltered during the polarization reconfiguration process, the return loss bandwidth remained the same.

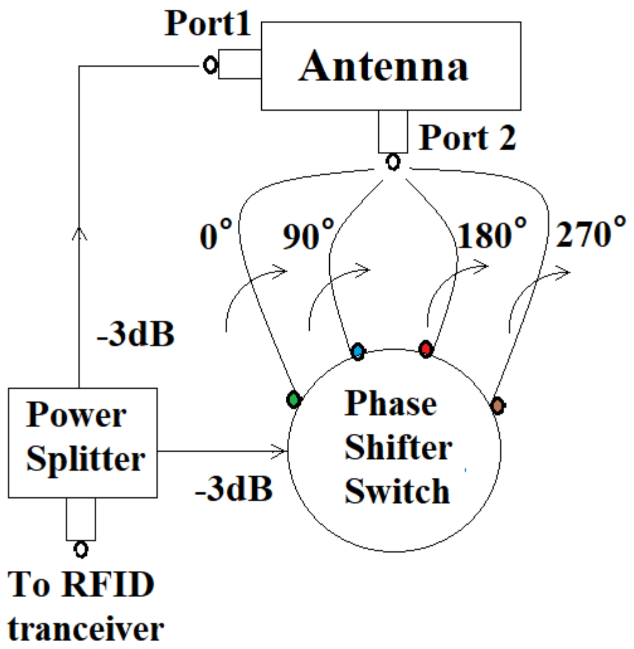

Figure.4.9. Schematic of a polarization reconfigurable module.

Polarization reconfigurability can be achieved as illustrated in Figure.4.9, when a non-smart RFID transceiver is used. The output power from the RFID transceiver is split equally (half power, -3dB) using a power splitter. One arm of the power splitter is fed into the antenna's port 1 while the other arm is connected to a switchable phase shifter. Depending on the phase shifter's configuration: 0°, 90°, 180° and 270°, the polarization can be configured as vertical, RHCP, horizontal and LHCP, respectively.

4.6 Discussion

The recycled polyolefin substrate can be used to design and manufacture high performance patch antennas at low-cost. The antenna is fully recyclable (both substrate and metal), making it environmentally friendly for a sustainable future. The inherited mechanical properties of the substrate make the antenna suitable for various applications. For instance, in UHF RFID applications, when the antennas are embedded on-floor to track mobile assets such as shopping carts or trolleys, the antennas are expected to withstand impact loads and be reasonably waterproof. The recycled polyolefin substrate is a suitable candidate as its surface tensile strength is 18 Mpa and has a hardness rating of Rockwell M-65 [10]. The substrate is also waterproof, UV resistant, self-lubricating, mold and bacteria growth resistant [10], and thus on-floor ground as well as outdoor antenna implementation is feasible at a lower cost.

Despite several advantages, the substrate is vulnerable to variation in dielectric constant value among different production batches. As the substrate production was not primarily intended for RF applications and since recycled materials are used, these variations can be expected. To avoid having to re-characterize the dielectric constant for every sample of this substrate and consequently retuning the antenna, a wideband patch antenna design is suggested. A wideband antenna's response centred at the frequency of interest can be used to accommodate the frequency shift due to changes to its dielectric constant value. Current antenna bandwidth enhancement techniques [17-19] can be adopted for the design of such wideband patch antennas constructed from recycled substrates

4.7 Conclusion

This manuscript presents a dielectric substrate made from recycled polyolefin for patch antenna design in UHF applications. The ISM band of 902-928 MHz is chosen for antenna design and demonstration for RFID applications. The proposed substrate can be similarly used for patch antenna design in other RF applications such as smartphones, Bluetooth or Wi-Fi devices. The dielectric constant of the substrate was first analyzed through patch antenna's resonance method by creating a simple patch antenna. A well matched multi-polarizable complex patch antenna was designed using the calculated dielectric properties. A very high port isolation and return loss was observed with a 28 MHz 10 dB return loss bandwidth. The antenna has a symmetric beam shape with ~80° HPBW in both planes. The low front-to-back ratio of <15 dB shows that the antenna is directional and less leaky on its back. As part of our future work, the antenna's performance will be measured at varied temperature and humidity to investigate their relative effects on the antenna's performance.

Prelude to Manuscript 2

This manuscript presents a scalable ultra-high-frequency (UHF) radio frequency identification (RFID) reader antenna for retail checkout counters. The antenna's simultaneous near-field and far-field operation enable effortless and reliable asset identification. A virgin polyethylene material HDPE is chosen as the substrate whose relative permittivity and loss tangent values are available from the manufacturer (2.256 and 0.0002, respectively, at 1 GHz). Although the material is virgin, it is considered to be non-conventional as it uncommon to see PE as a patch antenna substrate.

Near field and far-field components are generated by two different techniques. The former used microstrip lines' fringe fields to generate intense magnetic fields and the latter generates propagating circularly polarized electric fields from a resonant patch. The microstrip line is made as narrow as possible and meandered to increase the proximity magnetic fields, leading to no surface dead-zones when used for RFID applications. Thus, 113Ω impedance was chosen instead of a simple 100Ω. Two meandered microstrip lines that are 90° out-of-phase form the near-field antenna rim around a far-field patch antenna. The phase shift is created by a hybrid coupler chip. The coupler has 4 ports: input, isolation, and two output ports. The isolation port is connected to a pad where a resistor is connected, and it is grounded via a pad that has a grounding pin. The input is connected to a pad where a SMA connector is probed in. The two output ports of the coupler are fed to the meandered transmission lines. The patch antenna is fed by those meandered lines along the vertices on its orthogonal points, resulting in circular polarization. The near-field energy (as a result of electric and magnetic field generation above the antenna's surface) is evenly distributed with no surface dead zones, and the far-field radiation pattern is symmetrical with a 90° half-power beam-width in both azimuth and elevation planes.

The circular patch antenna's axial ratio was deteriorated due to the proximity of meandered lines' coupling. The asymmetry in the patch antenna's shape i.e., the resonant length on the other TM mode, fixes the axial ratio. The electrical length of the patch is increased by the stub and the 'V' slot – as the surface currents take a longer path along the resonance. As the substrate thickness in only 6 mm, obtaining a wideband operational bandwidth is challenging and thus the slot also enhances the bandwidth. Currents travelling on the surface of the patch antenna takes longer path when it travels past the 'V' slot. Thus, the electrical length is longer than the physical length, in both orthogonal directions.

The antenna was simulated using ADS software and the port impedance was set and calibrated (transmission line 'TML calibration) to 50Ω. The antenna is simulated with a finite ground plane using a bottom conductor structure. Excitation port's positive and negative terminal are referenced to the microstrip line's input (top conductor), and ground plane (bottom conductor), respectively. The antenna operates in the North American UHF RFID band (902-928 MHz) with a 50 MHz impedance bandwidth. The simulated radiation parameters included the antenna's effective angle (or antenna aperture) – a theoretical measure of the effectiveness of an antenna's power reception calculated from the antenna's frequency of operation and its gain. The software reported a theoretical aperture area in steradians.

The fabricated antenna's gain and axial ratio at the band's centre frequency of 915 MHz is 3.3 dBi, and 1.4 dB, respectively. This antenna is low-profile, low-cost and recyclable, and is scalable (making meandered lines wider to cover larger perimeter of a checkout counter as it will not affect the far-field that is solely contributed by the centre patch antenna) with increasing checkout counter sizes and insusceptible to proximity assets and metal frames. The antenna inherits mechanical ruggedness and other properties from the substrate which are proven by the commercial manufacturer. A protective radome can also be made from the same material to protect metallic foil layers.

Chapter 5

Manuscript 2

Scalable near-field fed far-field RAIN RFID reader antenna for retail checkout counters

5.1 Introduction

UHF RFID is a part of the Automatic Identification and Data Capture (AIDC) system which collects information from an object or an individual without needing a manual data entry. Industry associations such as the Advancing Identification Matters (AIM) and RAdio frequency IdentificatioN (RAIN) promote the global adoption for UHF RFID that utilizes the GS1 UHF Gen2 protocol as per ISO/IEC 18000-63 standard. The industry 4.0 focus on automation of manufacturing and data management demands the need for UHF RFID along with other Internet-of-Things (IoT) devices. A typical UHF RFID system consists of a reader and antenna to transmit and receive RF signals, a tag with a unique identifier, and a computer with appropriate software to post-process the data. This manuscript proposes a new UHF RFID reader antenna design with simultaneous near-field (NF) and far-field (FF) operations for retail checkout counters, otherwise known as the point-of-sale (POS). UHF RFID is attractive for retail industries due to its simplicity, compatibility, and cost-effectiveness in installation and maintenance [1]. Asset tracking is often challenging at the POS as the assets are heterogeneous, varying from paper, plastics, linen to metals and liquids.

Assets will be at proximity to the reader antenna at POS while billing and checking out. Traditional FF antennas are susceptible to these proximity assets. High dielectric assets and metal assets detune the FF antenna, whereas liquid assets limit the antenna's read range [2]. NF antennas can solve this problem as the magnetic fields are less affected by liquid and metal assets, but the read range is significantly less compared to the FF antenna. Antennas that can operate in both NF and FF simultaneously is an essential requirement for retail POS application. Other vital requirements for retail checkout counter reader antennas include:

- Customizable size in the 2-D plane to suit different checkout counters such that the scanning area is occupied by the NF and FF energy with no surface dead zones
- Low gain and uni-directional FF radiation to avoid reading unwanted proximity items

- Symmetrical wide-beam FF radiation to provide adequate coverage over the checkout counters
- Low-profile and embeddable under the table or checkout conveyor belt
- Mechanically sturdy to accustom heavy assets laid on them
- Low-cost construction for ease of adoption by the retail industry

In this manuscript, a perimetric meandered line fed patch antenna for UHF RFID reader is presented where the meandered line creates a square rim of NF radiation, and the center patch produces directional FF radiation. The NF perimetric rim has a uniform energy distribution on its surface with no dead zones. The circularly polarized patch creates a symmetrical radiation pattern that enables accurate tag detection regardless of the asset's orientation. The perimetric NF antenna's size in 2D-plane is scalable with an increase in counter size and customizable for various retail checkout counters. Scaling the patch antenna is not required as its symmetrical wide-beam is sufficient to cover large- and small-sized counters.

The antenna is low-profile and constructed from non-conventional polyolefin substrate with inherent properties such as UV, impact, and chemical resistance, low coefficient of friction, lightweight and high durability [3]. The antenna is designed for the North American UHF RFID frequencies (902-928 MHz). With an impedance bandwidth of 50 MHz which is larger than the operating requirement of 26 MHz, the excess bandwidth of our antenna can be useful to accommodate any detuning (frequency shift) caused by the proximity assets. Power reflections induced by nearby metallic assets are drained through a resistor on the isolation port of a quadrature hybrid coupler (to achieve circular polarization in the patch), thus preventing permanent damage to the RFID readers [4]. This manuscript is an extended version of the work reported in [5].

5.2 Related works

Several UHF RFID reader antenna designs that can operate either in NF [6-8] or FF [9-11] have been recently proposed. The NF designs are typically based on segmented loops, meandered line, travelling wave and oppositely directed current (ODC) antennas [2], while the FF designs often used microstrip patch, stacked patch, quasi-Yagi, monopoles, dipoles, PIFA, helical, slot and loop antennas. Existing antenna designs that can operate in both NF and FF are not suitable for retail checkout counter/POS applications. The multiport reader antenna design in [12] is a dipole-based design where four dipoles are arranged in a square geometry and fed at a different location using three ports. The antenna behaves as an NF antenna when fed at port-A and resonates with two different orthogonal linear polarization when excited through port-B and port-C, respectively. The main disadvantage with this design is that the users will have to either use three different RFID readers (if they are 1-port readers) or a 3-port reader to use this antenna, which increases the cost and complexity of the system. The antenna's bidirectional radiation may read unwanted stray tags in a POS scenario, and its half-power beam-width (HPBW) is not measured. On the other hand, our proposed antenna in this manuscript can operate in both NF and FF simultaneously when excited using a single port. It is circularly polarized, has a directional radiation pattern, and customizable NF readable region.

A fragment type structure is designed in [13] for simultaneous NF and FF operation, producing bidirectional radiation with 60°, and 90° HPBW, respectively, which can introduce stray tag reads. The antenna's impedance matching and frequency of operation are dependent on the structure's length and width and internal connections. Fabrication cost and complexity are higher in this antenna, as there are a lot of variables that need high precision and attention. Although the NF and FF operation can be performed simultaneously, the FF radiation is only linearly polarized, which cannot detect tags in different orientations. In contrast, our proposed antenna in this manuscript can simultaneously operate in NF and circularly polarized FF. Furthermore, its directional radiation can create a predictable read zone that will not induce stray tag detection. Comparatively, it is a less-complex design that can scale without any significant modification of the antenna's critical parameters such as its impedance and frequency of operation.

A switchable NF/FF antenna is presented in [14], which has a PIN diode that operates the antenna in those two modes when biased with different voltages. Four dipole antennas arranged in a square geometry (as in [12]) are driven with equal phase for NF operation and with incremental phase delays of 0°, 90°, 180° and 270° for FF operation. The FF antenna is circularly polarized with an axial ratio of 1.5 dB. The antenna's 50° HPBW is narrow for POS applications and may miss assets that travel through the checkout counter conveyors. On the contrary, the proposed antenna in this manuscript is passive and can operate in both NF and FF simultaneously without the need for switching. Losses introduced by PIN diodes do not exist in our design. Moreover, there is no need for DC biasing in our design, which enhances the ease of installation.

The authors in [15] presented a linearly polarized coupled loop antenna design that operates in NF and FF simultaneously with bidirectional radiation whose HPBW is 90°, and 75°, respectively. As the loop is a function of the wavelength, scaling this antenna design is impossible without trading-off its performance. The antenna's overall thickness with a reflector is 80 mm. Unlike the above antenna, our proposed antenna in this manuscript is low-profile, mechanically sturdy, UV, impact, and chemical resistant, and low moisture absorbent. In addition, it has a unidirectional and symmetrical radiation pattern with 90° HPBW in both planes. The compact multiservice reader antenna designed for NF and FF application in [16] is a circularly polarized antenna with 3 dB axial ratio. The antenna is based on a rectangular slot design fed by L-shaped feed. The asymmetric slot perturbation yields the circularly polarized fields. The antenna's radiation is uni-directional and symmetrically spread in both planes with an HPBW of 80°. Unlike our proposed antenna, this antenna is hardly scalable as the dimensions of its slots cannot be altered to suit differently sized checkout counter. Moreover, its 3 dB axial ratio can make tag detection harder when assets are oriented differently. On the other hand, our proposed antenna's NF region is easily scalable by altering the meandered line to suit the dimensional requirements. Besides, its axial ratio is twice as large as the existing design. Reflections caused by nearby metallic assets are drained through a termination resistor in the proposed design while they are fed directly back to the RFID reader.

The meandered line antenna presented in [17] is a near-field antenna that can also detect far-zone items. These antennas cannot detect tags whose orientations are orthogonal to the prescribed orientation, unlike our proposed design. The meandered lines are unterminated (by a load) and their width, spacing and turns have to be fixed as otherwise the antenna's resonance will be affected, highlighting its inability to scale to different sizes. On the other hand, our patch antenna terminates the meandered lines and can scale in both axes of the 2-D plane.

5.3 Antenna design

Our antenna design features a radiating patch that is driven along the vertices by two meandered microstrip lines. To achieve circular polarization, the patch must be driven 90° out-of-phase with an equal magnitude on its orthogonal points which can be either along the vertices or along the perpendicular bisectors intersecting the sides where TM_{01} and TM_{10} modes exist. A 6 mm high-density polyethylene (HDPE, a type of polyolefin) sheet is used as the substrate whose dielectric constant (ε_r) and loss tangent is 2.256 and 0.0002, respectively [3]. The patch is inset-fed at a location 21 mm along the diagonals, which is 16.8 mm away from the sides (Figure.5.1). The patch's impedance at this location is found to be 113 Ω. The microstrip line consists of a quarter-wave transformer that transforms the 50 Ω input impedance into 113 Ω patch impedance. The length and width of the quarter-wave transformer are 61 mm and 9 mm, respectively. The 113 Ω microstrip line is meandered around the patch in all four directions to inset feed the patch along its diagonals.

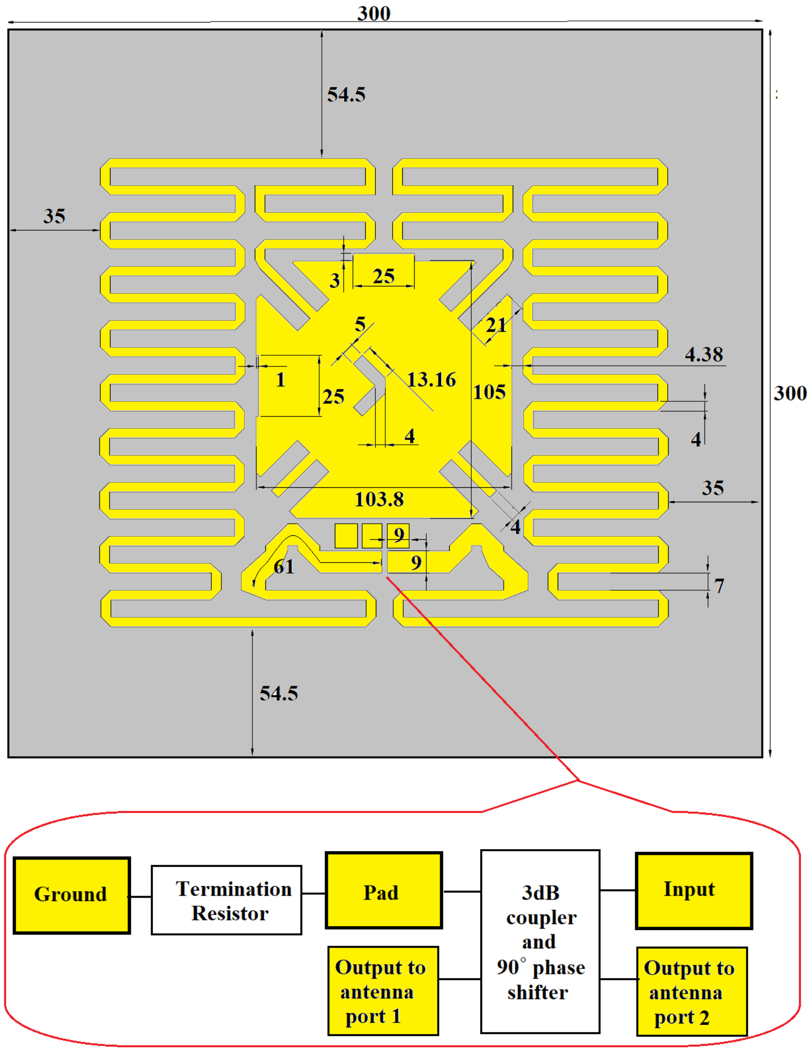

Figure.5.1. Proposed antenna design with input components

The meandered microstrip line creates a strong magnetic field on the antenna surface contributing to the NF radiation while the patch produces the FF radiation. The magnetic field is evenly distributed on the surface of meandered lines with no dead zones. The NF area can be extended along the antenna's surface in its X and Y axes just by lengthening the meanders in the microstrip line, thereby enhancing the scalability. A low-loss, thin-film, 3dB hybrid coupler with four ports: input port, isolation port and two output ports with nominal 50 Ω impedances, is used. The small-sized coupler helps to eliminate dead zones around it. The input power is divided equally through two output ports with 90° phase difference.

Although the coupler offers high isolation, it is recommended to terminate the isolation port with a 50 Ω thin-film resistor to maintain balanced coupling. The coupler's output ports are connected to the patch via the meandered lines to generate circularly polarized waves. The patch is tuned using tuning stubs and 'V' slots to withstand the electromagnetic coupling experienced between the meandered lines and the patch. The patch's size is calculated to be 105 mm long and 103.8 mm wide, which are dependent on the substrate's ε_r and thickness. For more compact patch size, a thicker substrate with higher ε_r may be used. Although the patch width is physically shorter, the 'V' slot makes the patch electrically wider. The D4 symmetry of the patch is maintained by introducing a dummy replica of the inset feed on its other half [18]. Figure.5.1 shows the design of the meandered line fed patch antenna.

5.4 Simulation

The designed antenna is simulated using ADS electromagnetic simulation software. ADS use Method-of-Moments (MoM) solver for computation. A 3D-model of the antenna is designed with 6 mm HDPE substrate spanning 300 mm in length and width (see Figure.5.2). The HDPE's ε_r is defined as 2.256 with 0.0002 *tan δ*. 0.1 mm copper sheet with a conductivity of 5.96×10^7 S/m with 1.68×10^{-8} σ-m resistivity is defined for the copper conductor sheet. Tin sheet is defined for the ground plane whose conductivity and resistivity are 9.17×10^6 S/m and 1.09×10^{-7} σ-m, respectively. The ground plane extends to the entire substrate's surface area.

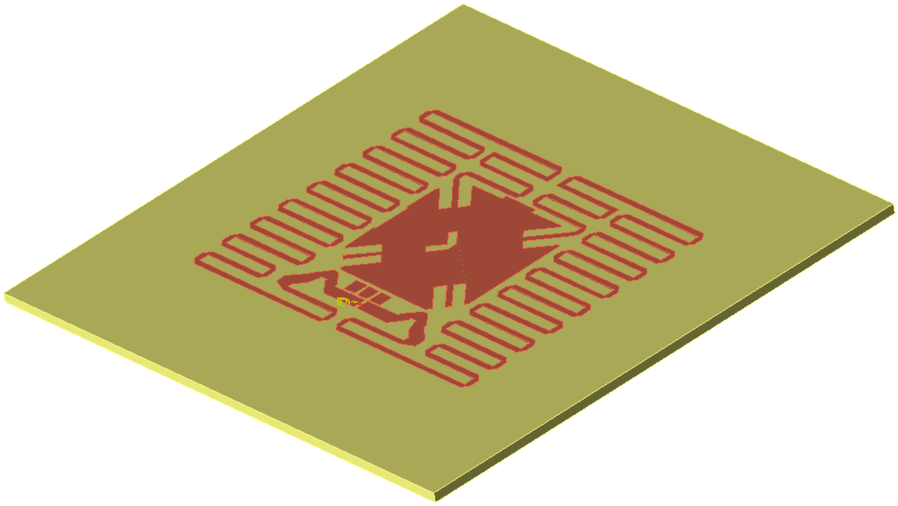

Figure.5.2. ADS 3D model

The 3dB hybrid coupler's model is imported for use with the antenna. All four ports have 50 Ω impedance. The coupler's output ports are connected to antenna's ports. Lumped resistor component with pad artwork is created with 50 Ω resistance for use with coupler's termination port. 'Port 1' with 50 Ω impedance is defined with 'TML' transmission line calibration to excite the coupler. The port's negative terminal is referenced to the antenna's ground plane. Simulation frequency is swept between 800-1000 MHz. The mesh frequency is set as 915 MHz with a mesh density of 20 cells per wavelength. The simulated antenna's current density distribution is shown in Figure.5.3. A uniform surface current distribution with no dead or null zones is observed. The antenna's 3D radiation pattern is shown in Figure.5.4 with its gain, directivity, radiation efficiency and effective angle.

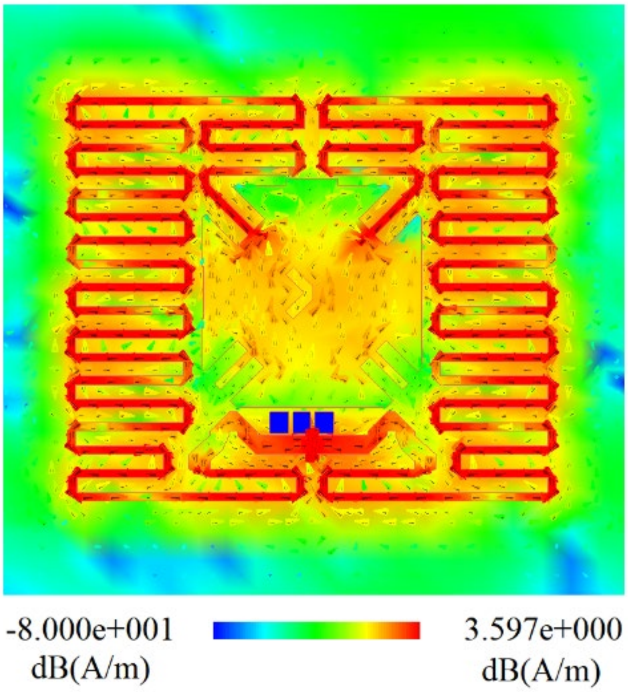

Figure.5.3. Surface current density distribution

The simulated antenna's return loss and gain over the frequency range are plotted against the measured results of the fabricated antenna in Section 5.6. Similarly, the simulated 2D radiation pattern is plotted against the measured beam plots in Section 5.6.

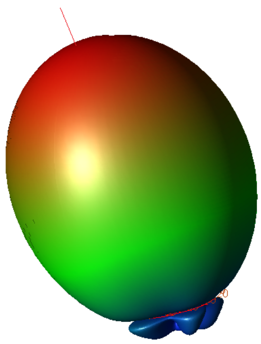

Frequency	:	915 MHz
Directivity	:	3.6 dBi
Peak Gain	:	3.2 dBi
Radiation efficiency	:	91.05%
Effective angle (Steradians)	:	1.764

Figure.5.4. 3D Radiation pattern

5.5 Fabrication

The patch antenna and microstrip line feed network is fabricated using 0.1 mm copper foil. The copper foil is adhered to the HDPE sheet using a non-conductive acrylic adhesive that has 125 N/100 mm adhesion to metal and 86 N/100 mm adhesion to plastic. The patch antenna is centered to the substrate, as mentioned in Section III. The ground plane is constructed using a 0.2 mm tin sheet, and the same adhesive is used to adhere the ground plane to HDPE. The coupler's input port is connected to a rear-mount SMA connector. The coupler, SMA connector, 50 Ω resistor and its grounding pin used are soldered directly onto the copper foil. Figure.5.5 shows the coupler and 50 Ω termination resistor in the fabricated antenna. The thin film multilayer 3dB hybrid coupler (DB0805A0880ASTR) used in the fabrication is manufactured by AVX. It operates at 880 MHz ± 30 MHz. The coupler's output ports have equal magnitude and a 90° phase difference.

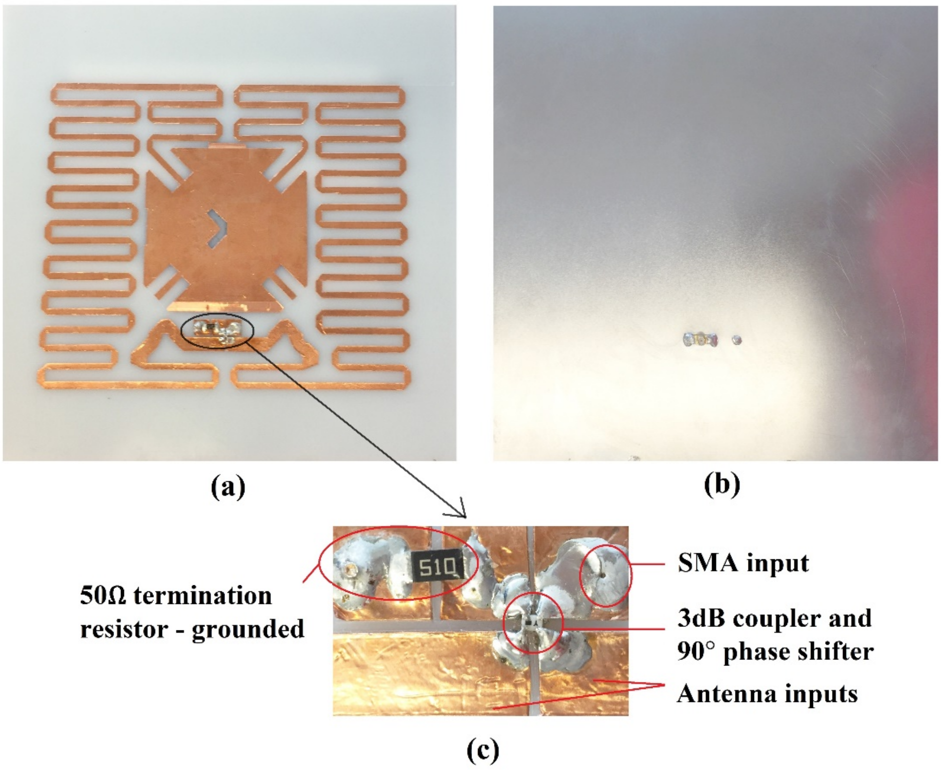

Figure.5.5 Fabricated antenna (a) radiator and feed network (b) ground plane with SMA connector (c) components at the input

5.6 Measurement and Analysis

The fabricated antenna's performance was measured using a TR/1300 VNA in an anechoic chamber. The linear gain of the antenna is measured for both vertical and horizontal polarizations by the comparative method using a calibrated reference antenna. The antenna's return loss and gain values are shown in Figure.5.6 (highlighted), and in Table.5.1 for low, mid and high frequencies of the FCC band. The fabricated antenna has a 50 MHz and 42 MHz return loss bandwidth at -10 dB, and -15 dB cut-off, respectively. The simulated antenna has 65 MHz and 45 MHz return loss bandwidth at -10 dB, and -15 dB cut-off, respectively. The fabricated antenna's peak gain at 915 MHz in vertical polarization is 3.3 dBi with 1.4 dB axial-ratio. Simulated antenna's peak gain is 3.2 dBi in the same polarization with 0.7 dB axial ratio. The fabricated antenna's best- and worst-case axial-ratio is 0.8 dB at 902 MHz and 2.2 dB at 928 MHz, respectively. The simulation adheres to the measured gain profile while the return loss profile has less ripple compared to the measured antenna. The EM solver considers perfect materials and other assumptions for its calculations leading to variations between the simulated and the measured results.

Table.5.1. Return loss and gain measurement at frequency of interest

Parameter	**902 MHz**		**915 MHz**		**928 MHz**	
	Simulated	**Measured**	**Simulated**	**Measured**	**Simulated**	**Measured**
Return loss (dB)	-20.2	-17.2	-28.2	-16.4	-21.5	-19.6
Vertical pol. gain (dBi)	2.3	2.4	3.2	3.3	2.4	0.5
Horizontal pol. gain (dBi)	2.2	1.6	2.5	1.9	2.2	2.7

The simulated and measured far-field radiation pattern is given in Figure.5.7, which shows a symmetrical radiation pattern with 90° HPBW in both elevation and azimuth planes. Back radiation of the fabricated antenna is minimal in azimuth plane compared to the elevation plane. The fabricated antenna is tag tested to benchmark the RFID metrics. An Impinj speedway R420 RFID reader [19] (FCC band) is used for testing purposes. Smartrac's 'Miniweb' and 'Bling' tags are used for testing. The former is specially designed for general asset tracking and supply-chain applications [20] while the latter is for jewelry, cosmetics and other close-coupled applications [21]. The antenna's NF and FF radiation are tested by presenting the tag directly on top of, and above the antenna, respectively.

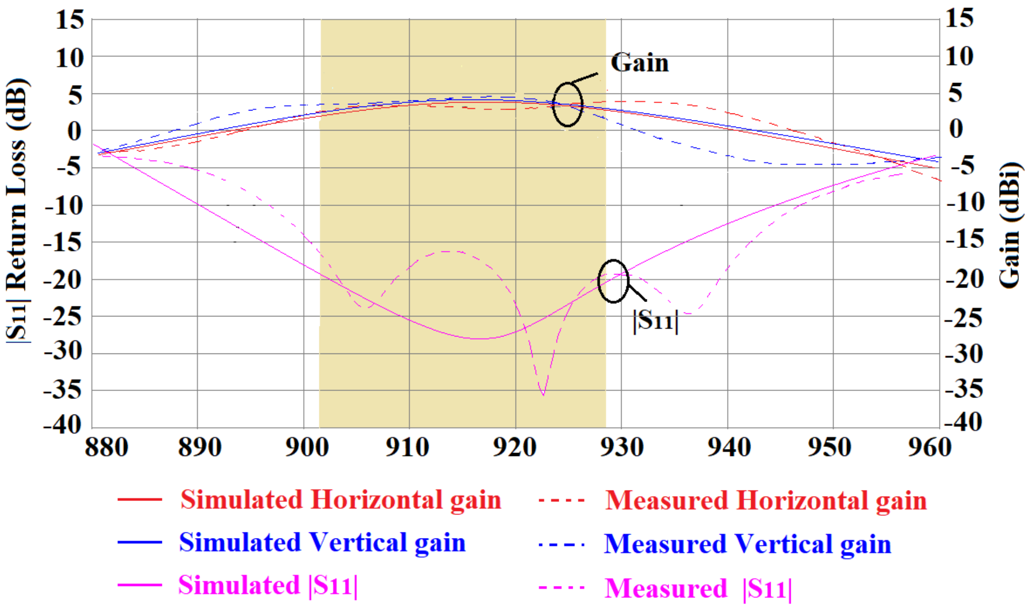

Figure.5.6 Return loss and gain measurements

The 300 mm × 300 mm antenna is divided into 36 cells, each being 50 mm × 50 mm. Figure.5.8 shows the test setup with grids marked on the antenna's surface. One tag per cell is placed and tested for its received signal strength indicator (RSSI) for vertical and horizontal tag-orientation. The bling tag and the Miniweb tag spans 25 mm × 15 mm and 42 mm × 16 mm, respectively.

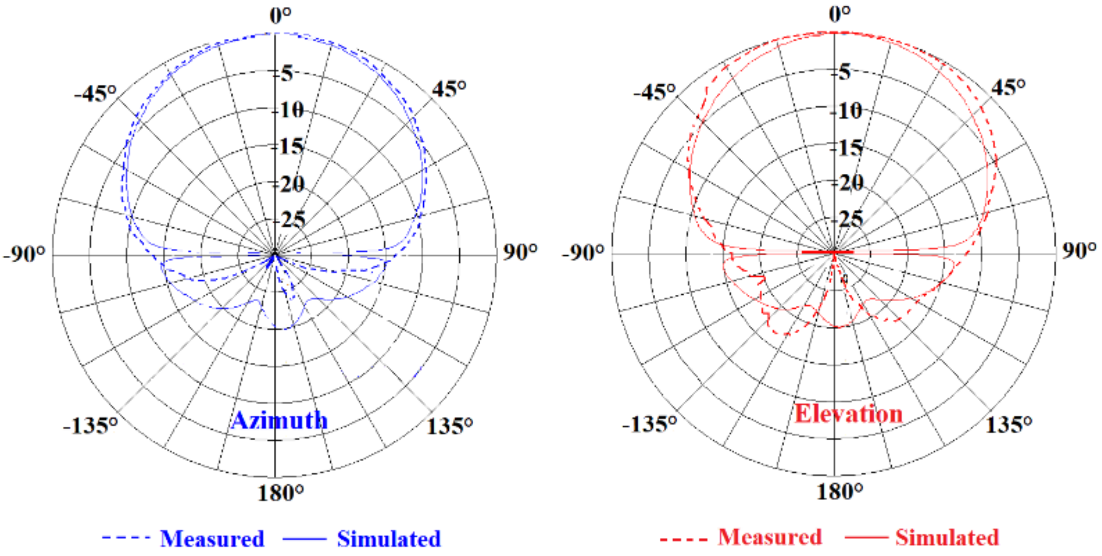

Figure.5.7 Far-field radiation pattern

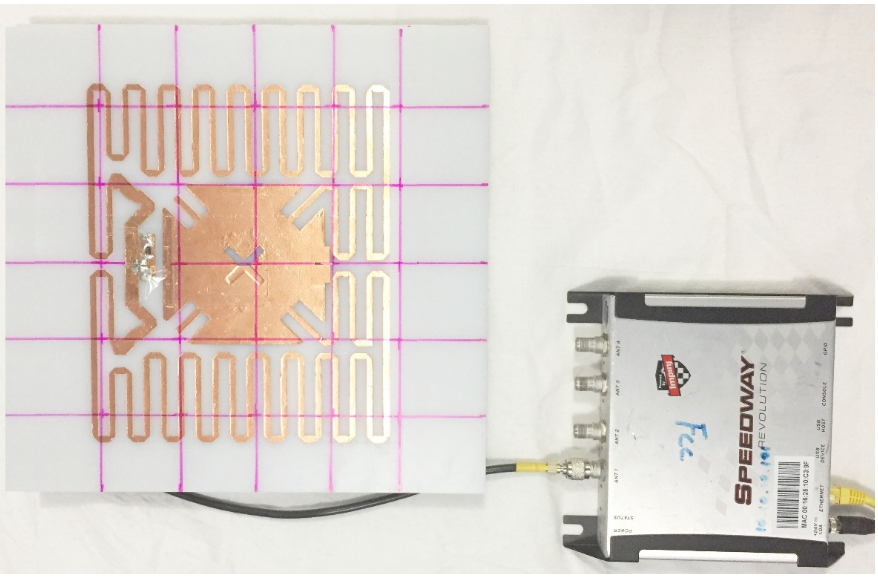

Figure.5.8 Tag testing setup

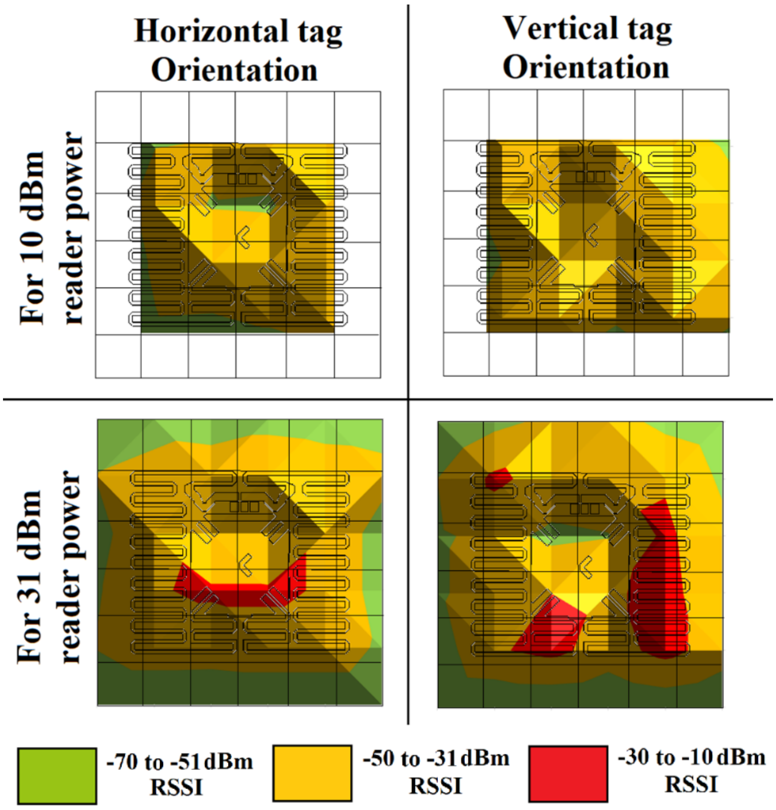

Figure.5.9 Bling tag's RSSI measurements

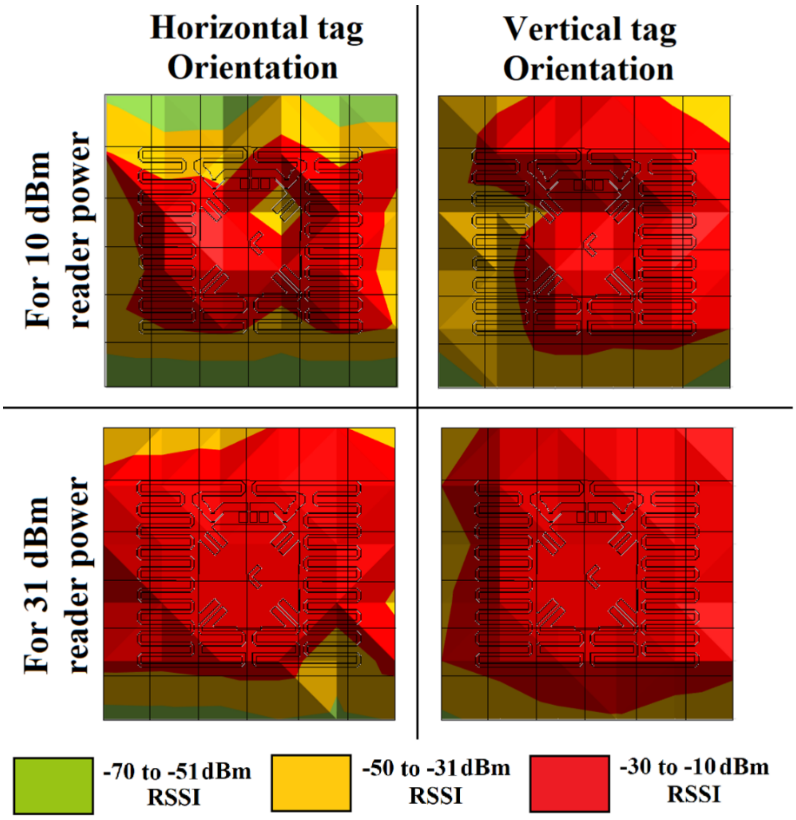

Figure.5.10 Miniweb tag's RSSI measurements

The Impinj's item-test software is used to retrieve RSSI information by setting the reader to two different power levels: 10 dBm (min) and 31.5 dBm (max). It is observed that the NF distribution is concentrated on the antenna's surface for Bling and the surface detection range is extended by 50 mm laterally in both axes for Miniweb tag. Figure.5.9 and Figure.5.10 shows the contour plot of the Bling and Miniweb tag's RSSI, respectively, over the antenna's surface for two power settings (min, max) and orthogonal tag orientations (vertical, horizontal). Figure.5.11 shows the maximum read distance plot for both tags at 10 dBm power.

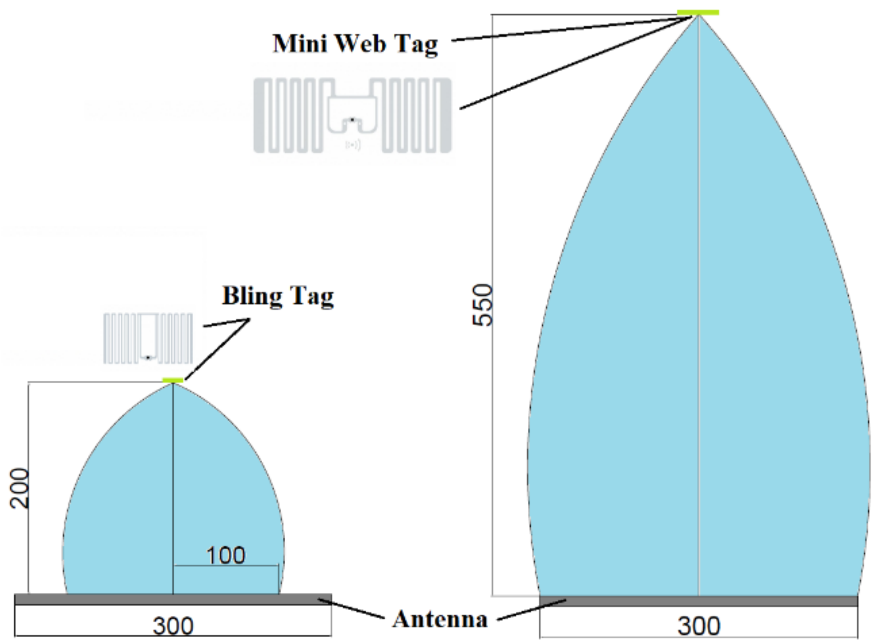

Figure.5.11. Read distance measurements (units in mm) for Bling and Mini-web tag

A summary of the performance differences between the proposed and existing antenna designs is provided in Table.5.2. The change in color per unit cell implies that the transmitted signal strength in those zones with respect to the tag's ability to receive the signals. It is clear that the Miniweb tag has a greater ability than the Bling tag to receive the signal in the unit cells. On the other hand, the Bling tag was not detected in some cells at 10 dBm reader power as shown by the uncolored cells in Figure.5.9 (top row). Figure.5.11 shows the maximum read distance plot for both tags at 10 dBm power.

Table.5.2. Performance comparion of proposed vs existing antenna designs

Ref.	FF Polarization	Gain (f_c)	Axial ratio (f_c)	FF HPBW (f_c)	FF radiation	DC Bias required?	Ports required	Simultaneous NF and FF operation?	NF zone scalability	Reflection handling ability
[11]	Linear	-3.2 dBi	Infinity	Not measured	Bi-directional	No	Three	No	No	No
[12]	Linear	5 and 6 dBi	Infinity	60° and 90°	Bi-directional	No	One	Yes	No	No
[13]	Circular	7 dBiC	1.5 dB	50°	Directional	Yes	One	No	No	Yes (Wilkinson power dividers)
[14]	Linear	6.8 dBi	Infinity	90° and 75°	Bi-directional	No	One	Yes	No	No
[15]	Circular	5.5 dBiC	3 dB	80°	Directional	No	One	Yes	No	No
[16]	Linear	-5 dBi	Infinity	Not measured	Directional	No	One	Yes	No	No
This work	Circular	3.3 dBi (5.3 dBiC)	1.4 dB	90° in both planes	Directional	No	One	Yes	Yes	Yes (Quadrature hybrid coupler)

5.7 Real-life testing and Discussion

The antenna's susceptibility to change in return loss due to the presence of mounting frames and proximity assets are tested and discussed in this section.

5.7.1 Effect of metal frames

Checkout can be a desktop counter with conveyors or standalone self-checkout kiosk with a weight-scale. The antenna can be mounted under the conveyor or over the scale to read all the assets that are checked out. Holes can be drilled in the corner of the antenna to be mounted using screws. Alternatively, the antenna can be slided through a metal frame. The effect of the metal frame is tested by pushing two aluminium extrusions on either side of the antenna, as shown in Figure.5.12. The antenna's return loss is measured to find the changes due to the effect of frames. Figure.5.13 compares antenna's performance in free space, edge framing and inner framing.

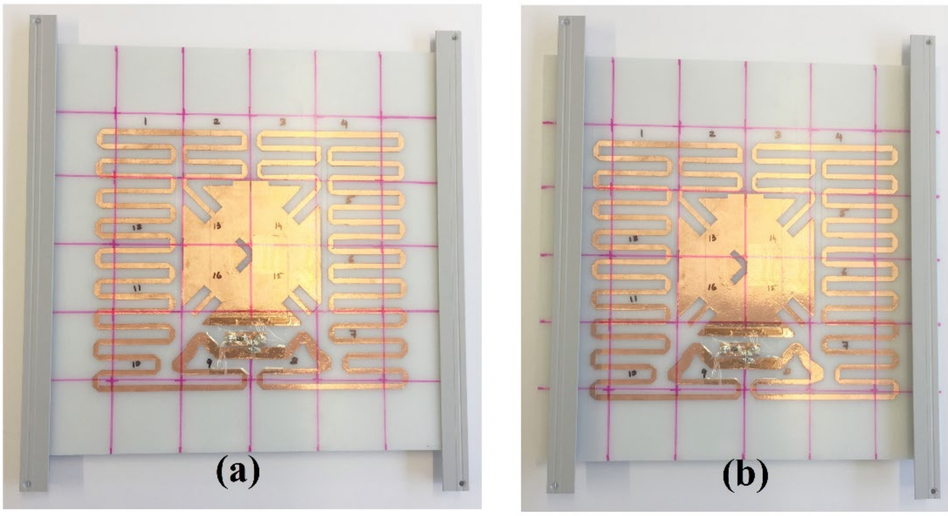

Figure.5.12. Metal frame mounting: (a) Edge framing and (b) Inner framing

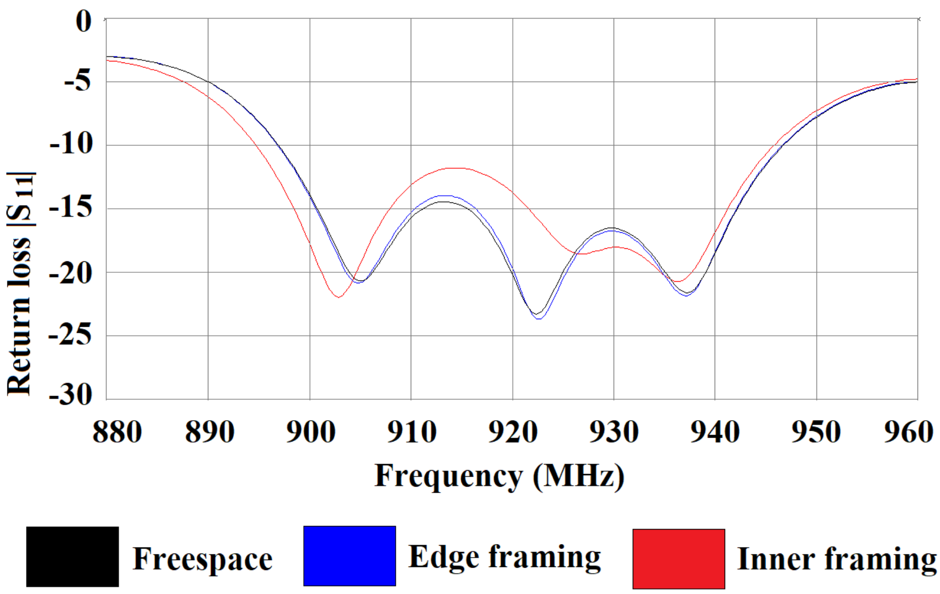

Figure.5.13. Active test cells

Edge framing affected the antenna's return loss negligibly. The antenna's performance is maintained to that of its operation in free space. Inner framing caused slight reflections to change the return loss pattern. The antenna's -10 dB bandwidth remained unchanged

5.7.2 Effect of proximity assets

A protective radome will be used over the antenna's radiating face in real life, and tagged assets will be placed over the antenna at different locations when used in retail checkout counters. The antenna's radome is not manufactured rather a 3 mm thick polystyrene sheet is used as a radome for testing purposes. Polystyrene is chosen because it induces minimal changes in the antenna's performance due to its dielectric properties that are similar to air. This enables us to use the antenna as it is for testing without tuning for a radome. As mentioned in Section 5.4 , the antenna is virtually divided into 50 mm × 50 mm cells. Among 36 cells, 16 cells in the centre of the antenna are active as they bear the NF and FF elements. Figure.5.14 shows test cells with numbering over the active region. Six different common assets found in a retail grocery store are used for testing. Assets include handwash, perfume spray can, powdered spices, bath soap, hair wax and pack of razors. These assets represent different mediums viz., liquid, metal, powder, solid, wax and air-filled packets. The antenna's response will be affected by these mediums when they are proximity to the radiating surface. Radio frequency (RF) waves travel slower in denser mediums such as solids, causing detuning effect compared to lighter mediums such as air-filled packets (Figure.5.15).

The liquid medium can absorb RF, while metal mediums cause reflections. Changes in antenna's performance due to absorption, reflection, attenuation and detuning effect is captured and reported in this section. The tags are usually attached to these mediums using a thin adhesive layer. A dipole-like tag's performance can be varied significantly by different mediums that offer different attenuations. Metal asset requires a unique tag that is designed to work by using the asset as the tag's ground plane.

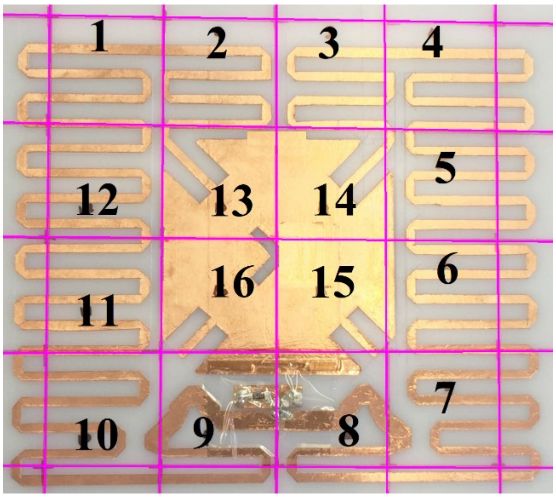

Figure.5.14. Test points (cells) formed by 50 x 50 mm grids

Vortex R-6A is a dipole-like tag that is designed and manufactured by ‘Checkpoint systems’ for retail assets using Impinj Monza R-6 chips. The tag antenna is hybrid, consisting of a FF wiggled-dipole and an NF loop. It is optimized to use with various assets except for metal. Vortex R-6A wet inlay comes with an acrylic adhesive to adhere to the tag. All assets are tagged using the Vortex tag except the metal asset. The metal asset bears a ‘Pico-On-Plus’ on-metal tag that is designed and manufactured by ‘Xerafy’. Tags were predominantly put under the asset such that the tags are closer to the antenna when scanned. Some assets were challenging to tag due to their physical profile and tags were put non-conventionally. For instance, the hair wax is a small cylindrical shaped asset, and the tag has to be bent to conform with the asset’s curvature. A bent dipole’s radiation pattern is different from that of a conventional straight dipole tag.

Figure5.15. Tagged assets: 1. Liquid (Vortex tag), 2. Metal (Pico-On-Plus), 3. Powder (Vortex tag), 4. Solid (Vortex tag), 5. Wax (Vortex tag) and 6. Air-filled packet (Vortex tag).

The reader antenna's return loss performance is measured by loading different assets directly on top of the 3 mm foam spacer. Change in performance is tracked by moving the assets from cell 1 to cell 16. Liquid, metal, powder and wax assets can fit into the 50 mm × 50 mm cells. Solid asset spans ~50 mm × 100 mm, consuming two cells and air-filled pack consumes four cells (see Figure.5.16). Changes in antenna's return loss are recorded for each asset in each test cell. The antenna's tag detection ability for different assets in different test cells is also tested by using the Impinj speedway r420 RFID reader. The reader is turned on for 10 seconds to record read counts, average RSSI and the minimum power required to energize the tag. The antenna's return loss and tag read performances are reported for each test cells in this section.

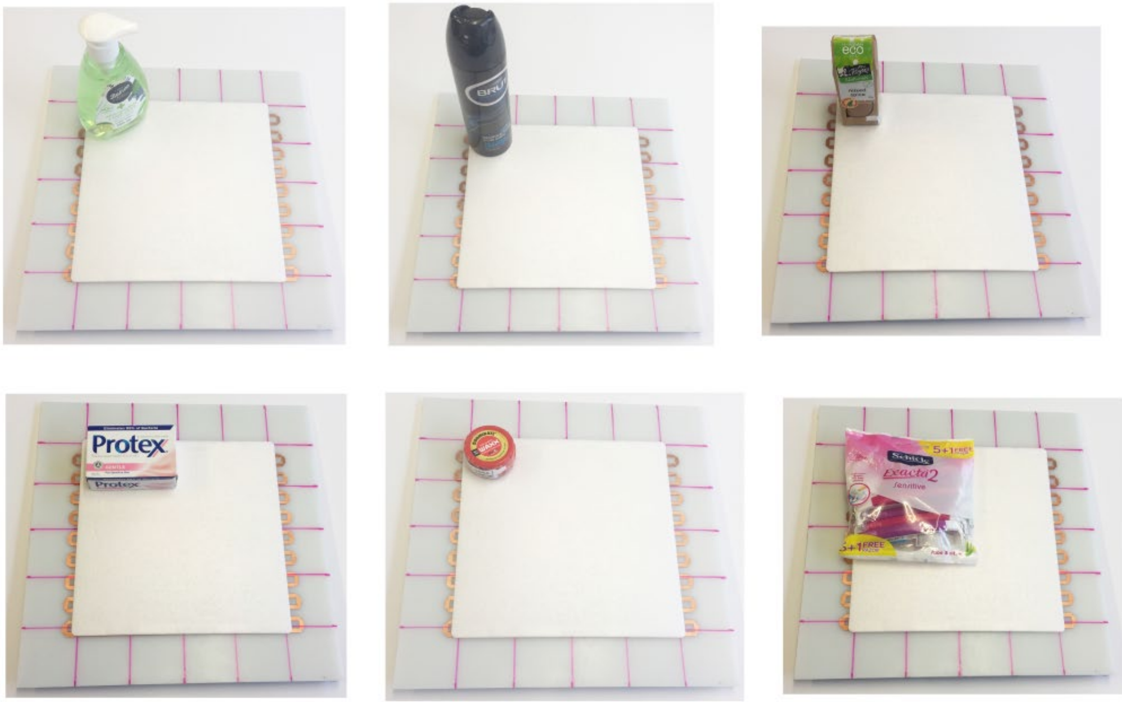

Figure.5.16. Assets' cell occupancy: Liquid, Metal, Powder and Wax = 1 cell, solid = 2 cells and Air-filled pack = 4 cells.

1) Cell 1

Cell 1 (refer location in Figure.5.14) is part of the meandered microstrip line that emerges out from the 3dB coupler's port 1. A strong magnetic field is present in this section of the meandered line. The antenna's return loss has changed slightly, shifting the pattern to the lower end of the band. The antenna's operational bandwidth has not changed, and the return loss is below -10 dB for the operating frequencies (see Figure.5.17). Only 10 dBm power is required to detect all the assets in this location. Read rate was similar for all the assets. Tag attached to the air-filled pack has the highest RSSI due to minimal attenuation offered by the asset. The solid asset has the lowest RSSI as the medium is dense. Table.5.3 details different RSSI and read count values for different assets.

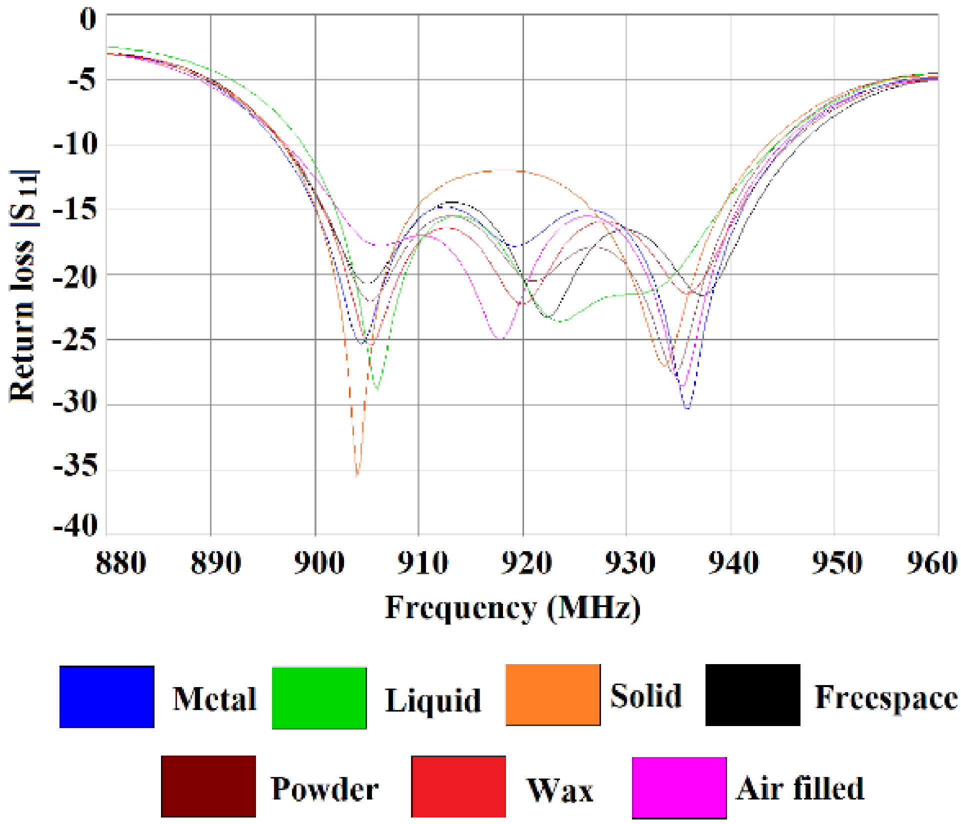

Figure.5.17. Effect of proximity assets on cell 1

Table.5.3. RFID Asset testing: Cell 1

Asset type	Minimum Power required to energize	Reads per 10 seconds	Average RSSI
Metal	10 dBm	438	-36 dBm
Liquid	10 dBm	439	-33 dBm
Solid	10 dBm	438	-44 dBm
Powder	10 dBm	416	-35 dBm
Wax	10 dBm	438	-32 dBm
Air-filled	10 dBm	429	-26 dBm

2) Cell 2

Cell 2 (refer location in Figure.5.14) is also part of the coupler's port 1 microstrip line. The microstrip line is close to the feed point and patch's edge. Magnetic fields are stronger in this meandered region. Fringe fields from the side of the patch in cell 13 are strong enough to read tags in cell 2. Return loss measurements for different assets in cell 2 is similar to cell 1. The -10 dB bandwidth is unaltered. Solid asset's RSSI is the lowest and powder asset's RSSI is the highest. There are no dramatic read rate differences. Table 4 shows different RSSI and read count values for different assets.

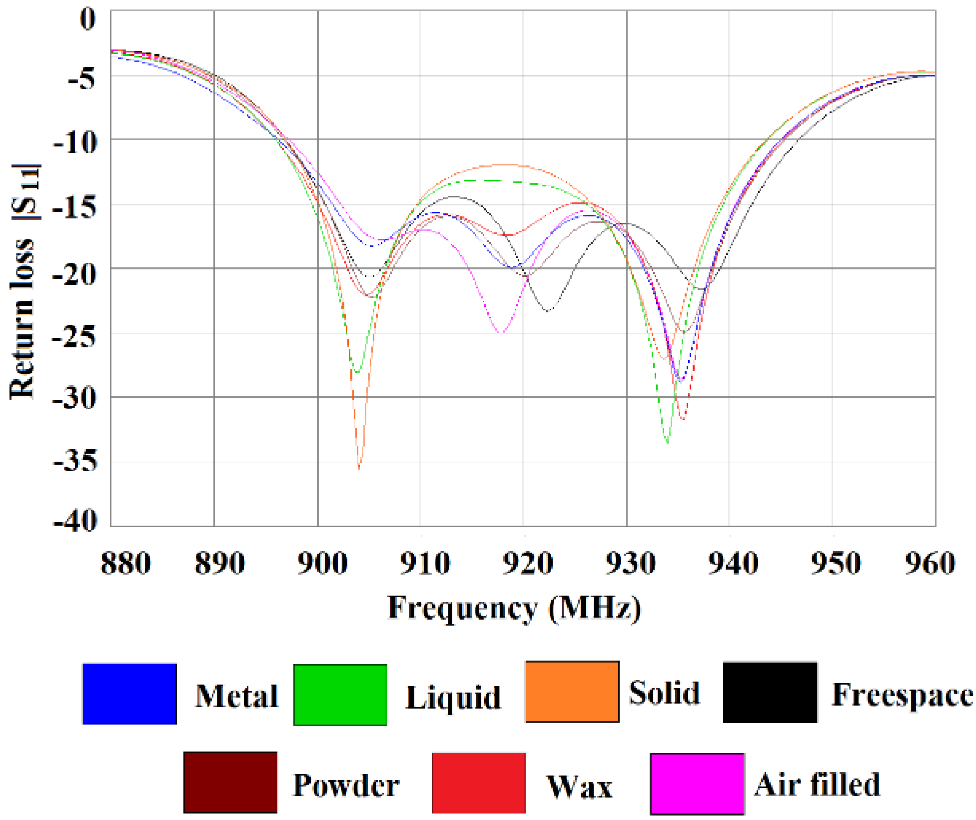

Figure.5.18. Effect of proximity assets on cell 2

Table.5.4. RFID asset testing: Cell 2

Asset type	Minimum Power Required to energize	Reads per 10 Seconds	Average RSSI
Metal	10 dBm	431	-36 dBm
Liquid	10 dBm	432	-35 dBm
Solid	10 dBm	438	-44 dBm
Powder	10 dBm	440	-22 dBm
Wax	10 dBm	442	-31 dBm
Air-filled	10 dBm	429	-26 dBm

3) Cell 3

The return loss profile has slightly changed to foam a valley at the centre frequency in cell 3 (refer location in Figure.5.14) when the assets are loaded. The meandered microstrip line is from the coupler's second port. Cell 3 is close to the edge of the patch in cell 14. Tags in cell 3 can be quickly excited by the fringe fields produced in cell 14. Solid and powder asset are the least and most sensitive with respect to the return signal strength, respectively. Read rates of all the assets are relatively similar (Table.5.5).

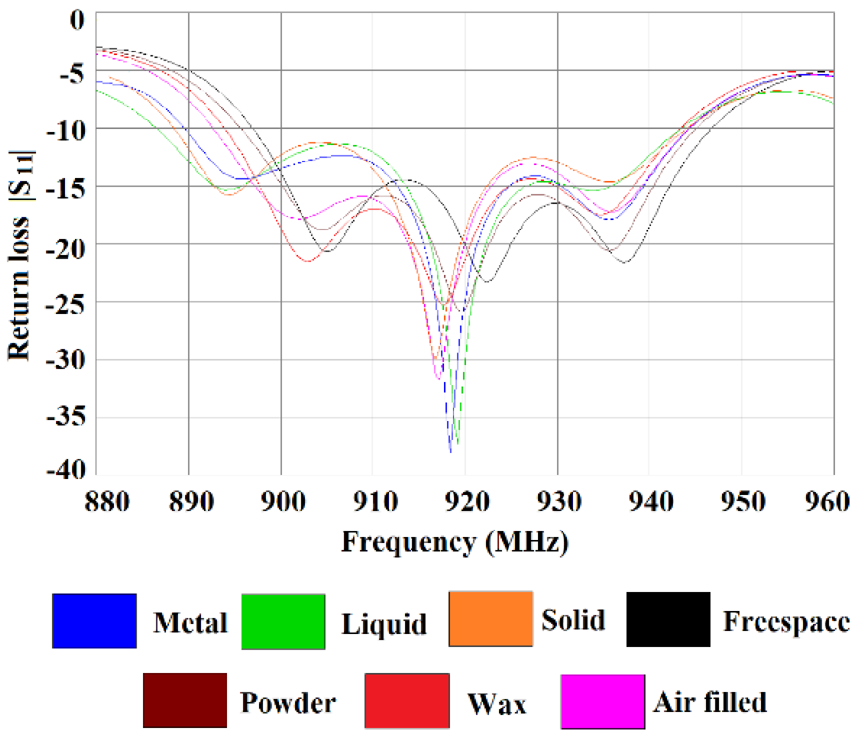

Figure.5.19. Effect of proximity assets on cell 3

Table.5.5. RFID asset testing: Cell 3

Asset type	Minimum Power Required to energize	Reads per 10 Seconds	Average RSSI
Metal	10 dBm	443	-37 dBm
Liquid	10 dBm	431	-30 dBm
Solid	10 dBm	435	-43 dBm
Powder	10 dBm	439	-25 dBm
Wax	10 dBm	440	-38 dBm
Air-filled	10 dBm	432	-32 dBm

4) Cell 4

The return loss performance in cell 4 (refer location in Figure.5.14) is similar to that of cell 3 except for the frequency shift caused by wax and air-filled package assets. The return loss bandwidth is not disturbed and is maintained below -10 dB. Read rates of the powder asset is the lower although the asset had the highest RSSI. Wax and liquid assets yielded the most top read rate performance. Solid asset has the lowest RSSI with a second highest read rate. The meandered line in cell 4 emerged out from port 2 of the 3 dB coupler. The signal in this port is 90° out-of-phase compared to port 1. The meandered line has powerful magnetic fields to detect challenging assets such as liquids and metals. RSSI and read count values for different assets are listed in Table.5.6.

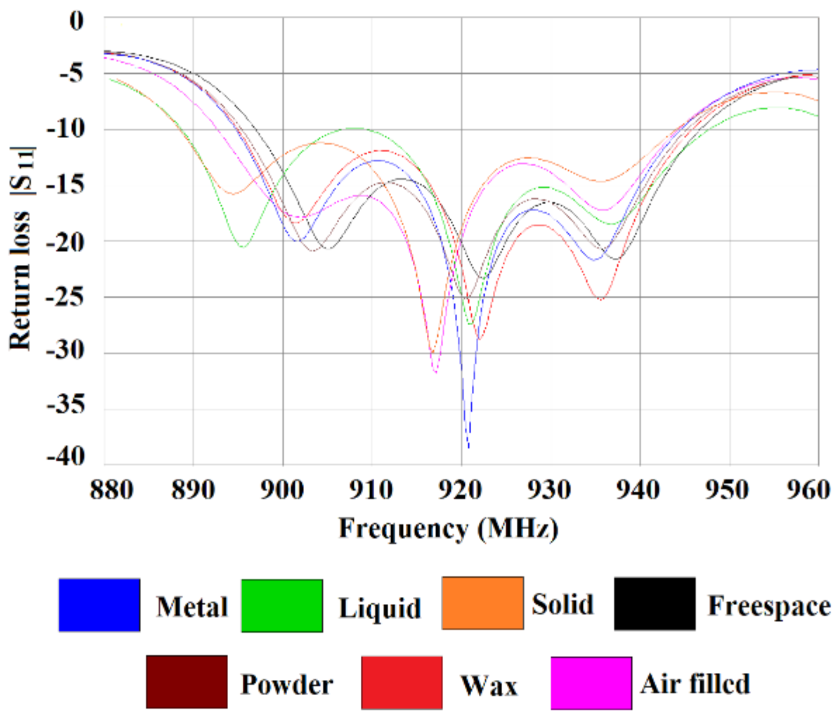

Figure.5.20. Effect of proximity assets on cell 4

Table.5.6. RFID asset testing: Cell 4

Asset type	**Minimum Power Required to energize**	**Reads per 10 Seconds**	**Average RSSI**
Metal	10 dBm	304	-33 dBm
Liquid	10 dBm	438	-33 dBm
Solid	10 dBm	435	-43 dBm
Powder	10 dBm	280	-29 dBm
Wax	10 dBm	438	-42 dBm
Air-filled	10 dBm	432	-32 dBm

5) Cell 5

The meandered lines in this cell 5 (refer location in Figure.5.14) are close to the radiating patch. Both fringe fields and meandered line's magnetic field contribute to tag detection. These fields interact with the assets differently causing changes in return loss distribution over the frequencies. The liquid asset's response has shifted the most compared to any other assets. Read rate and RSSI of the liquid asset is, however, not affected significantly. The solid asset has the highest RSSI due to the fringing fields from the patch. Read rates of all the assets are consistent (Table.5.7).

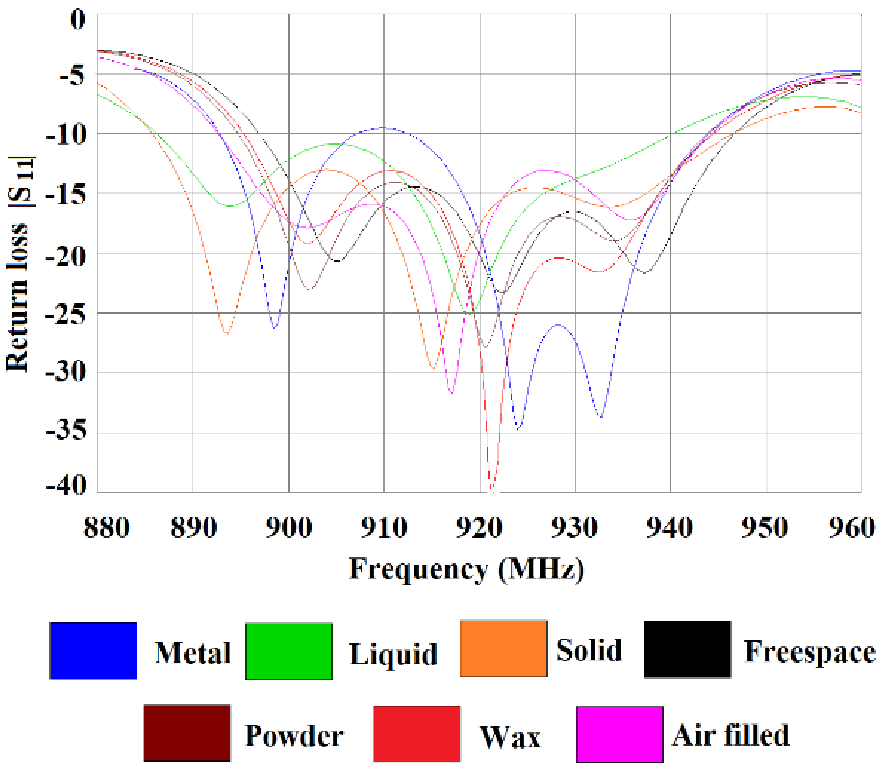

Figure.5.21. Effect of proximity assets on cell 5

Table.5.7. RFID asset testing: Cell 5

Asset type	Minimum Power Required to energize	Reads per 10 Seconds	Average RSSI
Metal	10 dBm	442	-31 dBm
Liquid	10 dBm	441	-30 dBm
Solid	10 dBm	435	-27 dBm
Powder	10 dBm	441	-24 dBm

Wax	10 dBm	439	-35 dBm
Air-filled	10 dBm	432	-32 dBm

6) Cell 6

The meandered line in cell 6 (refer location in Figure.5.14) is also near the patch antenna, and thus the effects are similar to that of the effects reported in cell 5. The -10 dB return loss bandwidth is maintained throughout the frequencies of interest even though the antenna's response has shifted slightly towards the lower side of the frequency band. Air-filled package has the highest RSSI followed by powder, solid and wax asset. Liquid and metal assets have the lowest RSSI (Table.5.8).

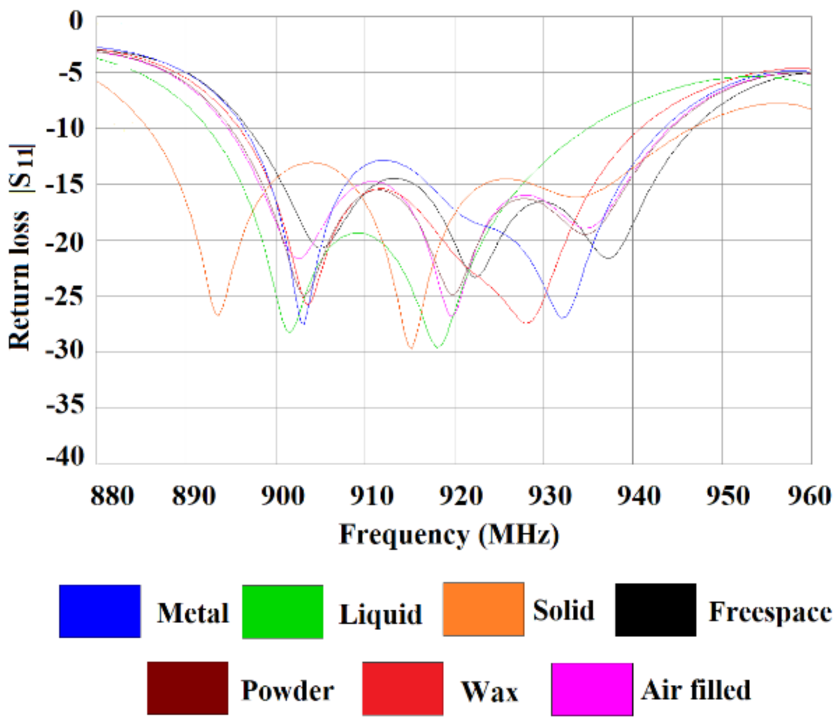

Figure.5.22. Effect of proximity assets on cell 6

Table.5.8. RFID asset testing: Cell 6

Asset type	Minimum Power Required to energize	Reads per 10 Seconds	Average RSSI
Metal	10 dBm	405	-36 dBm
Liquid	10 dBm	440	-36 dBm
Solid	10 dBm	435	-27 dBm

Powder	10 dBm	441	-24 dBm
Wax	10 dBm	440	-31 dBm
Air-filled	10 dBm	431	-22 dBm

7) Cell 7

The return loss performance in cell 7 (refer location in Figure.5.14) is interesting. The meandered line comes out of the coupler's second port with a 90° phase shift. Liquid, metal, solid and wax assets experienced a significant frequency shift towards the lower side of the frequency band. The return loss at higher operating frequencies viz., 924 MHz, 925 MHz, 926 MHz, 927 MHz and 928 MHz for liquid and metal assets are slightly higher than -10 dB. Read count for the metal asset is dropped by half compared to other assets, although its RSSI is -33 dBm. A liquid asset with the same RSSI has a read count of 441 per 10 seconds. The air-filled packet has the highest RSSI, while the wax asset has the lowest. Table.5.9 details different RSSI and read count values for different assets.

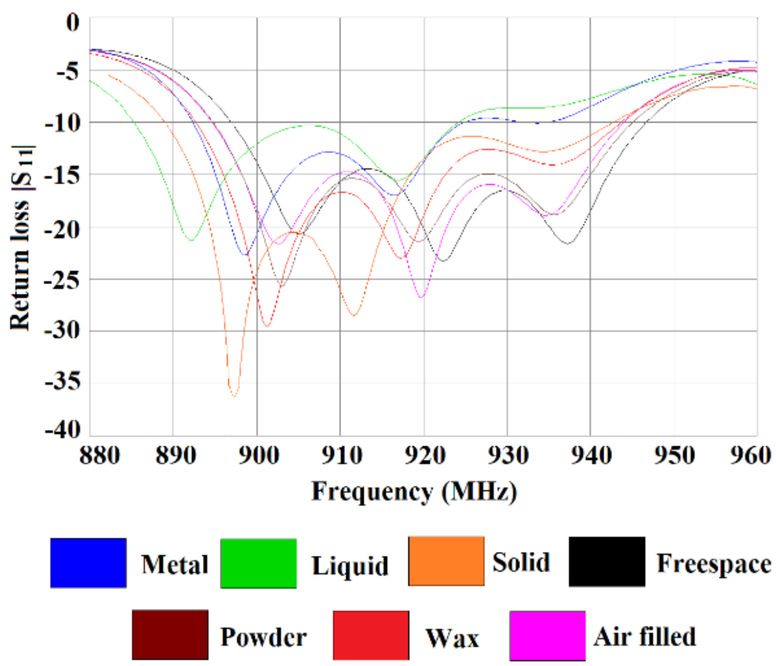

Figure.5.23. Effect of proximity assets on cell 7

Table.5.9. RFID asset testing: Cell 7

Asset type	Minimum Power Required to energize	Reads per 10 Seconds	Average RSSI
Metal	10 dBm	269	-33 dBm
Liquid	10 dBm	441	-33 dBm
Solid	10 dBm	438	-32 dBm
Powder	10 dBm	441	-23 dBm
Wax	10 dBm	442	-38 dBm
Air-filled	10 dBm	431	-22 dBm

8) Cell 8

The return loss is not deteriorated for any assets in cell 8 (refer location in Figure.5.14), unlike cell 7. The -10 dB operating bandwidth is maintained. The microstrip lines in cell 8 have fewer meanders compared to all the cell discussed previously. Cell 8 consists of a 75.16 Ω quarter-wave transformer transforming the impedance from 50 Ω to 113 Ω. The signal travelling through this line is delayed by 90°. The signal strength in these lines is higher as they are directly connected to the coupler's output. The read count of almost all the assets are higher but the wax.

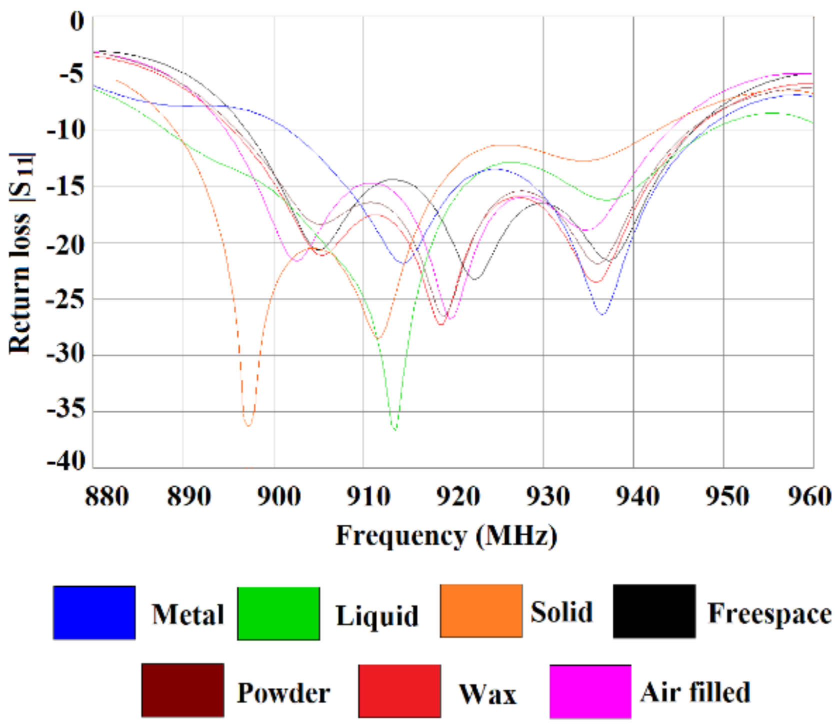

Figure.5.24. Effect of proximity assets on cell 8

As the tag was laid on its side and when the tag was facing away from the microstrip line (facing towards the inactive antenna regions), the read rate is dropped to 354 (Table 10).

Table.5.10. RFID asset testing: Cell 8

Asset type	Minimum Power Required to energize	Reads per 10 Seconds	Average RSSI
Metal	10 dBm	435	-32 dBm
Liquid	10 dBm	432	-34 dBm
Solid	10 dBm	438	-32 dBm
Powder	10 dBm	354	-32 dBm
Wax	10 dBm	441	-38 dBm
Air-filled	10 dBm	431	-22 dBm

9) Cell 9

Cell 9 (refer location in Figure.5.14) is similar to cell 8 except for the signal travelling through this quarter-wave transformer. There is no delay introduced by the coupler's port 1. The RSSI for all the assets were lower compared to the RSSI reported in cell 8. The metal asset's read count is dropped to 285 compared to other assets whose read counts were about 435 on an average. The surface area of the Pico-On-Plus tag is smaller compared to the Vortex tag, and when the tag lies in between the microstrip line gaps, it may not be detected as efficiently as a vortex tag that spans across the meandered microstrip lines. The Pico-On-Plus tag was right over the microstrip line when tested in cell 8, yielding a higher read rate (Table.5.11).

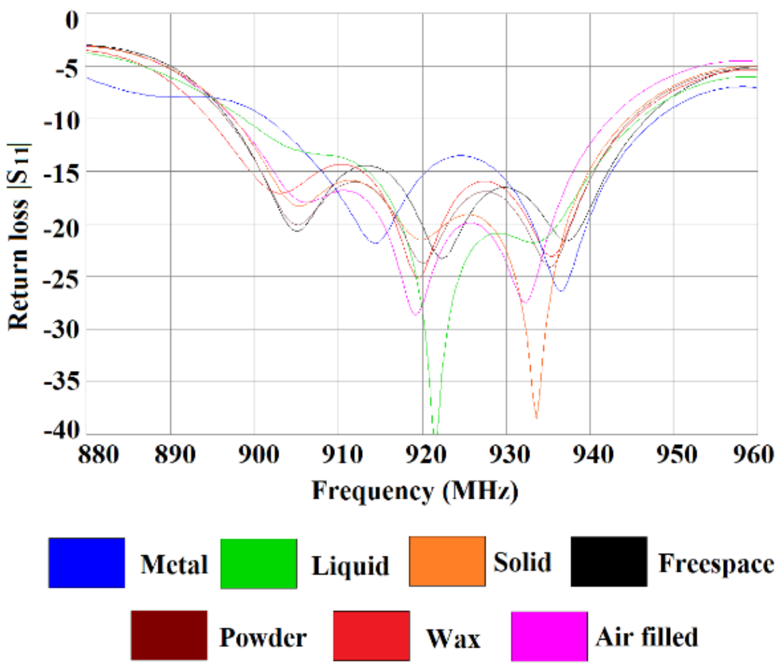

Figure.5.25. Effect of proximity assets on cell 9

Table.5.11. RFID asset testing: Cell 9

Asset type	Minimum Power Required to energize	Reads per 10 Seconds	Average RSSI
Metal	10 dBm	285	-40 dBm
Liquid	10 dBm	433	-40 dBm
Solid	10 dBm	430	-40 dBm
Powder	10 dBm	439	-31 dBm
Wax	10 dBm	438	-38 dBm
Air-filled	10 dBm	426	-21 dBm

10) Cell 10

In cell 10 (refer location in Figure.5.14), the microstrip line from the coupler's output is extended to form a 113 Ω meandered line. Antenna detuning was not significant, and the -10 dB return loss bandwidth is maintained for the operational frequency band. Although RSSI for different assets varies between -21 and -44 dBm, read counts were all similar (Table.5.12).

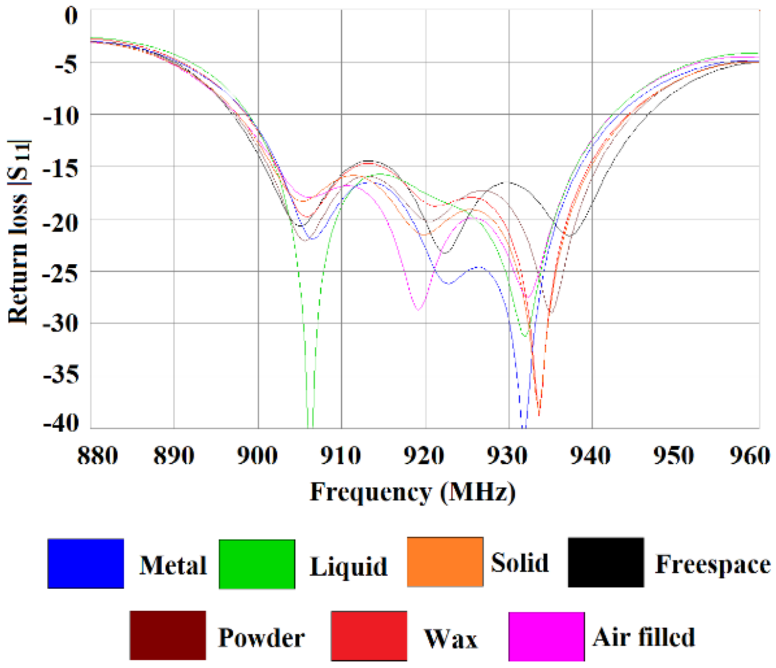

Figure.5.26. Effect of proximity assets on cell 10

Table.5.12. RFID asset testing: Cell 10

Asset type	Minimum Power Required to energize	Reads per 10 Seconds	Average RSSI
Metal	10 dBm	425	-36 dBm
Liquid	10 dBm	438	-44 dBm
Solid	10 dBm	430	-40 dBm
Powder	10 dBm	440	-26 dBm
Wax	10 dBm	408	-38 dBm
Air-filled	10 dBm	426	-21 dBm

11) Cell 11

This cell (refer location in Figure.5.14) is similar to cell 6 where the microstrip line from the coupler's port 1 is carried over as a meandered line but without any phase shift. The patch's edge lies close to the meandered line, and its fringe fields help reading the tags. The antenna's return loss is maintained less than -10 dB in our frequency of interest. The air-filled pack has the highest RSSI, and metal asset had the highest read count. The wax asset has the least RSSI and least read count. Table.5.13 details different RSSI and read count values for different assets. Table.5.13 details different RSSI and read count values for different assets.

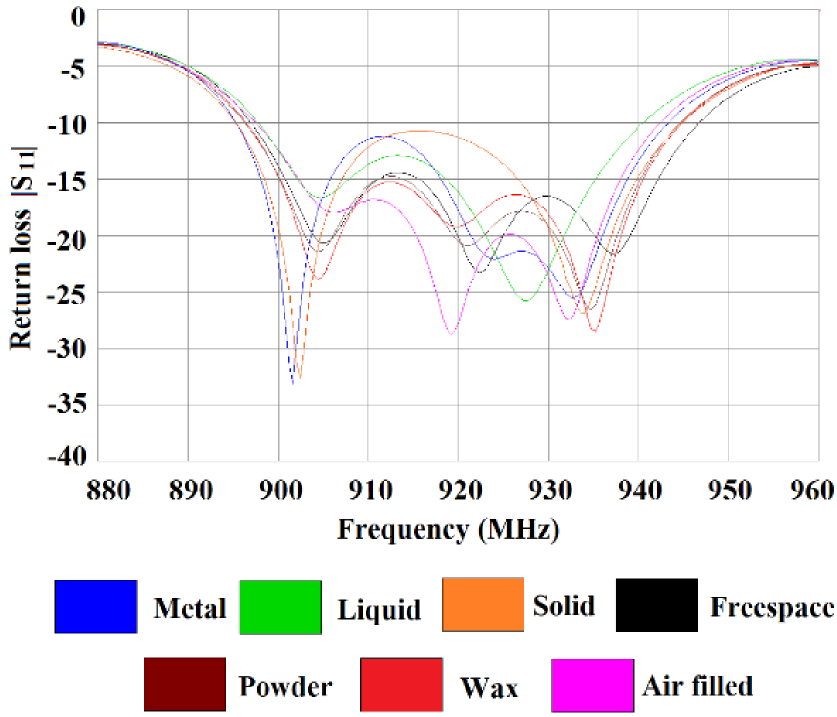

Figure.5.27. Effect of proximity assets on cell 11

Table.5.13. RFID asset testing: Cell 11

Asset type	Minimum Power Required to energize	Reads per 10 Seconds	Average RSSI
Metal	10 dBm	443	-35 dBm
Liquid	10 dBm	431	-36 dBm
Solid	10 dBm	432	-31 dBm
Powder	10 dBm	436	-22 dBm
Wax	10 dBm	377	-44 dBm
Air-filled	10 dBm	426	-21 dBm

12) Cell 12

Cell 12 (refer location in Figure.5.14) is similar to cell 5 and an extension of the meandered line explained in cell 11. Solid asset's return loss was deteriorated slightly in the centre of the operating band, but it did not exceed -10 dB. All assets have good read counts and their RSSI were equally high (refer to Table.5.14). The antenna's -10 dB bandwidth is unaltered in the operational frequencies.

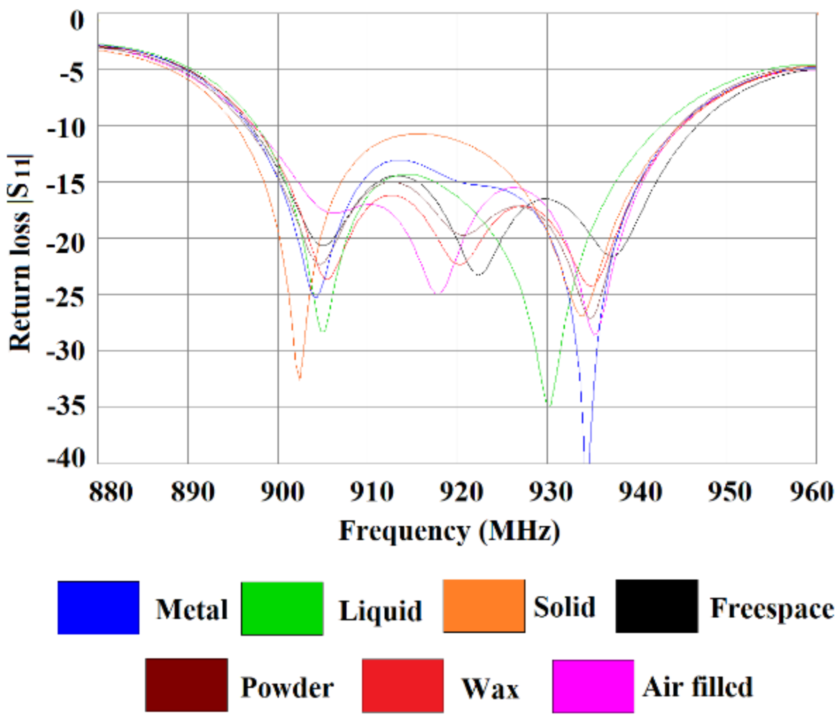

Figure.5.28. Effect of proximity assets on cell 12

Table.5.14. RFID asset testing: Cell 12

Asset type	Minimum Power Required to energize	Reads per 10 Seconds	Average RSSI
Metal	10 dBm	441	-33 dBm
Liquid	10 dBm	431	-37 dBm
Solid	10 dBm	432	-31 dBm
Powder	10 dBm	436	-23 dBm
Wax	10 dBm	441	-39 dBm
Air-filled	10 dBm	429	-26 dBm

13) Cell 13

The top left quadrant of the patch antenna constitutes Cell 13 (refer location in Figure.5.14). The patch antenna in this cell is driven by the meandered line with 0° phase shift. The feed line is inset to match the 113 Ω input impedance. The patch antenna has concentrated fringe fields in its edges. Metal asset caused reflections in the centre of the frequency band in this cell, but it did not exceed -10 dB. The assets are read seamlessly with a higher read count. The RSSI of most of the assets are higher except for the liquid asset (see Table.5.15).

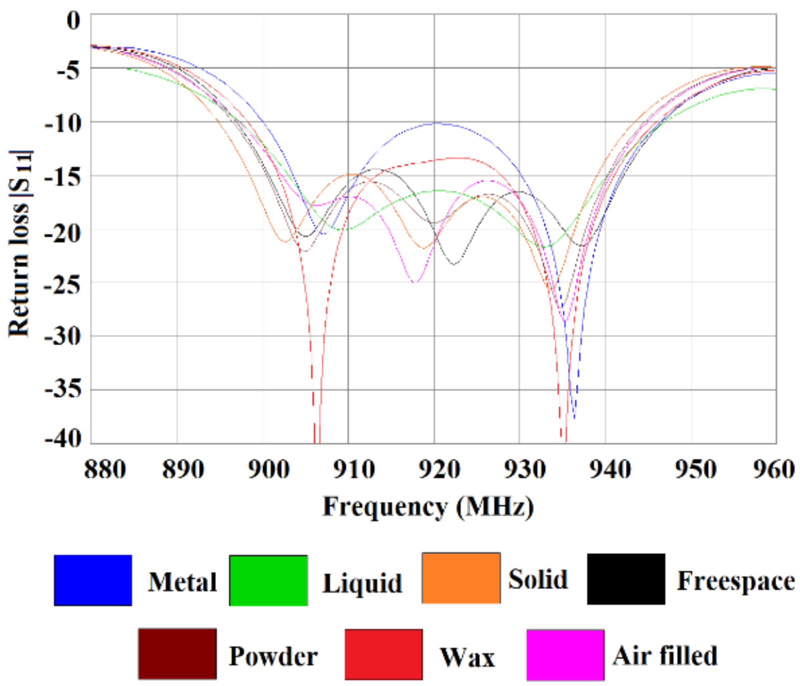

Figure.5.29. Effect of proximity assets on cell 13

Table.5.15. RFID asset testing: Cell 13

Asset type	Minimum Power Required to energize	Reads per 10 Seconds	Average RSSI
Metal	10 dBm	429	-37 dBm
Liquid	10 dBm	431	-41 dBm
Solid	10 dBm	440	-24 dBm
Powder	10 dBm	428	-27 dBm
Wax	10 dBm	441	-31 dBm
Air-filled	10 dBm	429	-26 dBm

14) Cell 14

The cell 14 (refer location in Figure.5.14) corresponds to the top right quadrant of the patch antenna. The patch antenna in this cell is driven by the meandered line with 90° phase shift. The feed line is inset to match the patch impedance. Changes in return loss are not dramatic, and the -10 dB bandwidth is maintained in the operating frequencies. Read counts were high enough for all the assets and the lowest RSSI is noted for the metal asset (see Table.5.16).

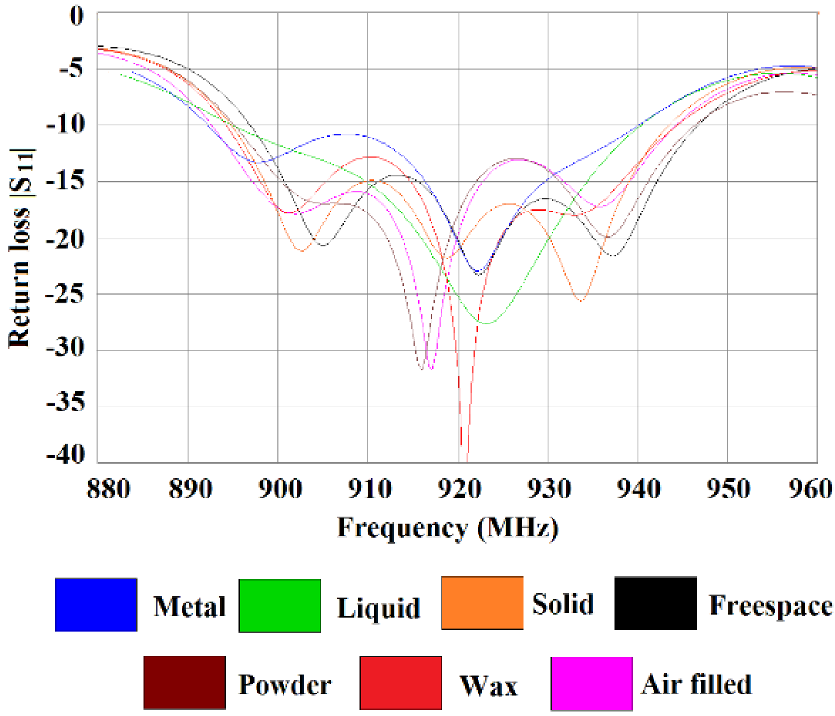

Figure.5.30. Effect of proximity assets on cell 14

Table.5.16. RFID asset testing: Cell 14

Asset type	Minimum Power Required to energize	Reads per 10 Seconds	Average RSSI
Metal	10 dBm	409	-41 dBm
Liquid	10 dBm	431	-31 dBm
Solid	10 dBm	440	-24 dBm
Powder	10 dBm	440	-19 dBm
Wax	10 dBm	440	-36 dBm
Air-filled	10 dBm	432	-32 dBm

15) Cell 15

The bottom left quadrant of the patch antenna comprises cell 15 (refer location in Figure.5.14). This region of the patch has the dummy inset replica to maintain the D4 symmetry. Fringe fields are prominent in the patch's edges. Although the return loss is not altered too much by the assets, metal and liquid assets' read count are lower compared to others. The liquid asset's RSSI is -53 dBm, which is the least value among all the assets and across different cells. However, the read count of the liquid asset is higher compared to the metal asset whose RSSI is -44 dBm. Table 17 details different RSSI and read count values for different assets.

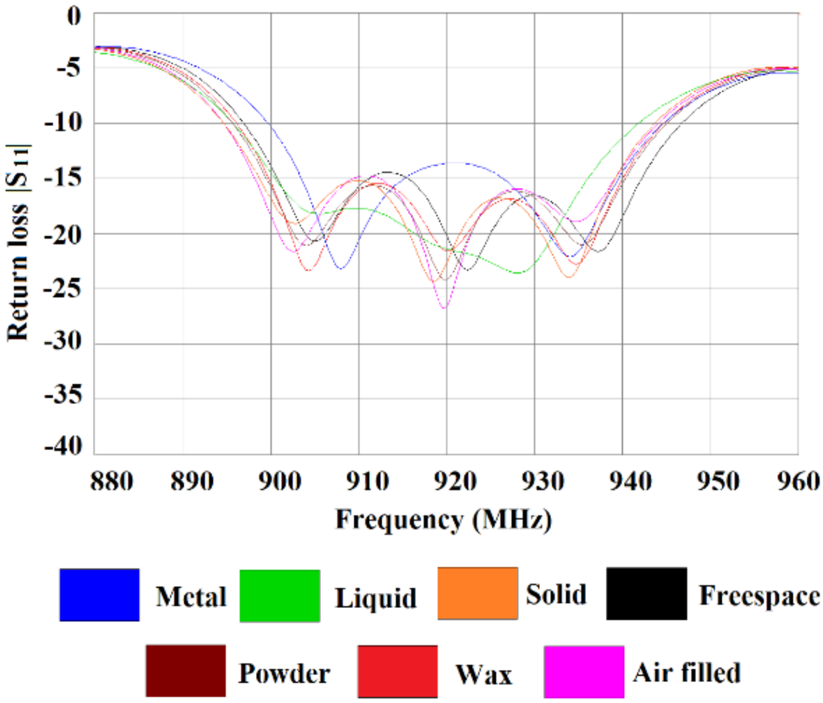

Figure.5.31. Effect of proximity assets on cell 15

Table.5.17. RFID asset testing: Cell 15

Asset type	Minimum Power Required to energize	Reads per 10 Seconds	Average RSSI
Metal	10 dBm	114	-44 dBm
Liquid	10 dBm	132	-53 dBm
Solid	10 dBm	441	-45 dBm
Powder	10 dBm	442	-24 dBm
Wax	10 dBm	440	-34 dBm
Air-filled	10 dBm	431	-22 dBm

16) Cell 16

The bottom right corner of the patch antenna forms the cell 16 (refer location in Figure.5.14). Cell 16 is similar to cell 15 with D4 symmetry and strong fringe fields. The metal asset affects the antenna's return loss slightly at the low side of the operating frequency band. The read count of metal asset is the least with -43 dBm RSSI. However, the solid asset's RSSI is -45 dBm with very high read count (Table.5.18).

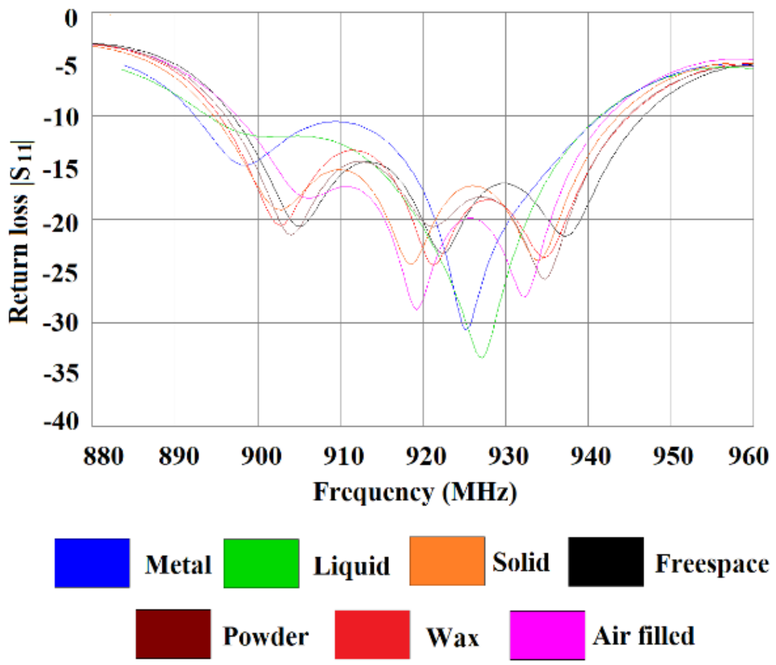

Figure.5.32. Effect of proximity assets on cell 16

Table.5.18. RFID asset testing: Cell 16

Asset type	Minimum Power Required to energize	Reads per 10 Seconds	Average RSSI
Metal	10 dBm	149	-43 dBm
Liquid	10 dBm	391	-51 dBm
Solid	10 dBm	441	-45 dBm
Powder	10 dBm	443	-20 dBm
Wax	10 dBm	441	-29 dBm
Air-filled	10 dBm	426	-21 dBm

5.8 Conclusion

A new scalable UHF RFID near-field fed far-field reader antenna design is proposed to meet the requirements for POS reader antenna at retail checkout counters. The design features a meandered line fed patch antenna that yields a 3.3 dBi (5.3 dBiC) peak gain with a 90° half-power beam-width in both planes. The antenna's axial ratio is 1.4 dB at f_c. The antenna operates between 902-928 MHz and has uniform surface energy distribution with no dead zones. Furthermore, it is low-cost, planar and mechanically sturdy with excellent UV/chemical/impact resistant properties and low friction coefficient. The antenna is tested for its susceptibility to mounting metal frames and proximity assets.

Prelude to Manuscript 3

In this manuscript, an ultra-rugged UHF RFID reader antenna made from a concrete substrate that is sandwiched between a stubbed quarter-wave monopole radiator and a folded ground plane is proposed for fixed UHF RFID readers. The antenna's ruggedness is not dependent on the antenna's radome unlike traditional rugged antenna designs. Instead it is dependent on the ruggedness of the antenna's substrate and metal layers, which are already proven by commercial manufacturers. Although a typical monopole antenna radiates omni-directionally, when the antenna is spaced above the ground plane (quarter wavelength above), the monopole antenna becomes directional. The concrete's dielectric constant of ~4.3 is obtained from the literature for a Portland cement concrete brick. The composition of the concrete brick could vary and the antenna design can work efficiently despite the variation within a range.

This linearly polarized antenna operates between 865 and 868 MHz with a 3.5 dBi peak gain and a 160 MHz -15 dB $|S_{11}|$ bandwidth. The 3.5 dBi and 2.0 dBi gain bandwidth are 80 MHz and 140 MHz, respectively. The antenna is intended to use in convention center loading docks, thus tested for extreme environmental conditions such as high temperature, humidity, condensation, rain, the effect of superstrates and metals. The antenna's gain and return loss were measured but not the radiation pattern (which is a plot of gain vs direction) due to practical difficulties. More than one concrete tile antenna can be operated using one RFID reader to realize a distributed antenna system (DAS). The antenna is conformal and can blend with the environment without affecting the existing aesthetics. The antenna creates a wide circumferential read zone (~5.6 m diameter) and reads tags up to 6.5 m at the boresight in free space. The radiation pattern is asymmetric as the antenna is linearly polarized and has a folded ground plane emulated by using a conducting via strip to connect the top and bottom ground plane to form a metal side wall.

Chapter 6

Manuscript 3

Ultra-rugged UHF RFID reader antenna for convention centre loading docks

6.1 Introduction

Auto Identification and Data Capture (AIDC) is a technology that automatically identifies objects, collects and records the data about them. A wide range of auto-ID technologies is available which include optical character recognition (barcodes), speech recognition, biometric recognition (fingerprint and iris), RFID (passive and active) and so on are available. Passive RFID is more popular due to its low cost and low complexity benefits. UHF RFID is a type of passive RFID which can detect tags at greater distances. The power, frequency, and other spectral standards are region specific, which are defined by the regional telecommunications equipment standards association. However, the air-interface protocol, tag data standard, reader protocol and so on are defined by GS1 [1].

The UHF RFID is an integral part of the Internet of Things (IoT) in environmental sensing, real-time monitoring and ambient assisted living [2]. Due to this integration, UHF RFID is not only used for auto-identification but also as a sensor that senses and shares the information about a product in a closed-loop or an open-loop supply chain, enhancing the product traceability [3]. The UHF RFID system can either be fixed or a mobile using a WiFi/Bluetooth enabled battery powered hand-held scanner with a built-in RFID antenna. The fixed scanner consists of the RFID reader that acts as a transceiver, RFID antennas connected externally using coaxial cables and other accessories such as the power and data cables. Some fixed readers may have an integrated antenna with a few RF ports for the external antenna connection. The fixed reader antennas are deployed in the area where data capture is required. In practice, the fixed readers cannot be protected in a protective metal enclosure (they would block the RF transmission) from mechanical damages, unlike the readers. Antennas with other types of RF transparent radomes are still vulnerable to mechanical destructions. A broken radome makes the antenna susceptible to physical and environmental damages. A concrete antenna is not vulnerable to a broken radome as the concrete substrate is strong enough to handle the knocks. This demands the need for ultra-rugged antennas (not just the radomes) in RFID applications especially when they are amid heavy-duty vehicles such as trucks and forklifts.

Figure.6.1. A typical convention center loading dock

A convention center loading dock (shown in Figure.6.1) is one among the aforementioned environment that requires an ultra-rugged reader antenna. RFID reader antennas are used to detect the assets that are loaded and unloaded at the dock-doors. Commercial RFID reader antennas cannot handle greater mechanical stress or strain, leading to permanent damage and deformation. Besides, the traditional antennas cannot be installed seamlessly and may not handle extreme environmental conditions without a significant change in RF properties. The proposed concrete substrate antenna is ultra-rugged and can handle a variety of mechanical stress and strain without getting damaged significantly. This enables a conformal deployment that does not affect the aesthetics of the environment. Moreover, the antenna can be installed in-floor seamlessly or on the wall to create a distributed antenna system using a single RFID reader.

6.2 Related works

Traditional UHF RFID reader antennas are made from conventional RF materials such as FR4, Rogers, Taconic, etc. Copper clad (80 to 140 μm thick) is attached to the substrates and the antenna pattern is often formed by photoengraving and etching the copper. These antennas are not rugged and cannot handle a lot of mechanical stress or strain without damaging the antenna pattern and the substrate itself. As there are no existing works on UHF RFID reader antennas that are used in conventional dock-door applications, this section discusses (a) rugged UHF RFID reader antenna designs, (b) rugged but non-UHF RFID reader antenna designs, and (c) antennas made from concrete and other non-conventional materials for non-UHF RFID applications.

Commercially available rugged antennas such as [4, 5] and [6] are made from plastic and metal housing, respectively. Former designs are a patch antenna and patch antenna array enclosed in polyphenylene ether (PPE) and glass-reinforced plastic enclosures, respectively. The antenna's radome provides the ruggedness and strength. The latter is a patch coupled resonant metal cavity aperture antenna where the patch couples to a square cavity and it in-turn couples to a cross-slot [7]. The plastic housing has a limited load-bearing capability and can easily be deformed to damage the internal patch antenna. A dented metal cavity resonator will no longer resonate at the intended resonant frequency. The proposed antenna is made from a concrete brick which has a very high load-bearing capability that will not allow a permanent deformation or damage to the antenna without using a radome.

Rugged but non-UHF RFID reader antennas found in the literature are [8, 9] where rugged UHF RFID hand-held reader antennas are reported. Handheld reader antennas' definition of ruggedness is very different from the fixed reader antenna. Their ruggedness is associated with day-to-day handling such as dropping or knocking the handheld reader. The proposed antenna can operate in harsh industrial environments such as strong impacts/shocks, wet, dusty and extreme temperatures. [8] is a compact yagi antenna consisting of molded 6 mm ABS plastic with stamped metal traces. The plastic used here can be perceived as a protective cover (radome). Similarly, a monofilar backfire helical antenna is proposed in [9] that uses an ABS plastic core and radome for ruggedness. Both yagi and the helical antennas are not lo-profile unlike the proposed antenna and are 100 mm and 130mm long, respectively. These non-planar antennas are not conformal to the convention center dock-door environment and are vulnerable to impact hazards (such as trucks running into the antennas).

A microstrip patch antenna is designed to operate at 2.45 GHz inside a reinforced concrete slab for wireless communications. [10]. The antenna is made from Rogers' substrate (RO4003C). and its S_{11} and the S_{21} values were measured. Another patch antenna made from Roger's TMM 10i and TMM 6 substrate is designed and embedded into a concrete structure for wireless monitoring applications at 900 MHz [11]. The antenna's performance is simulated and analytically calculated for different dielectric constant values (ε_r = 4 to 9). Different from the works mentioned above, the proposed antenna in this manuscript is not made from an expensive RF material such as Rogers or Taconic but a non-conventional substrate. The proposed antenna is not embedded in a concrete material for protection (like a radome) rather the substrate itself is made from a concrete brick. The reported antenna in [11] become vulnerable when the radome is broken whereas the proposed antenna offers the ruggedness without a radome. The proposed antenna's substrate is made from Portland cement concrete whose dielectric constant variation can be controlled using mix proportion (as provided in Table III) unlike [11] where neither the type of concrete nor the mix proportion is advised.

A square loop antenna designed in a paper substrate for UHF RFID tags is attached under a concrete tile in [12] to form a localization matrix. This manuscript antenna is not robust when it is subjected to mechanical stress and strains, on its own unless protected by a concrete tile cover. Thus, this design is not suitable to be used as UHF RFID reader antennas. Moreover, the antenna design is fabricated from a conventional RF substrate, and the ruggedness relies on the concrete cover. The multi-layer patch antenna design in [13] is also an embedded tag antenna design where the antenna consists of a ceramic driven patch separated by a plastic housing and a parasitic patch. The tag antenna rests on a metal cavity that is embedded into the concrete floors. This antenna design cannot be used with an RFID reader because the antenna is not different than the other antennas explained in the literature with no ruggedness built in and the strength is added by the concrete outer shell when the antenna is embedded into it. The proposed antenna will be suitable for both reader and tag antennas. The higher gain specification of the proposed antenna would make the tag highly sensitive that could be read at very long distances if the proposed antenna is used as a tag antenna. To make this antenna as a tag antenna, an RFID tag chip can be attached at the antenna's feed point replacing the coaxial cable.

Table 1 summarize the advantages and the disadvantages of existing works over the proposed antenna design. The antenna type, construction, ruggedness and material used to provide the ruggedness is also compared and reviewed. The proposed antenna has a lot of advantages over existing works. The disadvantages are also mentioned, and ways to mitigate them stated under the 'comments' column.

Table.6.1. Summary of existing works and proposed work with their advantages and disadvantages

Ref.	**Antenna type and construction**	**Ruggedness provider**	**Rugged material**	**Main Advantages**	**Main Disadvantages**	**Comments**
[4] and [5]	Patch antenna and patch antenna array inside a plastic enclosure	Radome	PPE and glass reinforced plastic	1. UHF RFID reader antenna 2. Commercially available	1. The radome provides ruggedness 2. Non-conformal and expensive 3. Plastics, in general, has limited load bearing capability	Antenna becomes vulnerable when the radomes are damaged. Damaged antenna's efficiency drops and leads to unreliable RFID asset tracking.
[6] and [7]	Patch coupled resonant metal cavity aperture	Cavity aperture radome	Metal	1. All metal structure from the outside 2. Commercially available	1. Damage to the metal cavity affects the antenna's performance 2. Damages are permanent and non-revocable	Damaged metal cavity can destroy the antenna's impedance matching. The poorly matched antenna offers very high RF reflections. This can

					3. Non-conformal and expensive	damage the RFID reader permanently.
[8] and [9]	Yagi antenna and helical antenna on plastic	Radome and plastic core	ABS	1. Antennas are attached to the molded plastic radome 2. Rugged for hand-held RFID reader applications	1. Cannot handle harsh industrial environments 2. Non-conformal and protruding 3. Poor impact resistance	Protruding antennas can be crushed by trucks running into them. Thus, their ruggedness is irrelevant for the industrial use case.
[10] and [11]	Patch antenna inside concrete slab	Radome	Concrete	1. The antenna is used for wireless monitoring application	1. The radome provides ruggedness 2. Antennas are made from conventional RF substrate materials 3. The type of concrete used, and its composition is not explained	Antenna becomes vulnerable when the radomes are damaged. Damaged antenna's efficiency drops and leads to unreliable RFID asset tracking.
[12] and [13]	Loop and multi-layer patch antenna	Radome	Concrete	1. low-cost tag antenna design	1. Not suitable for reader antenna application 2. The radome provides ruggedness 3. Damages to the internal antenna are permanent and non-revocable	Antenna becomes vulnerable when the radomes are damaged. Damaged antenna's efficiency drops and leads to unreliable RFID asset tracking.
This Work	Quarter-wave monopole antenna on a concrete substrate with a reflector ground plane	Substrate and conductor layers	Concrete substrate and steel sheet (radiator and ground plane)	1. Does not require a protective radome 2. Can operate in a harsh industrial environment 3. Construction is simple and low-cost 4. The antenna is planar, conformal and has directional radiation with a wide beam-width.	1. The antenna introduces higher losses compared to conventional RF substrates 2. The substrate's relative permittivity and loss tangent are uncontrolled.	The antenna's wideband design can mitigate the risk of change in antenna's resonance due to relative permittivity changes. The type of concrete brick with its mixing proportion is advised to control the inherited substrate's losses.

6.3 Antenna design and fabrication

The ultra-rugged antenna consists of a quarter-wave radiating element and a folded-ground plane separated by a concrete substrate. The substrate's size is 230 mm (length) x 190 mm (width) × 40 mm (height) and is a 'concrete-only' structure without metal reinforcement (See Figure.6.2(a)). The commercially available substrate's dimensions define the antenna's physical dimension. The radiating element is 55 mm long and 25 mm wide. The radiating element is impedance matched using an open-stub that is 12 mm × 25 mm in dimension. The overall dimensions of the ground plane are 310 mm (length) × 230 mm (width). The ground plane is folded along its length and made to remain close to the radiating element, for ease of cable soldering. The ground plane spans 70 mm, 190 mm and 40 mm on the top layer, bottom layer and the side of the substrate, respectively (Figure.6.2(b)). The antenna is designed for the frequencies 865-868 MHz prescribed by the European Telecommunication Standards Institute (ETSI) [14] and [15]. The 55 mm long monopole (quarter wave radiator's length for the center frequency (f_c) 866.5 MHz) is half immersed in the concrete and half exposed to air with an effective (mean) dielectric constant of 1.25. The radiator is placed in the center of the concrete and it is 2 mm away from the folded ground plane in the top layer. The 50 Ω feed point is at the edge of the radiator where the excitation takes place.

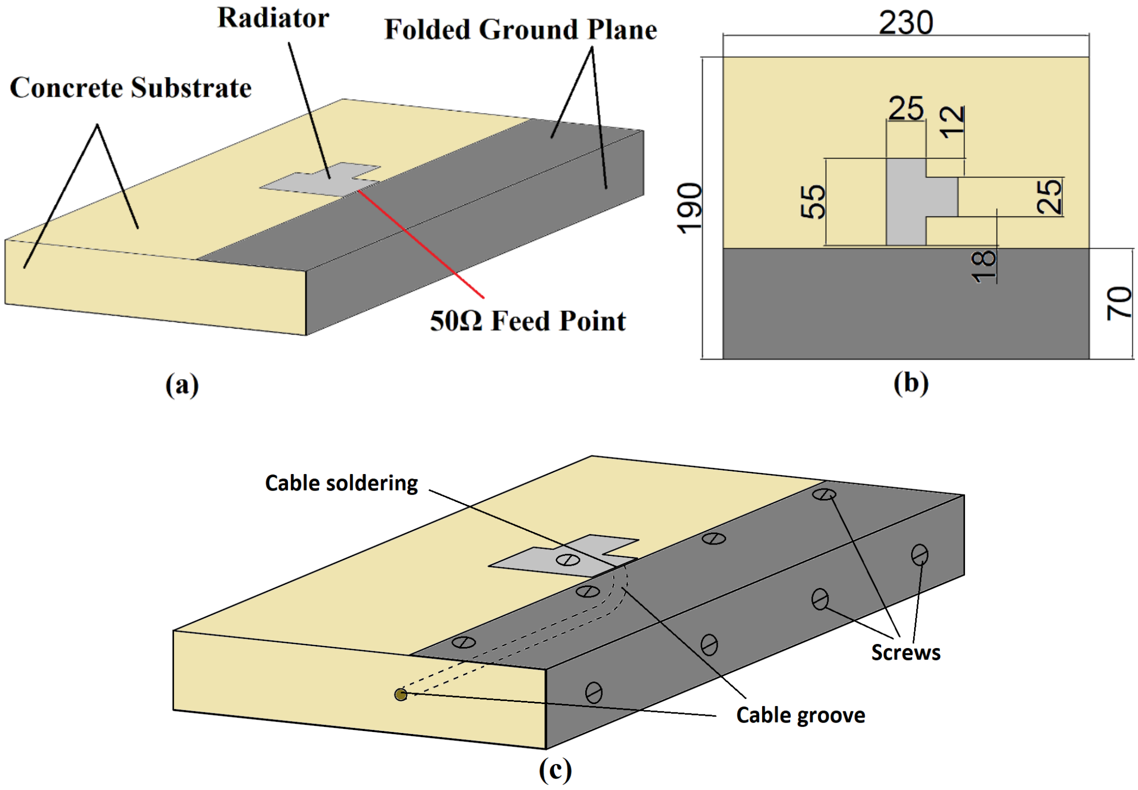

Figure.6.2. Antenna design (dimensions are in mm): (a) 3D-Model, (b) Top-view (c) Manufacturing essentials – cable groove and fastening screws

The antenna is fabricated using a 0.3mm thick, tinned-steel sheet for the radiating element and the ground plane. Tinned- steel sheets are low-cost and robust with electrical conductivity and an electrical resistivity of 8.7×10^{6} Siemens/m and 11.5×10^{-8} Ωm, respectively. The concrete substrate adheres with the radiating element and the ground plane using a 0.05 mm non-conductive acrylic adhesive. Coaxial cable is soldered directly onto the radiating element and the folded ground plane as shown in Figure.6.3(a). The folded ground plane continuous to extend on the bottom of the substrate (Figure.6.3(b)). The fabricated antenna can be enhanced by making a custom concrete brick with a provision for cable protection and fastening holes to mechanically secure the tinned sheets using screws (Figure.6.2(c)). The cable will be pulled through the cable groove to solder with the radiator and the ground plane in the same feed point described in Figure.6.3(a). The proposed antenna is cost-effective and, its bill of materials (BOM) including assumed labor for manufacturing is listed in Table.6.2.

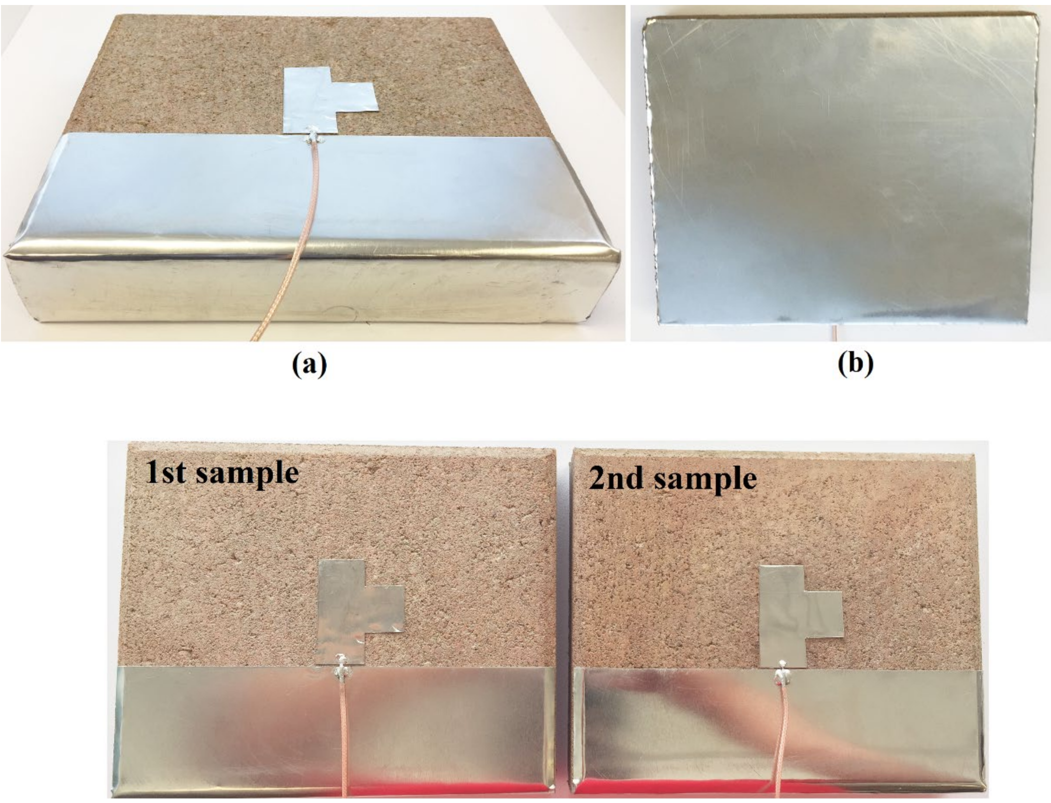

(a) **(b)**

(c)

Figure.6.3. Fabricated Antenna: (a) Top-view and (b) Rear-view (c) Second identical sample fabricated

Table.6.2. Proposed antenna's bill of materials

Part Description	Cost (USD)	Quantity Used	Sub-Total (USD)
Tinned steel	$3.74 (300 x 500 mm)	300 x 190 mm	$1.44
Concrete brick	$2.95	1	$2.95
RG-316 cable	$1.50	1	$1.50
Solder	$50	0.001	$0.05
Adhesive	$20 (10 m reel)	0.05	$1.00
Assumed labor	@ $12 per hour	10 minutes	$2.0
Total			$8.94

6.4 Results and analysis

The antenna is analyzed using a Method of Moments (MoM) based Electromagnetic field (EM) solver, ADS momentum. It is a 2.5-dimension EM solver that is preferred for planar antenna simulations [16]. A concrete substrate of 40 mm thickness is defined with a ε_r and a loss tangent (tanδ) values of 4.38 and 0.125, respectively. 0.3mm thick conductor layers with a conductivity of 8.7×10^6 Siemens/m is defined, and the folded ground plane is emulated using conductive vias with the same conductivity. A 50 Ω port (transmission line calibrated) is defined between the ground plane and the radiator for excitation. The simulation is set up at a meshing frequency of 866.5 MHz with 20 'cells per wavelength' mesh. Edge mesh is enabled, and the antenna is simulated between 0.8 and 1 GHz.

The fabricated antenna (first sample) is measured using a TR1300/1 Vector Network Analyzer (VNA) in an anechoic chamber over the same frequency range specified in ADS simulation. Figure. 4(a) is the obtained $|S_{11}|$ and the far-field gain plot through the ADS simulation and the VNA measurements. The far-field gain is measured by a comparative method using a reference antenna at the boresight. The -15 dB $|S_{11}|$ bandwidth of the fabricated antenna is 160 MHz while the simulated -15 dB $|S_{11}|$ bandwidth is only 120 MHz. The peak gain of the fabricated antenna is 3.5 dBi, and it remains constant for 80 MHz. The gain bandwidth is measured to be 140 MHz at a 2.0 dBi gain cut-off. The simulated antenna's peak gain is 2.8 dBi for 28 MHz bandwidth. At 866.5 MHz (f_c), the $|S_{11}|$ of the fabricated antenna is -18.55 dB while the simulated antenna yielded -20 dB. The fabricated antenna's efficiency is measured to be 50.47% using the Wheeler cap's constant loss-resistor method.

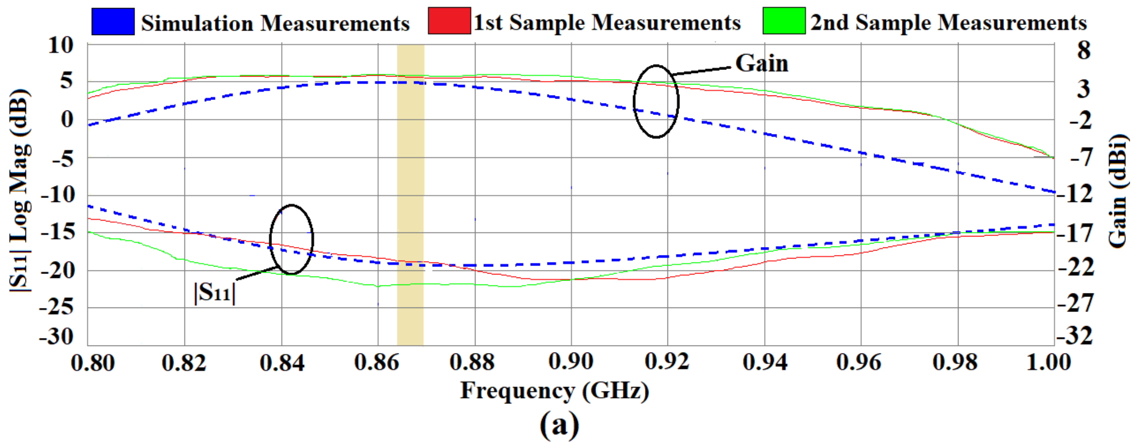

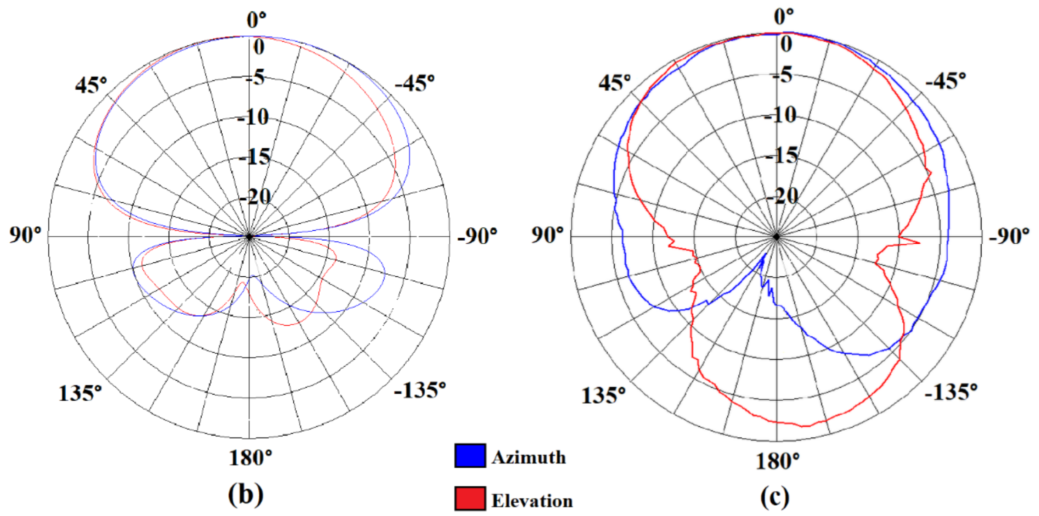

Figure.6.4. Simulated and measured results: (a) |S11| and Gain (b) 2-D Simulated Radiation Pattern (c) 2-D Measured Radiation Pattern

To confirm that this favorable performance was not achieved by chance, another antenna of the same design is manufactured and measured for its performance under the same setup (to also imply the performance is repeatable). Figure.6.3(c) shows the second fabricated sample which is identical to the one that is fabricated before. Figure.6.4(a) shows the second sample's measured $|S_{11}|$ and gain bandwidth which bears similar to those of the first sample. Figure.6.4(b) and (c) shows the antenna's simulated and measured 2-dimensional radiation pattern, respectively. Both the simulated and the measured Half-Power Beam-Width (HPBW) is found to be 145° and 116° in azimuth and elevation planes, respectively. The fabricated antenna has a Front-to-Back Ratio (FBR) of 3dB in the elevation plane and ~25 dB in the azimuth plane. The FBR in the fabricated antenna can be improved by having a larger ground plane attached to the antenna. The simulation assumes a larger ground plane, and thus the back radiation is smaller compared to the measured antenna, otherwise, the simulation results are similar to the measured results.

The concrete substrate used is a nonconventional radio-frequency (RF) substrate whose electrical parameters such as ε_r and tanδ can vary. These variations will impact the antenna's resonant frequency [17]. The change in ε_r can either shift the antenna's resonant frequency lower or higher. An increase in ε_r will induce a shift towards the lower band and vice-versa for the decrease in ε_r. The response of the fabricated antenna ($|S_{11}|$ and gain) is wide enough to cover the four channels (865-868 MHz) even when there is a shift in the antenna's resonant frequency (center frequency of the bandwidth) due to the change in substrate's ε_r. This phenomenon is noticed in the results reported in Figure.6.4(a) where the second fabricated Sample's $|S_{11}|$ and the gain response is shifted towards the lower side of the band compared to the first sample. The antenna's bandwidth is wide enough to accommodate the changes in substrate's ε_r. It is worth mentioning that this wideband antenna would not interfere with other closer bands such as the 4G uplink (800 MHz band) and the 4G downlink (900 MHz band) as the antenna will be connected to an RFID reader which will strictly transmit and receive only in the 865-868 MHz RFID band. Although the antenna with its wide bandwidth may receive from nearby 4G uplink transmitters, the RFID reader will filter them so that only received signals falling within the desired frequencies (865-868 MHz) will be further processed.

Table.6.3. Recommended concrete brick proportion

Water Kg/m^3	Cement Kg/m^3	Sand Kg/m^3	Coarse Aggregate Kg/m^3	Water-to-cement ratio
205	513	560.21	1087.47	0.40

The concrete brick that is used in this paper is made from Portland cement that is similar to the GB-C50 concrete with a strength rating of 50 MPa. The Portland cement consists of 61.2% CaO, 22.4% SiO_2, 5.6% Al_2O_3, 3.5% SO_3, 1.9% MgO, 2.2% FeO, 0.4 K_2O and 2.8% LOI. The ε_r of concretes, in general, can vary between 3.5 to 5.5 depending on the grades for 800 MHz to 1 GHz [18]. The ε_r variation for higher frequencies such as 6 GHz is from 3.3 to 4.9 [18]. The ε_r of concrete is dependent on the water-to-cement ratio. The concrete mix proportion listed in Table.6.3 is recommended to be followed while manufacturing the custom concrete brick with cable provision [19].

6.5 Environmental Testing

This section discusses on the fabricated antenna's performance over the environmental effects such as temperature, humidity, rain, condensation and the impact of antenna deployments namely, on-metal deployment, mounted on a concrete wall, recessed within the concrete wall and covered with protective covers is tested. The first fabricated sample is used throughout the testing.

6.5.1 Effect of temperature and humidity

The temperature and the humidity are often uncontrolled in convention center loading docks, and the antenna's performance can be affected by these parameters [20]. The antenna's performance is evaluated for various temperature between -20°C and +70°C from 50% to 85% relative humidity (RH) in 10°C and 5% steps, respectively. The antenna had a noticeable change in response when the temperature is varied at 85% RH (Figure.6.5). The $|S_{11}|$ is improved by 10 dB at higher temperatures (60°C and 70°C) while the gain dropped by 0.5 and 1 dB, respectively. Conversely, the gain is improved by 1 dB at lower temperatures (-10°C and -20°C) with 2 dB improvement in $|S_{11}|$. The antenna's bandwidth has a negligible impact on temperature and humidity changes. The acrylic adhesive did not undergo any noticeable changes, and the antenna is intact mechanically throughout the testing.

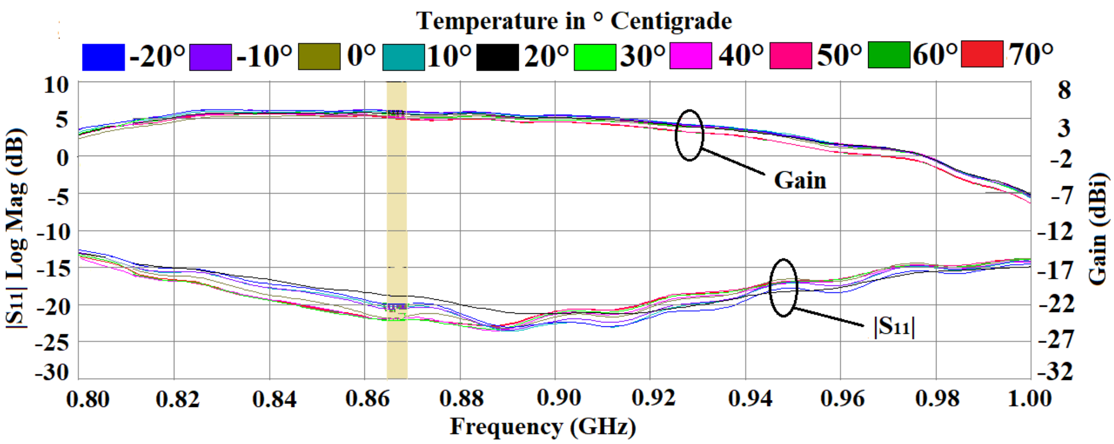

Figure.6.5. Effect of Temperature at 85% Relative Humidity

6.5.2 Effect of condensation and water splash

The loading docks are semi-indoor, and the antennas installed will be subject to a drizzle of rain and condensation. Condensation occurs when the air cools to its dew point through contact with a surface that is colder than the air. Damp concrete's absorption losses are greater GHz and sub-GHz frequencies [20]. Therefore, the antenna's performance evaluation due to the condensation and a drizzle of rain is necessary. The antenna is cooled at -10°C and is exposed to an ambient room temperature of 20°C to initiate condensation. Figure.6.6 shows that the condensed water droplets on the radiator have no significant change in the antenna's response (both $|S_{11}|$ and gain). A drizzle of rain is simulated by splashing water on the antenna (Figure.6.6). The antenna's $|S_{11}|$ is distorted by 5 dB with a 1 dB reduction in gain. The wideband response of the antenna is not affected by both condensation and splash of water. Tinned steel is rust-proof, and the antenna can be installed outdoor, permanently without any protective casing.

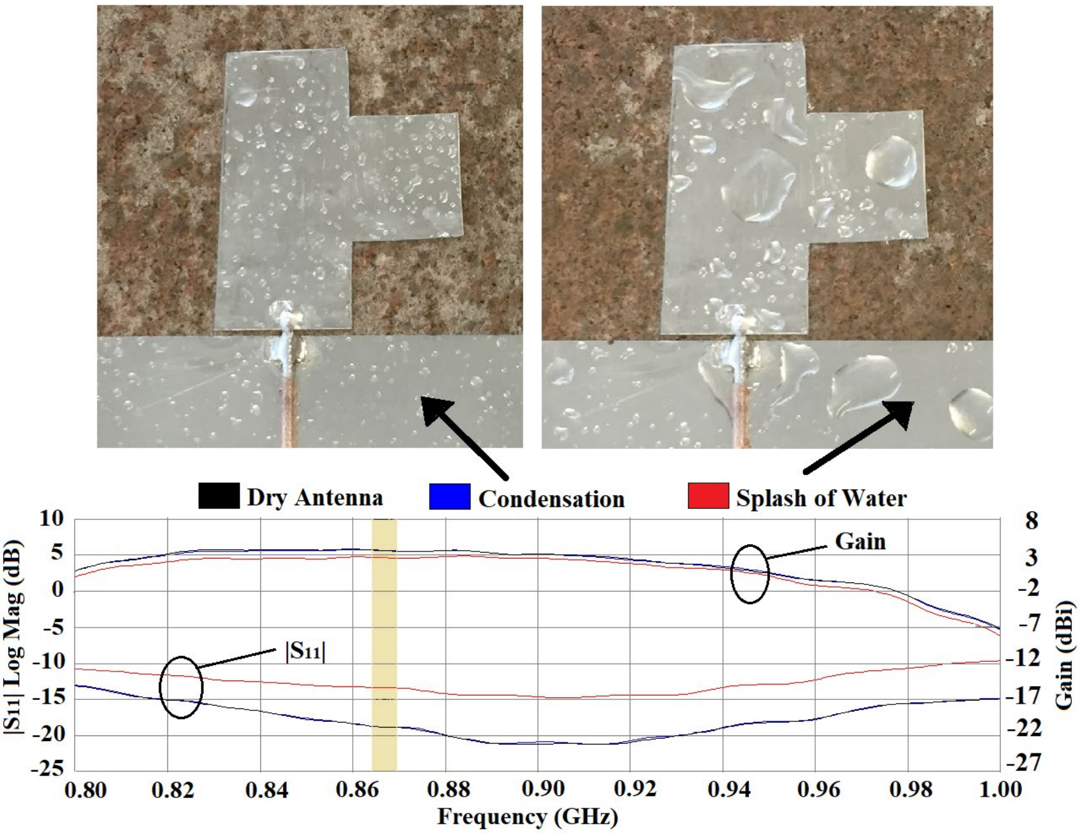

Figure.6.6. Effect of Condensation and Water splash

6.5.3 Effect of superstrates

The antennas can be covered with materials to match the convention center dock-door's color and aesthetics. These covers can be perceived as a superstrate when it is loaded directly on the top face of the antenna. High-density Polyethylene (HDPE), poly-vinyl Chloride (PVC) and fiberglass are some of the commonly used RF transparent cladding materials. Figure.6.7 shows the responses of different types of superstrates with different thicknesses. The $|S_{11}|$ improved for all three superstrate materials. The gain remained similar to the antenna in free space for the HDPE and PVC superstrates while it dropped by 0.3 dBi for the fiberglass superstrate. A frequency shift towards the lower side of the band is noticed. The change in velocity of the radiating fields due to the dense superstrates leads to the frequency shift.

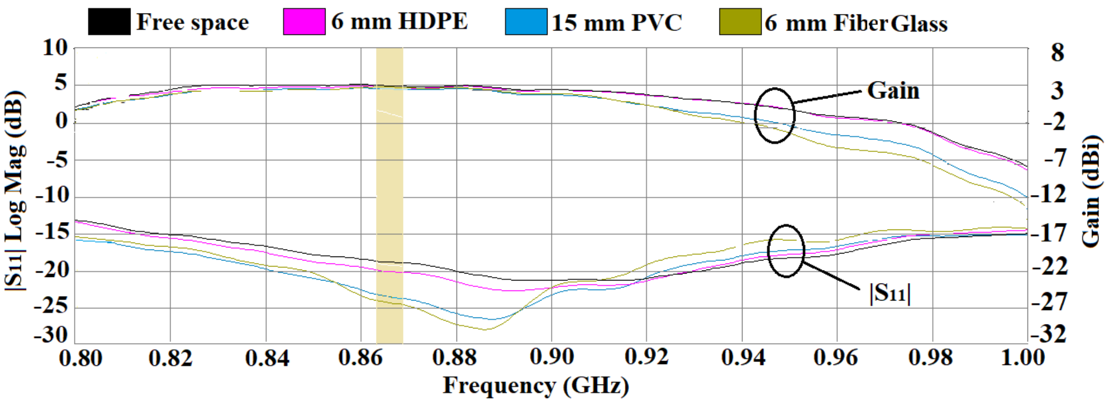

Figure.6.7. Effect of Superstrates on the Radiating Face of the Antenna

6.5.4 Effect of antenna attached-to and recessed-in concrete

The antenna deployment can either be an external attachment to a concrete wall or recessed within the wall or the floor. A recessed antenna enables seamless and conformal installation. A distributed antenna systems (DAS) is viable when the antennas are recessed in the wall creating multiple RFID read-zones. The antenna's gain is reduced by 1.5 dB with an improvement in $|S_{11}|$ when it is attached to the concrete wall (Figure.6.8). The recessed antenna's gain is further dropped by 0.5 dB along with slight $|S_{11}|$ detuning. The gain bandwidth is decreased by 50% for the recessed antenna while the $|S_{11}|$ bandwidth is improved by 40%. Although the gain reduction appears to be significant, the RFID tag reading ability is not affected significantly. The assets traversing between the truck and the dock-doors will be in the range of 2-3 meters to the antenna. Assets can easily be detected in this range regardless of the type of antenna attachment. A detailed RFID testing is reported in Section 6.6.

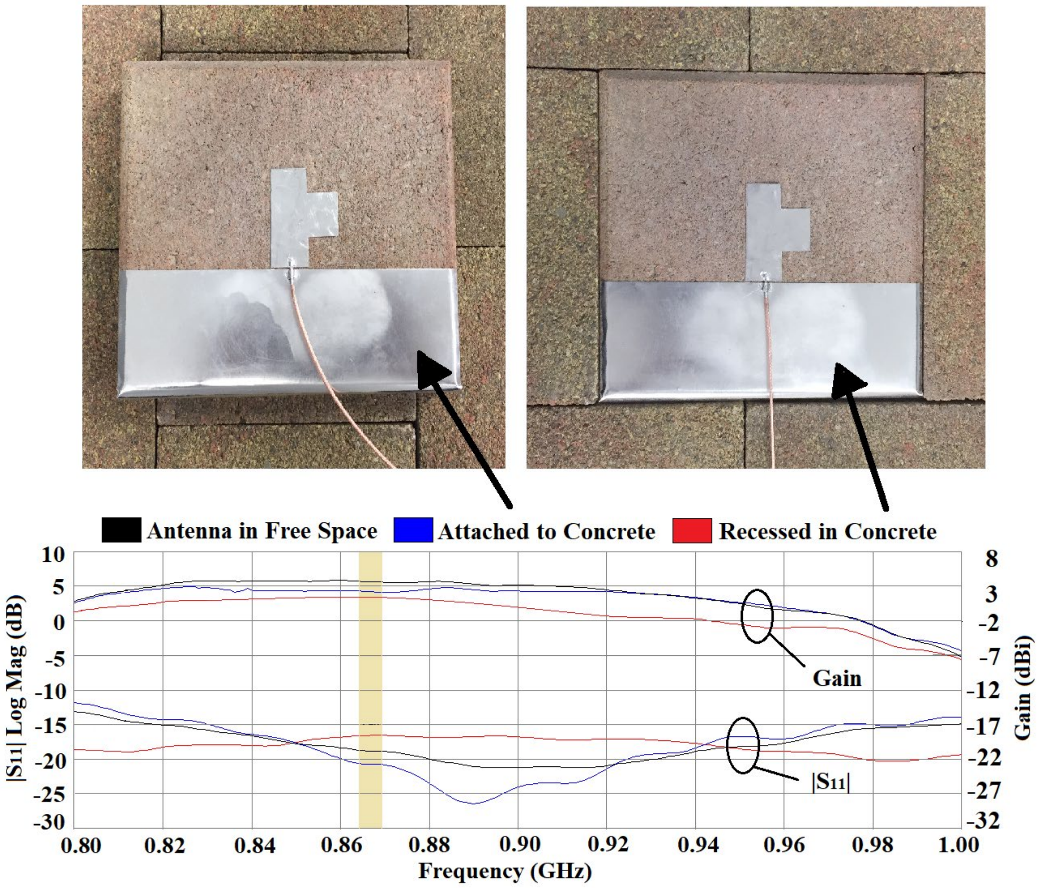

Figure.6.8. Effect of Surrounding Concrete – Recessed and Attached

6.5.5 Effect of reinforcing mesh and metal sheets

Some of the loading docks bear metal cladding or reinforced concrete pillars and beams where the antennas will potentially get deployed. The ultra-rugged antenna is tested with metal sheets and reinforcing steel mesh for the $|S_{11}|$ and gain responses. The gain and the $|S_{11}|$ is improved by 0.5 dBi and 5 dB, respectively when the steel mesh is attached to the back of the antenna (Figure.6.9). A standard steel mesh with150 mm spacing is used for testing [21].

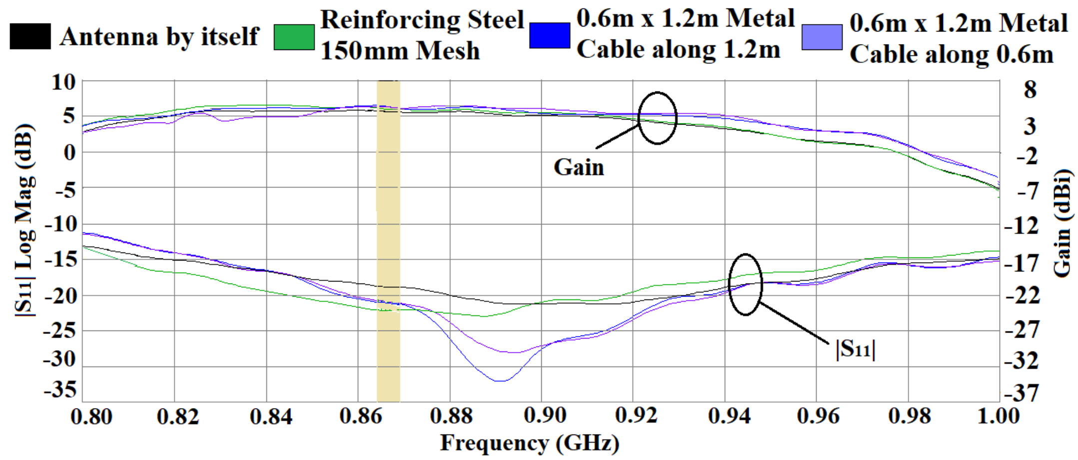

Figure.6.9. Effect of Reinforcing Mesh and Metal sheets

A rectangular metal sheet spanning 0.6m × 1.2m is chosen to simulate a large metal cladding. The sheet was placed in two different orientations, namely a) the shortest length is along the direction of the cable and b) the longest length is along the direction of the cable. The antenna's $|S_{11}|$ and the gain is improved for both rectangular sheets in both orientations. The gain is improved by 1 dBi for both orientations whereas the $|S_{11}|$ is improved by 3 dB and 4 dB for orientation (a) and (b), respectively (Figure.6.9). Table 4 shows the advantages of the proposed antenna compared to the existing works. The antenna's gain, bandwidth, return loss, radiation pattern, beam-width, substrate material, impact strength, protective cover/radome usage and their manufacturing complexity and costs were compared. The manufacturing complexity is estimated through the antenna's construction and special parts required such as an injection molded radome/cover, ceramic structures and so on. The manufacturer's suggested retail price (MSRP) is included for the commercial rugged antennas from which an estimate of the antenna's manufacturing cost can be calculated. For instance, the manufacturing cost for a $395 MSRP antenna at 50% gross profit margin would be ~$197.

Table.6.4. Advantages of proposed antenna vs existing rugged antennas

Ref.	Substrate	Gain (dBi)	$\lvert S_{11}\rvert$ Bandwidth (MHz)	Return loss at f_c (dB)	Radiation pattern and Azimuth and Elevation HPBW	Operating Temperature and Humidity without a radome	Impact strength (MPa)	Radome / cover material	Need for protective radome?	Manufacturing complexity and costs
[4]	Undefined	2.0	26	-15.56	Directional 70° and 90°	Not specified	Not Specified	PPE	Yes	High $395 MSRP
[5]	Undefined	9.6	26	-20.0	Directional 90° and 27°	Not specified	Not Specified	Glass reinforced plastic	Yes	High $365 MSRP
[6]	Undefined	3.0	26	-13.97	Directional 80° and 80°	Not specified	Not Specified	Polycarbonate and metal	Yes	High $199 MSRP
[8]	ABS plastic	6.0	50	-17.69	Not measured	Not specified	Not Specified	ABS plastic	Yes	High
[9]	ABS plastic	6.3	20	-18.0	Directional 70° and 70°	Not specified	Not Specified	ABS plastic	Yes	High
[10]	Rogers RO4003C	Not specified	40	-20.0	Not measured	Not specified	Not Specified	Concrete	Yes	Very High
[11]	TMM 10i and TMM 6 Rogers	-1.75	10	-19.9	Bi-Directional. Gain is focused in ±30° beam angle	Not specified	Not Specified	Concrete	Yes	High
[12]	Paper	4	5	-16.5	Bi-directional	Not specified	Not Specified	Concrete	Yes	Moderate
[13]	Ceramic	3.8	10	-15.0	Directional 60° and 60°	Not specified	Not Specified	Concrete	Yes	Very High
This Work	Concrete (Portland Cement)	3.5	160	-18.55	Directional 145° and 116°	-20°C to +70°C	50	None	No	Very Low $8.94

6.6 UHF RFID Performance

The fabricated antenna (first sample) is tested for its UHF RFID performance. An Alien Higgs-3 Squiggle tag is the preferred transponder tag for test purposes which has a dipole-like linearly polarized antenna [22]. An Impinj speedway-R420 RFID reader is used for testing [23]. The reader and the antenna are connected with a 2-meter LMR-195 type coaxial cable which has a cable loss of 0.73 dB [24]. The reader is programmed to ETSI region, and the reader is set to 'auto-set dense reader' mode with a frequency set to 'reader selects frequency' where the reader would transmit in one of the four channels, namely 865.7, 866.3, 866.9 and 867.5 MHz for 4 seconds if tags are being detected and for 1 second if no tags are detected. According to the ETSI standards [14] and [15], the reader must stop transmitting for a period of at least 100 milliseconds. The reader is set to 'dual target' search mode and session '2' for a 'single target inventory' run mode, using Impinj's 'multi-reader' reader control software. The power is set to maximum, 31.5 dBm and the maximum tag detection distance at the antenna's boresight is measured for twelve different configurations.

Table.6.5 lists the maximum read distance for various configurations at the antenna's boresight. The tag's readability away from the antenna's boresight, namely anterior, posterior and bilateral directions are also measured with the same power and cable losses and is documented in Table.6.6. Since the antenna's azimuth and elevation beam is wider, the read range is also extended to its sides. This shows that the proposed antenna can create a very wide RFID read zone. A convention center's dock-door can span up to 18×9 meters [25] and efficient RFID read zone creation is viable with a smaller number of proposed ultra-rugged antennas. Multiple tag performance test is conducted to measure the antenna's ability in detecting a cluster of tags and to measure the antenna's power distribution at far-field distances. The setup mentioned above, and reader configuration is used for this test. A 0.6×1.2-meter polystyrene sheet is constructed for this test. The sheet is divided into six rows and twelve columns where 72 Alien squiggle tags are laid in each cell. The tag sheet is located at 900 mm (< 3 wavelengths) away from the antenna for multiple tag testing. The antenna's input power is varied from 10 dBm in 1 dBm steps and the minimum power required to excite all tags is recorded along with the tag's return signal strength indicator (RSSI). The test is conducted only for two deployment configurations namely, a) antenna attached to concrete and b) antenna recessed in concrete as they both are the worst-case scenarios in comparison with other ten configurations explained before. The tags' and the antenna's polarization are maintained to be the same throughout the testing.

Table.6.5. Boresight read range

Antenna Configuration	Read distance (mm)
Free space configuration at room temperature (20°C) with 85% RH	6500
At high temperature (70°C) with 85% RH	6000
At low temperature (-20°C) with 85% RH	7000
With condensation at 20°C at 20°C and 85% RH	6500
With a splash of water (rain) at 20°C and 85% RH	6000
With 6 mm HDPE superstrate	6500
With 15 mm PVC superstrate	6500
With 6 mm Fiberglass superstrate	6200
Attached to concrete wall (non-reinforced)	5500
Recessed to concrete wall (non-reinforced)	4600
Attached to reinforced steel mesh	6800
Attached to metal sheet (both orientations)	7000

Table.6.6. Circumferential read range

Antenna Configuration	Anterior (mm)	Posterior (mm)	Bilateral (mm)
Free space configuration at room temperature (20°C) with 85% RH	5500	2300	2800
At high temperature (70°C) with 85% RH	5000	2000	2400
At low temperature (-20°C) with 85% RH	6000	2500	3100
With condensation at 20°C at 20°C and 85% RH	5500	2300	2800
With a splash of water (rain) at 20°C and 85% RH	5000	2000	2400
With 6 mm HDPE superstrate	5500	2300	2800
With 15 mm PVC superstrate	5500	2300	2800

With 6 mm Fiberglass superstrate	5200	2100	2600
Attached to concrete wall (non-reinforced)	5200	3200	3000
Recessed to concrete wall (non-reinforced)	5100	2300	1800
Attached to reinforced steel mesh	5800	2400	2900
Attached to metal sheet (both orientations)	6000	2500	3100

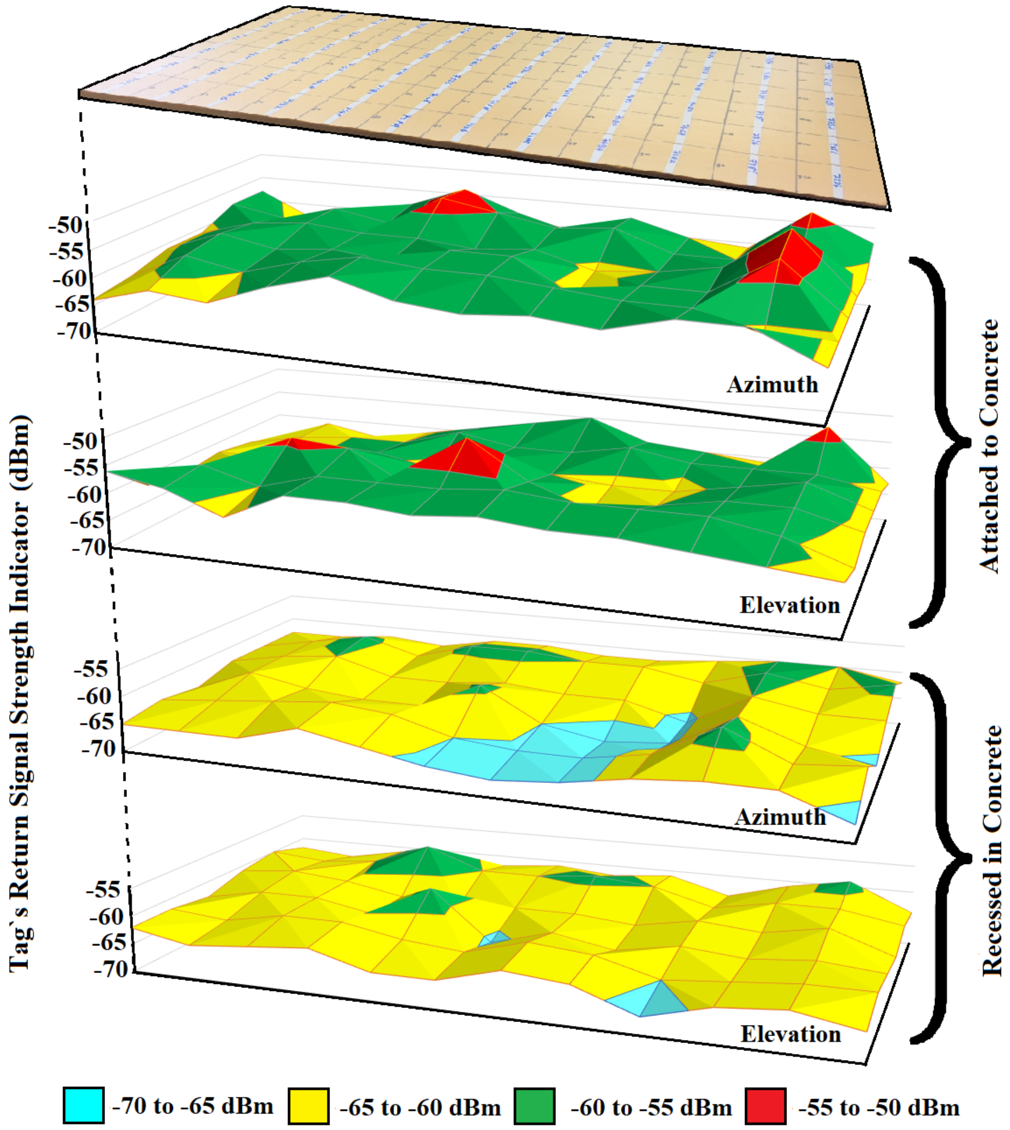

Figure. 6.10. RSSI of Alien Squiggle tag array in azimuth and elevation planes

The antenna that is attached to the concrete required 22 dBm whereas the recessed antenna required 24 dBm as the minimum power to detect all the 72 tags. The power measurement does not include 0.73 dB loss within the cable. The measured RSSI is plotted in a 3D-contour plot to realize a rectangular power distribution. The overall tag's RSSIs were in the range of -60 to -50 dBm and -70 to -60 dBm for the attached and recessed antenna, respectively (See Figure.6.10).

6.7 Conclusion and future work

An ultra-rugged UHF RFID reader antenna is designed in a non-conventional concrete substrate and tested for ETSI UHF RFID frequencies. This robust antenna has a high impact resistance towards mechanical stress and strain and can operate in extreme environmental conditions with and without the presence of superstrates. The antenna is low-cost and suitable for permanent outdoor installation. The antenna deployment is practical as it can be mounted on a concrete wall or recessed into it. The antenna can also be fixed onto a metal cladding or on a pillar that contains reinforcing mesh. The antenna's performance is satisfactory for convention center dock-doors although the gain and the read range reduction is experienced in certain circumstances.

As part of the future work, an antenna will be designed for RFID frequencies prescribed by the Federal Communications Commission (FCC) which operates for 26 MHz in the range of 902 to 928 MHz. A reinforced concrete substrate's effects on the antenna's performance will be analyzed. The antenna's beam-width reduction techniques will be considered in future to limit the stray tag reads (unwanted tags read by the wide beam-width). A circularly polarized antenna version will also be designed for both ETSI and FCC frequencies.

Prelude to Manuscript 4

This manuscript presents an unconventional bandwidth enhancement technique for thin substrate UHF RFID linearly polarized patch antennas. The patch antenna is made from polyethylene dielectric substrate and aluminum adhesive strip conductive layers. A microstrip fed rectangular patch antenna is designed to operate between 902 and 928 MHz UHF RFID frequencies. Impedance bandwidth is enhanced by intentional impedance mismatch at the edge of the patch. An 88.98 MHz impedance bandwidth was achieved through a -32% intentional impedance mismatch. In general, an impedance mismatch will cause RF reflection yielding a poor $|S_{11}|$. The percentage of mismatch offered optimises the bandwidth increase without causing significant reflections.

Antenna`s gain and other parameters were not majorly affected by this technique. This technique is also suitable for other applications operating in 433 MHz or 2.4 GHz. Transceivers that can handle reflected power is recommended to use with this type of bandwidth enhancement.

As patch antenna designs require to be wideband when made from non-conventional materials, this technique can be adopted on its own or in conjunction with other existing techniques.

Chapter 7

Manuscript 4

Bandwidth enhancement of thin substrate UHF RFID patch antenna

7.1 Introduction

Most commercial UHF RFID patch antennas are either made from thick substrate (usually $1/_{10}{}^{\text{th}}$ of the wavelength) or has a stacked patch configuration to achieve the necessary operating bandwidth. This manuscript presents an unconventional and inexpensive way to enhance the impedance bandwidth of a thin substrate ($^1/_{35}$th of the wavelength) microstrip fed patch antenna. The 902–928 MHz RFID band was chosen for demonstration as it is the widest RFID bandwidth allotted by Federal Communications Commission (FCC). One major operational disadvantage of patch antenna is its very narrow frequency bandwidth [1]. Traditionally patch antenna`s bandwidth can be enhanced by insertion of slits and slots in both radiating patch and ground plane [2] or using a thicker substrate [3] or by stacking radiators over the driven patch [4]. Addition of material such as increased substrate or stacked elements increases the cost and size of the antenna. Slotted radiating element and ground planes yield enhanced bandwidth at the cost of poor antenna efficiency and front to back ratio. Bandwidth and gain can also be enhanced with loaded parasitic elements next to the radiating patch [5] or by loaded loops over the radiating patch [6]. Though parasitic elements contribute in gain and impedance bandwidth enhancement of a linearly polarized antenna, a circularly polarized antenna`s axial ratio will get affected. The proposed bandwidth enhancement technique in this manuscript is unconventional and is focused on the feed rather the radiating patch.

7.2 Related works

Conventionally bandwidth of a patch antenna can be enhanced by offsetting the microstrip feed to one side of the patch [7] or using multiple feeds where the same patch is fed by two different locations with 180° phase shift [8]. The antenna`s gain was compromised quite a bit in the former method while the antenna`s maximum radiation was not at the bore sight in the later, which means its directivity is altered. The proposed design in this manuscript would not alter the antenna`s radiation parameters such as beam-width, front to back ratio, directivity, etc., as the shape of the radiating patch remains undisturbed. Bandwidth can also be enhanced by differential feeding technique mentioned in [9-10]. Antennas operate in different modes and bandwidth enhancement is a consequence of dual mode operation. Though the antenna design has a stable radiation pattern, the design required two input feed and not all application such as UHF RFID could afford sacrificing two ports for a single antenna. In addition to this the antenna in these designs are not fed through a microstrip line but are coax-fed.

This means that the design is not low profile and antenna array realization will be complex. The proposed antenna uses a microstrip line feed, an antenna array realization is practical as the patch and the feed network will be in the same plane. The proposed antenna design is simple, as it does not use differential inputs. Electromagnetic coupling is also one among those traditional bandwidth enhancement technique where coupled lines are used to feed the patch antenna [11]. Antenna`s resonant frequency is deviated when this method is used, and H-plane radiation squint is observed due to unsymmetrical feed [11]. The proposed antenna has a symmetrical feed as the patch antennas are edge fed. Defected ground structure (DGS) is an evolving technique to enhance the performance of patch antennas [12]. The antenna`s ground plane is defected either symmetrically or asymmetrically to obtain a DGS. DGS creates a parallel-tuned circuit that offers multiband operation [12]. As the ground plane is defected, the antenna`s radiation efficiency and its directivity are altered. The proposed antenna`s radiation parameters were not altered yet bandwidth enhancement is achieved. Unconventionally bandwidth enhancement was achieved by using a holey superstrate, described in [13]. The problem with this design is when this antenna is covered by a radome there is no guarantee that the enhanced bandwidth will remain unaffected. The proposed bandwidth enhancement technique is based on a single substrate design and does not incorporate a superstrate yet unconventional.

The proposed design can be distinguished from the traditional bandwidth enhancement techniques due to the following reasons;

1. No significant addition of material such as increased substrate or addition of a superstrate or stacked elements. Size and cost of the antenna is not increased therefore.

2. Antenna parameters such as resonant frequency, directivity, beam-width, front-to-back ratio, radiation efficiency is not altered when bandwidth is enhanced.

3. Shape of the radiating patch remained the same and the bandwidth enhancement was achieved through the feed.

4. The patch and the feed network will be in the same plane, thus array realization is easy and cost effective.

5. No differential inputs were used, making the system less complex.

6. Intentional impedance mismatch is an unconventional technique.

7.3 Antenna design and fabrication

A simple microstrip fed rectangular patch antenna is used in this bandwidth enhancement experimentation. The patch antenna operates only in one mode and thus it is linearly polarized. The antenna is designed in polyethylene substrate. This substrate is preferred over other traditional substrates (such as air) in RFID applications for physical robustness. HDPE`s dielectric constant ($\varepsilon_r$) is 2.5 and loss tangent ($\tan\delta$) is 0.0005 [15]. The patch antenna`s length and width are calculated through the following steps [1].

Step 1: Patch antenna`s width (W) is calculated using the free-space velocity of light (v_0), resonant frequency (f_r) and dielectric constant (ε_r), shown in (1).

$$W = \left(\frac{v_0}{2f_r}\right)\left(\sqrt{\frac{2}{\varepsilon_r+1}}\right) \tag{1}$$

Step 2: The effective dielectric constant (ε_{reff}) is calculated using the formula shown in (2). Substrate thickness (h) is 6 mm which is a thin substrate as it is $\frac{1}{35}$th of the wavelength in polyethylene substrate.

$$\varepsilon_{reff} = \frac{\varepsilon_r+1}{2} + \frac{\varepsilon_r+1}{2}\left(1 + 12\,\frac{h}{W}\right)^{-(\frac{1}{2})} \tag{2}$$

Step 3: The free-space velocity of light (v_0), resonant frequency (f_r) and effective dielectric constant (ε_{reff}) are used to find the effective length (L_{eff})

$$L_{eff} = \left(\frac{v_0}{2f_r\,(\sqrt{\varepsilon reff})}\right) \tag{3}$$

Step 4: Length extension (ΔL) is calculated using the width of the patch antenna (W), height or the thickness of the dielectric substrate (h) and the effective dielectric constant (ε_{reff}), shown in (4).

$$\Delta L = 0.412\,h\left[\frac{(\varepsilon_{reff}+0.3)\left(\frac{W}{h}+0.264\right)}{(\varepsilon_{reff}-0.258)\left(\frac{W}{h}+0.8\right)}\right] \tag{4}$$

Step 5: Actual length of the patch is found using the effective length (L_{eff}) and the Length extension (ΔL), shown in (5)

$$L = L_{eff} - 2\Delta L \tag{5}$$

Based on the calculation, patch antenna`s length and width is found to be 100.45 mm and 126.9 mm for 915 MHz resonant frequency. The patch antenna is fed by a microstrip-line. The microstrip-line is also a quarter wave transformer transforming the input impedance 50 Ω to the patch antenna`s edge impedance 137.8 Ω. The quarter wave transformer is 7.08 mm wide and 60 mm long (see Figure.7.1(a)).

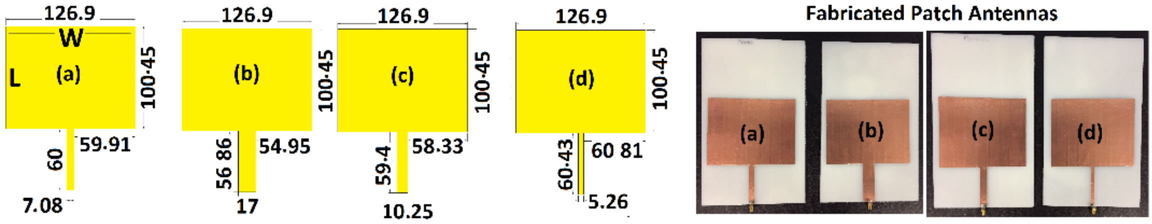

Figure.7.1. Antenna designs and fabrications (dimensions are in mm):

(a) Matched patch antenna design (b) -64% Intentional input mismatch

(c) -32% Intentional input mismatch (d) +32% Intentional input mismatch.

Traditional bandwidth enhancement techniques are based on impedance matching feed network [14] where the antenna`s edge impedance is matched to the input impedance through tuned stubs, etc. The proposed bandwidth enhancement is based on intentional impedance mismatch at the patch antenna`s point of excitation. The radiating rectangular patch antenna`s shape and size are unaltered. Thus, intentional impedance mismatched excitation was applied on the same rectangular patch antenna geometry. The antenna designed in Figure.7.1(b) has an abrupt impedance mismatch at the edge of the patch antenna. The input impedance 50 Ω was carried all the way through a 50 Ω microstrip line and terminated at the edge of the patch antenna. The 50 Ω microstrip line was made quarter wavelength long to maintain the consistency with the matched patch antenna shown in Figure.1(a). The 50 Ω microstrip line is -64% of the patch antenna`s actual edge impedance, 137.8 Ω. Antennas designed in Figure.7.1(c) and (d) has intentional impedance mismatches in its quarter-wave transformer`s impedances. The antenna shown in Figure.7.1(c) uses a quarter wave transformer whose impedance is 68.33 Ω. This transformer will be ideal to transform the 50 Ω input impedance to 93.5 Ω load impedance. As the designed patch antenna`s edge impedance (load impedance) is 137.8 Ω, the quarter wave transformer designed for a -32% edge impedance produces an impedance mismatch. The antenna shown in Figure.7.1(d) uses a quarter wave transformer whose impedance is 95.50 Ω. 95.50 Ω quarter wave transformer is suitable to transform the 50 Ω input impedance to 181.9 Ω. As the designed patch antenna`s edge impedance (load impedance) is 137.8 Ω, the quarter wave transformer designed for +32% edge impedance produces an impedance mismatch. The designed antenna was fabricated (see Figure.7.1) in polyethylene substrate. The substrate is 6 mm thick. Radiating patch is made from strips of copper tape. Ground plane is made from tinned steel sheet. The conductive layers are adhered to the dielectric substrate using non-conductive acrylic adhesive. A SMA flange mount connector is used for excitation.

7.4 Analysis

The fabricated antennas are measured using TR1300/1 vector network analyzer for its return loss. The antenna`s path loss was measured across the frequency using a receiving dipole antenna. Fabricated antenna`s gain is found by comparative method [15]. Using a reference patch antenna (whose gain is known), -29.5dB path loss measured is translated to 0dBi antenna gain. Figure.2 shows the return loss and path loss measurements for all the fabricated antennas. The impedance matched patch antenna resonated at 915.0 MHz with a -26.12 dB return loss. The antenna`s -5dB return loss bandwidth is 79.13 MHz. The return loss at low (902 MHz) and high (928 MHz) RFID frequencies were -12.64 dB and -12.02 dB respectively (see Figure.7.2). Most fixed RFID antennas bear long coaxial cables when installed in sites and the reflections happening within the cable gets attenuated [16]. Moreover, antennas with good SWR will undergo SWR deterioration due to the way assets are tracked in RFID applications (assets sit right on top of the antenna in a point of sale, shelving systems, etc). Modern RFID interrogators has an embedded SWR tuning module and thus they can handle reflected power by the antenna. So, the bandwidth of the antenna is measured at -5 dB return loss. The +32% and -64% impedance mismatched antennas resonated at 918.0 MHz and 928.7 MHz respectively. This resonance is higher than the intended resonant frequency. This is because the quarter wave microstrip lines were not only feeding the antennas but were also acting as tuning stubs, thus changing the F_c [17]. The -32% impedance mismatched antenna was found to be the optimal design as it did not induce a shift in resonant frequency. The antenna resonated at 915 MHz with a return loss of -14.27 dB. Table.7.1 lists the return loss, path loss and the gain parameters for center, low and high frequency of different designs, respectively. The -32% mismatched antenna`s -5dB return loss bandwidth is 88.98 MHz. The return loss at low (902 MHz) and high (928 MHz) RFID frequencies were -11.44 dB and -11.55 dB respectively (see Figure.7.2). This shows that with a -32 % intentional impedance mismatch, the impedance bandwidth is enhanced by 12.5% (9.85 MHz) without significantly altering the return loss at the operating frequencies.

Table.7.1. Measured return loss, path loss and gain.

Antenna Type	Measured Loss	Low Freq		Mid Freq		High Freq	
		F_{low} (MHz)	Loss (dB)	F_c (MHz)	Loss (dB)	F_{high} (MHz)	Loss (dB)
Matched Antenna	Return loss	877.1	-5.04	915.0	-26.1	954.2	-5.08
	Path loss	857.32	-27.4	915.0	-23.7	951.93	-27.4
	Gain (dBi)	857.32	2.08	915.0	5.71	951.93	2.10
-64% Ω mismatch	Return loss	901.7	-4.95	928.7	-5.93	960.7	-5.03
	Path loss	901.73	-26.9	928.7	-26.8	960.71	-27.2
	Gain (dBi)	901.73	2.59	928.7	2.66	960.71	2.22
-32% Ω mismatch	Return loss	870.8	-5.06	915.0	-14.2	959.7	-5.05
	Path loss	849.58	-27.4	915.0	-24.4	955.92	-27.4
	Gain (dBi)	2.01	915.0	5.01	955.92	2.06	2.01
+32% Ω mismatch	Return loss	893.2	-5.07	918.0	-32.3	942.87	-5.04
	Path loss	893.27	-25.3	918.0	-24.3	942.8	-25.9
	Gain (dBi)	4.18	918.0	5.17	942.8	3.55	4.18

The linear gain of fabricated antennas at their resonant frequencies. F_c remained unaltered between matched and the -32% mismatched antenna whereas the other two designs has their Fc shifted to higher frequencies viz., 928.7 and 918 MHz respectively. The gain of the -32% mismatched antenna is 0.7dB less than that of the matched antenna at 915 MHz (F_c). At -5dB bandwidth points, the -32% mismatched antenna has 0.07 dB (at 849.58 MHz) and 0.04 dB (at 955.92 MHz) less gain compared to the -5dB bandwidth points of the matched antenna (at 857.32 and 951.93 MHz respectively). Antenna gain at the edge of the band is not deteriorated significantly. Figure.3 shows the azimuth and elevation radiation pattern of the -32% mismatched antenna. Gain was ~3dB high at 915 MHz compared to the low (870.8 MHz) and high (959.7 MHz) side of the band and thus their beam is smaller than 915 MHz`s pattern. The front to back ratio is -10 dB for 915 MHz. The front-to-back ratio can be improved by using a larger ground plane [1]. Table.7.2 shows the measured beam-width for low, mid and high frequency in both azimuth and elevation planes. Beam-width remained the same regardless of the frequency. Figure.7.3 as well reveals that the antenna`s directivity is not spoiled. Peak radiation is at the antenna`s bore-sight. Both matched and -32% mismatched antennas are tested for UHF RFID applications. Antennas can be deployed in portals, shelves, benchtops, etc where assets may directly be placed over the antennas for inventory tracking. When an object is in contact with the antenna`s radiating element, the antenna`s parameters such as return loss and gain may get affected. Comon objects that comes in contact with the reader antennas are plastic, glass and wood (see Figure.7.3). Figure.7.4 shows the frequency sensitivity of matched and mismatched antennas when objects are in contact with the antennas. The return loss and the path loss of the matched antenna varied quite a bit compared to the intentional mismatched antenna. The frequency shift of a matched antenna varied upto ~30 MHz where as for the -32% mismatched antenna it was limited to ~13 MHz. Results in Figure.7.5 also show that the antenna`s gain is insensitive when items contact the -32% mismatched antenna.

Table.7.2. Measured return loss, path loss and gain.

Antenna Type	**Azimuth Beam-width**			**Elevation Beam-width**		
	F_{low}	F_c	F_{high}	F_{low}	F_c	F_{high}
-32% mismatch	83°	87°	89°	85°	90°	87°

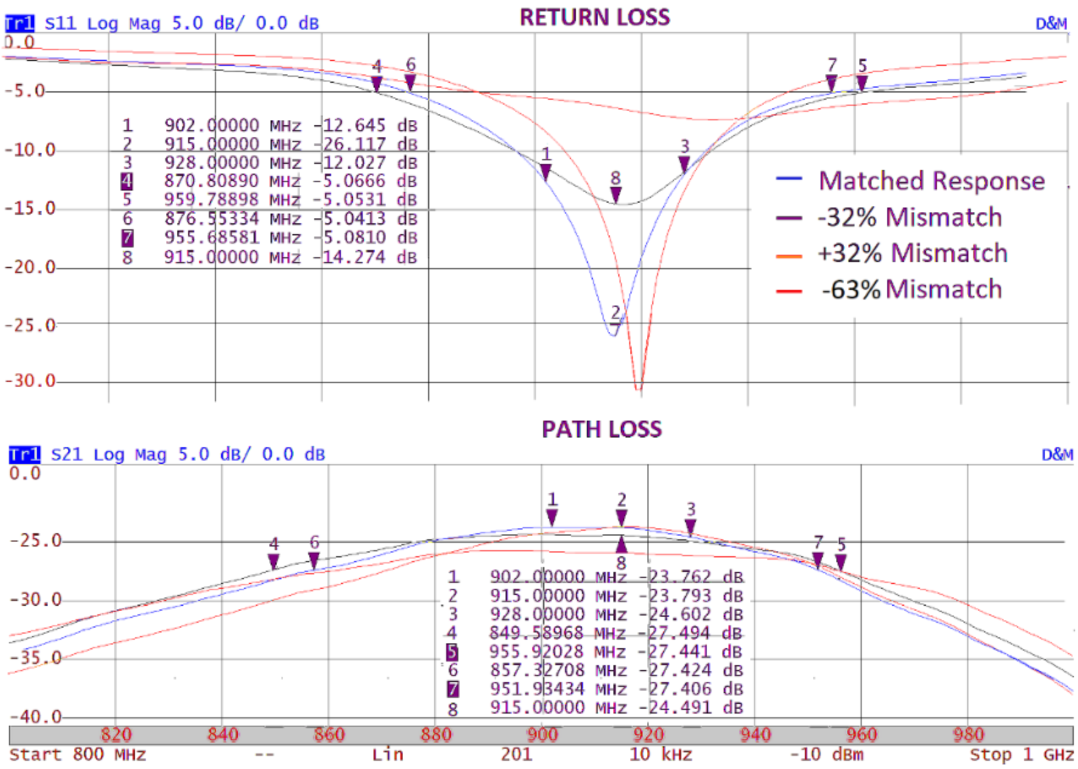

Figure.7.2. Return loss |S11| (top) and path loss |S21| (bottom) measurements.

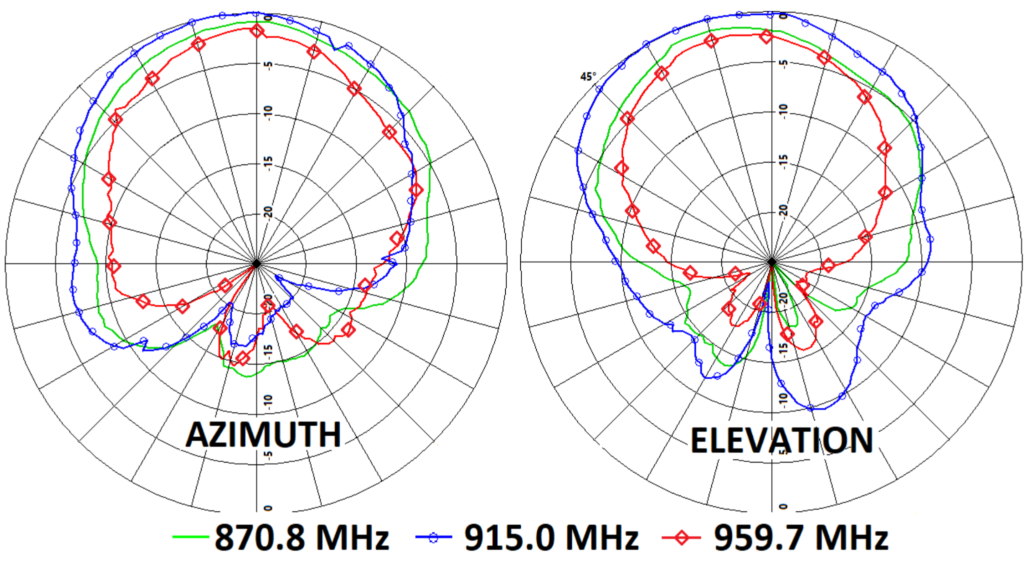

Figure.7.3. Radiation pattern of -32% mismatched patch antenna.

Figure.7.4. -32% mismatched patch with wood, glass and plastic assets.

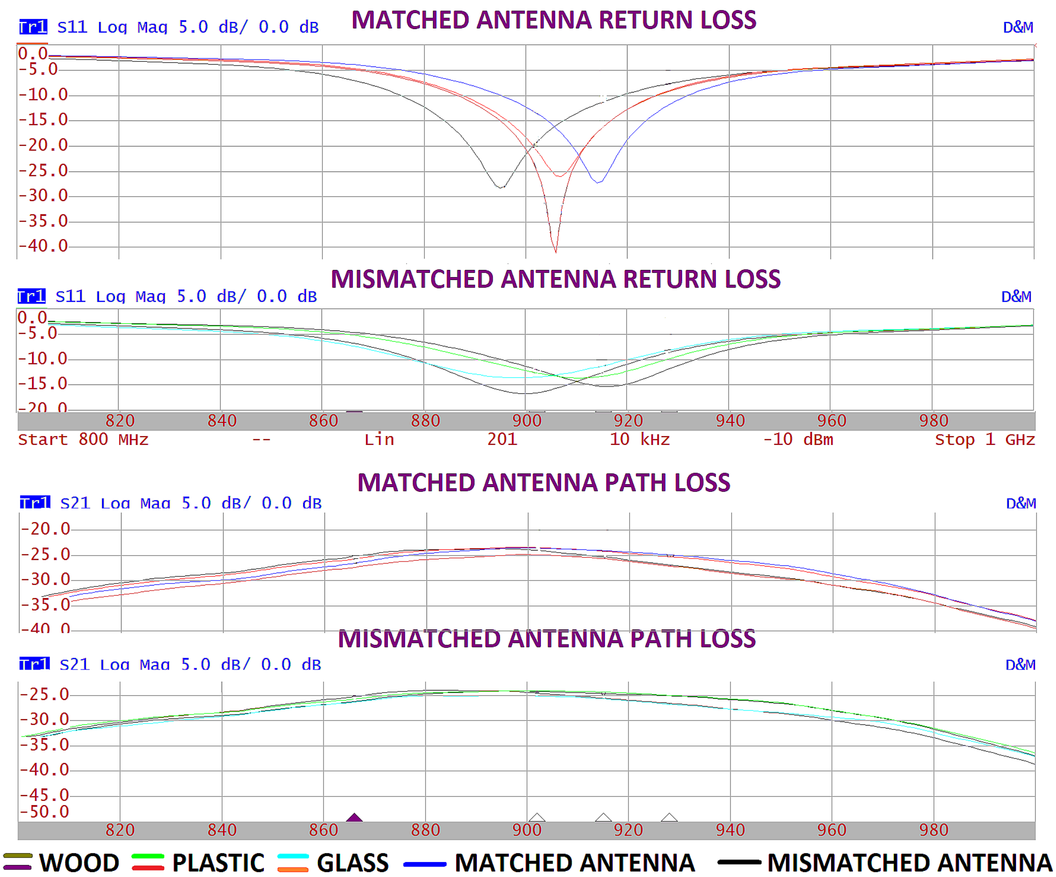

Figure.7.5. Frequency sensitivity on matched vs -32% mismatched antenna.

Table.7.3. Measured RSSI

Reader Output	Frequency (MHz)	902	915	928	902	915	928	902	915	928	902	915	928
10 dBm	**Material**	**Free Space**			**Wood**			**Plastic**			**Glass**		
	RSSI (dB)	-51	-52	-49	-67	-68	-69	-82	-84	-85	-86	-84	-84
20 dBm	**Material**	**Free Space**			**Wood**			**Plastic**			**Glass**		
	RSSI (dB)	-54	-52	-49	-69	-68	-68	-79	-79	-80	-82	-83	-83
30 dBm	**Material**	**Free Space**			**Wood**			**Plastic**			**Glass**		
	RSSI (dB)	-50	-48	-47	-67	-68	-70	-83	-84	-82	-83	-82	-84

The antenna is tested with 'Impinj speedway r420' UHF RFID reader for FCC frequencies (Figure.7.4). The items were tagged using an 'Alien Squiggle Higgs-4' tag. Table.7.3 shows the tag`s return signal strength indicator (RSSI) when the antenna is powered by the Impinj reader (with no cables) at 10, 20 and 30 dBm levels. When the tag was tested at full power (30 dBm) in free space, it reported a highest RSSI value of -47 dB at 928 MHz. When items were placed over the radiating patch, the reported RSSI for different materials remained similar for different frequencies. This is because the antenna`s gain remained similar across the band.

7.5 Conclusion

This manuscript presented a novel and unconventional bandwidth enhancement technique for RFID applications. This single substrate, less complicated technique enhances bandwidth withrout substantially degrading other antenna parameters such as gain, directivity, radiation pattern, etc. This impedance mismatch technique is frequency independent as the microstrip line feed`s impedance stays constant across the frequencies for a given substrate thickness and its dielectric constant. This method is recommended for transceivers like UHF RFID readers that can handle reflected power. As part of future work the same technique will be applied for circularly polarised antenna and antenna array. A circular polarization antenna design uring intentional mismatch will be challanging because of the two modes existing in the same radiator.

Prelude to Manuscript 5

This manuscript presents a low cost, scalable far-field antenna array design with multiple beam and polarization configurations. The scalability of the antenna, i.e., realizing larger antenna with more array elements, can be achieved with less effort and cost than those made from conventional materials. Low cost nature ensues from thin substrate layer and foil conductors. The antenna architecture comprises of four patch elements excited by microstrip lines and a finite ground plane made from aluminium foil sheets sandwiched by a High-Density Polyethylene (HDPE) substrate, whose dielectric constant is determined by the manufacturer.

Standard patch antenna arrays are limited by the inability to scale, non-reconfigurable beam shapes and polarizations, thus relatively expensive. The proposed antenna architecture has the ability to reconfigure beam shapes and switch between vertical linear, horizontal linear and circular polarizations. Furthermore, the antenna's properties of being lightweight, durable, chemical/UV/impact resistance will add more value for various industrial and retail applications. The antenna inherits these properties from the substrate which are proven by the manufacturer. A protective radome may be designed from the same material to protect the antenna. The antenna operates in the FCC frequencies with an operational bandwidth of 28 MHz. Bandwidth enhancement techniques are not applied to this antenna design that is made from a thin substrate.

Chapter 8

Manuscript 5

Low-cost low-profile UHF RFID reader antenna with reconfigurable beams and polarizations

8.1 Introduction

UHF RFID is preferred over the High Frequency (HF) and Low Frequency (LF) tracking systems due to its ability to read tags at a greater distance, inexpensive tag manufacturing potential, higher data rate, and unified Generation-2 (Gen2) standard. Therefore, contemporary industries prefer UHF RFID to traditional barcode, LF and

HF systems. Nevertheless, UHF RFID reader antennas lack smartness in their design. Conventional antenna designs are predominantly used for UHD RFID applications [1-2]. Traditional antennas are realized from materials such as Taconic, FR4 or Rogers, which usually contains copper laminate. These materials are distinctively fabricated in pursuit of high frequency designs and hence they are not cheap. Scaling antenna arrays made from these materials for RFID frequencies results in massive structures and corresponding high costs.

The proposed antenna array design conversely uses High Density Polyethylene (HDPE) as the substrate material and aluminium foil for conductor layers, which are less expensive as they are not specifically used for RF purposes but for other engineering applications. Besides its low cost nature, the proposed design has reconfigurable beam shapes and polarization features, opening doors to different tracking needs such as beam tilt in one direction for eliminating stray tag detection, grating lobes for doorway tracking applications, and so on. The antenna is scalable to suit custom requirement if needed. The suggested manufacturing process to maintain the cost efficacy is by using a decal foil for patch antennas and microstrip line feed network. The decal can be obtained by stamping antenna, feed network patterns and ground plane. This antenna array design shall be considered as smart antenna when combined with software development that can track directions by changing the beam shapes, or changing polarization in environments that require high isolation between wanted and unwanted tags. This design will be very useful for inventory tracking in industries and retail.

8.2 Related works

Most of the existing antennas for UHF RFID applications used traditional substrate and conductors unlike the proposed design using inexpensive materials. The reconfigurable modular antenna designed in [3] is an uncommon spiral antenna with one main port and four additional ports on the spiral boundaries. Curved slots were placed adjacent to the spiral to resonate at 865-868 MHz RFID frequencies. The configurability described by the authors refers to the ability to configure their antenna to work as either a spiral or a slot antenna, unlike the proposed antenna in which polarization and beam patterns are configurable. Moreover, the proposed antenna is a patch antenna array as opposed to spiral and slots. The near-field modular antenna presented in [4] was made from PET substrate. The antenna structures are dipole like meandered lines arranged in a block. The meandered lines are modular and tuned for 865-868 MHz RFID frequencies. Another near-field antenna was designed in [5], which is also based on meandered lines. The authors claimed their antenna is highly scalable and has uniform field distribution. On the other hand, our proposed antenna is a far-field patch antenna and is designed for 902-928 MHz FCC RFID frequencies.

In [6], a single patch antenna design with cut corners is presented where the antenna's polarization can be configured between linear and circular by shortening or opening the truncated corners. This antenna is designed for FCC RFID frequencies but the f_c is off centered at 922.5 MHz instead of 915 MHz. Our proposed antenna can be distinguished from this design by its array configuration, beam steer-ability, low cost nature and the f_c, which is centered at 915 MHz for FCC RFID frequencies. A shaped beam antenna array described in [7] is a rectangular antenna array made from traditional FR-4 substrate. It consists of five elements and a down tilt of 27˚. Our proposed antenna`s beam can tilt to different directions unlike the design in [7], which can tilt only to a fixed direction. Its antenna`s gain was only 6.1 dBi as compared to 10.3 dBi of our proposed antenna. The proposed antenna is made from inexpensive substrate and conductor materials, yielding a low-cost antenna design.

8.3 Antenna design and fabrication

PE100 natural HDPE is a type of polyolefin, which is durable, light weight, non-water absorbent, chemical/ultra violet (UV)/impact resistant, and has low coefficient of friction [8]. The antenna made from this material inherently inherits all these aforementioned properties. PE100 is a virgin natural polyethylene substrate that has a dielectric constant of 2.256 and a loss tangent of 0.0002. The designed antenna array, as shown in Figure.8.1, consists of four square patches each of dimensions 106.5 mm × 106.5 mm. These square patches are designed to resonate at 915MHz (center of FCC band for UHF RFID) and are separated 44.57 mm from each other. The edge impedance of the patch is calculated to be 213.11 Ω. Feed network is designed such that two patches are fed by one input port. The 50 Ω input is split into two 100 Ω branches, and each is matched to the patch`s edge impedance of 213.11Ω through a quarter wave transformer. The quarter wave transformer is 2 mm wide and 68 mm long, translating to an impedance of 145Ω and electrical length of 90˚. The input impedance is stub-matched to compensate the extra inductance induced by the SMA connector. The antenna has a footprint similar in size (300 mm x 300 mm) to common RFID reader antennas [9-10], where however beam steering is not possible as they are single patch antennas made from air dielectric (with a λ/2 of ~160 mm).

As shown in Figure.8.2, a 0.1 mm thick aluminium foil was used for patch elements, feed network and the ground plane. The foil was secured to the HDPE substrate using a non-conductive acrylic adhesive [11], which has 125N/100mm adhesion to metal and 86N/100mm adhesion to plastic. This adhesive has good UV- and solvent-resistant properties, and can withstand temperatures of up to 120°C. Since a special solder was required for soldering onto aluminium, adhesive copper tapes are used, which are capacitively coupled to the aluminium foil at the input where SMA connector is soldered. The total thickness of the antenna without a radome is close to 6.1 mm.

The scalability of the antenna, i.e., realizing larger antenna with more array elements, can be achieved with less effort and cost than those made from conventional materials. A rear connector can also be used and soldered (using special solder) to avoid usage of copper tape. A small air gap of ~1-2 mm is preferred between the patches and radome to avoid superstrate effect from the radome. The total material cost per array module is $9.35 USD (See Table.8.1). Future work will further consider the labor and tooling costs (e.g. die-stamp for antenna pattern) involved in manufacturing the antenna, and will include gauge repeatability and reliability (R&R) study and yield analysis.

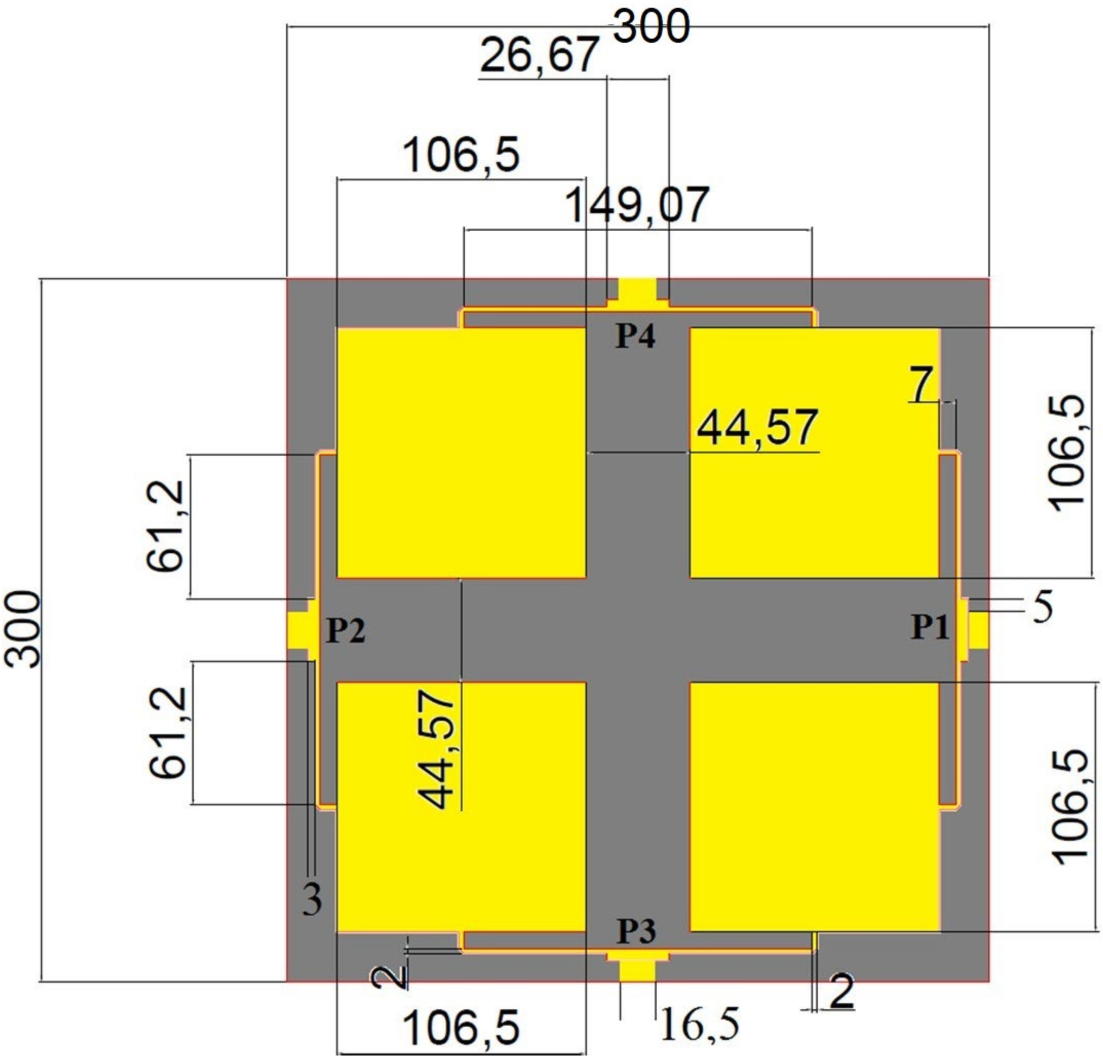

Figure.8.1. Antenna design (dimensions are in mm)

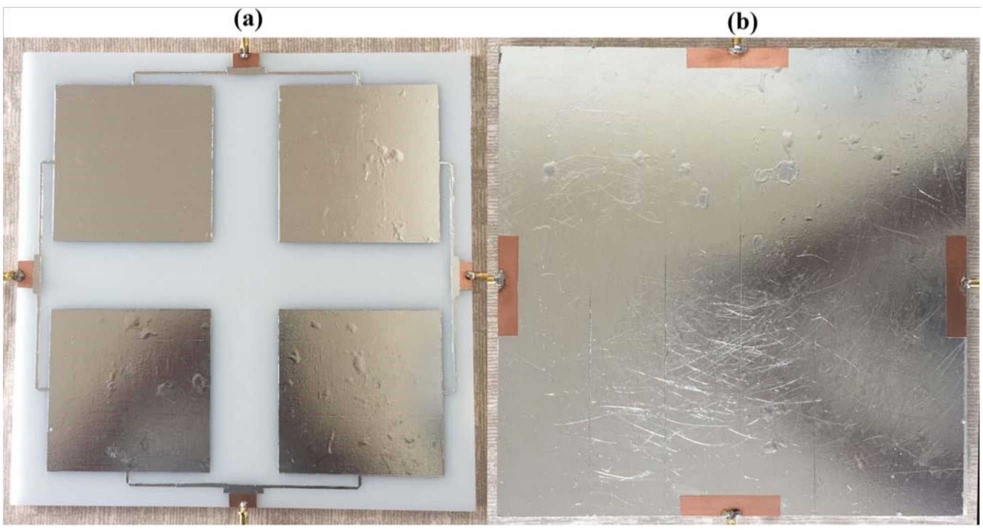

Figure.8.2. Fabricated antenna: (a) front face (b) back face

Table.8.1. Proposed antenna's bill of materials

Part Description	Cost (USD)	Quantity Used	Sub-Total (USD)
Aluminium foil	$3.50 (W-0.3m, L-30m)	W-0.3m, L-0.3m	$0.035
HDPE Substrate	$53.36 (W-1.2m, L-2.4m)	W-0.3m, L-0.3m	$1.6675
3M Copper Tape	$32.87 (W-10mm, L-73m)	W-10mm, L-25mm	$0.052
SMA connector	$1.90	4	$7.60

8.4 Analysis

Method of moments (MoM) based EM simulator was used to design the antenna, which was then fabricated based on the antenna pattern acquired from the simulation, and characterized using a HP8753D vector network analyzer.

8.4.1 Simulation

MoM based ADS momentum software was used for simulating the antenna design, which is less complex for planar RF structures such as patch antennas. The HDPE substrate`s ε_r, tanδ and thickness were defined as 2.3, 0.0002, and 6 mm, respectively. The aluminium conductors do not have any surface roughness, and their conductivity and thickness were defined as 3.72×10^7 Siemens/m, and 0.1 mm, respectively. The patch antennas, feed network and finite ground plane share the same conductor`s properties. Ports P1, P2, P3 and P4 were 50Ω + 0i and are transmission line calibrated. The simulation frequency was chosen to range between 800-1000 MHz. Mesh frequency was defined to be the maximum simulation frequency, and the mesh density used is 20 cells per wavelength.

Figure. 8.3 shows the return loss (S_{11}, S_{22}, S_{33}, S_{44}) and isolation (S_{21}, S_{41}, S_{31}; S_{42}, S_{32}, S_{12}; S_{43}, S_{23}, S_{13}; S_{34}, S_{24}, S_{14}) plots for all four ports. The results show that resonance is consistent and the array resonates at f_c = 915 MHz. The worst case isolation loss was noted to be -14 dB. Different polarizations: horizontal linear, vertical linear, right hand circular (RHCP), left hand circular (LHCP) can be obtained by modifying the magnitude and phase at the input (See Table.8.2). Figure.4 shows the azimuth and elevation beam pattern for both linear and circular polarizations. Beam-width is symmetrical as all four patches are equidistant from each other. Maximum gain at bore sight is noted to be 10.3 dBi for linear polarization and 10.3 dBiC for circular polarization array. Half power beam-width (HPBW) is noted to be 53˚ and 55˚ for linear and circular polarization configurations, respectively. Front-to-back ratio is 10.25 dB and 10.3 dB for both polarizations.

Figure.8.5 shows the axial ratio for circularly polarized array is 0.8 dB at bore sight and 1.7 dB at the half power site, along with other antenna parameters such as the antenna`s directivity, radiation efficiency, and so on. Beam tilts can be achieved by changing the phase between ports (See Table.8.3) and are only possible with linear polarization. When the beam is tilted, its symmetry is no longer maintained, and thus the HPBW will be different for azimuth and elevation beam patterns. Figure.8.6 shows the left and right tilted beams when P1 and P2 are configured according to Table.8.3. Tilt angle can be changed by varying the phase. Current tilt angle is ~21˚. When beam is tilted, minor side lobe emerges. The side lobes can be suppressed by energizing the third port (See Table 4).

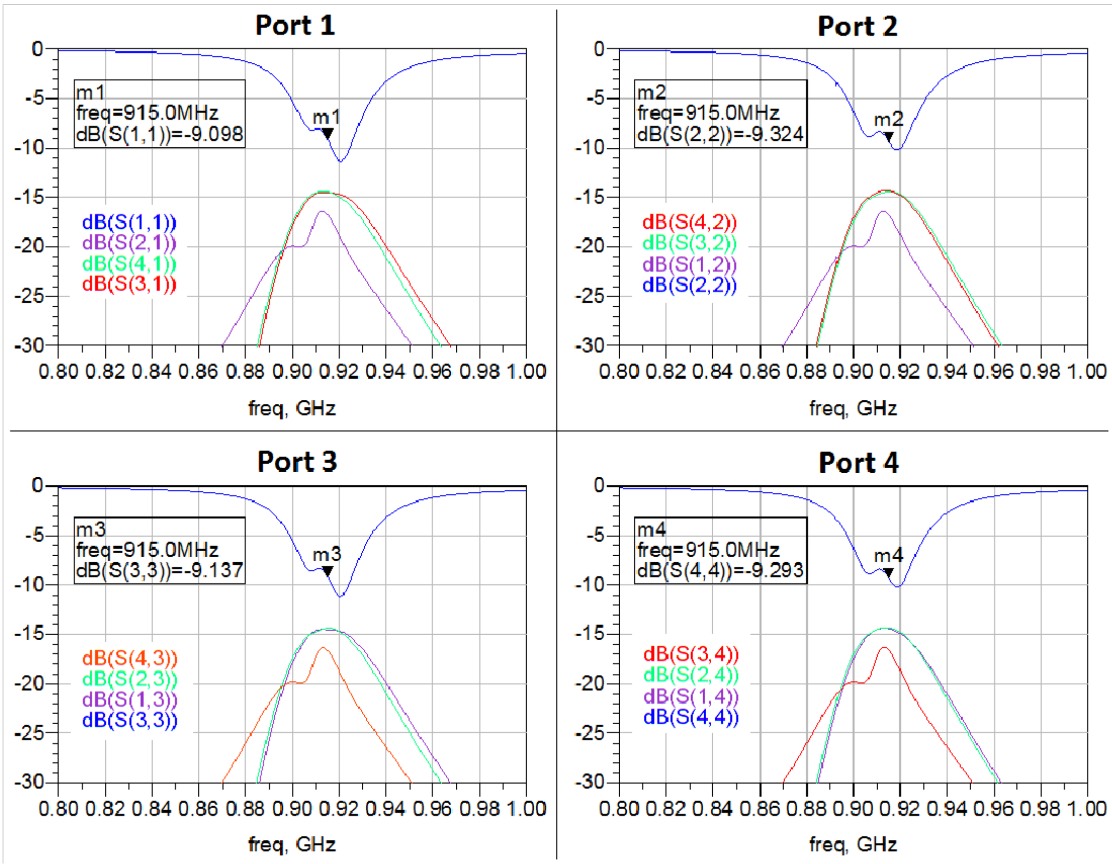

Figure.8.3. Simulated return loss (S_{11}, S_{22}, S_{33}, S_{44}) and isolation (S_{21}, S_{41}, S_{31}; S_{42}, S_{32}, S_{12}; S_{43}, S_{23}, S_{13}; S_{34}, S_{24}, S_{14})

Table.8.2. Polarization configurations

Polarization / Orientation	**Port 1**		**Port 2**		**Port 3**		**Port 4**	
	Mag	**Phase**	**Mag**	**Phase**	**Mag**	**Phase**	**Mag**	**Phase**
Horizontal Linear	Hi†	0°	Hi†	180°	Lo‡	n/a	Lo‡	n/a
Vertical Linear	Lo‡	n/a	Lo‡	n/a	Hi†	0°	Hi†	180°
Circular RHCP	Hi†	0°	Hi†	180°	Hi†	90°	Hi†	270°
Circular LHCP	Hi†	0°	Hi†	270°	Hi†	180°	Hi†	90°

†7.07 Vrms with a 30 dBm transmitter
‡ 0 Vrms (i.e. transmitter is off)

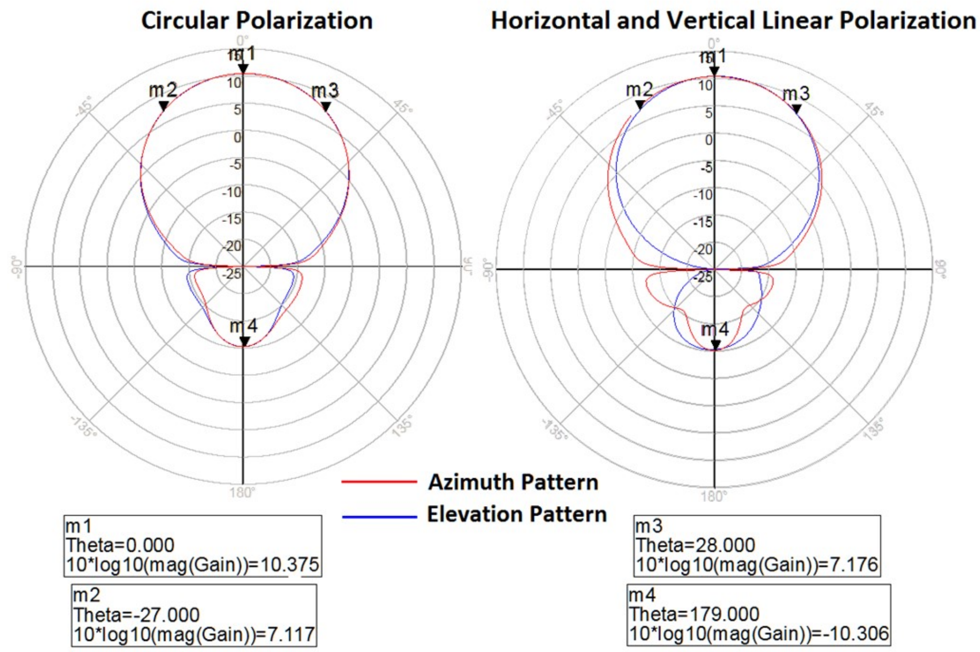

Figure.8.4. Simulated beam pattern for circular and linear (horizontal and vertical) polarizations

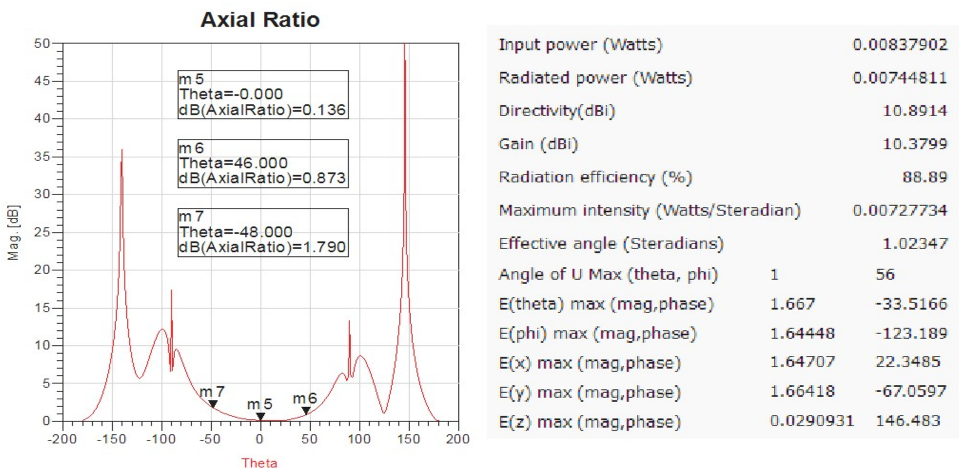

Figure.8.5. Axial ratio and antenna parameters

Table.8.3. Beam tilt configurations

Tilt	Port 1		Port 2		Port 3		Port 4	
	Mag	**Phase**	**Mag**	**Phase**	**Mag**	**Phase**	**Mag**	**Phase**
Right: towards P1	Hi†	0°	Hi†	90°	Lo‡	n/a	Lo‡	n/a
Left: towards P2	Hi†	90°	Hi†	0°	Lo‡	n/a	Lo‡	n/a
Front: towards P4	Lo‡	n/a	Lo‡	n/a	Hi†	90°	Hi†	0°
Back: towards P3	Lo‡	n/a	Lo‡	n/a	Hi†	0°	Hi†	90°

†7.07 Vrms with a 30 dBm transmitter

‡0 Vrms (i.e. transmitter is off)

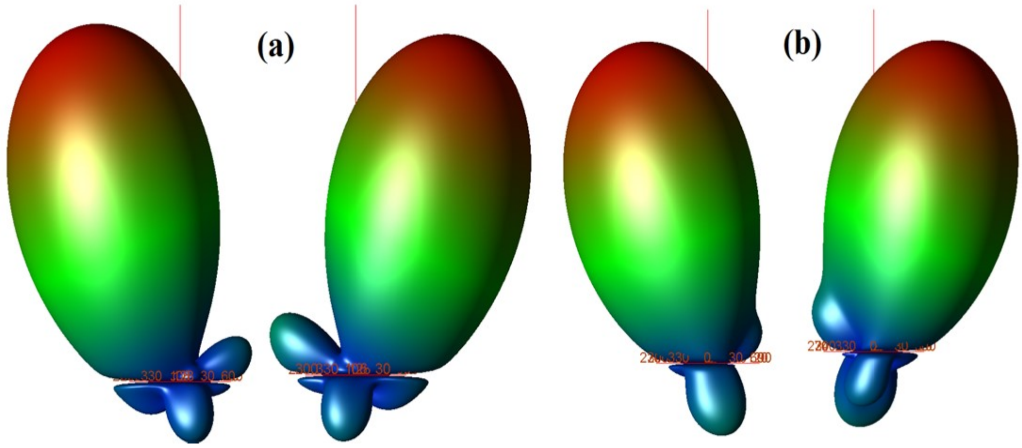

Figure.8.6. Left and right tilted beam: (a) with side lobes; (b) suppressed side lobes

Different corner beam tilts configurations are achieved by energizing all four ports with different delays, as shown in Table.8.5. Figure.8.7 shows the beams towards right and left corner.

Table.8.4. Sidelobe suppression

TILT	Port 1		Port 2		Port 3		Port 4	
	Mag	**Phase**	**Mag**	**Phase**	**Mag**	**Phase**	**Mag**	**Phase**
Right: towards P1	Hi†	0°	Hi†	90°	Lo‡	n/a	Hi†	0°
Left: towards P2	Hi†	90°	Hi†	0°	Hi†	0°	Lo‡	n/a

†7.07 Vrms with a 30 dBm transmitter
‡0 Vrms (i.e. transmitter is off)

Table.8.5. Corner beam tilts

TILT	Port 1		Port 2		Port 3		Port 4	
	Mag	**Phase**	**Mag**	**Phase**	**Mag**	**Phase**	**Mag**	**Phase**
Right bottom corner	Hi†	0°	Hi†	90°	Hi†	0°	Hi†	90°
Left top corner	Hi†	90°	Hi†	0°	Hi†	90°	Hi†	0°

†7.07 Vrms with a 30 dBm transmitter

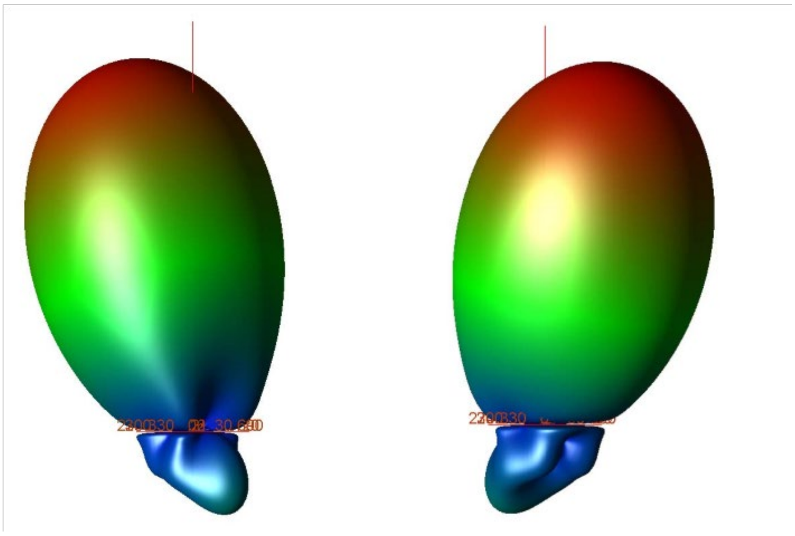

Figure.8.7. Left top and right bottom corner tilts

Grating lobes can be generated by energizing P1 and P2 180˚ out of phase. Similarly, P3 and P4 can be powered 180˚ out of phase to generate grating lobes. An antenna with grating lobes can be used on doorways where the beam is focused on the stores rather filling up the doorway, increasing the chance of finding a nonstationary tag. Figure..8.8 shows grating lobes protruding in store 1 and 2 when the antenna is mounted on a doorway.

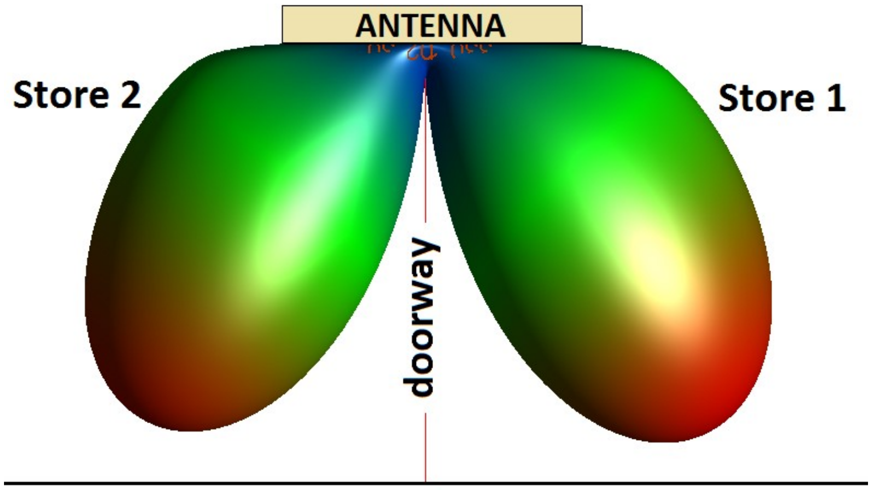

Figure.8.8. Grating lobe doorway configuration

8.4.2 Hardware measurements

The fabricated hardware was measured using VNA in an anechoic chamber for its return loss and isolation (Figure.8.9). The fabricated antenna`s performance is slightly better than the simulated results as ADS momentum is only a 2.5D simulator, which considers only RF currents traveling in x and y directions unlike a 3D simulator. Since HP 8753D is a 2 port VNA, all four ports cannot be measured at once, but rather were swapped for measurements. Figure.8.9 shows the return loss for all four ports. The antenna array module resonates at 915 MHz (marker 2) in all four ports with a worst case return loss of -16.8 dB. Resonances span between 902 (marker 1) and 928 MHz (marker 3) covering all FCC frequencies. –7dB bandwidth is measured to be 46 MHz in all four ports. The antenna may require slight tuning to accommodate a radome, as it may detune the antenna`s performance. As shown in Figure.8.10, the worst case isolation of -10.5 dB is noted in S_{43}. The results show that there is minimal RF leakage through other ports when input port is powered. The antenna gain at 915 MHz was measured to be 7.525 dBi for the 2-patch array at port 1−4. Port 1 and 2 were driven 180° out of phase using an external power divider and a phase shifter to find the gain of the 4patch array. The gain was measured to be 10.173 dBi for the 4patch array configuration, linearly polarized (for both port 1+2 and port 3+4 excitation) and 7.6 dBi (10.6 dBiC) for the 4-patch array configuration, circularly polarized. Figure.8.11 shows the measured gain when comparing the path loss measurements (S_{21}) against a 6 dBi reference antenna. The axial ratio for the circularly polarized 4-patch array was found to be less than 2 dB.

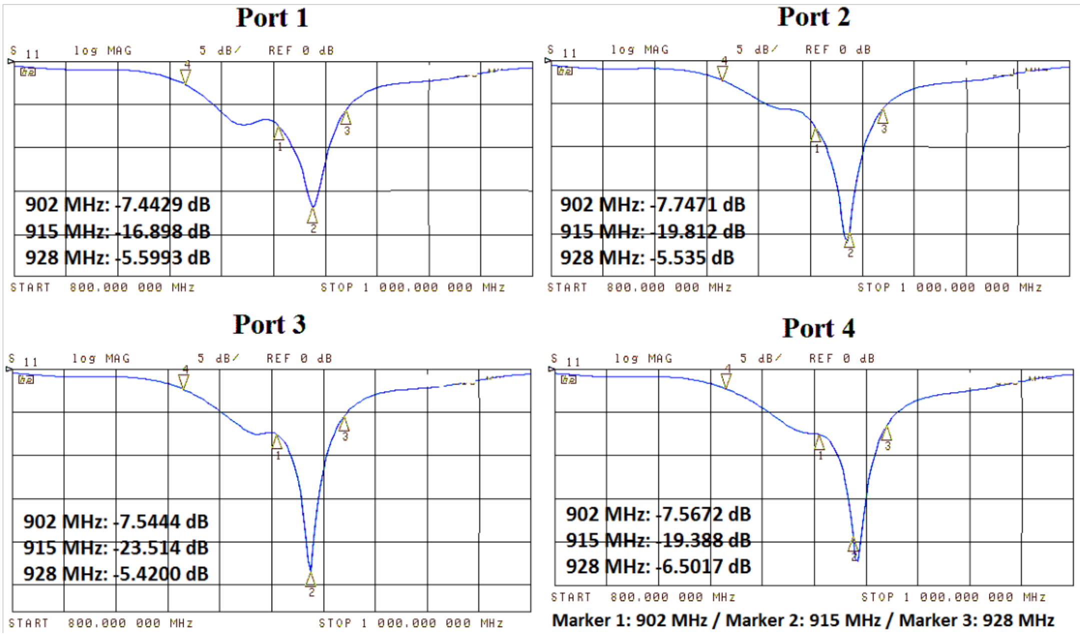

Figure.8.9. Return loss (S_{11}, S_{22}, S_{33} and S_{44}) of fabricated antenna

Figure.8.12 shows the measured beamwidth for linear and circular polarization configurations. The azimuth and elevation beam patterns are more or less symmetric yielding a half power beamwidth of ~60° in both planes. The front-to-back ratio was measured to be -17 dB. Since the ground plane is relatively small for this 4 element array, the antenna experiences back radiation. Electrically the ground plane can be increased by putting a series of slots which can improve the front-to-back by a few dBs. In practice, when these antennas are mounted on surfaces such as walls or ceilings, the antenna`s back radiation shall not be a problem and may be ignored completely.

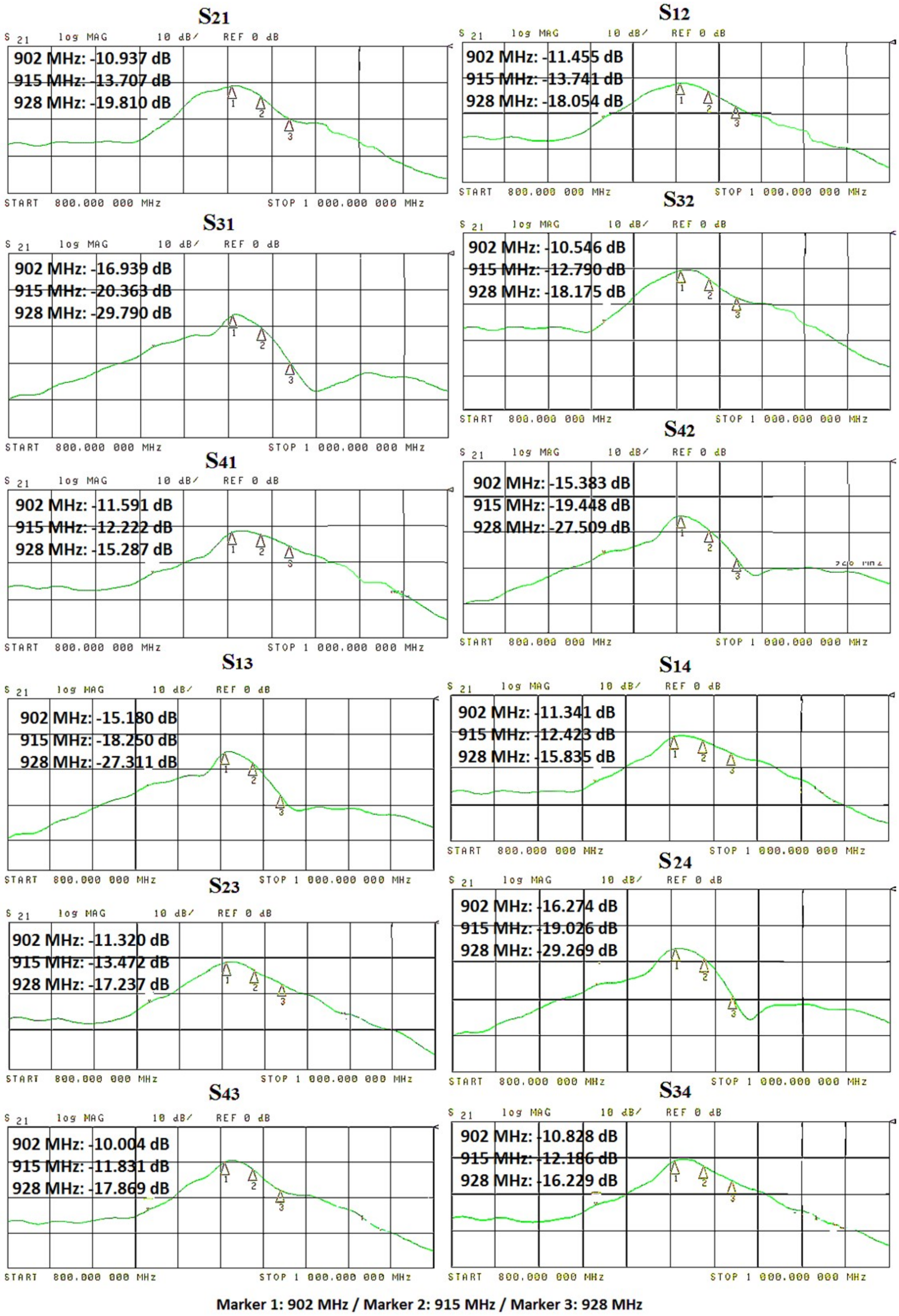

Figure.8.10. Isolation (S_{21}, S_{41}, S_{31}; S_{42}, S_{32}, S_{12}; S_{43}, S_{23}, S_{13}; S_{34}, S_{24}, S_{14}) of fabricated antenna

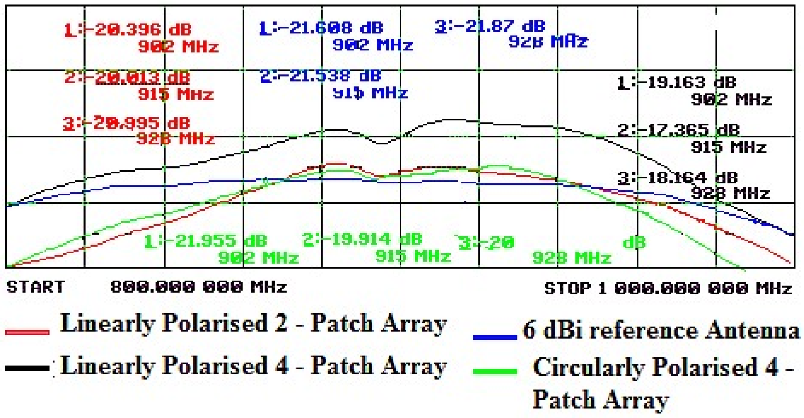

Figure.8.11. Pathloss measurements

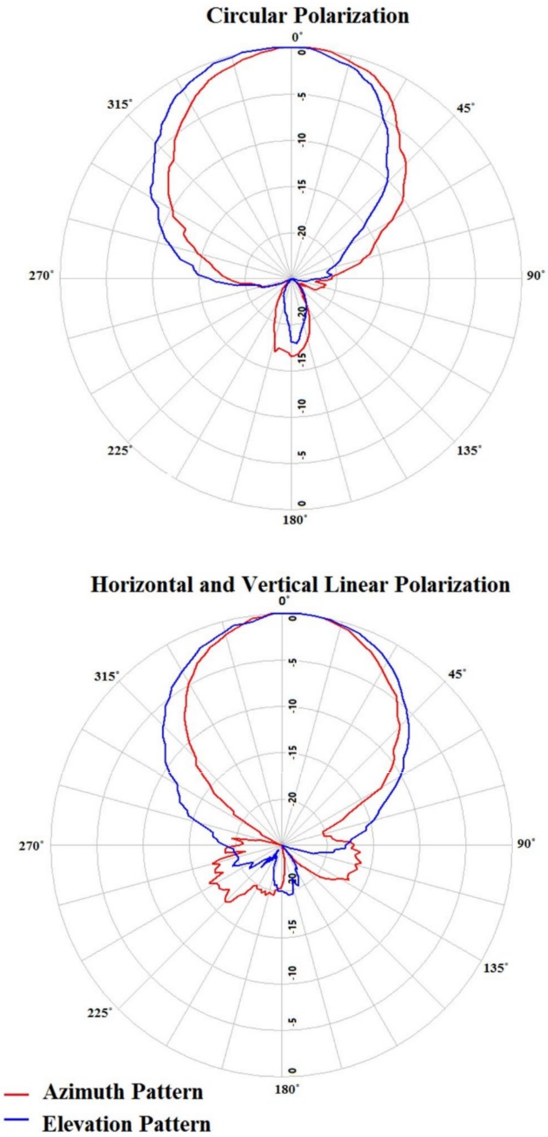

Figure.8.12. Measured beam pattern for circular and linear (horizontal and vertical) polarization

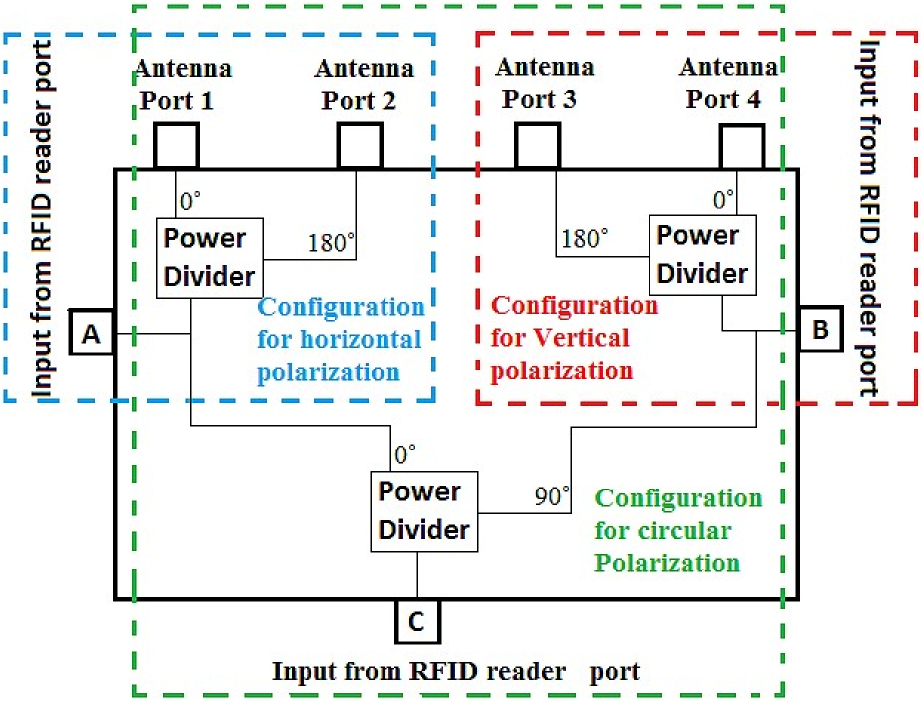

Figure.8.13. External module for changing polarizations

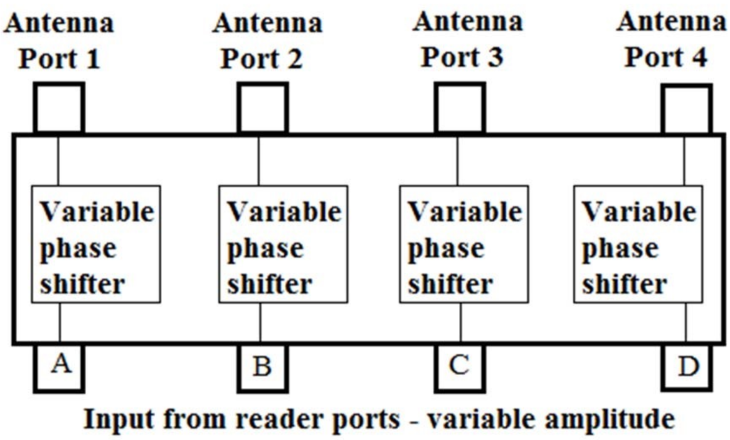

Figure.8.14. External module for changing beam angles

Unlike commercially available beam forming antennas such as Impinj X-array gateway (integrated reader-antenna module) [12] the proposed design is a standalone antenna that can be used with any UHF multi-port RFID reader module. Customization is possible with the proposed antenna system. Polarization can be altered between vertical linear, horizontal linear and circular which are not possible with X-array gateways.

Different beam shapes and polarizations are achievable by altering the signal power and phase in RFID readers. The phase can be altered simply by having different length coaxial cables between the antenna and RFID reader whereas power can be set through the RFID reader user interface. Alternatively, as shown in 2017 IEEE International Conference on RFID (RFID) Figure.8.13, an external module can be designed that connects to all four ports of the antenna to obtain the desired polarizations. Figure.8.14 shows that various beam tilt angles (including grating lobes) can be achieved by changing reader`s input amplitude in conjunction with phase using a variable phase shifter.

8.5 Conclusion and future work

A low-cost and low-profile UHF RFID antenna with reconfigurable beam shapes and polarization has been designed and characterized for FCC RFID frequencies. The substrate`s inherited properties makes the antenna durable, light weight, non-water absorbent, chemical/UV/impact resistant. As part of the future work, an external module connecting to all four ports of the antenna with a select switch for selecting the desired polarization and/or beam shapes, will be designed, and the antenna`s grating lobe configuration will be field tested using RFID tags. A similar antenna will also be designed for ETSI RFID frequencies (865–868 MHz) and its manufacturing cost, gauge R&R and process yield will be analysed.

Prelude to Manuscript 6

In this manuscript, a novel design of a probe-fed circularly polarized (CP) patch antenna on a 3D-printed concave-shaped substrate is proposed. The substrate is a combination of two virgin materials: air and PLA. Using the 'Maxwell-Garnett equation' with dielectric constant 1 for air and 3.2 for PLA whose volume fraction δ is 10%, the theoretical effective dielectric constant is calculated to be 1.1295. The measured effective dielectric constant using patch antenna resonance method is 1.222. This discrepancy of 0.0925 in the dielectric constant may be attributed to the tolerances of the 3D printer used.

The radiating patch conforms to the concavity of the substrate surface, and the circular polarization is achieved by two pairs of asymmetric slot perturbation. These arc- slot perturbations create asymmetry in the resonant lengths, making the currents to take longer path to add the 90° phase shifts, similar to how a traditional corner-truncated patch will have varying resonant lengths between their diagonals. The centre slot is used to tune the antenna's resonance as it was resonating at a higher frequency. The varying substrate thickness due to the concavity across the cross-section enhances the antenna's bandwidth by 20 MHz (2%) compared to traditional flat substrates. As the height of the substrate increases, the patch antenna's 'Q' decreases, thus increasing the bandwidth. The spherically curved surface focuses the antenna's radiation by narrowing its half-power beam-width (HPBW). The gain, HPBW and axial ratio of the antenna are also less susceptible to the effects of having a large ground plane. A large reflector ground plane was to simulate the effect of the antenna's performance when attached to a metal surface. In practice, the antenna may be installed on a metal wall or on a metal chassis, in the case of a vehicle mount application. Moreover, the small foot-printed low-gain antenna's gain can be boosted by simply installing on to a bigger ground plane surface.

The results are verified by comparing the measured performance of the proposed antenna with that of a conventional corner truncated circularly polarized patch on a 3D-printed flat substrate. The comparison is made to show that the proposed antenna's performance is superior. The proposed antenna is designed for sub-GHz industrial, scientific and medical radio (ISM) band (865-868 MHz) and has 7 dBiC gain and near 0 dB axial ratio with 65° and 61° HPBW in elevation, and azimuth planes, respectively.

Chapter 9

Manuscript 6

3D printed circularly polarized concave patch with enhanced bandwidth and radiation pattern

[P. Parthiban, B. Seet and X. J. li, "3D Printed Circularly Polarized Concave Patch with Enhanced Bandwidth and Radiation Pattern," *Submitted to a journal*, 2020].

9.1 Introduction

3D printing technology has attracted significant attention in recent years due to its customizability, affordability, continuous manufacturability, and versatility in prototyping. This manuscript discusses a novel patch antenna design for sub-GHz ISM band (865-868

MHz) that has enhanced radiation and bandwidth properties. The antenna substrate is 3D printed to form a concave shape only on one side of the substrate, and the other side is maintained flat. The radiating patch takes the shape of the concave substrate. As the substrate thickness varies across the length and width of the patch, the antenna resonates at different frequencies to enhance the operating bandwidth. The concave-shaped patch focuses the beams at boresight direction to enhance the radiation pattern. Besides, the *bio-degradable* PLA substrate (used for 3D printing) and *recyclable* copper foils (radiator and ground plane) yield an *eco-friendly* antenna design, which is also light weight and low cost.

9.2 Related works

A wide range of recent 3D printed antenna designs such as the 3D printed lens antenna in [1], 3D printed antenna cavity for liquid metal alloy elements in [2] and 3D printed antenna with conductive filaments [3] are prevalent. These novel works did not include any patch antenna designs. 3D printed patch antenna designs discussed in [4, 5] are relevant to compare. The authors in [4] proposes an inhomogeneous flat (cuboid) shaped substrate with air slots for patch antennas. A shunt varactor diode is used to tune the patch antenna's frequency of operation bearing L-shaped slots while maintaining the circular polarization. The proposed manuscript is distinguishable from this work as it has a concave-shaped substrate that is homogeneous. A compact 3D printed antenna technology is introduced for nano-sat/cube-sat applications in [5]. The substrate printed with hollow structures is still cuboid in shape rather concave as proposed in this manuscript.

There are a few works reported in the literature that are known as concave patch antennas. These works refer to the two-dimensional patch's shape rather the three-dimensional concave shape. A patch can be designed from any geometry viz., square, rectangle, circle, hexagon, and so on. Works reported in [6, 7] bears a concave-shaped geometry on a flat cuboid-shaped substrate. This should not be confused with the proposed concave-shaped substrate and the patch conforming to this shape. Hence, the proposed antenna design is completely different from [6, 7]. A concave shaped lens in [8] is 3D printed from a dielectric material and is used to shape the antenna's beam by loading it directly on top of /the patch antenna that is made from a cuboid substrate. Although a concave dielectric is 3D printed in [8], this design is not the same as the proposed one where the printed dielectric is used as the patch antenna substrate. The three-dimensional circular patch design mentioned in [9] is not 3D printed. The substrate with a hole in the center is electroplated to obtain an indent in the circular patch at its center. This is not a concave patch, but rather it has a stepped indent at the center. This work supports better impedance matching, but it does not provide improved bandwidth and radiation pattern characteristics like the proposed work.

A conformal bent dielectric resonator antenna (DRA) with a bent ground plane proposed in [10] is probably the comparable prior art that needs to be critically analyzed. This work focusses more on the DRA design which includes a curved ground plane and a curved substrate with a slot to excite a curved dielectric resonator located over the substrate. This design is compared with a curved microstrip patch antenna to prove that the DRA's performance is better. The patch antenna reported in this work is wholly curved into a concave shape (including the ground plane) whereas the proposed work has a flat ground plane and the substrate is concave only on one side. Curving the substrate does not change the dielectric substrate's thicknesses along its length and width, whereas, in the proposed work, the continual change in substrate thicknesses enhances the antenna's bandwidth. Although the reported bent antenna's beam-width is focused, it is not as directional as the proposed work. Finally, the proposed concave shape is three-dimensional (bent in both x and y-direction and concavity is along the z-direction) whereas the work in [10] is bent only in one direction (along the x-direction and concavity towards z-direction). Therefore, the proposed antenna is distinguished from [10], and this manuscript presents for the first time, the design of a patch antenna on a 3D-printed PLA substrate that is concave shaped for sub-GHz ISM-band applications.

9.3 Substrate design and fabrication

An ANET-A8 3D-printer is used for fabricating an 18 mm thick concave-shaped substrate with 18° edge and 36° inner concavity (Figure.9.1) at a 10% density using PLA filament. The concave angles are obtained by interconnecting the 6 mm substrate thickness at the center to 18 mm thickness at the edges and 12 mm thicknesses at the center of the edges.

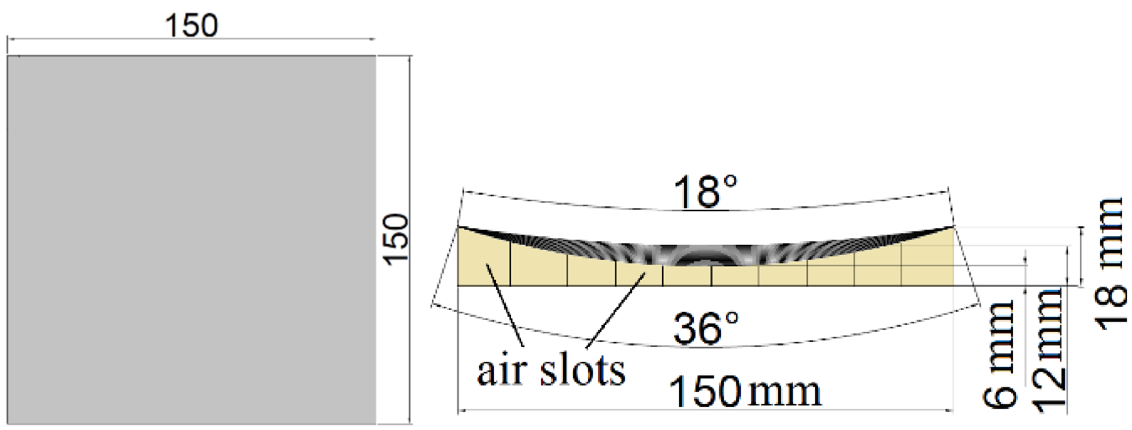

(a) (b)

Figure.9.1. (a) Concave Substrate's top view; and (b) Concave substrate's cross section view

The 10% substrate density consists of a solid outer skin and honeycomb core with air slots. Figure.9.2(a) illustrates the air-filled honeycomb core and solid skin, for the concave substrate. As the fabricated substrate (Figure.9.2(b)) includes air slots, its effective dielectric constant (D_k) can be different from that of PLA at 3.549. Hence, effective D_k is estimated section 9.4 by employing the resonant frequency method [11].

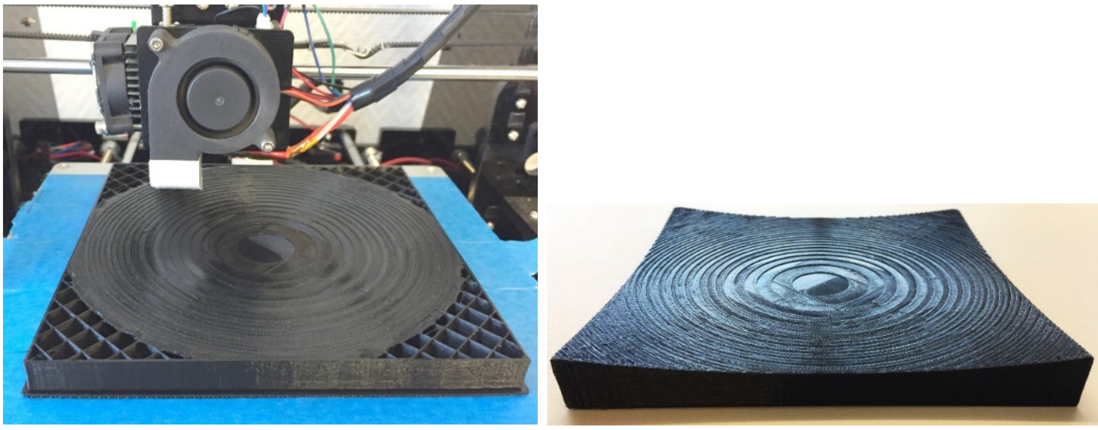

(a) (b)

Figure.9.2. (a) ANET-A8 3D-printer printing the concave substrate; and (b) Fabricated concave substrate

9.4 Substrate characterization

An 18 mm thick flat (cuboid) substrate (Figure.9.3) is printed with 10% density using the same PLA material that is used to print the concave substrate. A similar air-filled honeycomb core with solid skin (Figure.9.4) is designed for the D_k characterization. A 140 mm × 140 mm linear patch antenna is designed (Figure.9.5) and fabricated on the 3D printed cuboid substrate. The radiating element and the ground plane are made from copper sheets and are attached using non-conductive acrylic adhesives. The patch's dimensions are approximated using an assumed dielectric constant of 1.2, which is slightly higher than the free space D_k value. The ground plane size is 150 mm x 150 mm. The antenna is excited using a rear 50 Ω SMA connector.

When measured using a TR/1300 vector network analyzer (VNA), we found that the antenna resonates at 850 MHz with -19.248 dB return loss. When this resonant frequency

(f_r) and the antenna's length and width are equated back in equations (1-3), we can obtain the effective substrate D_k (air + PLA) as 1.222. As the substrate is a honeycomb structure with only 10% PLA and 90% air, 1.222 D_k is probably right. The antenna is simulated using ADS EM software to verify the estimated D_k (Figure.9.6). The simulated and measured D_k results are similar, and thus, the patch antenna resonance method used to characterize the substrate's D_k is accurate.

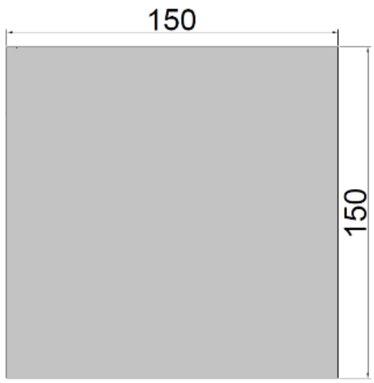

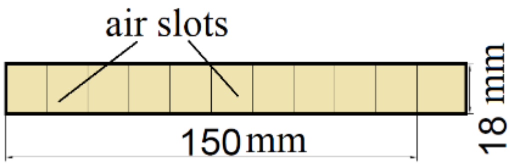

(a) (b)

Figure.9.3. (a) Cuboid Substrate's top view; and (b) Cuboid substrate's cross section view

The width (w) of the patch antenna is given by

$$w = \left(\frac{v_0}{2f_r}\right)\left(\sqrt{\frac{2}{\varepsilon_r+1}}\right) \tag{1}$$

where, v_0 = free-space velocity of light

f_r = resonant frequency

ε_r = dielectric constant

The patch antenna's length is given as

$$L = \frac{v_0}{2f_r\sqrt{\varepsilon_{reff}}} - 2\Delta L \tag{2}$$

where, $\varepsilon_{reff} = \frac{\varepsilon_r+1}{2} + \frac{\varepsilon_r+1}{2}\left(1+\frac{12h}{w}\right)^{-\left(\frac{1}{2}\right)} \qquad \frac{w}{h}>1$

h = height of dielectric substrate (thickness)

ε_{reff} = effective dielectric constant.

$$\Delta L = 0.412h\left[\frac{(\varepsilon_{reff}+0.3)\left(\frac{w}{h}+0.264\right)}{(\varepsilon_{reff}-0.258)\left(\frac{w}{h}+0.8\right)}\right] \qquad (3)$$

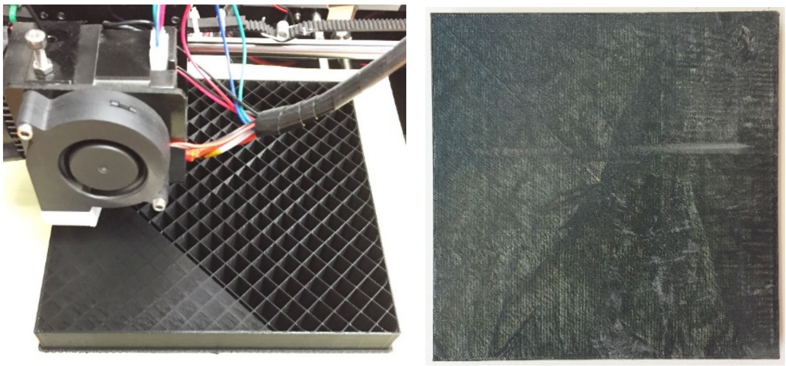

(a) (b)

Figure.9.4. (a) ANET-A8 3D-printer printing the cuboid substrate; and (b) Fabricated cuboid substrate

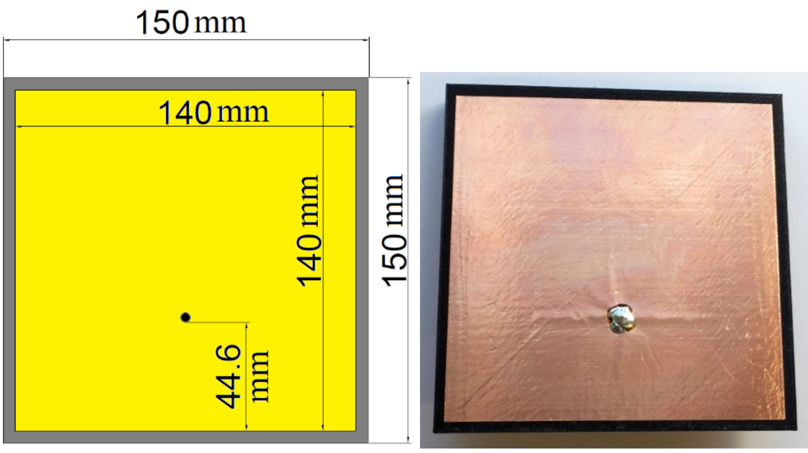

(a) (b)

Figure.9.5. (a) Linearly polarized antenna design on cuboid substrate; and (b) Fabricated cuboid antenna for dielectric constant measurement

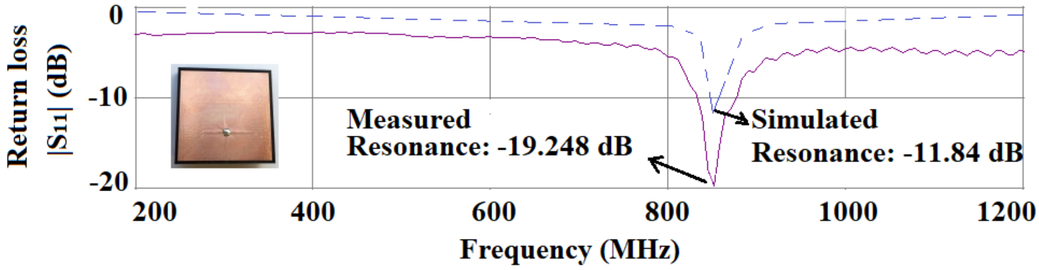

Figure.9.6. Characterizing antenna's resonance to determine effective substrate D_k.

9.5 Concave antenna design and fabrication

Utilizing the characterized D_k and the fabricated concave substrate, a circularly polarized patch antenna is designed. Figure.9.7 shows the proposed concave patch with asymmetric perturbating 'arc' slots on the edges and a circular slot centered on the 3D-printed concave substrate with radiating patch conforming to the substrate's concavity. The patch is symmetric and spans 141 mm x 141 mm. The asymmetric perturbating 'arc' slots make the patch longer in one direction and shorter in other. This degenerates the fundamental TM_{10} mode into two orthogonal modes that realize right-hand circular polarization (RHCP). The antenna is probe-fed using a rear 50 Ω SMA connector, and circular polarization is achieved through the asymmetric patch shapes. The ground plane of the antenna takes the size of the substrate (150 mm × 150 mm). The radiating patches and ground planes are fabricated using 0.1 mm thick copper foils and adhered to the substrate using non-conductive pressure sensitive acrylic-based adhesive (similar to the construction discussed in Section 9.6).

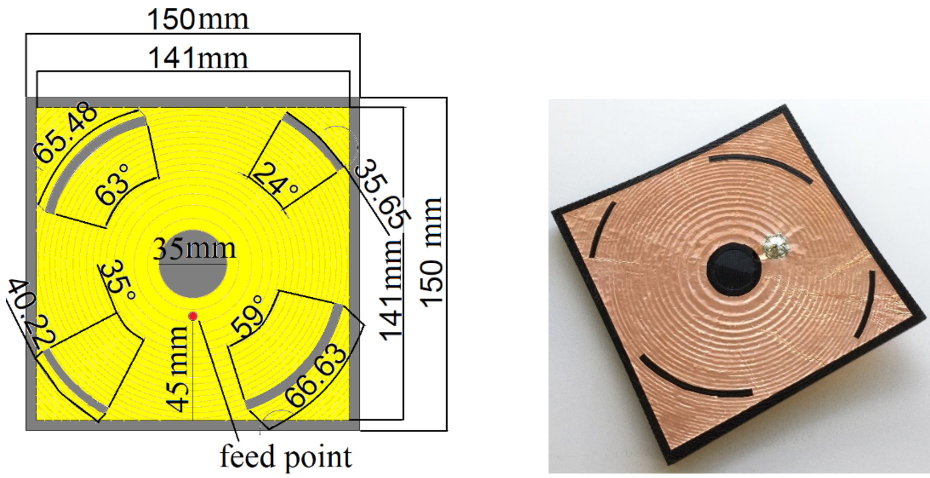

(a) (b)

Figure.9.7. (a) Circularly polarized patch antenna design on 3D-printed concave substrate; and (b) Fabricated concave patch antenna.

9.6 Concave antenna measurements

The antennas' performances are measured with TR1300/1 VNA in an anechoic chamber. The concave antenna's return loss at 866.5 MHz (f_c) is found to be -16.2 dB. The antenna yielded a 35 MHz bandwidth, when measured at −15 dB $|S_{11}|$ cut-off. The antenna's circular gain is measured by gain-transfer method. Results show that the gain of the concave antenna is 7 dBiC (Figure.9.8). The antenna was also evaluated with a larger reflector ground plane by mounting them onto a 250 mm × 250 mm aluminium plate. The aluminium plate was touching the antenna's ground plane to simulate a ground plane extension. As shown in Figure.9.8, the concave antenna's return loss is reduced by only 0.8 dB while still maintaining its 35 MHz bandwidth. The concave antenna's gain was increased by 2.5 dB, making it powerful 9.5 dBiC antenna. Figure.9.9 shows that the concave antenna is circularly polarized with near 0 dB axial ratio without a reflector. The reflector ground plane increases the axial ratio only by 2.5 dB the operating frequency range.

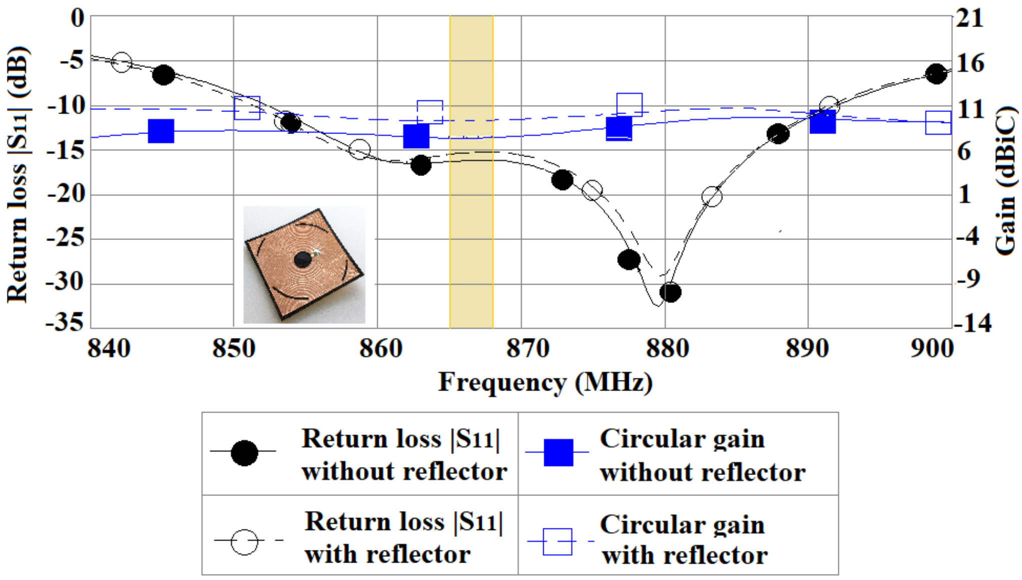

Figure.9.8. Return loss and gain measurements for circularly polarized concave antenna.

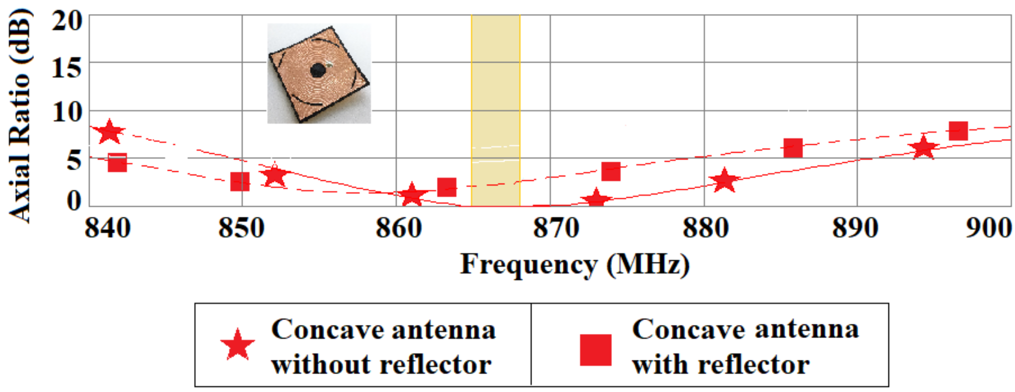

Figure.9.9. Axial ratio measurements

Figure.9.10 shows the far-field radiation pattern of both antennas with and without a reflector ground plane. Without a reflector, the concave antenna has a poor front-to-back ratio (FBR) of ~4 dB. With reflector, the FBR is improved to 12 dB. The half-power beam-widths (HPBW) of azimuth and elevation planes are shown in Table.9.1. It is observed that the concave antenna's HPBW is decreased only by 3° and increased by 5° in elevation and azimuth plane, respectively, when operating with a reflector. The concave antenna is less susceptible to changes in the beam-width with a reflector. The gain is boosted by adding the back radiation in-phase to the direction of radiation and hence the FBR improvement.

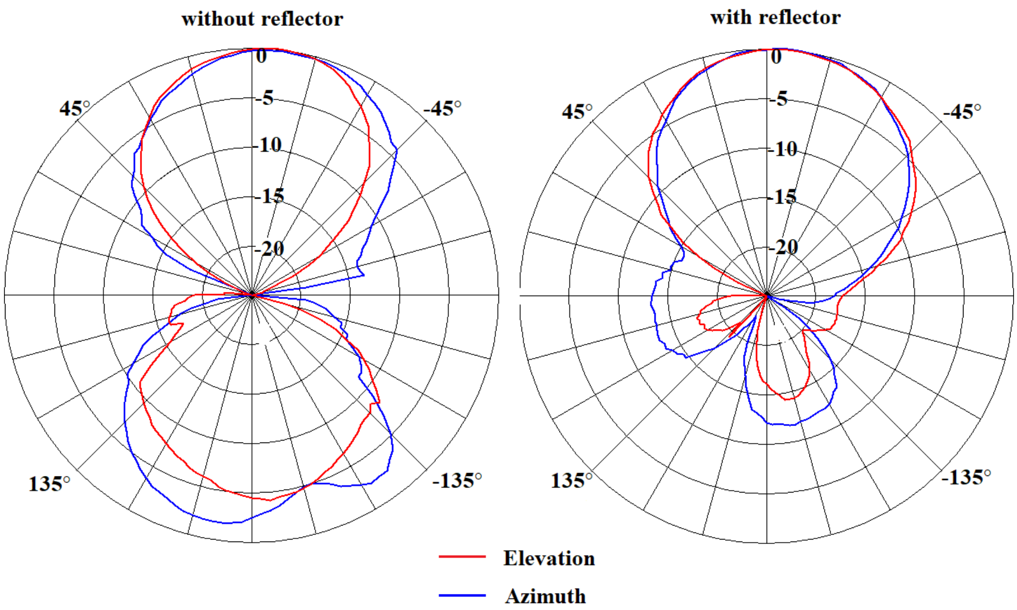

Figure.9.10. Radiation pattern of concave antenna without (left) and with a reflector (right)

Table.9.1. Concave antenna's half-power beam-width

Antenna under test	Elevation HPBW	Azimuth HPBW
Concave antenna on its own	65°	61°
Concave antenna with reflector	62°	66°

9.7 Design comparison

The results show that the concave antenna has the following merits;

1. Bandwidth enhancement is achieved just by the substrate and patch's concavity and not by implementing bandwidth enhancement techniques.
2. Axial-ratio and return loss are less-susceptible to changes when a reflector ground plane is added.
3. Beam-width is narrower compared to traditional flat substrate design (with and without the presence of reflector).
4. Beam-width it is less-susceptible to significant changes in the presence of a larger

reflector.

To show that the concave antenna has achieved all the merits mentioned above, it is compared with a traditional 3D printed cuboid substrate antenna that has similar functionalities such as, circular polarization, 865.5 MHz resonance, and so on. The linearly polarized square patch fabricated in section IV is tuned to operate circularly at 865.5 MHz by truncating the corners and by adding a perturbating slot in the center (Figure.9.11). The cuboid antenna's return loss is -16.2 dB (same as that of the concave antenna), but the -15 dB bandwidth is only 15 MHz (Figure.9.12). Moreover, the cuboid antenna's return loss is significantly reduced by 4.5 dB to 11.7 dB at f_c, whereas, the concave antenna's return loss is reduced by only 0.8 dB while still maintaining its 35 MHz bandwidth. This clearly shows that the concave antenna has an improved impedance bandwidth without adopting any bandwidth enhancement techniques.

Figure.9.13 shows the comparison between the axial ratios of the cuboid and concave antenna with and without the reflector. The concave antenna is circularly polarized with near 0 dB axial ratio, whereas the cuboid antenna is elliptically polarized with 5 dB axial ratio. The reflector ground plane increases the axial ratio by 7 dB and 2.5 dB for the cuboid and concave antenna, respectively, over the operating frequency range. Thus, proving that the concave antenna is less susceptible to return loss and axial ratio changes when in the presence of the reflector ground plane. Figure.9.14 shows the far-field radiation pattern of both antennas with and without the reflector ground plane. Without reflector, both antennas have a poor front-to-back ratio (FBR) of ~4 dB. With reflector, the FBR of cuboid and concave antennas are improved to 10 dB and 12 dB, respectively. The concave antenna achieves better directivity than the cuboid antenna, without using traditional beam-width enhancement techniques such as using dual-ring resonator [12] or auxiliary antennas to spread the transmitted power [13]. One of the predominant sub-GHz ISM band application is UHF RFID. A focused reader antenna beam helps UHF RFID readers to eliminate unwanted stray tag reads in applications such as retail point-of-sale and library returns chute. In the presence of a reflector ground plane, the concave antenna's boresight radiation is unaltered in both planes, while that of the cuboid antenna is tilted by 15° in the azimuth plane. The half-power beam-widths (HPBW) of the cuboid antenna is shown in Table II. The concave antenna has achieved more directivity without implementing any beam-width enhancement techniques. Besides, the radiation is also not spoiled by the addition of the reflector plate. Hence, proved that the concave antenna has an enhanced radiation pattern with beam-width being narrower and less-susceptible to be influenced by large reflector plates. Table.9.3 shows the advantages of the proposed design over existing 3D printed concave patch antennas.

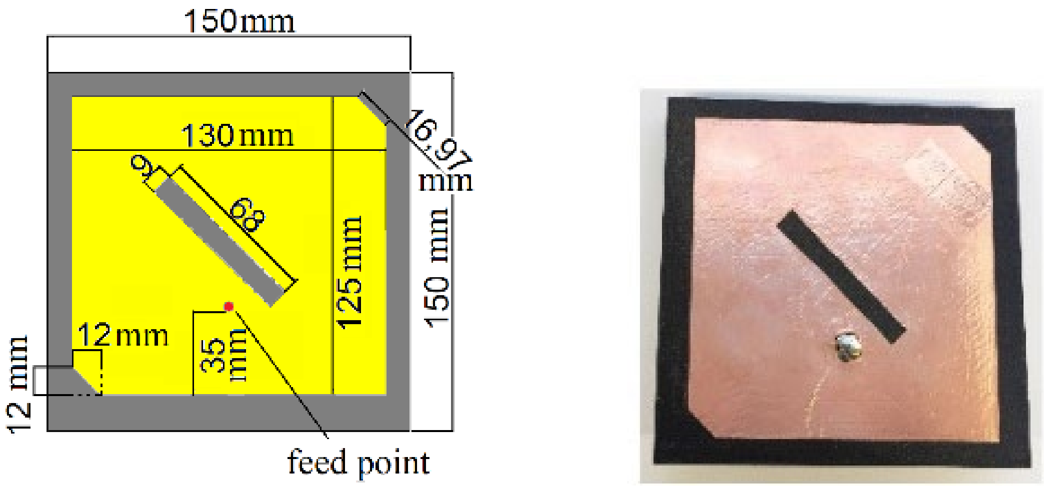

(a) (b)

Figure.9.11. (a) Circularly polarized antenna design on cuboid substrate; and (b) Fabricated cuboid antenna

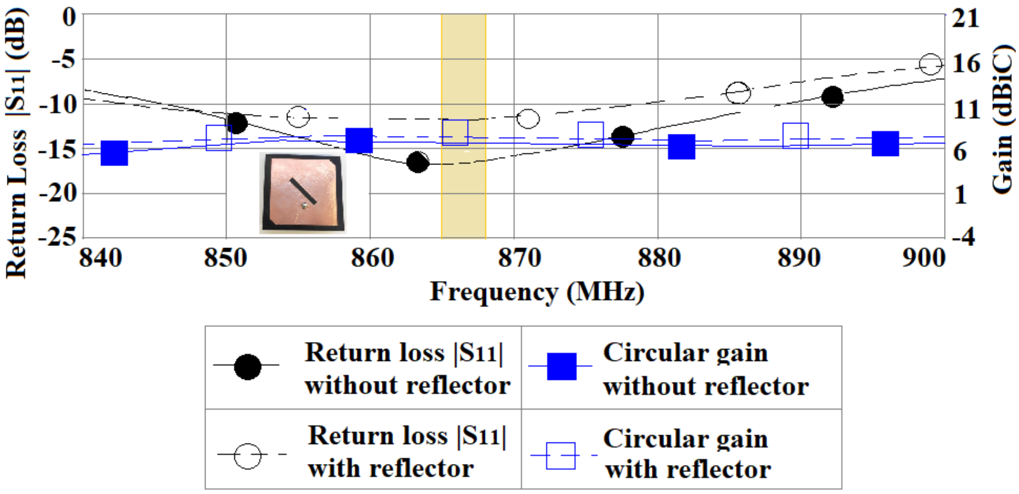

Figure.9.12. Return loss and gain measurements for circularly polarized cuboid antenna.

Table.9.2. Cuboid antenna's half power beam-width

Antenna under test	Elevation HPBW	Azimuth HPBW
Cuboid antenna on its own	85°	83°
Cuboid antenna with reflector	72°	78°

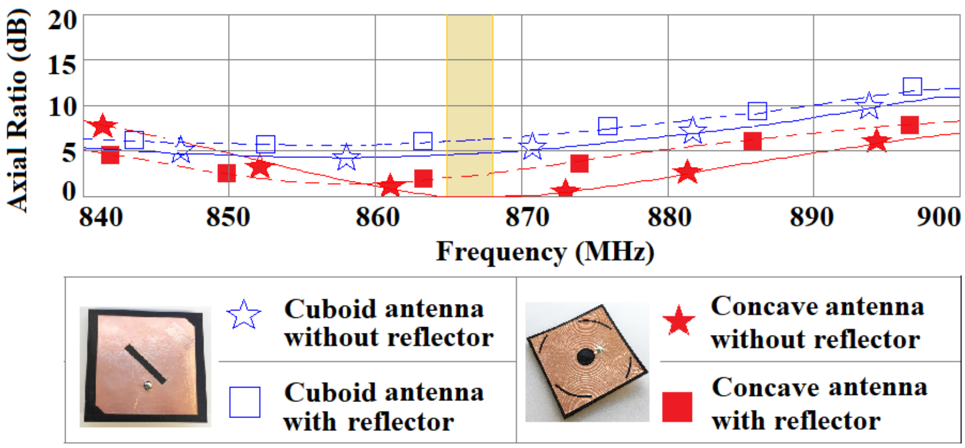

Figure.9.13. Comparison of axial ratio measurements

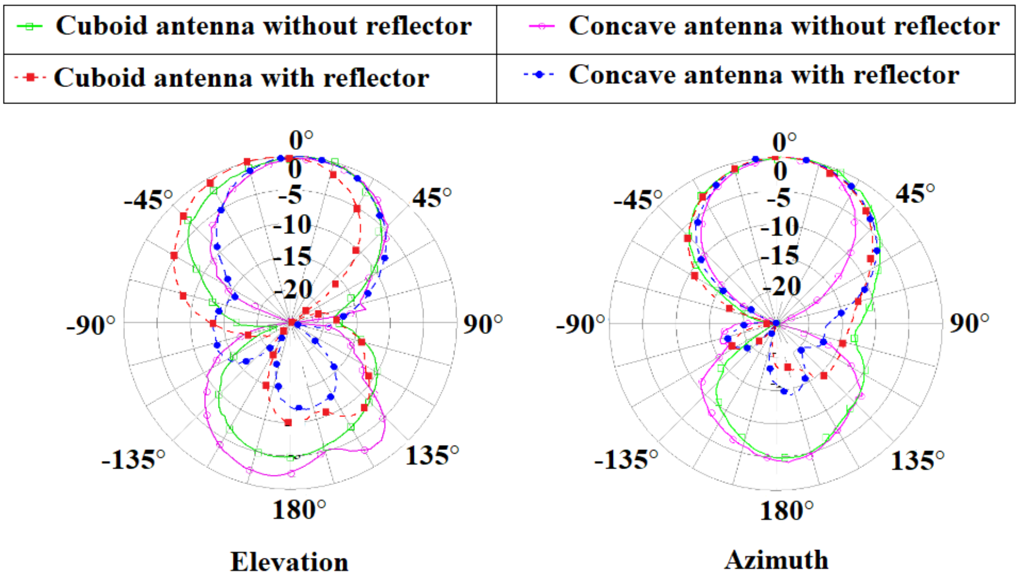

Figure.9.14. Comparison of radiation patterns

Table.9.3. Advantages of proposed design vs existing 3D printed concave antennas

Reference	Substrate concavity with flat ground plane	Patch concavity	Bandwidth enhancement	Radiation pattern enhancement	Reflector insusceptibility	Bio-degradable substrate	Eco-friendly antenna	Cost
[4]	No	No	No	No	No	No	No	High
[5]	No	No	No	No	No	No	No	Moderate
[6 & 7]	No	No, only 2D concave geometry	No	No, but enhanced Gain	No	No	No	High
[8]	Yes, as a lens superstrate	No	No	Yes	No	No	No	Moderate
[9]	Substrate with hole	Indent and not concave	No	No	No	No	No	Moderate
[10]	No, the ground plane is also bent with the substrate	Yes	No	No	Not tested	No	No	High
This work	Yes, the substrate is concave with a flat ground plane.	Yes	Yes	Yes	Yes	Yes	Yes	Extremely low

9.8 Conclusion and future work

This manuscript proposes a novel circularly polarized 3D-printed concave patch antenna design that is light-weight, low-cost and eco-friendly for sub-GHz ISM band (865-869 MHz) applications. The proposed antenna is fabricated and evaluated against a traditional circularly polarized cuboid patch antenna. Measured results show that the proposed antenna exhibits enhanced performance in terms of bandwidth, radiation pattern, return loss, and axial ratio, while remaining resilient to the effects of large reflector ground plane. As part of the future work, the evaluation of impedance bandwidth and radiation enhancement behaviour of the concave antenna will be supported by theoretical analysis and discussion.

Prelude to Manuscript 7

This manuscript presents a radiative quadrature hybrid coupler designed using a non-conventional substrate material for ultra-high frequency (UHF) radio-frequency identification (RFID) applications. One of the biggest problems in UHD RFID is the stray reads, which is the detection of unwanted tags that are lying around. For certain applications such as point of sale, a very-low gain antenna is preferred to create a confined read zone that does not over-lap the neighbouring counter (the phenomenon is commonly referred to as RF spill). Using an appropriately designed antenna with high performance in this scenario will cause the RFID system to fail. Thus, a radiating hybrid coupler is a better choice of antenna than a standard high-performing antenna that fosters stray reads. The coupler generates radiation above the microstrip-lines for near-zone UHF RFID tag detection. The coupler is designed to be wideband by intentionally mismatching the port impedances.

The concept of ‘intentional mismatch’ is not to create a complete impedance mismatch in a circuitry that destroys the performance, rather it creates a slight mismatch to the input impedance. For instance, in this case, instead of using a 50 Ω matched input, a 45 Ω impedance line is used with which a minimum 15 dB (instead of 17 dB) return loss is obtained, resulting in a slightly enhanced bandwidth. This -10% impedance mismatched (45 Ω) microstrip line is connected between the 50 Ω connector and two λ/4 junctions. Using standard microstrip calculations as mentioned in chapter 7, a 50 Ω microstrip line is 17.9 mm while a 45 Ω line is 21.4 mm. The coupler's return loss is −15 dB while its isolation bandwidth is 155 MHz, which more than meets the UHF RFID requirements. The coupler is insusceptible to performance variations due to the presence of proximity assets. The coupler can read tags up to 1.3 m at 1 W RFID reader power. The surface magnetic field distribution is uniform with no surface dead zones (due to fields generated by currents), making it suitable for liquid and metal asset tracking. The coupler is balanced and yields equal power split with 90° phase difference, which also makes it practical for driving external beamforming antennas. Several of this coupler can be cascaded to form a distributed antenna system for various smart applications. Connected antennas will not impact the read performance of the hybrid coupler. Instead of terminating the hybrid's output ports with 50 Ω loads, they will be terminated with 50 Ω antennas. Thus, the return loss and isolation plot may change (depending upon the antenna) but the ability to read tags above the hybrid will not be altered.

Traditionally, couplers are used in static array for beam formation. In applications like RFID, assuming that the input and isolation ports are connected to the RFID reader's ports (that transmits at different time instances) and the outputs are connected to two separate antennas operating at the same frequency and are spaced half-wavelength apart, will have a beam formation that appears to be an active beam steering. The 0° and 90° phase inputs to the patch antennas alter from time to time to create tilted beams that appear to be steered; thus, beam steering can be achieved using couplers. The coupler's half-power beam-width is narrow (~60° in both E and H planes) and its front-to-back ration (FBR) is ~6 dB.

The coupler's return loss is insusceptible to proximity assets. When an asset is put over the antenna, the antenna's return loss is disturbed and when the return loss goes beyond 5 dB or so, the reader shuts down to protect itself from the reflected power. The figure of merit is 5 dB threshold. Measurements of this coupler design show that the return loss has not deteriorated significantly (within the threshold, 5dB) when various assets such as liquids, ceramics, wood, plastic, metals are proximity to the antenna. Tests have proven that RFID tags can be excited even at regions where the microstrip lines are not present, meaning there is no nulls on the coupler's surface.

Chapter 10

Manuscript 7

Radiative quadrature hybrid coupler for near-zone UHF RFID applications

10.1 Introduction

Radio-Frequency Identification (RFID) has become prevalent in this Internet-of-Things (IoT) era where fast and accurate data handling is necessary. UHF RFID is better than other forms of RFID for the same reasons. UHF RFID system comprises of a tag (transponder), reader (interrogator), reader antenna and software for data processing [1]. The UHF Gen2 standard uses leading main frequency bands viz., region-1 (864-868

MHz) and region-2 (902-928 MHz) and are generally referred to as ETSI and FCC frequencies, respectively. The former is being used in most European nations, while the latter is adopted by North and Latin American nations. The rest of the countries uses either of the bands or its sub-bands, e.g. Malaysia uses 919 to 923 MHz – a sub-band of region-1 frequencies. GS1 prescribed the over-the-air protocol and the reader-to-tag communication techniques such as FHSS and LBT are governed by country-specific regulatory authorities [1]. High performing reader antennas are necessary for a viable over-the-air communication with the tag. In certain applications, such as retail checkout counters and cabinet asset management, overreading unwanted tags is a major problem. Eliminating stray tag reads can be controlled using the software only to an extent. Limiting the RF spill in reader antennas even when operating at high power, is crucial in most applications [1]. Some applications demand reader antennas be less susceptible to the effect of proximity assets, metals and human intervention.

The proposed quadrature hybrid coupler design is novel due to the following reasons.

- The microstrip line quadrature hybrid coupler is made from a low-cost non-conventional radio-frequency (RF) substrate.
- The coupler is radiative and becomes the RFID reader antenna on its own.
- The coupler's focused and near-zone radiation helps to avoid unwanted stray tag detection.
- The uniform magnetic field distribution on the microstrip line's surface creates no surface dead or null zones.
- The coupler is insusceptible to the effect of detuning by proximity assets during scanning.

Besides, the coupler's output ports can be terminated by antennas with 50 Ω characteristic impedance, to extend the read range. Antennas' beam can also be steered using the 90° phase difference between the ports. A 50 Ω RF energy harvesting LED module connected to the coupler's output port can indicate the liveliness of the reader antenna during operation. Distributed antenna systems (DAS) can be realized by cascading several of the proposed hybrid coupler in such applications as smart shelves, smart workbenches, and so on.

10.2 Related works

There are several quadrature hybrid coupler designs [2, 3] in literature that are intended for use as a splitter with quadrature phasing. A lumped element-based quadrature hybrid coupler is discussed in [2] for X-band microwave integrated circuits (MMIC). A printed ridge gap waveguide hybrid coupler for millimeter-wave applications is presented in [3]. Some incremental works, such as the hybrid coupler design to suppress harmonics from $2f_o$ [4] and a tunable substrate integrated waveguide (SIW) cavity-based quadrature coupler [5], are also presented. These existing works differ from our proposed work because they are intended for use only as a splitter and not a radiator. Lumped element and cavity-based designs do not have spurious radiation that can contribute to RFID tag detection. As our proposed radiative hybrid coupler is used as a reader antenna, existing UHF RFID near-field (NF) antenna designs are critically analyzed in the following segment.

Low-gain patch antenna arrays in [6, 7] are used for near-zone tag detection. All far-field (FF) antennas have near-field and radiative near-field regions to contribute to the near-zone area. Although FF antennas' near-zone region can detect metal and liquid assets, the surface magnetic field distribution has lots of dead zones. The far-field components of these array antennas are compelling that unwanted tags can be read meters away from the antenna. On the other hand, our proposed radiative hybrid coupler has confined radiation to limit stray tag reads. The coupler is active throughout the microstrip line as opposed to having dead zones (where voltage is zero) in the center of the patch.

Loop and segmented antennas are most commonly used as NF antennas due to their uniform surface magnetic field distribution. Dipole antennas are curved to form a loop-like structure in [8], which still suffers from an extended read range due to the FF gain. Circular and square-shaped zero-phase-shift-line (ZPSL) loop antennas in [9], and [10], respectively, are very narrow band and can only work in UHF RFID region-2. These narrow-band antennas are vulnerable to both environmental and proximity asset detuning. A detuned antenna offers very high return loss, leading to RFID reader damages. Some antennas are built with an antenna detection circuitry to avoid reader damages during antenna disconnection by measuring its return loss [1]. These readers stop its transmitting function when the antenna's return loss has detuned beyond a cut-off point. Our proposed radiative coupler can operate in both region-1 and 2 frequencies. Detuning effect will be minimal due to its wide bandwidth and the presence of 50 Ω termination resistor in the isolation port where the reflected energy gets dissipated.

An electrically large segmented dipole array antenna design in [11] comprises of one active segmented dipole and seven parasitic elements. The uniform surface energy distribution relies on an effective coupling between the active and parasitic segmented dipoles. When dense assets are placed very close to the active dipole, it gets detuned, and the subsequent parasitic segments will get very little energy. This induces dead zones and is not acceptable for certain RFID near-field applications. A near- and far-field antenna with no surface dead zones is proposed in [12, 13]. In [12], the antenna consists of four dipole antennas arranged in a square and driven in-phase (0°) as well as incremental quadrature phases (0°, 90°, 180° and 270°) to obtain NF and FF performances. A PIN diode is used to switch between NF and FF operations. The antenna is intended to read tags at farther distances using its far-field gain, and thus it is not suitable for all near-zone UHF RFID applications. Moreover, the antenna has a null zone in its center during its NF operation.

Our previous work in [13] has two meandered microstrip lines (with quadrature phase shifts) to feed a single patch antenna. The meandered microstrip line creates a near-field rim, and the central patch antenna produces far-field radiation. The antenna operates in NF and FF modes simultaneously, unlike [12] where it is switched between them. The antenna is designed in a non-conventional RF substrate, and it is planar in nature. Meandered microstrip lines are driven 90° out-of-phase to achieve circular polarization in the patch antenna. The 90° phase shift is achieved using a thin film miniatured hybrid coupler chip. Although this work also used a non-conventional RF substrate and a coupler chip, our new work in this manuscript is still novel due to the following reasons:

- Our current proposed design features a *radiative* hybrid coupler whereas the coupler used in [13] is a non-radiative thin-film miniatured-hybrid coupler.
- The non-conventional substrate used in [13] is for the design of meandered lines and patch antenna, while current work utilizes it for designing a microstrip line hybrid coupler.
- The current design is wideband and can operate for both regions-1 and 2 as opposed to region-2 only in [13].
- There are no surface dead zones in the current design while the patch antenna's center in [13] has a null zone.

10.3 Radiative quadrature hybrid coupler

10.3.1 Design

Quadrature hybrid coupler is otherwise known as a branch-line (refer Figure.10.1(a)), which consists of four lines that are quarter wavelength long [14]. Two parallel lines have the characteristic impedance (Z_0), and the other two lines have a higher impedance i.e. $\frac{Z0}{\sqrt{2}}$. The hybrid coupler maintains D-2 symmetry and is matched from all four ports. The S-parameter matrix after even and off mode analysis is given in (1). Traditional microstrip line quadrature hybrid coupler is shown in Figure.10.1(b) is usually made from conventional RF substrates.

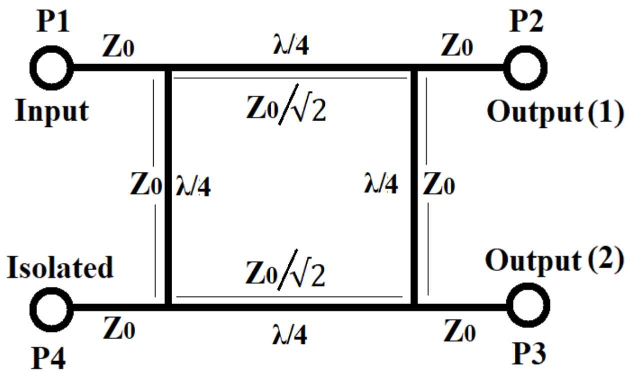

(a)

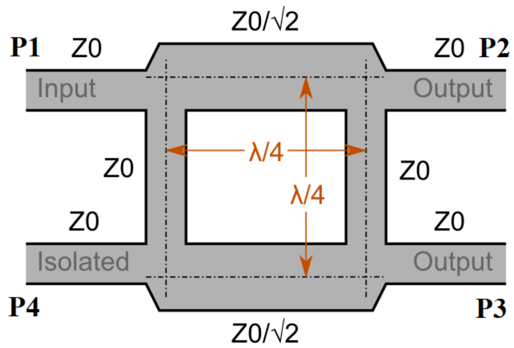

(b)

Figure.10.1. (a) Quadrature hybrid coupler design and (b)Traditional microstrip quadrature hybrid design

$$
S = \frac{-1}{\sqrt{2}}\begin{pmatrix} 0 & j & 1 & 0 \\ j & 0 & 0 & 1 \\ 1 & 0 & 0 & j \\ 0 & 1 & j & 0 \end{pmatrix} \tag{1}
$$

Non-conventional virgin high-density polyethylene (HDPE) substrate is used to design the quadrature hybrid coupler. HDPE's dielectric constant (ε_r) and loss tangent (tan δ) are 2.256, and 0.0002, respectively [13]. Substrates with lower ε_r is necessary to generate spurious microstrip line emissions. The substrate is 6 mm thick and spans 150 mm in length and width. The substrate is cut to an octagon shape to ease the 50 Ω SMA connection. The input impedance is the same as the characteristic impedance in a traditional branch-line coupler (see Figure.10.1(b)), whereas the proposed design adopted an intentional input impedance mismatch as suggested by [15]. A -10% impedance mismatched (45 Ω) microstrip line is connected between the 50 Ω connector and two $\frac{\lambda}{4}$ junctions. The $\frac{Z0}{\sqrt{2}}$ lines are curved to shrink the height of the hybrid coupler so that the center of the coupler does not become a dead zone. The surroundings can generate enough magnetic fields for efficient tag detection. A 6 mm notch is introduced at the center of the curved $\frac{Z0}{\sqrt{2}}$ line to keep the quarter wavelength right. Figure.10.2 shows the proposed corner excited radiative quadrature hybrid design.

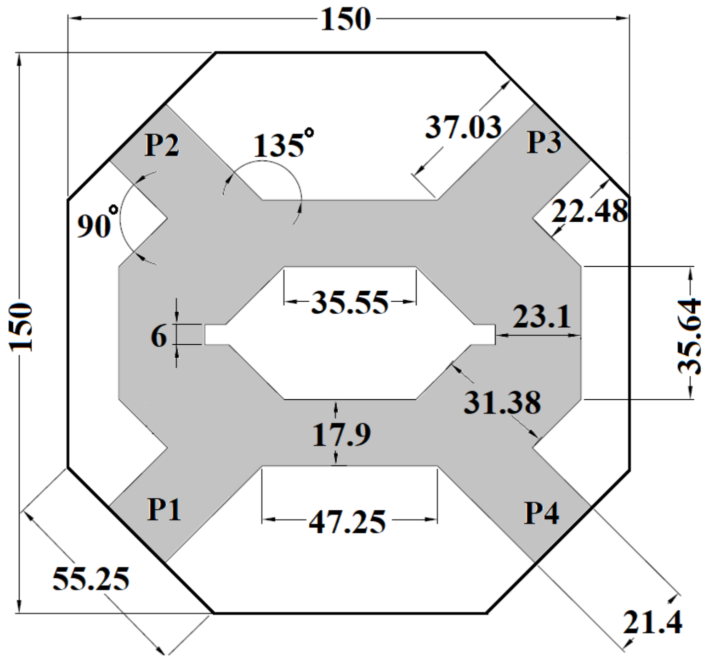

Figure.10.2. Proposed coupler design (dimensions are in mm)

10.3.2 Fabrication

The coupler is fabricated using 0.2 mm thick steel-plated tin -electrolyte (SPTE) metal for the microstrip line and ground plane (see Figure.10.3). Both conductor patterns are laser cut with very high dimensional accuracy. The conductors are adhered to the substrate using a non-conductive acrylic adhesive that has 80 N/100 mm and 125 N/100 mm adhesion to metal, and plastic, respectively [13]. Four 50 Ω SMA connectors are edge mounted.

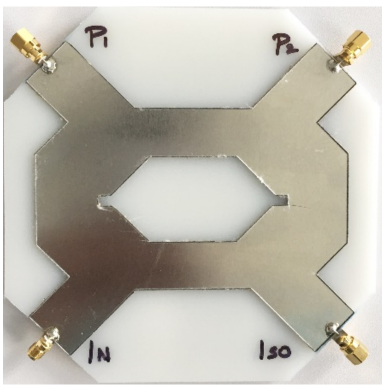

(a)

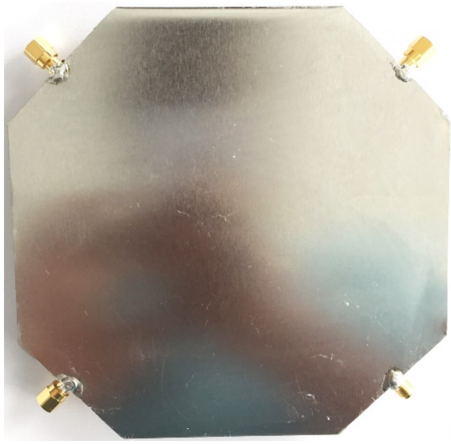

(b)

Figure.10.3. Fabricated design: (a) Front view and (b) Rear view

10.4 Simulation

The quadrature hybrid coupler design is simulated using ADS electromagnetic simulation software. ADS is a powerful Method of Moments (MoM) based simulator that is accurate for planar components such as power dividers, couplers and patch antennas. The substrate is defined as HDPE using the (ε_r) and tan δ values. Two conductor layers are set directly on the top and bottom of the substrate with no surface roughness. The material is chosen to be tin-plated steel with 9.17 x 10^7 σ (S/m) conductivity. Four 50 **Ω** transmission line calibrated ports are defined at the edge of the conductor layers. Port 1, 2, 3 and 4 are defined for input, first output, second port and isolation ports, respectively. Twenty cells per wavelength mesh are defined at 900 MHz meshing frequency. The simulation is swept between 0.8 and 1.0 GHz. Figure.10.4(a) shows port1's return loss $|S_{11}|$ and port 4's isolation $|S_{44}|$ plot when the output ports 2 and 3 are terminated with a 50 **Ω** load.

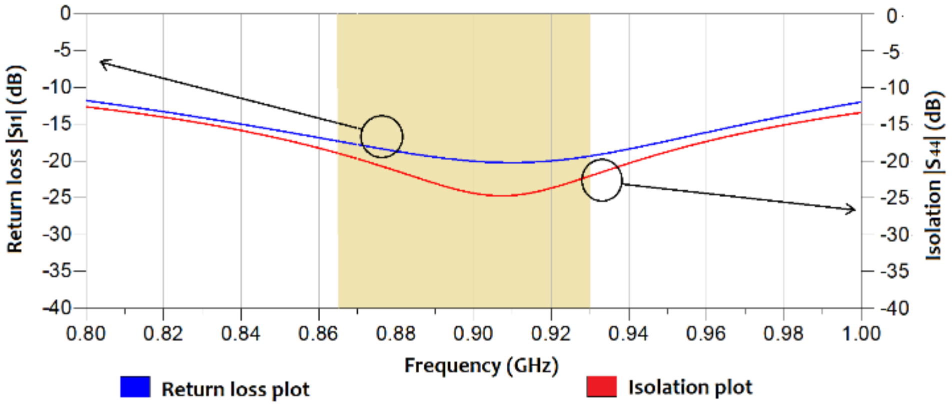

(a)

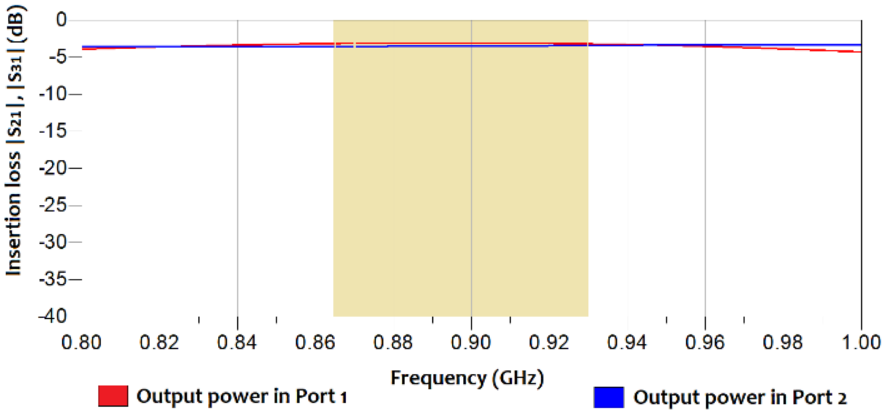

(b)

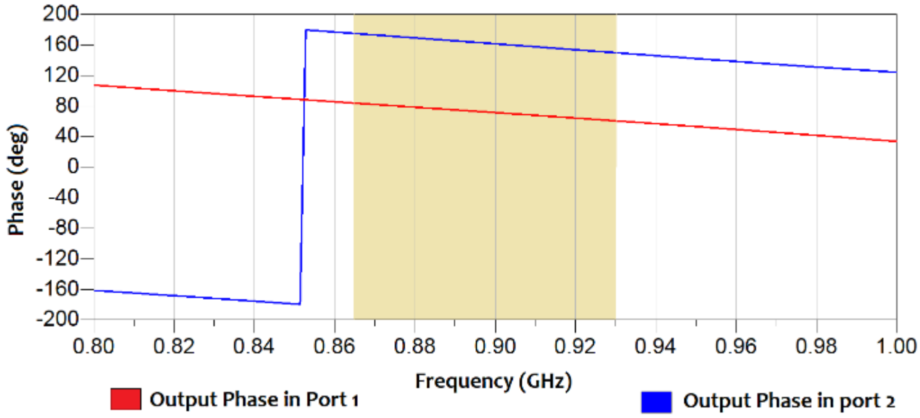

(c)

Figure.10.4. Simulation results: (a) Return loss and Isolation, (b) Power distribution at output ports (Insertion loss) and (c) Phase at output ports.

The coupler resonates at 900 MHz, which is the center for both region-1 and 2 frequencies. The -15 dB return loss bandwidth is 150 MHz. The achieved wide bandwidth offers insusceptibility to proximity asset's detuning. The isolation is better than the return loss, meaning there is very little power dissipation through that port. The coupler is highly efficient as the power split in both output ports are close to equal. The phase difference of ~90° is maintained between the output ports. Table.10.1. shows the return loss, isolation, power and phase distribution and differences for region-1 and 2 frequencies.

Table.10.1. Simulated Results

Parameter	**Region-1**	**Region-2**		
	866.5 MHz	**902 MHz**	**915 MHz**	**928 MHz**
Return loss terminated	-17.33 dB	-20.10 dB	-20.17 dB	-19.47 dB
Isolation	-18.99 dB	-24.55 dB	-24.35 dB	-22.36 dB
Port 1 Power	-3.52 dB	-3.47 dB	-3.44 dB	-3.40 dB
Port 2 Power	-3.13 dB	-3.05 dB	-3.09 dB	-3.17 dB
Power difference	0.39 dB	0.42 dB	0.35 dB	0.23 dB
Port 1 Phase	174.89°	160.67°	155.79°	150.52°
Port 2 Phase	83.66°	70.61°	66.13°	61.22°
Phase difference	91.23°	90.06°	89.66°	89.30°

Measurements are recorded at region-1's and region-2's center frequencies, 866.5 and 915 MHz, respectively. As region-2's is a broader band, measurements at 902 and 928 MHz (band edges) are also recorded to note any performance deviations. The surface current distribution (J) is plotted in Figure.10.5 for different input phases. The current flow can be noticed at different phases. The coupler has no null region to introduce surface dead zones. Far-field 3-D radiation plot is shown in Figure. 6. The coupler's radiation is very narrow. The coupler's front-to-back can be limited by having a larger ground plane.

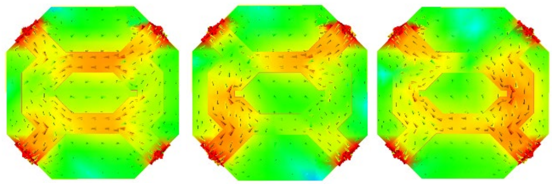

(a) (b) (c)

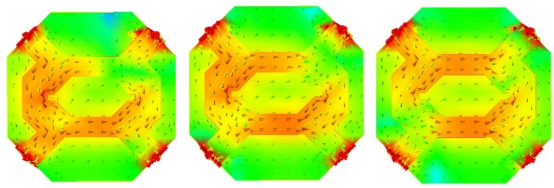

(d) (e) (f)

Figure.10.5. Surface current distribution at different input phases: (a) 0°, (b) 30°, (c) 60°, (d) 90°, (e) 120° and (f) 150°.

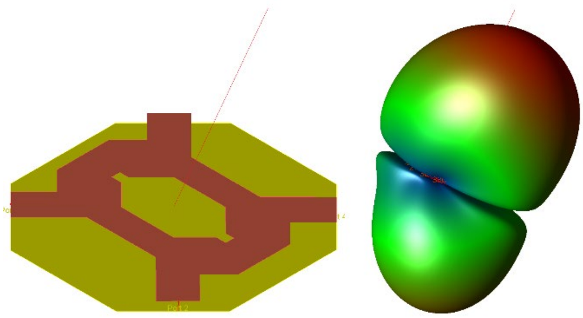

Figure.10.6. 3-D Radiation Pattern

10.5 Measurement results and analysis

The fabricated is measured using a vector network analyzer (VNA) over 200 MHz frequency span with 900 MHz as the center frequency. Figure.10.7(a) shows the return loss $|S_{11}|$ plot in continuous line when all three ports were terminated. As the VNA is fitted only with two 50 Ω measurement ports, 50 Ω SMA load terminations were used in the other two ports throughout the measurements. For instance, to measure the isolation (|S44| as described in the previous section), two output ports were terminated with 50 Ω loads, and the VNA's port 1 is connected to the input port and port 2 to the isolation port (P4).

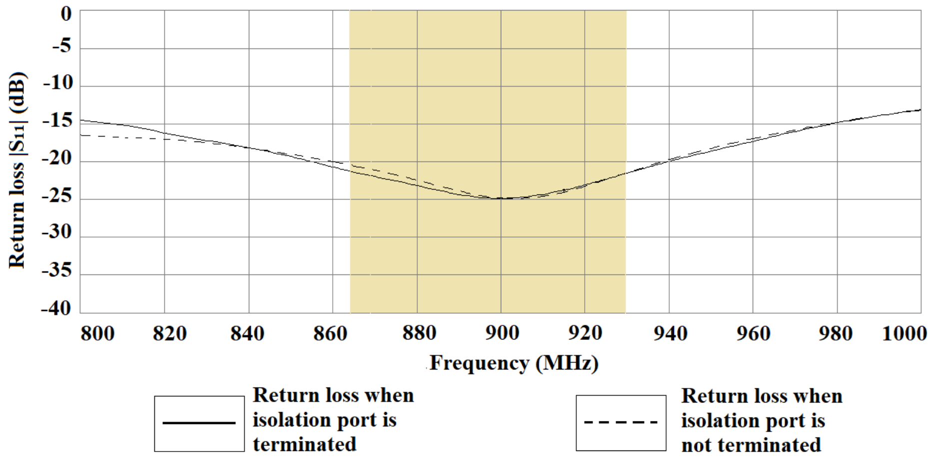

(a)

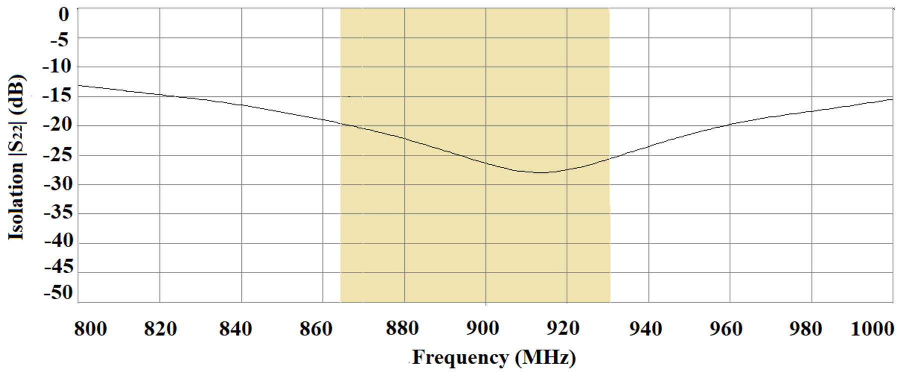

(b)

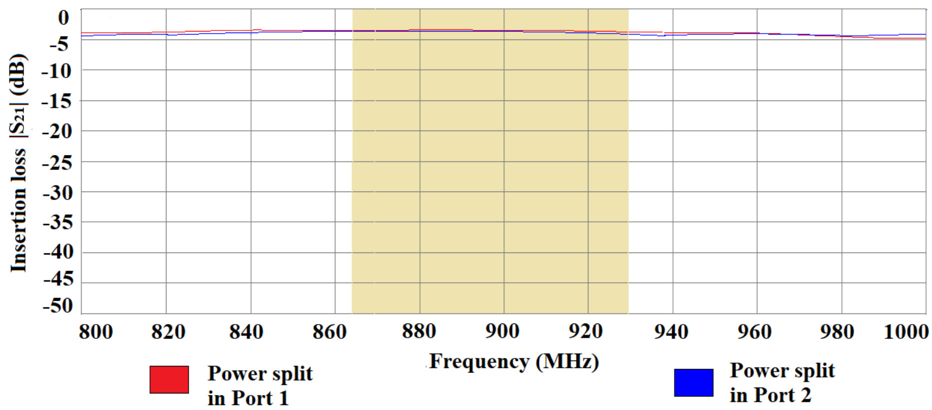

(c)

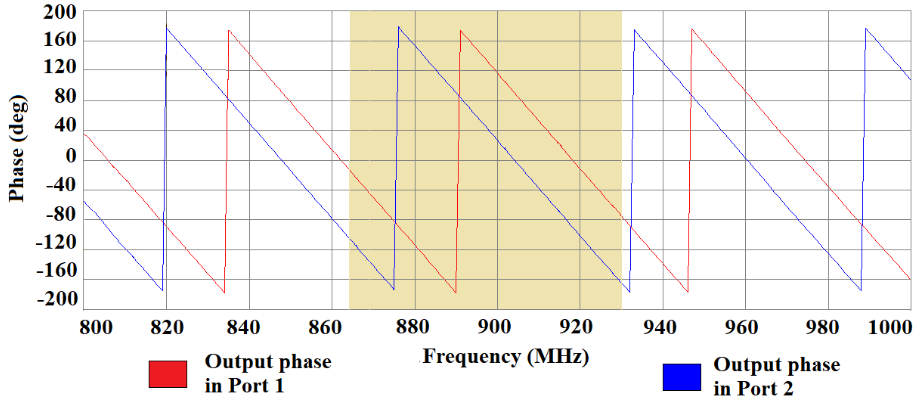

(d)

Figure.10.7. Measured Output: (a) Return loss: Terminated and unterminated, (b) Isolation, (c) Power split (insertion loss) and (d) Phase at output ports

This way, by measuring the |S21| parameter, we can find the isolation. The termination load from the isolation port is removed to show that there are no significant changes in the return loss (dashed lines in Figure.10.7(a)). This demonstrates that the coupler is well balanced, although it has been intentionally mismatched at the feed point. This statement is further supported by the plot at the isolation port shown in Figure.10.7(b). The -15 dB return loss bandwidth is found to be 155 MHz. Figure.10.7(c) shows the power distribution in output ports by measuring the insertion losses. Ideally, the power split has to be -3 dB (half power) for each port. As the coupler has radiation losses, the power split is not quite -3 dB. This radiation loss is used productively to read RFID tags. The phase balance between the ports is ~90° (see Figure.10.7(d)). The coupler's return loss, isolation, phase and power differences across the frequencies are tabulated in Table.10.2. The coupler's radiation is measured in an anechoic chamber, and its gain is plotted by the comparative method [6] in Figure.10.8. Gain is measured in four different orientations for different polarizations viz., vertical, horizontal, slant 45° and negative slant 45°. The radiative coupler is vertically polarized with a peak gain of -5.6 dBi. The lowest gain, -14.6 dBi is noted in horizontal polarization. Gain values of UHF RFID frequencies are tabulated in Table.10.3. Figure.10.9 shows the azimuth and elevation radiation pattern. Near-field antenna with a low far-field gain is essential to eliminate detecting unwanted tags due to surplus RF spill.

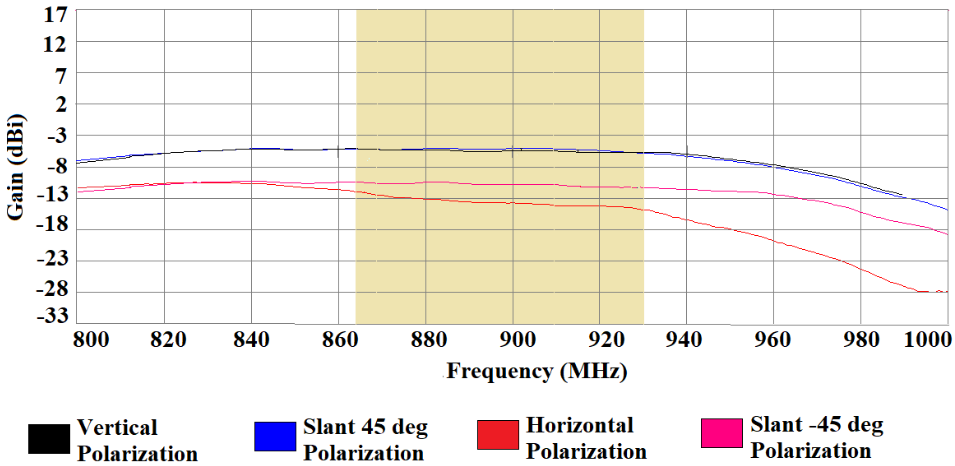

Figure.10.8. Measured gain

Table.10.2. Measured results

Parameter	**866.5 MHz**	**902 MHz**	**915 MHz**	**928 MHz**
Return loss terminated	-21.52 dB	-24.82 dB	-23.79 dB	-21.84 dB
Return loss unterminated	-20.66 dB	-24.87 dB	-24.04 dB	-21.82 dB
Isolation	-19.84 dB	-26.74 dB	-27.94 dB	-26.13 dB
Port 1 Power	-3.40 dB	-3.39 dB	-3.46 dB	-3.63 dB
Port 2 Power	-4.04 dB	-4.06 dB	-4.08 dB	-4.12 dB
Power difference	0.64 dB	0.67 dB	0.62 dB	0.49 dB
Port 1 Phase	-24.82°	104.40°	20.50°	-62.68°
Port 2 Phase	-115.86°	13.66°	-69.87°	-152.86°
Phase difference	91.04°	90.74°	90.37°	90.18

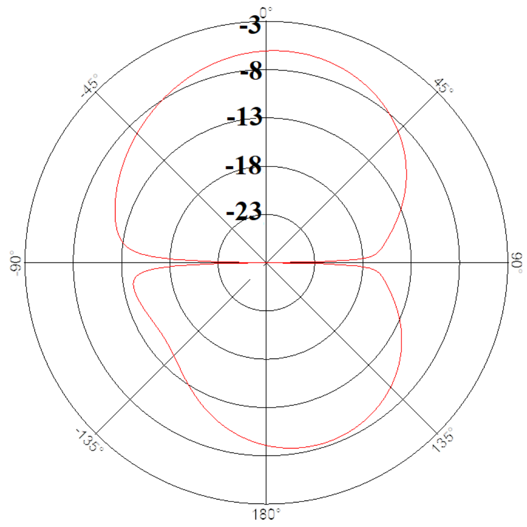

(a)

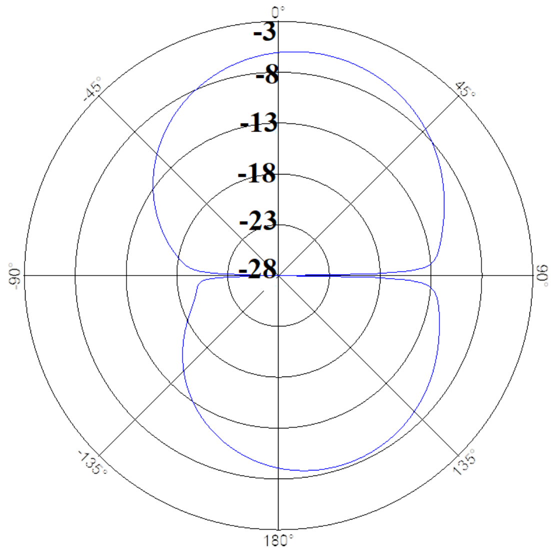

(b)

Figure.10.9. Radiation Pattern: (a) Azimuth and (b) Elevation

Table.10.3. Gain Measurements

Polarization	**866.5 MHz**	**902 MHz**	**915 MHz**	**928 MHz**
Slant 45°	-5.1 dBi	-5.1 dBi	-5.3 dBi	-5.7 dBi
Horizontal	-12.1 dBi	-13.9 dBi	-14.2 dBi	-14.6 dBi
Vertical	-5.2 dBi	-5.5 dBi	-5.6 dBi	-5.7 dBi
Slant -45°	-10.5 dBi	-10.8 dBi	-11.1 dBi	-11.3 dBi

Table.10.4. Advantages of proposed design vs existing near-zone antenna designs

Reference	Design	Cost / Complexity	Return loss insusceptible design	Uniform surface energy distribution	-15 dB Operational bandwidth	DC Bias Required?	Stray tag detection	DAS ability
[6 and 7]	Patch antenna array	Medium / High	No	No	20 MHz	No	Yes	No
[8]	Loop like dipole	Medium	No	Yes	35 MHz	No	Yes	No
[9 and 10]	ZPSL	Medium	No	Yes	~15 MHz	No	No	No
[11]	Segmented dipole	High	No	No	~20 MHz	No	No	No
[12]	Dipole array	Medium	No	No	26 MHz	Yes	Yes	No
[13]	Meandered line and patch	Low / Medium	No	No	42 MHz	No	Yes	No
This work	Radiative quadrature hybrid coupler	Low / Very low	Yes	Yes – No dead zones	155 MHz	No	No – Very confined read zone	Yes – using cascaded couplers and external antennas

10.6 Test application

The radiative coupler is compatible with all UHF RFID readers and tags in the market. For test purposes, Impinj R420 reader [16] and Smartrac's bling tags are used. As per the test methodology mentioned in [13], the coupler is virtually divided into 25×25 mm squares and comprises of 36 cells as shown in Figure.10.10. The cell size is chosen based on the length of the Smartrac's bling tag [17]. The radiative hybrid coupler is powered at ¼ W (24 dBm) to measure the RSSI at each cell.

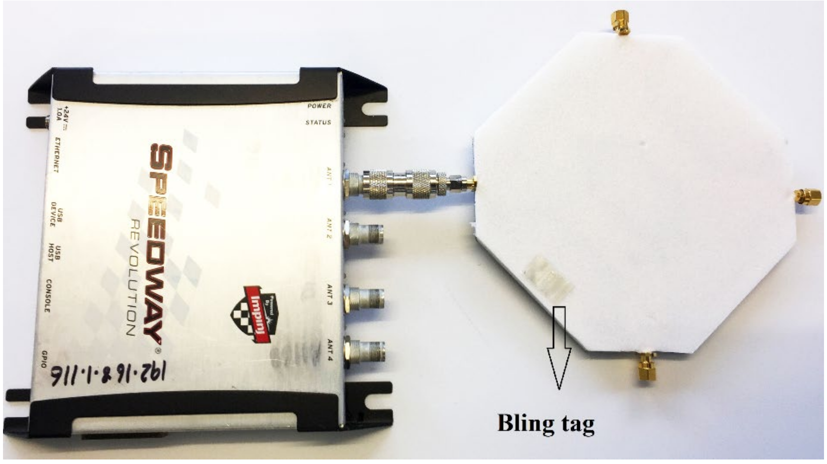

Figure.10.10. Test setup with Impinj reader

A contour plot of these RSSI values is given in Figure.10.11 to show that the energy distribution is uniform with no dead zons even in places where the microstrip line is not present. A 3 mm foam spacer is used to simulate an airgap between the hybrid and the radome that will be used in practice. The maximum read distance at 1 W (30 dBm) input power is 1.3 meters at the bore-sight. The radiation was confined with very little spillover of ~110 mm on all 4 sides.

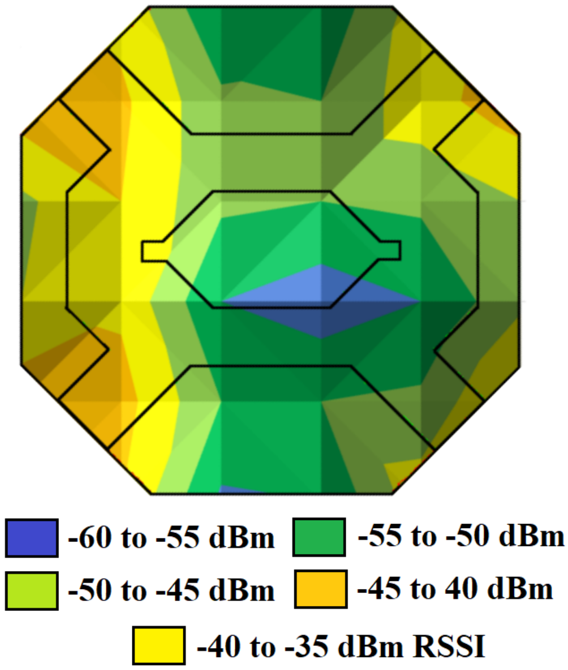

Figure.10.11. Contour plot of RSSI values

The return loss insusceptibility of proximity assets is measured by putting various assets over the microstrip line coupler. The 3 mm foam spacer is used during this test. Various assets used for testing include, glass jar, dishwashing liquid filled in plastic bottle, metal aerosol spray can, metal sheet, electronic item in a plastic casing and ceramic coffee mug. Figure.10.12 shows the assets and the 3 mm foam spacer used over the quadrature coupler. The assets were placed directly on top of the foam to measure the return loss insusceptibility. None of the assets detuned the coupler's return loss below -15 dB in the UHF RFID frequency range. The coupler's wide operating bandwidth offers the insensitivitiness towards the frequency shift caused by dense assets.

Figure.10.12. Various assets used for testing

Figure.10.13 shows the return loss plots under the interference of various assets. When metal assets interfere with the coupler and induce RF reflections, the reflected signal is drained through the resistor in the isolation port. Other assets induce a slight frequency shift as the coupler is loaded with a dense medium as the coupler's wideband performance makes it insusceptible and robust.

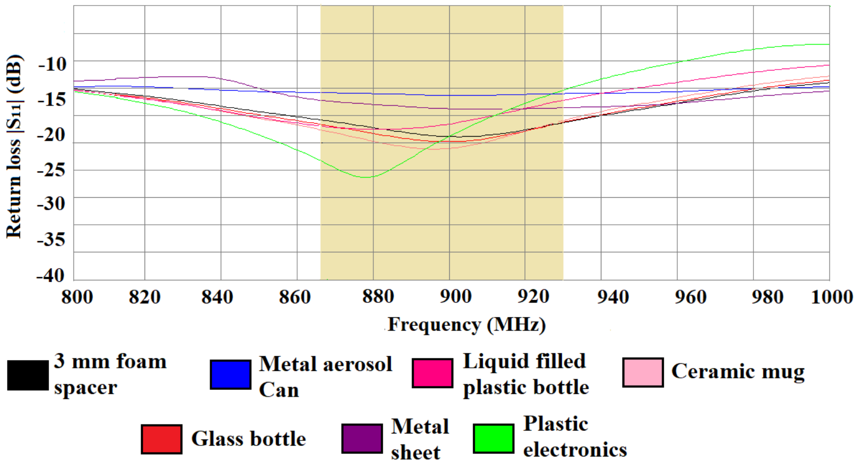

Figure.10.13. Return loss insusceptibility

10.7 Conclusion and future work

A radiative quadrature hybrid coupler design is proposed as a near-zone UHF RFID reader antenna. It has uniform surface energy distribution with no dead zones. The radiation is very confined and does not read unwanted stray tags. The coupler is very wideband and has equal power split and 90° phase differences. The coupler operates for both FCC and ETSI regions. The maximum tag read distance (at 1 W reader power) is 1.3 m at the bore-sight. The coupler's design is low-cost and low-complexity. External patch antennas can be attached to enhance the read range or to beamform. Distributed antenna systems (DAS) can be realized by cascading the proposed couplers in smart applications. As part of the future work, the radiative hybrid's performance as DAS with and without external beamforming antennas will be tested.

Prelude to Manuscript 8

This manuscript presents a scalable NF antenna design that utilizes a non-conventional but commercially available RF material that makes the antenna inexpensive. A standard antenna's definition is not applicable for an UHF RFID antenna due to the reasons explained in the section 2.3. UHF RFID reader antenna has its own unique requirements. The antenna architecture comprises of a rectangular spiral microstrip line (equivalent to a travelling-wave antenna) with intentional impedance mismatches and a finite ground plane made from conductive tapes and sheets sandwiched by a non-conventional substrate material. As this structure is used to detect tags, by connecting it with the RFID reader ports, in place of a standard antenna, this structure is termed as an antenna as well.

Traditional patch and loop NF antennas suffer from size limitation, surface dead spots and have far-field (FF) component that introduces stray tag reads. The proposed antenna design has no surface blind spots from the RFID perspective. Nulls or dead zones are places where RFID tags cannot be detected at all on the surface of the antenna. It has a uniform magnetic field distribution for near-field operation. The antenna is made from a non-conventional RF substrate: foamed PVC, which is not contaminated unlike the recycled substrate mentioned in chapter 4, and thus, its electrical property variation is minimal. The antenna has an 80 MHz bandwidth tolerance to accommodate slight variations in the material's composition. It is easily scalable by increasing the spiral size without altering the performance as the design is simply a long transmission line when unwound. It also has a potential for building an inexpensive tracking shelve with confined read zones that can detect both NF and FF tags. The light weight, chemical resistant, non-toxic, and self-extinguishing properties of the antenna can significantly expand the range of applications and deployment environments of UHF RFID

Chapter 11

Manuscript 8

Low-cost scalable UHF RFID reader antenna with no surface dead zones

11.1 Introduction

UHF RFID systems have many advantages over the High Frequency (HF) and Low Frequency (LF) systems such as, enabling fast transfer of data, low-cost tag production, long read distance, and a unified global Gen2 standard. Due to these advantages, modern industries prefer UHF RFID over traditional barcode, LF and HF systems. However, UHF RFID system has a limitation in reading tagged liquid items due to absorption of electric fields by the liquid. On the other hand, magnetic fields are not altered by liquids as opposed to electric fields [1].

Planar antennas such as patch and loop antennas have been traditionally used for NF RFID applications. These antennas fail to produce uniform magnetic field over the surface and the surface regions with weak magnetic fields are commonly termed as blind spots or dead zones. Patch antennas have dead zones at its centre where the voltage is zero [2] and loop antennas introduce phase inversion and null current when current flows along the loop, leading to dead zones [3]. By avoiding changing the current`s direction within the loop, such dead zones can be eliminated. Conventional antennas are made from materials such as FR4, Rogers, and Taconic, which are specifically manufactured to suit RF applications, and thus are generally expensive. Furthermore, these antennas are not scalable and are difficult to customize as their dimensions are a factor of their wavelength of operation, and thus are constrained to certain length and width.

On the contrary, the proposed antenna uses commercially and widely available material as substrate material. In addition, the proposed antenna is scalable, and can accommodate shelves, desks and racks of any size. Cost effectiveness can be achieved from low cost substrate material and ease of manufacturing by using a decal aluminum foil (with precut antenna pattern) for conductor layers. In particular, most of the existing works have FF radiators as part of the design which emits FF components that propagates for a longer distance. This increases the chance of reading stray tags. The proposed antenna has a confined read zone that can detect both NF and FF tags in close proximity. Radiation in this antenna is due to the reactive and radiative NF component. NF component would not propagate unlike FF components, thus enhancing isolation between inventories. This antenna would be the ideal choice for RFID systems for inventory with shelves containing metals and liquids, kiosk, check-out and point-of-sale applications.

11.2 Related works

Existing NF antennas for UHF RFID applications are based on loop and patch antennas. Dead zones in a loop antenna are avoided through enhancements such as segmented loop, RLC addition in loop segments [3-5] and having loops in different shapes [6, 7]. Parasitic loop [10] and Capacitively loaded loop [12] are also used for NF detection. Folded dipole antennas are used for NF applications in [8] and [9] which in principle appear to be a loop antenna in a different geometry. On the other hand, patch antennas for NF applications typically have a segmented loop around the patch [2, 17]. These antennas suffer from dead zones in the center of the patch. A three element patch array is proposed in [18] for a conveyor belt application where the central patch is intentionally driven out of phase to cancel the FF radiation. As tags are not stationary, dead zones in the patch's center is not a concern. The proposed antenna in this manuscript is intended for applications where the tags can be either stationary or non-stationary.

Apart from the aforementioned works based on traditional antennas, a novel antenna is designed in [13] based on travelling wave coplanar waveguide made in FR4 with multiple segments. The authors in [14] and [15] proposed a circular 50Ω spiral travelling wave design in FR4 material for NF radiation. The former has a segmented loop antenna on both sides and the latter has a patch antenna for FF radiation. The circular 50Ω microstrip line was used to feed both the segmented loops and the patches. The patch antennas and microstrip lines are separated by some distance that would introduce surface dead zones. The meandered line antenna proposed in [16] does not have a bandwidth wide enough to cover FCC band. In contrast, the proposed antenna in this manuscript has a uniform surface field distribution to avoid surface dead zones. It has confined Fresnel zone for detecting both near- and FF tags that can be stationary or in motion. Moreover, it does not pick up stray tags as its FF gain is negligible.

11.3 Antenna design and fabrication

A non-conventional commercially available building material known as *Palight* was chosen as the substrate for this antenna. Palight is a type of foamed PVC which is light weight, durable, highly chemical resistant, non-toxic, and self-extinguishing if exposed to fire [11]. As this material is not manufactured for RF applications, its dielectric properties such as dielectric constant and loss tangent are unknown. Moreover, the material is not always manufactured from virgin but recycled or reground PVC and the properties are subject to change. In this manuscript, a 50Ω microstrip line for 900MHz is designed using electrical parameters of virgin PVC and constructed in Palight to investigate its frequency of resonance. The constructed structure is simulated in ADS to obtain the same frequency deviation by altering the dielectric parameters. Palight`s dielectric constant (ε_r) is found to be ~1.45 with a loss tangent ($\tan\delta$) of 0.0001. The antenna design shown in Figure.11.1 is essentially a microstrip line laid in a rectangular spiral fashion. The 50Ω input impedance is transformed to a 100Ω microstrip line that runs as a rectangular spiral (7mm wide) using a quarter wave transformer 70.71Ω (14mm wide, 73mm long) and terminated with two 50Ω surface mount resistors in series. This arrangement is laid on a ground plane of dimensions 275×295mm.

The resonant frequency may shift due to small changes in dielectric constant. As microstrip lines are wide band in nature, this frequency shift will hardly be noticeable for operational band 902–928 MHz (FCC band for UHF RFID). Compared to a microstrip line made from traditional PCB, our 100Ω microstrip line is physically narrower, experiences more radiation loss, and its fields are not self-contained. This microstrip line design has to encounter a number of 90˚ bends to realize a rectangular spiral. Traditionally, these 90˚ bends will be mitered (45˚ cut) or curved to avoid abrupt reflections from the turns. However, in our design, these bends are not mitered to create an intentional impedance mismatch that leads to radiation at every 90˚ bend. The H-fields on the antenna surface help in detecting NF tags whereas the radiated E-fields contribute to energizing FF tags. The distance of separation between the microstrip lines in the spiral is only 3mm and this contributes coupling among the lines. Surface mount resistors are used to minimize the inductances. RG316 cable with SMA termination is soldered right on the panel edge. Copper tapes are used at the points of excitation and termination to facilitate soldering.

This antenna is fabricated using a non-conductive adhesive aluminum tape (0.1mm thick) to create the rectangular spiral microstrip transmission line on a 275×295×6mm Palight piece and a 275×295× 0.3mm scrap steel sheet for the ground plane (Figure. 7). The overlapped aluminum has minimal or no effects in RF performance as currents travel on surface of the microstrip line through capacitive coupling. Adhesive does not need to be conductive for the same reason. This is confirmed by measuring the insertion loss of an overlapped microstrip line. The ground plane is attached to the substrate by a double-sided clear tape. Adhesive copper tapes are used in places where soldering is essential, which otherwise requires special solder for soldering onto aluminum. The ground plane can also be constructed using strips of adhesive aluminum tapes.

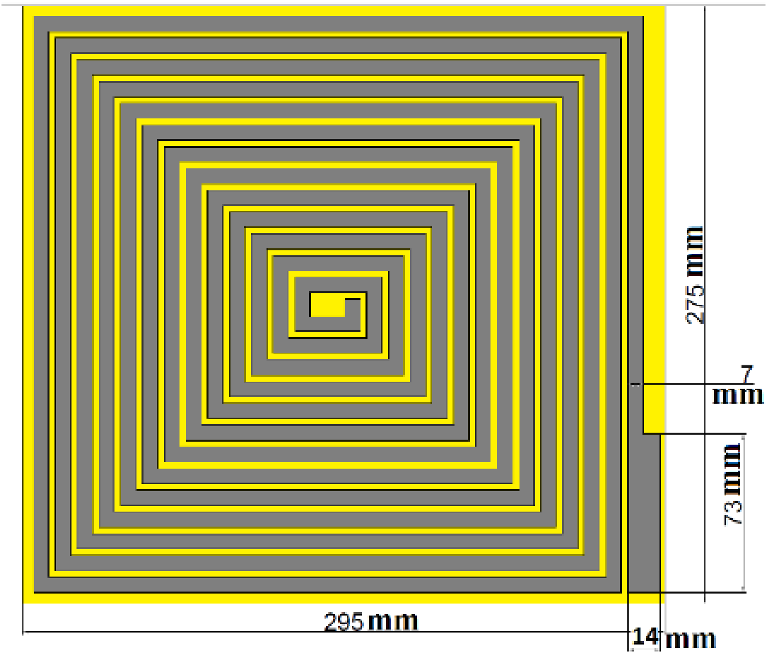

Figure.11.1. Antenna design

The presented antenna is easily scalable unlike antennas made of RF boards such as Taconic, Rogers or FR4s which have a size restriction and are often expensive for large sizes. This not only can be used as a standalone NF antenna for point-of-sale (POS) applications, but also can be realized as a RFID shelve by securing a sheet of Palight to the metal shelve and adhering a decal aluminum sheet that has the antenna pattern on top of the Palight material. Antenna can be fed via an edge mount connector or cables can be soldered (using special solder to avoid usage of copper tape) and run through to reach a RFID reader. The same Palight material can be used as radome to cover and protect the antenna artwork. Thickness of the radome can range from 1–3mm. Total material cost per antenna is $7.39 USD (Table.11.1)

Table.11.1. Proposed Bill of Materials

Part Description	**Cost (USD)**	**Quantity Used**	**Sub-Total (USD)**
3M Aluminium Tape	$10.68 (W-48mm, L-45m)	W-48mm, L-2.25m	$0.534
Scrap Steel	$0.83 / kg	0.15 kg	$0.1245
Palight Substrate	$53.36 (W-1.2m, L-2.4m)	W-0.3m, L-0.3m	$1.6675

3M Copper Tape	$32.87 (W-10mm, L-73m)	W-10mm, L-25mm	$0.052
RG316 Cable with SMA connector	$4.98	1	$4.98
SMD Resistor	$0.01	2	$0.02
Ground Pin	$0.01	1	$0.01

11.4 Analysis

Analysis of the proposed antenna commenced with method of moments (MoM) based electromagnetic (EM) simulation for matching and tuning. Hardware is fabricated based on the acquired pattern from simulation and tested using a vector network analyzer (VNA).

11.4.1 Simulation

Keysight's ADS momentum EM simulation software is used for simulating the antenna design as it is based on MoM that is far more accurate for planar antenna and transmission line simulation compared to FEM or FDTD calculation methods. Palight substrate of 6mm thickness, and εr and tanδ values of 1.5 and 0.0001, respectively, are chosen. Top conductor layer is considered to be made of 0.1mm thick aluminum sheet with a conductivity of 3.72×10^7 Siemens/m with no surface roughness. Bottom conductor of 275×295 mm dimensions and same properties as top conductor is designed for finite ground plane. Transmission line calibrated 50Ω port (P1) is used to excite the microstrip line and 100Ω port (P2) is where the microstrip line is terminated. An adaptive frequency sweep plan is opted between 800MHz and 1GHz and the frequency for meshing is mapped to the highest frequency for simulation. 20 cells per wavelength mesh density in conjunction with mesh reduction are found to be optimum in terms of calculation speed and CPU usage. Figure.11.2 shows the return loss (S_{11}) plot with multiple resonances. From 3D visualization of magnetic field distribution, it is observed that the microstrip line effectively radiates for the desired 902–928MHz frequency band. The −5dB bandwidth is found to be 7MHz with −20.2dB return loss at the center of the band. Figure.11.3 shows the current density (J) distribution over the surface. The distribution has high intensity over the surface showing no nulls.

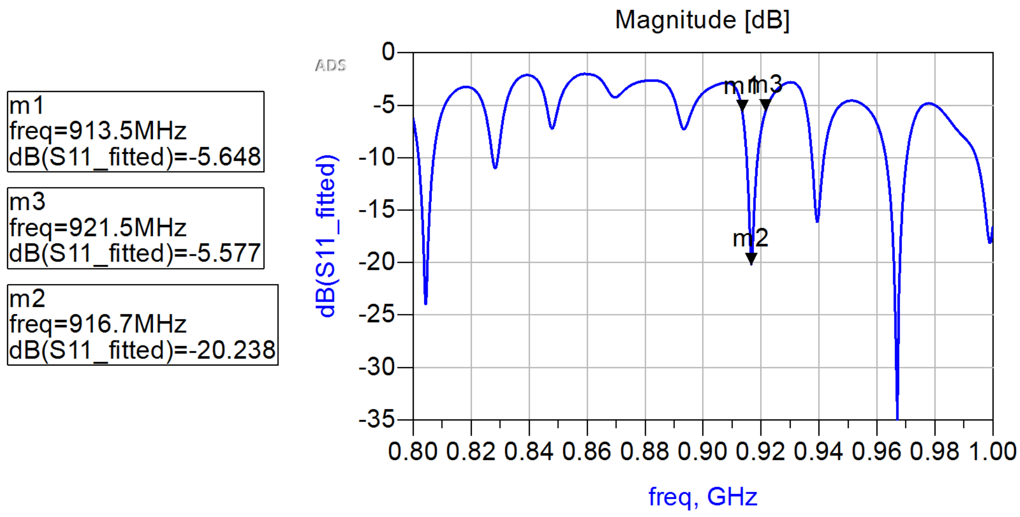

Figure.11.2. Simulated return loss (S_{11})

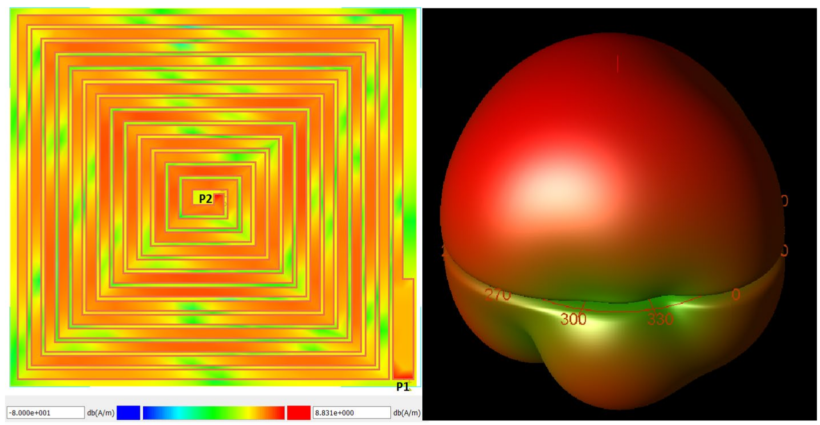

Figure.11.3. Current density distribution (left) and radiation pattern (right)

11.4.2 Hardware measurements

Unlike in the simulation, the fabricated hardware has a 100Ω resistor terminated to the ground plane. When measured with VNA (Figure.11.4) for its return loss (Figure.11.5), it is found that the hardware exhibits a wide band response across FCC's RFID frequencies with −17.7dB for 915MHz (centre of the band). The −10dB bandwidth is measured to be 55MHz, which provides sufficient tolerance to handle possible dielectric constant variation within the Palight material used here due to their less stringent and lower quality construction as compared to conventional RF boards. Using a radome made of Palight material over this antenna results in a frequency shift of ~ 2MHz towards the lower side of the band. Most RFID readers such as Impinj Speedway can effectively handle a return loss of −10dB [19]. A dipole antenna tuned for 800 – 1000 MHz was connected to VNA`s second port to measure the radiated power from the fabricated antenna through $S_{21}$ measurements to demonstrate that the antenna`s radiated power is much lower than a traditional far-field antenna. Power was measured at a distance greater than 1 wavelength (1λ is 327.8mm for 915MHz) where the transition from NF to FF occurs. A 9dBi patch antenna`s radiated power was measured to be -14.5dB at 360mm. The fabricated antenna`s power was measured to be -34.6dB and -46.4dB in horizontal and vertical orientation respectively. (Figure.11.6). By comparing the power to 9dBi antenna, the proposed antenna has -11.1dBi and -22.9dBi gain in horizontal and vertical orientation respectively

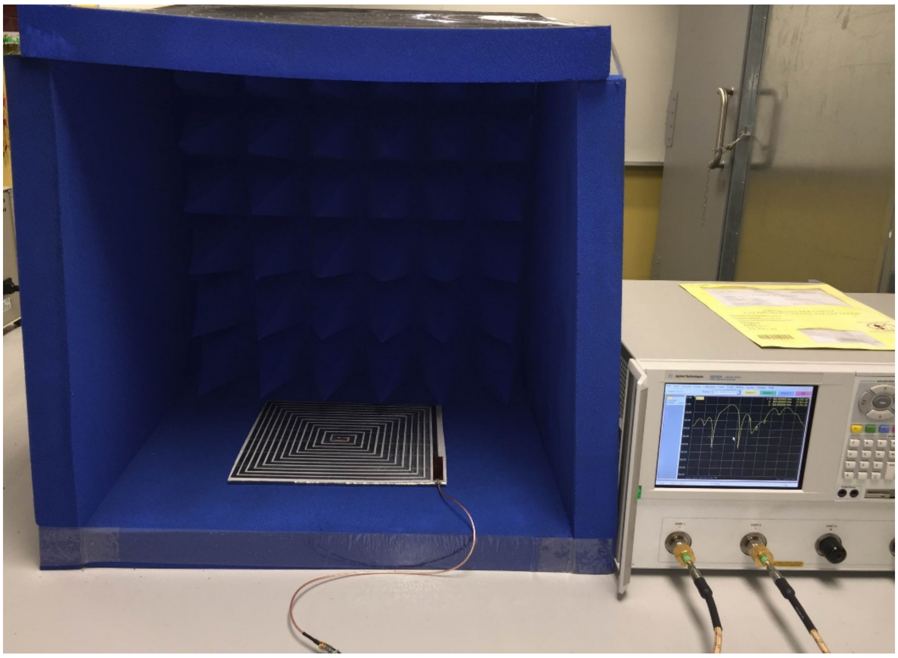

Figure.11.4. Measurement Setup

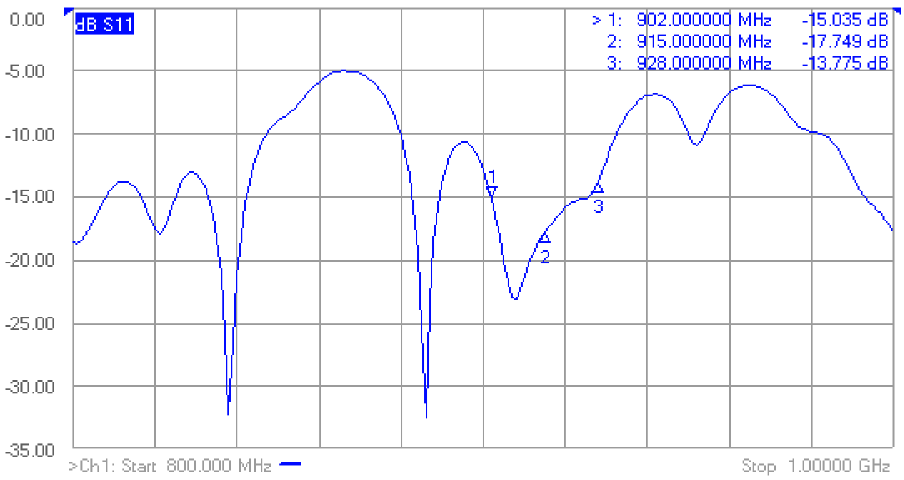

Figure.11.5. Return loss (S_{11}) of fabricated antenna

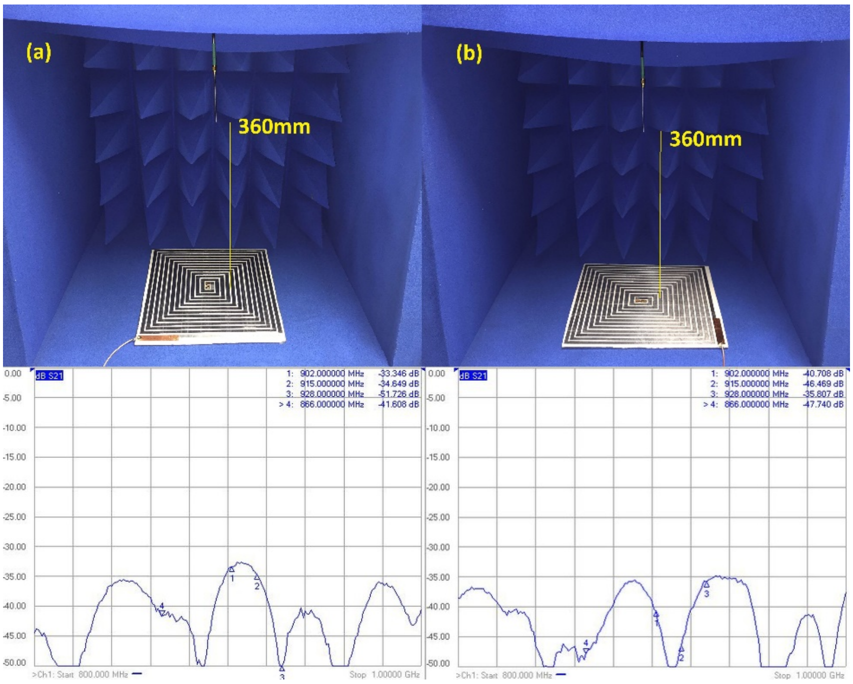

Figure.11.6. (a) Horizontal and (b) Vertical radiated power measurement (S_{21})

11.5 RFID tag testing

RFID tag testing is usually conducted to verify the antenna's performance in real time application, and the following metrics are recorded: (i) minimum power required to read a NF and FF tag; (ii) received signal strength indicator (RSSI measurements; (iii) surface dead spot analysis; and (iv) stray reads. The RFID tags used are: a) Alien SIT NF tag [20]; b) Impinj M5 FF tag [21]. FF tags consist of both loop antenna (for NF detection) and a dipole (for FF detection) whereas the NF tag has only a magnetic loop dedicated for NF tracking only. Impinj Speedway R420 Reader [19] is chosen to excite the antenna at the desired band (902–928 MHz). The reader complies with GS1 regulations. Impinj multi-reader software (factory read/write software for UHF RFID) is used to benchmark the performance with the setup shown in Table.11.2 [22].

Table.11.2. Impinj reader settings

Settings	Configuration/Value
Reader Mode	Auto Set Dense Reader
Search Mode	Dual Target
Session	Session 2
Population Estimate	32
Run Mode	Single Inventory
Tx Power	Variable (10 to 31dBm)
Rx Sensitivity	Up to -70 dBm

11.5.1 Test setup

Test zones are defined by virtually segmenting the antenna's surface into 9 equal parts (Figure.11.7), each of size ~98×92 mm. Test tag sheets, made from polyethylene foam having minimal RF absorption (Figure.11.8) are cut to this dimension. The tag sheets are 3mm thick to emulate the radomes`s incorporation at a later stage which introduces a similar height. 10 NF tags are randomly oriented and adhered to the sheet. Similarly, 3 FF tags are randomly oriented and adhered without overlapping each other. As the FF tags are physically bigger, each tag sheet is limited to 3 unique tags. The tag sheet is rotated 0˚, 90˚, 180˚ and 270˚ in each zone to test the antenna under different orientations. 4 orientations and 9 test zones yield a total of 36 measurements (Figure.11.9). 1mm deep notch was created on the rear side of the tag sheet to keep the sheet flush while testing at zone 9 where the sheet goes over the resistors.

Minimum power required to excite all 10 tags, $P_{t,\ min}$ is noted. Minimum and Maximum RSSI values ($P_{r,min}$ and $P_{r,max}$) of the tag signal detected by the antenna are noted for each zone. Purpose of the zone definition is to evaluate the energy distribution, and thus the presence or absence of any dead zones on the antenna`s surface.

11.5.2 Tag test results

RF power was increased in 1dBm steps from 10dBm start level, until all the tags are read in each zone. Styrofoam spacers (induced minimal attenuation) are used to position the tags at heights to find the maximum height until all tags are read in a tag sheet. Most commercial shelf racks are 15” high and so FF tags were tested at 380mm height to simulate the environment and benchmark its performance for stock inventory applications. Table III shows that a minimum power of 17dBm is required to excite all 10 NF tags for four different tag orientations in all defined zones at the surface except zone 9 which needed 20dBm. Tag which sits hard on the resistor is invisible at low power. By increasing the power, the intensity of the fields associated with the microstrip line adjacent to the resistors are also increased, leading to tag vicinity. Thus zone 9 needed more power. 25mm was the maximum height noted to read all 10 NF tags at 31dBm max power (Figure.11.8(a)). This shows that the antenna has a uniform NF distribution up to 25mm from the antenna`s surface. For FF tags (Figure.11.8(b)), it is noted that the antenna required only 13dBm as minimum power to read all 3 tags at the surface and 26dBm to read tags at 380mm high (Table.11.4). Number of tags would not affect the amount of power required to read them in a given surface area. When tags are piled in a dense environment, tags farther away from the antenna`s surface requires more power to be read compared to the ones at the surface. Min and Max RSSI value remained consistent in all zones, proving the uniformity in field distribution. It was also found that at 31dBm max power a NF and a FF tag cannot be read more than 100mm and 1.5m away from the antenna`s surface. This reveals that the antenna does not have radiative far-field component and thus avoids reading stray tags.

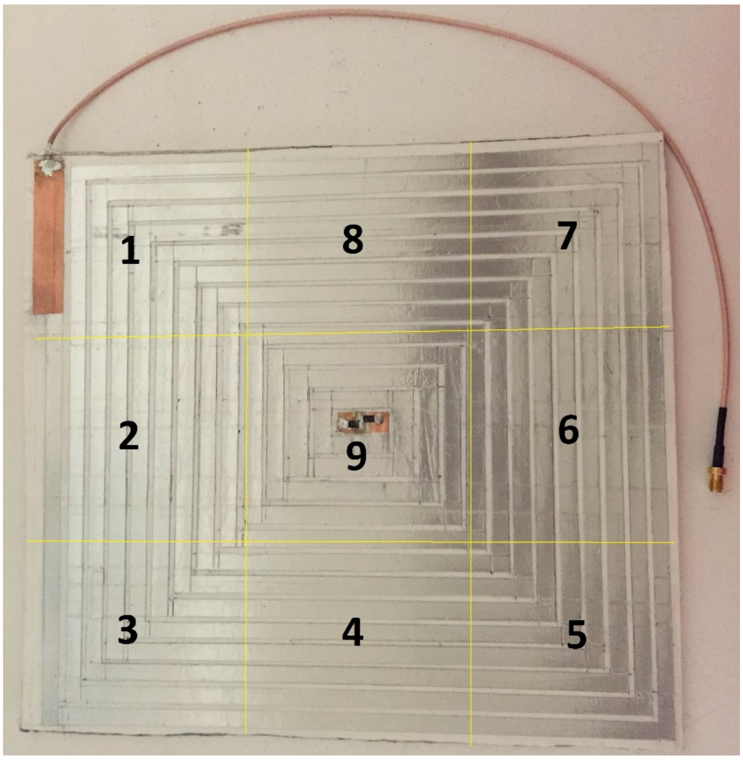

Figure.11.7. Test zone definition on fabricated antenna

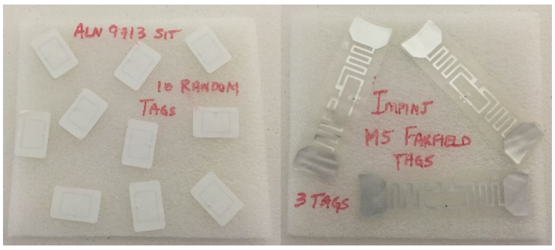

Figure.11.8. Randomly oriented NF and FF tags on test sheets

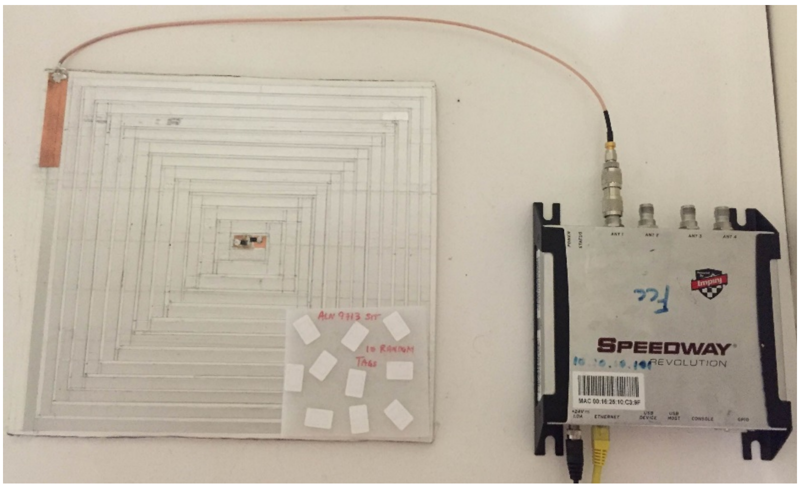

Figure.11.9. Surface tag test setup

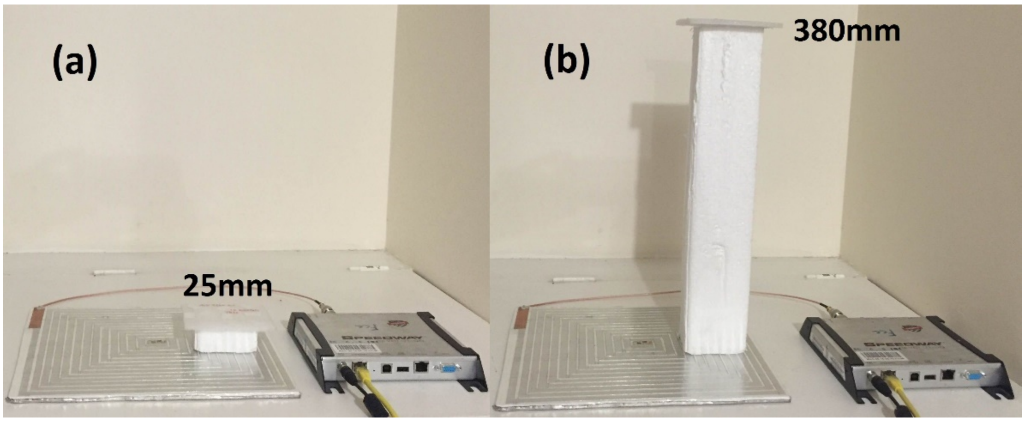

Figure.11.10. (a) NF tags 100mm high; (b) FF tags at 380mm high

Table.11.3. NF tag test results

Zone	Tags on the surface			Tags at 25mm height		
	$P_{t,\ min}$ (dBm)	$P_{r,max}$ (dBm)	$P_{r,min}$ (dBm)	$P_{t,\ min}$ (dBm)	$P_{r,max}$ (dBm)	$P_{r,min}$ (dBm)
1	17	-40	-53	31	-60	-73
2	17	-39	-54	31	-62	-74
3	17	-39	-51	31	-70	-73
4	17	-37	-52	31	-70	-73
5	17	-38	-54	31	-71	-72
6	17	-37	-54	31	-70	-73
7	17	-38	-55	31	-72	-75
8	17	-39	-53	31	-71	-72
9	20	-53	-60	31	-66	-77

Table.11.4. FF tag test results

Zone	Tags on the surface			Tags at 380 mm height		
	$P_{t,\ min}$ (dBm)	$P_{r,max}$ (dBm)	$P_{r,min}$ (dBm)	$P_{t,\ min}$ (dBm)	$P_{r,max}$ (dBm)	$P_{r,min}$ (dBm)
1	13	-18	-19	26	-59	-62
2	13	-19	-20	26	-62	-64
3	13	-18	-20	26	-59	-61
4	13	-18	-19	26	-63	-65
5	13	-17	-19	26	-60	-62
6	13	-18	-20	26	-60	-63
7	13	-17	-20	26	-62	-62
8	13	-18	-19	26	-60	-63
9	13	-19	-21	26	-63	-64

11.5 Conclusion and future work

A low-cost scalable UHF RFID antenna with uniform surface field distribution has been designed and tested for FCC RFID frequencies in accordance with GS1 standards. The designed antenna is not prone to detuning as it does not involve a FF radiator. Furthermore, stray tag detection is eliminated due to its low FF gain. The antenna can read tags in all considered orientations on the surface and at distances with no surface dead zones, leading to high accuracy in detection. Fabrication is easy and inexpensive with decal aluminium foil over a commercially available non-conventional substrate material. The antenna is scalable to custom sizes, and the substrate`s light weight, durability, high chemical resistance, non-toxicity and self-extinguishing (fire retardant) properties enhance the antenna's usability and regulatory compliance in different environments. As part of the future work, a similar antenna will be designed for ETSI RFID frequencies (865–868 MHz) and will have a radome, ready to implement in RFID smart shelves.

Prelude to Manuscript 9

A conformal display frame ultra-high frequency (UHF) radio frequency identification (RFID) reader antenna design is proposed for museums in this manuscript. The need of RFID in museum is essential as there are business benefits of tracking visitors who wear RFID enabled lanyards. When they approach and spend some time in-front of a particular artifact, the time spent can be identified and the reason for that person to spend time can be analysed. Different age group's interests can be found. The conformal antenna can seamlessly hide and blend with the museum environment. RFID asset tracking, personnel tracking and anti-theft surveillance, can be accomplished without altering the display artifacts or disturbing the aesthetics of the museum. Other similar designs have a patch antenna at the back of the picture or the artifact while this design does not need that antenna backing as the frame itself is an antenna.

The series fed patch antenna array, arranged in a circular fashion makes the RFID tag detection viable in any orientation at the near zone. The patch element's width is constrained by the width of the frame and thus, the length is calculated for 915 MHz centre frequency using the well-known patch antenna's resonant length formulae. The patch array is series fed with a 90° delayed microstrip line. The first and second elements;

and the third and fourth elements in the array are physically orthogonal. The first and third element; and the second and fourth elements are physically in the same plane. Thus, when driving them with serially, the realized polarization is slant along the diagonal axis.

At far-field distances, the antenna can detect tags up to 6 meters. The antenna has a bandwidth of 28 MHz and is designed for Region-2 RFID frequencies. It uses an unconventional substrate that is lightweight, non-toxic, chemically resistant and self-extinguishing if exposed to fire. These properties are inherited by the substrate, metal and adhesive layers as determined by their manufacturers. More than one frame antennas can be operated using multi-port RFID readers to realize a distributed antenna system within the museum. The antenna's half-power beam width is 60°, 45° in azimuth (E-plane or XZ plane, X being the short edge of frame and Z is the direction of propagation) and elevation (H-Plane or YZ plane, Y being the long edge of frame) planes with a 5dB front to back ratio. The antenna's read zone expands as the transmit power increases and the actual read range increase is dependent on the tag's sensitivity.

Chapter 12

Manuscript 9

Display frame UHF RFID antenna for museums

12.1 Introduction

The demand for automation is increasing to improve work productivity and life quality by reducing labor expenses, human errors and related costs. Passive ultra-high frequency (UHF) radio frequency identification (RFID) is an emerging technology that performs well if not better, while its cost and complexity are less than barcode or Near Field Communication (NFC) technologies. Museums which exhibit high valued assets such as paintings, antiques, and other artifacts, are amongst the most visited places by the public. Passive UHF RFID has been employed for asset management and asset surveillance in museums to keep track of the status, location, condition and movement of the exhibits. Museum visitors and employees can also be tracked within the museums for safety and productivity reasons. Reader antennas, an important component of passive UHF RFID systems, is often colossal and non-conformal. This manuscript proposes a design of a display frame UHF RFID reader antenna that can employed in museums due to its properties of being lightweight, visually covert, chemically resistant and self-extinguishing.

Related works include picture frame antenna and display device (e.g. TV) frame antennas [1]. The former constitutes a metal dipole antenna or a folded dipole-like antenna in a circuit board as backing of the picture frame, while the latter employs coils and chip antennas within the frame. In [2], a mobile phone frame antenna comprising of monopoles with omni-directional radiation is proposed. In [3], the authors designed a conformal patch array, which composes of power dividers and impedance transformers in series, leaving the patch antennas to operate in parallel. Unlike the existing works, the display frame antenna proposed in this manuscript does not contain an antenna backing, while the frame consists of a conformal patch array which is series fed using the patches and whose radiation is far more directional.

12.2 Design and fabrication

The proposed display frame antenna has four equal-width patches connected in series unlike traditional broad-side series patch array [4] whose widths are unequal throughout its length. Further, the proposed antenna`s array elements are arranged in a circular fashion, whereas other equal-width series patch antennas (e.g. [5]) are in a linear fashion. Although the polarization of the antenna will be a slant-linear, the circular patch arrangement will enable the antenna to detect tags in both vertical and horizontal orientations at near-field distances. The equal-width array is inset fed and is in series to match the input impedance [6]. A type of foamed PVC named *Palight* is used as the antenna`s substrate. Its electrical properties such as dielectric constant (ε_r of ~1.45) and loss tangent (*tanδ* of 0.0001) as well as mechanical properties such as being lightweight, durable, chemical resistant, and self-extinguishing if exposed to fire makes the antenna more suitable for museums and art-galleries.

The antenna is designed for Region-2 UHF RFID frequencies (902–928 MHz). The radiating patches and feed network are designed from a 0.1 mm copper board and the ground plane is made from 0.3 mm tinned steel. Patch antenna's width (20 mm) is made consistent for all four patches. To achieve an operating bandwidth of 28 MHz in a 6 mm thin substrate (1/35th of signal wavelength) and to accommodate effects of a paper radome, the resonant length of all patches is not made identical. The resonant length of two patches along the vertical and horizontal axis is 142 mm, and 134 mm, respectively. The array as a whole with paper radome will resonate at the center frequency (f_c).

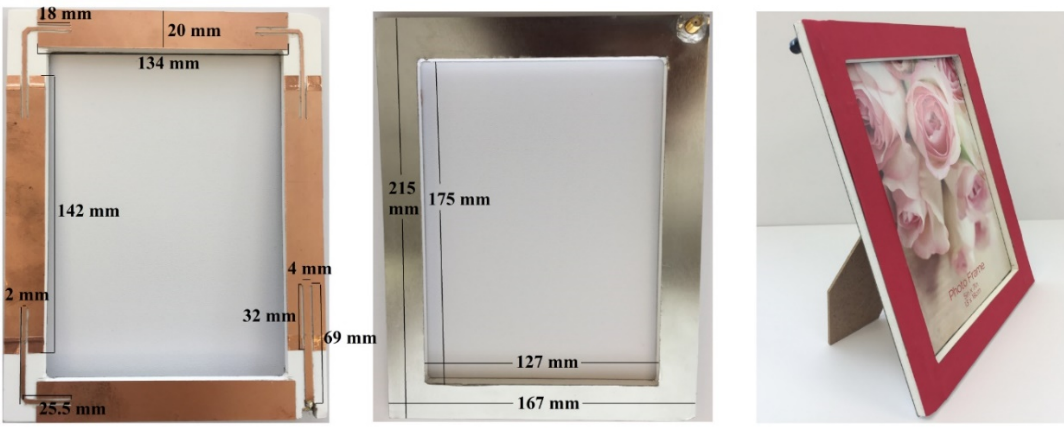

(a) (b) (c)

Figure.12.1. (a) Series fed patch antenna; (b) Ground plane with probe-fed connector; and (c) Antenna with paper radome on a frame stand.

The input impedance (50 Ω) is matched to the first patch`s load impedance (352 Ω) by a 132.6 Ω quarter-wave transformer. The load impedance is found at an inset of 32 mm from the edge of the patch using calibrated ports in ADS simulation software. A 169.9 Ω microstrip line is used for the series feed with an inset of 22 mm for the longer patches and 18 mm for the shorter patches. The antenna`s substrate and the ground plane form the 20 mm broad frame. The total frame length and width is 215 mm and 167 mm, respectively (Figure.12.1(b)). This enables the frame to display a standard 13 mm × 18 mm photo as a proof-of-concept for this work. In museums, display frames are often mounted on large metal embedded surfaces such as reinforced concrete wall, which in turn are expected to improve the antenna`s front-to-back ratio and gain due to a larger ground plane.

The fabricated antenna array and ground plane are adhered to the substrate using a 0.02 mm non-conductive acrylic adhesive. An SMA connector is probe fed through the substrate for the array excitation. The center pin and the ground of the connector are soldered. A 0.05 mm colored paper radome was affixed using the adhesive. A cardboard frame stand is bonded to the backside of the frame antenna where photos can be attached (Figure.12.1(c)).

12.3 Results and analysis

The fabricated antenna array is measured for its $|S_{11}|$ using a TR/1300 vector network analyzer (VNA). The $|S_{11}|$ at f_c is −33.269 dB. The low and high frequencies of the band have a $|S_{11}|$ of −11.43 dB, and −10.085 dB, respectively (Figure.2). The 10 dB return loss bandwidth of this antenna array is 28 MHz. The antenna`s far-field gain for different polarizations is measured by comparative analysis using a reference antenna at the boresight in different orientations. Figure.12.2 shows that the antenna`s peak gain is at slant 45° orientation. Table.12.1 shows the measured gains.

Table.12.1. Measured Far-field Gain

Polarization	**902 MHz**	**915 MHz**	**928 MHz**
Slant 45°	2.8 dBi	2.6 dBi	1.3 dBi
Horizontal (H)	0.7 dBi	1.6 dBi	1.4 dBi
Vertical (V)	0.4 dBi	−0.7 dBi	−3.4 dBi
Slant -45°	−10.5 dBi	−14.7 dBi	−29.3 dBi

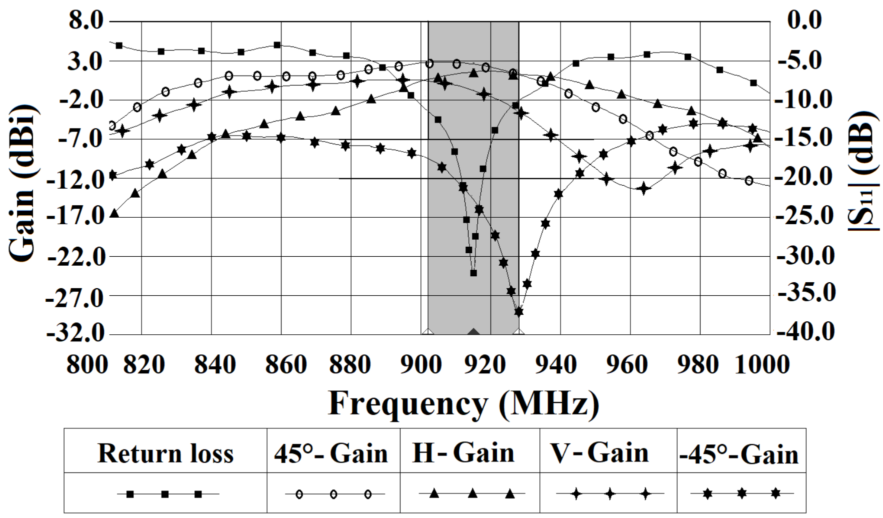

Figure12.2. Measured gain (left) and $|S_{11}|$ (right) performances

The maximum gain of the antenna array is 2.8 dBi at slant 45° polarization. The antenna has ~1 dB and ~2 dB less gain in horizontal and vertical polarization, respectively. Though the far-field gain for slant −45° polarization is less, the radiation at the near zone is useful for RFID tag detection. The antenna array`s radiation pattern was measured in azimuth and elevation planes and their corresponding half power beam-widths

(HPBW) are 60° and 45° (Figure.12.3(a)). The antenna`s front-to-back ratio is −5 dB and 4 dB in azimuth and elevation plane, respectively. The back radiation can be limited when the frame is mounted on-metal or on reinforced concrete walls containing steel mesh. The back-radiation can be advantageous in a two-sided frame where both side of the display frame bear antiques and vintages.

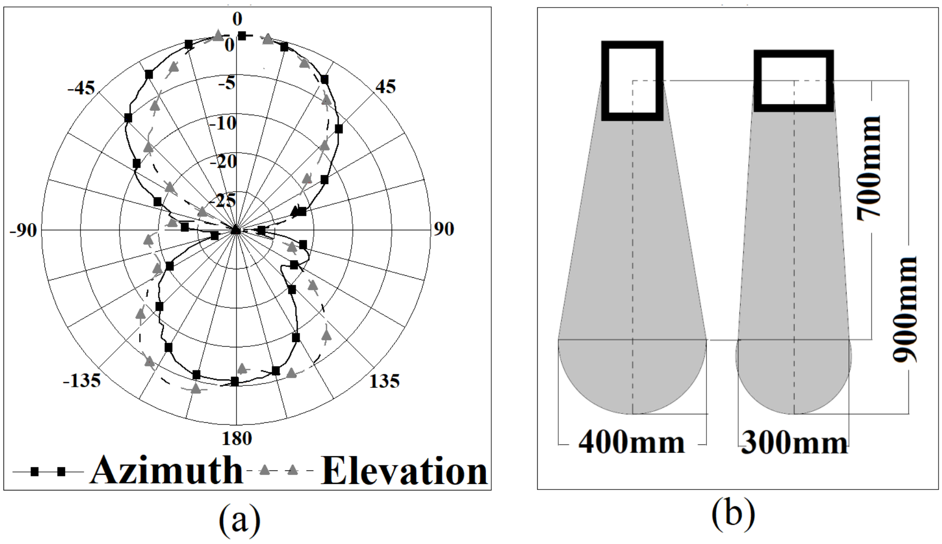

Figure.12.3. (a) Measured radiation pattern; and (b) 10 dBm read range

An Impinj r420 RFID reader and a Smartrac Dog-Bone Monza R6 RFID tag are used to test the RFID performance. The tag can be detected up to 6 m in antenna`s boresight at 31.5 dBm (max) transmitter ($t_x$) power. The maximum read distance at 10 dBm (min) $t_x$ power is 900 mm from antenna`s boresight. The antenna`s read-zone at 10 dBm $t_x$ power is 400 and 300 mm wide in azimuth and elevation plane, respectively, at 700 mm distance from antenna`s center (Figure.12.3(b)). The read-zone is shown to expand logarithmically as t_x power increases. Proximity visitors may absorb the RF energy but not significantly detune the antenna`s return loss [6].

12.4 Conclusion and future work

An RFID reader display frame antenna for museums is designed, fabricated and evaluated in this manuscript. An operational bandwidth of 28 MHz is achieved in a thin substrate antenna array for Region-2 UHF RFID frequencies. The antenna exibits a conformal and visually covert design with chemical resistance and self-extinguishing properties, which make them well-suited for museums. As future work, a distributed reader antenna system based on the proposed antenna will be experimentally evaluated for detection of embedded sensor tags in a museum environment.

Chapter 13

Conclusion

Five different commercially available non-conventional materials viz., recycled polyolefin, high-density polyethylene, foamed polyvinyl chloride, concrete brick and polylactic acid are analysed to design patch antenna and arrays. The commercial availability of these substrate materials enables the ease of fabrication. The substrate is characterized using the patch antenna resonance method. This method is accurate as the intended use is to make patch antennas and arrays at the same frequency. To ease the dielectric constant estimation process, a measurement jig is suggested with which different substrates can be measured non-invasively. The non-conventional substrates are low-cost, and their materials' costs are mentioned in the respective chapters. Non-conventional substrates enable conformal and seamless antenna designs. Non-conventional substrates' inherited physical and mechanical properties give rise to many other advantages viz., chemically resistant, fire retardant, and so on.

13.1 Summary of Contribution Chapters

Chapter 4 – Patch antenna from a recycled polyolefin substrate:

a) A commercially available substrate made from a recycled substrate is identified.
b) The dielectric constant is estimated using the patch antenna's resonance method. The same methodology is adopted for the rest of the manuscripts in this thesis.
c) A complex multi-polarizable patch antenna is designed, fabricated and tested for upper band UHF RFID frequencies.
d) A cross-shaped slot is incorporated to enhance the bandwidth of the patch antenna.
e) Substrate's low-cost nature is shown by comparing it with other conventional RF substrates.
f) The substrate is waterproof, UV resistant, self-lubricating, mould and bacteria growth resistant. It also has a surface tensile strength of 18 Mpa and has a hardness rating of Rockwell M-65. These inherited properties make the antenna advantageous.

Chapter 5 – Near-field fed far-field antenna from construction grade HDPE:

a) Thermoplastic, high-density polyethylene (HDPE), used for construction purposes is used as antenna's substrate.
b) The substrate is not made from recycled materials, but it is not manufactured in a controlled environment to keep up the dielectric properties' tolerances, either.
c) A wideband, near-field fed far-field antenna is designed in a thin substrate. Broad bandwidth is achieved by a V-slot and by the usage of a quadrature hybrid coupler.
d) The antenna's return loss is insusceptible to proximity assets and metal frames make it suitable for UHF RFID applications.
e) The antenna does not have any surface dead zones and has uniform energy distribution.

f) The antenna design, meandered line NF perimetric structures are scalable to different shapes and sizes.
g) The antenna is low-cost, and it is mechanically sturdy.
h) The antenna is tested for point-of-sale UHF RFID application.

Chapter 6 – Ultra-rugged antenna from concrete material:

a) Concrete brick is used as the antenna's substrate.
b) Monopole antenna is designed on the substrate with a ground plane. Substrate monopoles and dipoles with ground planes are similar to patch antennas.
c) The antenna is designed wideband to accommodate the potential dielectric constant changes in the substrate.
d) The antenna design is tested for its stability by varying temperature and humidity.
e) The antenna is also tested with different superstrates and different metallic structures, including reinforcing grids.
f) The effect of attaching and recessing to a concrete wall is tested under the influence of rain and condensation.
g) The antenna's read range is mapped along its boresight and circumferentially. Radiation fabric is also plotted using multiple UHF RFID tags.

Chapter 7 – Novel bandwidth enhancement technique for patch antennas:

a) A novel non-conventional bandwidth enhancement technique by intentional impedance mismatch is proposed.
b) The non-conventional material, HDPE, is as well used to apply this technique.

c) This technique is suitable for applications such as UHF RFID as the transceivers as they can handle higher RF reflections.
d) This technique not only enhances the bandwidth but also makes the design less susceptible to proximity assets' interference.

Chapter 8 – Reconfigurable patch antenna array in construction-grade HDPE:

a) HDPE substrate is used to design a low-cost quad-patch antenna array at USD \$9.35.
b) The antenna array's polarization and radiation pattern are reconfigurable using an external module.
c) The antenna has the ability to track RFID tag movement in a warehouse inventory tracking application using its grating lobe configuration.
d) Other configurations enable steered beam radiation to localize the scanning and eliminate stray reads by suppressing the sidelobes.
e) Both polarization and spatial diversity are achieved at very low-cost.

Chapter 9 – 3D printed concave shaped substrate and patch antenna in biodegradable substrate:

a) A bio-degradable substrate, PLA, is 3D printed to form a novel concave-shaped substrate. This novel shape enhances the patch antenna's bandwidth and beam-width.
b) The dielectric constant of the PLA substrate is estimated by patch antenna resonance method on a cuboid-shaped 3D printed substrate.

c) The patch conforms with the substrate's concavity, and thus the shape enhances the bandwidth and radiation pattern.
d) The antenna's bandwidth, radiation pattern or the axial ration does not get deteriorated with the inclusion of a large-sized ground reflector plate.

Chapter 10 – Radiative quadrature hybrid coupler in construction grade HDPE:

a) A microwave component, quadrature hybrid coupler is made from microstrip lines using an HDPE substrate.
b) It is a novel antenna design where the coupler's radiation is used for UHF RFID tag detection.
c) The design is non-conventional, yet the coupler's performance is comparable with that of a conventional coupler.
d) The intentional impedance mismatch technique discussed in chapter 4 is applied to obtain a wider operational bandwidth.
e) The hybrid design is insusceptible to proximity UHF RFID assets.

Chapter 11 – Near-field antenna from construction grade foamed PVC:

a) A non-conventional substrate, foamed-PVC (polyvinyl chloride) is used for a novel near-field antenna design.
b) The substrate's dielectric constant is estimated using a microstrip line's resonant method.
c) This non-conventional antenna is predominantly used as an insulation material in building construction.
d) The near-field antenna's length and width are scalable to larger or smaller sizes.

e) The antenna is suitable for pure near-field and close zone far-field operation.

f) The substrate is light-weight and has self-extinguishing properties.

Chapter 12 – Conformal patch antenna array from construction grade foamed PVC:

a) A conformal patch antenna array is made from a foamed-PVC substrate.

b) The substrate conforms to the shape of a display frame whereby the patch antenna array is formed in a circular fashion.

c) The antenna is aesthetically appealing, and it is intended to use in museums for personnel tracking using UHF RFID.

d) The display frame antenna is light-weight and mechanically sturdy with good chemical resistance and flammability specifications.

13.2 Limitations of current work

One of the main limitations of using a nonconventional substrate is its dielectric constant instability. Although the change is unpredictable, it was noted from experimentation that the changes would stay within a certain range for most of the non-conventional materials except for the recycled substrate mentioned in chapter 4. Non-conventional substrates such as HDPE, Palight (foamed PVC), PLA, etc., are virgin materials and are manufactured according to a specification such as a specific gravity (density) figure, chemical composition, etc. but not to RF specifications such as dielectric constant, loss tangent, etc. Different samples of HDPE and foamed PVCs are used in different antenna designs shown in chapters 5,7,8,11 and 12 and their dielectric constant did not vary significantly. Thus, the dielectric properties of these virgin materials do not vary as much as the recycled polyolefin material. The recycled substrate will also contain more impurities than other non-conventional substrates as they are intended to be a virgin. The manufacturing process is not strict enough to keep the dielectric constant tolerances on par in neither of the substrates. For an antenna to operate fine for various dielectric constant changes, it must have adopted one or more bandwidth enhancement techniques. Thus, another constraint is that only wideband antenna designs can use non-conventional substrates. A narrow band antenna design may need to be tuned every time when the substrate's properties changes.

Non-conventional substrates will have to be characterized for its dielectric constant value before an antenna can be designed. The substrate characterization process is a prerequisite whereas an antenna design from a conventional substrate does not need characterization. Some non-conventional substrates are lossy. This is a trade-off when compared with other advantages such as low-cost, ease-of-use, and so on. These substrates can still be used in applications where the antenna gain or directivity is not so significant.

13.3 Future work

As part of the future work, different substrates' dielectric constant stability over a wide temperature and humidity range will be studied. Current bandwidth enhancement techniques include slotted patch antenna, patch antenna array with multi-resonant patch elements, thicker substrate, intentional impedance mismatch technique and the usage of a wideband device in conjunction with the narrow band antenna. Other ways to enhance the antenna bandwidth will be studied and experimented. Along with this, an antenna optimization technique will be investigated to auto-tune the antenna's resonant length for various dielectric constant shifts that occur between different samples of the same non-conventional materials.

Moreover, the suitability of non-conventional substrate material in other applications such as 5G mobile communications, satellite communication, wireless power transfer and harvesting applications will be studied. Antenna design in higher frequencies such as the mm-wave will be challenging, and different non-conventional materials' properties at different frequencies will be investigated for efficient antenna design. LoRA WAN is yet another application that is similar to UHF RFID where the need for non-conventional material is required for low-cost novel antenna designs.

References

[1] Navy Radio Communications & Technology Publications, [Online]. Available: http://www.navy-radio.com/manuals/10228d/rm32_manual_64-08.pdf

[2] The Principle of Reciprocity in Antenna Theory, [Online]. Available: http://ieeexplore.ieee.org/stamp/stamp.jsp?arnumber=1694633

[3] Rashed, A, N, Z., & Sharshar, H, A., "Optical microstrip patch antennas design and analysis," Optik 124 – International Journal of Light and Electron Optics, Vol. 124, no. 20, pp. 4331-4335, 2013.

[4] Comparison of different types of patch antennas, [Online]. Available: http://research.ijcaonline.org/icaet2015/number5/icaet4062.pdf

[5] N. Nkordeh, F. Idachaba and O. Oni, "Microstrip Patch Antenna: Comparing Performance of a Rectangular and a Circular Patch at LTE Bluetooth and GSM Frequencies," in Proceedings of the World Congress on Engineering, London, Jul. 2015.

[6] Regulatory status for using RFID in the EPC Gen2 (860 to 960 MHz) band of the UHF spectrum, GS1, [Online]. Available: https://www.gs1.org/docs/epc/uhf_regulations.pdf, Accessed on: Sep. 3, 2018.

[7] EPC™ Radio-Frequency Identity Protocols Generation-2 UHF RFID, GS1, 2015.

[8] K. V. S. Rao, P. V. Nikitin and S. F. Lam, "Antenna design for UHF RFID tags: a review and a practical application," *IEEE Trans. on Ant. and Prop.*, vol. 53, no. 12, pp. 3870-3876, Dec. 2005.

[9] Guidelines for Choosing A Passive UHF RFID Antenna, [Online]. Available: https://blog.atlasrfidstore.com/choose-right-rfid-antenna, Accessed on: Sep. 3, 2018.

[10] Asset tracking in big organizations, [Online]. Available: https://www.rfidjournal.com/articles/view?507/2, Accessed on: Sep. 3, 2018.

[11] RFID becomes an overnight sensation for Sernam, [Online]. Available: http://www.rfidjournal.com/articles/view?2278/3, Accessed on: Sep. 3, 2018.

[12] All about the race: RFID is changing How we Race, [Online]. Available: https://blog.atlasrfidstore.com/all-about-the-timing, Accessed on: Sep. 3, 2018.

[13] What type of RFID system should we use to time a marathon race, [Online]. Available: http://www.rfidjournal.com/blogs/experts/entry?11089, Accessed on: Sep. 3, 2018.

[14] EPC bag tagging takes wing, [Online]. Available: http://www.rfidjournal.com/articles/view?2024/4, Accessed on: Sep. 3, 2018.

[15] IoT in pharmacies' refrigerators, [Online]. Available: https://www.rfidjournal.com/articles/view?17666, Accessed on: Dec. 31, 2018.

[16] UHF RFID in Russian toll collection points, [Online]. Available: https://blog.nxp.com/automotive/why-russians-dont-slow-down-to-pay-tolls, Accessed on: Dec. 31, 2018.

[17] Michel, M. R. Pino and P. Nepa, "Low-profile antennas for near-field UHF RFID systems: Design, measurements and system-level characterization," *Int. Conf. on EAA*, Verona, 2017, pp. 1563-1566.

[18] Low-friction plastics enhance performance under pressure, [Online]. Available: http://readingplastic.com/low-friction-plastics/, Accessed on: Sep. 3, 2018.

[19] S. Wang, X. Zhang, L. Zhu and W. Wu, "Single-Fed Wide-Beamwidth Circularly Polarized Patch Antenna Using Dual-Function 3-D Printed Substrate," *IEEE Ant. and Wire. Prop. Lett.*, vol. 17, no. 4, pp. 649-653, Apr. 2018.

[20] P. Kabacik and M. E. Bialkowski, "The temperture dependence of substrate parameters and their effect on microstrip antenna performance," *IEEE Trans. Ant. and Prop.*, vol. 47, no. 6, pp. 1042-1049, Jun. 1999

[21] *IEC*, 60068-2, 2018

[22] J. Lilja, P. Salonen, T. Kaija and P. de Maagt, "Design and Manufacturing of Robust Textile Antennas for Harsh Environments," *IEEE Trans. Ant. and Prop.*, vol. 60, no. 9, pp. 4130-4140, Sep. 2012.

[23] *ETSI*, EN300019-2-4, 2015.

[24] *IEC*, 60529, 2018.

[25] 3M Vibration damping tapes, [Online]. Available: https://multimedia.3m.com/mws/media/117317O/3mtm-scotchdamptm-vibration-434.pdf, Accessed on: Sep. 3, 2018.

[26] *IEC*, 60721-3-4, 1995.

[27] *ASTM*, G154, 2016.

[28] *UL*, UL-94, 2013.

[29] *IEC*, 60068-2-11, 1981.

[30] *ANSI*, TIA-222-G, 2005.

[31] *ETSI*, EN 1991-1-4, 2005.

[32] M6e Hardware Guide, [Online]. Available: http://www.dpie.com/manuals/rfid/M6eHardwareGuide_Sept13.pdf, Accessed on: Sep. 3, 2018.

[33] The Interaction of electrostatic Discharge and RFID, [Online]. Available: http://cdn.intechweb.org/pdfs/14424.pdf, Accessed on: Sep. 3, 2018.

[34] *FCC*, §15.247, 2015.

[35] *ETSI*, EN 302 208 V3.1.0, 2016.

[36] B. Shrestha, A. Elsherbeni and L. Ukkonen, "UHF RFID Reader Antenna for Near-Field and Far-Field Operations," *IEEE Ant. and Wire. Prop. Lett.*, vol. 10, pp. 1274-1277, Nov. 2011

[37] C.A. Balanis, *“Antenna Theory Analysis and Design”*, John Wiley & Sons, 1997, pp. 27-104.

[38] Gain correction factor to convert from dBiL to dBiC, [Online]. Available: https://www.cobham.com/media/83790/806-1.pdf, Accessed on: Sep. 3, 2018.

[39] *Conformité Européenne*, RED directive 2014/53/EU, 2014.

[40] *Conformité Européenne*, RoHS-3 directive 2015/863, 2015.

[41] *IEC*, IECEx-600079, 2014.

[42] *Conformité Européenne*, ATEX directive 2014/34/EU, 2014.

[43] *MIL-STD*, 464, 2010.

[44] *NFPA*, 90A, 2018.

[45] Brand, M., Osmun, S., Regnier, K., Lindstid, C., & Palangio, D. (2004). What we didn’t know about dielectric properties. Plastics Technology. Retrieved from http://www.ptonline.com/articles/what-we-didn't-know-about-dielectric-properties-of-plastics

[46] Reddy, R, J., Asmatulu, R., & Kahn, W, S. (2010). Electrical properties of recycled plastic nanocomposites produced by injection molding. Proceedings of the ASME 2010 International Mechanical Engineering Congress & Exposition.

[47] Ahmad, Z. (2012). Polymeric Dielectric Materials, University Sains Malaysia, Malaysia: Intech - Open Science, Open Minds. ISBN: 978-953-51-0764-4

[48] K. L. Lau and K. M. Luk, "A novel wide-band circularly polarized patch antenna based on L-probe and aperture-coupling techniques," *IEEE Transactions on Antennas and Propagation*, vol. 53, no. 1, pp. 577-582, Jan. 2005.

[49] Kin-Lu Wong and Hao-Chun Tung, "An inverted U-shaped patch antenna for compact operation," *IEEE Transactions on Antennas and Propagation*, vol. 51, no. 7, pp. 1647-1648, July 2003.

[50] N. Yan, K. Ma and H. Zhang, "A Novel Substrate-Integrated Suspended Line Stacked-Patch Antenna Array for WLAN," *IEEE Transactions on Antennas and Propagation*, vol. 66, no. 7, pp. 3491-3499, July 2018.

[51] A. Jaiswal, M. P. Abegaonkar and S. K. Koul, "Highly Efficient, Wideband Microstrip Patch Antenna With Recessed Ground at 60 GHz," *IEEE Transactions on Antennas and Propagation*, vol. 67, no. 4, pp. 2280-2288, April 2019.

[52] Y. Kim, H. Kim, I. Yoon and J. Oh, "4×8 Patch Array-Fed FR4-Based Transmit Array Antennas for Affordable and Reliable 5G Beam Steering," *IEEE Access*, vol. 7, pp. 88881-88893, 2019.

[53] X. Zhao and S. Riaz, "A Dual-Band Frequency Reconfigurable MIMO Patch-Slot Antenna Based on Reconfigurable Microstrip Feedline," *IEEE Access*, vol. 6, pp. 41450-41457, 2018.

[54] C. Deng, X. Lv and Z. Feng, "Low-profile circularly polarised patch–ring antenna with compact feeding network," in *IET Microwaves, Antennas & Propagation*, vol. 12, no. 3, pp. 410-415, 28 2 2018.

[55] F. Babaeian and N. C. Karmakar, "A High Gain Dual Polarized Ultra-Wideband Array of Antenna for Chipless RFID Applications," *IEEE Access*, vol. 6, pp. 73702-73712, 2018.

[56] M. S. Sharawi, S. Deif and A. Shamim, "An Electronically Controlled 8-ElementSwitched Beam Planar Array," in *IEEE Antennas and Wireless Propagation Letters*, vol. 14, pp. 1350-1353, 2015.

[57] N. Shoaib, S. Shoaib, R. Y. Khattak, I. Shoaib, X. Chen and A. Perwaiz, "MIMO Antennas for Smart 5G Devices," *IEEE Access*, vol. 6, pp. 77014-77021, 2018.

[58] T. Zhang *et al.*, "High-gain low-cost broadband 60 GHz differential integrated patch array antennas with wire-bonding packaging and on-board compensation network," *IET Microwaves, Antennas & Propagation*, vol. 11, no. 7, pp. 971-975, 2 6 2017.

[59] F. Faisal and H. Yoo, "A Miniaturized Novel-Shape Dual-Band Antenna for Implantable Applications," *IEEE Transactions on Antennas and Propagation*, vol. 67, no. 2, pp. 774-783, Feb. 2019.

[60] O. Abu Safia, M. Nedil, L. Talbi and K. Hettak, "Coplanar waveguide-fed rose-curve shape UWB monopole antenna with dual-notch characteristics," *IET Microwaves, Antennas & Propagation*, vol. 12, no. 7, pp. 1112-1119, 13 6 2018.

[61] H. Zahir *et al.*, "Design fabrication and characterisation of polyaniline and multiwall carbon nanotubes composites-based patch antenna," *IET Microwaves, Antennas & Propagation*, vol. 10, no. 1, pp. 88-93, 9 1 2016

[62] A. S. Eltrass and N. A. Elborae, "New design of UWB-MIMO antenna with enhanced isolation and dual-band rejection for WiMAX and WLAN systems," *IET Microwaves, Antennas & Propagation*, vol. 13, no. 5, pp. 683-691, 17 4 2019.

[63] G. Monti, L. Catarinucci, C. Vasanelli and L. Tarricone, "3D patch antenna using a cardbord substrate for RFID reader applications," *2012 42nd European Microwave Conference*, Amsterdam, 2012, pp. 884-887.

[64] I. Kharrat, P. Xavier, T. -. Vuong, J. -. Duchamp, P. Benech and G. E. P. Tourtollet, "Low-Loss Paper Substrate for Printed High Efficiency Antennas at 2.45 GHz," *IEEE Antennas and Wireless Propagation Letters*, vol. 14, pp. 1400-1403, 2015

[65] H. Saghlatoon, L. Sydänheimo, L. Ukkonen and M. Tentzeris, "Optimization of Inkjet Printing of Patch Antennas on Low-Cost Fibrous Substrates," *IEEE Antennas and Wireless Propagation Letters*, vol. 13, pp. 915-918, 2014.

[66] H. Saghlatoon, L. Sydänheimo, L. Ukkonen and M. M. Tentzeris, "Optimized RF/microwave antennas and circuits on low-cost fibrous substrates using inkjet-printing technology," *2014 IEEE Antennas and Propagation Society International Symposium (APSURSI)*, Memphis, TN, 2014, pp. 322-323.

[67] S. Wang, L. Zhu and W. Wu, "3-D Printed Inhomogeneous Substrate and Superstrate for Application in Dual-Band and Dual-CP Stacked Patch Antenna," *IEEE Transactions on Antennas and Propagation*, vol. 66, no. 5, pp. 2236-2244, May 2018.

[68] M. Ramadan and R. Dahle, "Characterization of 3-D Printed Flexible Heterogeneous Substrate Designs for Wearable Antennas," *IEEE Transactions on Antennas and Propagation*, vol. 67, no. 5, pp. 2896-2903, May 2019.

[69] S. S. Bukhari, W. G. Whittow, J. Joubert and J. (. C. Vardaxoglou, "Flexible three-dimensional printed antenna substrates," *The Journal of Engineering*, vol. 2015, no. 8, pp. 258-260, 8 2015.

[70] C. C. Njoku, W. G. Whittow and J. C. Vardaxoglou, "Microstrip Patch Antennas With Anisotropic and Diamagnetic Synthetic Heterogeneous Substrates," *IEEE Transactions on Antennas and Propagation*, vol. 63, no. 7, pp. 3280-3285, July 2015.

[71] S. Wang, X. Zhang, L. Zhu and W. Wu, "Single-Fed Wide-Beamwidth Circularly Polarized Patch Antenna Using Dual-Function 3-D Printed Substrate," *IEEE Antennas and Wireless Propagation Letters*, vol. 17, no. 4, pp. 649-653, April 2018.

[72] C. Mendes and C. Peixeiro, "A Dual-Mode Single-Band Wearable Microstrip Antenna for Body Area Networks," *IEEE Antennas and Wireless Propagation Letters*, vol. 16, pp. 3055-3058, 2017.

[73] L. Song and Y. Rahmat-Samii, "A Systematic Investigation of Rectangular Patch Antenna Bending Effects for Wearable Applications," *IEEE Transactions on Antennas and Propagation*, vol. 66, no. 5, pp. 2219-2228, May 2018.

[74] W. T. Li, Y. Q. Hei, P. M. Grubb, X. Shi and R. T. Chen, "Inkjet Printing of Wideband Stacked Microstrip Patch Array Antenna on Ultrathin Flexible Substrates," *IEEE Transactions on Components, Packaging and Manufacturing Technology*, vol. 8, no. 9, pp. 1695-1701, Sept. 2018.

[75] A. T. Castro and S. K. Sharma, "Inkjet-Printed Wideband Circularly Polarized Microstrip Patch Array Antenna on a PET Film Flexible Substrate Material," *IEEE Antennas and Wireless Propagation Letters*, vol. 17, no. 1, pp. 176-179, Jan. 2018.

[76] M. Y. Mat Zain, M. T. Ali, A. N. H. Hussin and B. Baharom, "2.4GHz Patch Antenna on Bio-Composite Substrate Using Quarter Wave Transmission Line," *2018 International Symposium on Antennas and Propagation (ISAP)*, Busan, Korea (South), 2018, pp. 1-2

[77] H. F. Khalili *et al*., "Biodegradable Dual Semicircular Patch Antenna Tile for Smart Floors," *IEEE Antennas and Wireless Propagation Letters*, vol. 18, no. 2, pp. 368-372, Feb. 2019.

[78] P. Rawat, M. Sharma, B. Kaur, D. Mittal, D. Singh and E. Sidhu, "Performance evaluation of microstrip patch antenna using plywood as substrate for fixed satellite and earth exploration applications," *2017 International Conference On Smart Technologies For Smart Nation (SmartTechCon)*, Bangalore, 2017, pp. 153-157.

[79] M. Akbari, J. Virkki, M. W. A. Khan, L. Sydänheimo and L. Ukkonen, "Towards eco-friendly and cost-effective passive RFID applications," *2016 10th European Conference on Antennas and Propagation (EuCAP)*, Davos, 2016, pp. 1-4

[80] D. E. Anagnostou, A. A. Gheethan, T. Amert and K. W. Whites, "A low-cost WLAN “Green” PIFA antenna on eco-friendly paper substrate," *2009 IEEE Antennas and Propagation Society International Symposium*, Charleston, SC, 2009, pp. 1-4

[81] J. Kumar, B. Basu, F. A. Talukdar and A. Nandi, "Graphene: A possible low-cost eco-friendly solution for antenna applications," *2017 IEEE Applied Electromagnetics Conference (AEMC)*, Aurangabad, 2017, pp. 1-2.

[82] Kumar, J., Gupta, N., "An eco-design of dielectric resonator antenna for wideband applications," *The IUP Journal of Telecommunications*, vol. 8, no. 1, pp. 47-52, 2016. Retrieved from http://search.proquest.com/openview/986732015a26dde9ff10fd3a91353908/1?pq-origsite=gscholar&cbl=2030006

[83] Manna, D., Majee, T., Patrs, S., Sarkar, B., Banik, S., Azim, N., Imdad, M, S., & Das, S., "Simulation of a rectangular patch antenna with polyolefin substrate from wasted materials by Zeland IE3D," *International journal of Scientific and Research Publications*, vol. 5, no. 4, pp. 1-3, 2015. Retrieved from http://www.ijsrp.org/research-paper-0415/ijsrp-p4098.pdf

[84] E. C. Moreira, A. S. B. Sombra and G. C. Barroso, "An UHF RFID reader antenna made of recycled and reutilized materials from construction debris," *2012 IEEE 23rd International Symposium on Personal, Indoor and Mobile Radio Communications - (PIMRC)*, Sydney, NSW, 2012, pp. 1779-1784.

[85] G. M. Turner and C. Christodoulou, "FDTD analysis of phased array antennas," *IEEE Transactions on Antennas and Propagation*, vol. 47, no. 4, pp. 661-667, April 1999.

[86] Kavkic, U., Pivar, M., Dokic, M., Gregor-Svetec, D., Pavlovic, L., & Muck, T., "UHF RFID tags with printed antennas on recycled papers and cardboards" *Materials and Technology*, vol. 48, no. 2, pp. 261-267, 2014. Retrieved from http://mit.imt.si/Revija/izvodi/mit142/kavcic.pdf

Chapter 4 reference list:

[1] C. Deng, X. Lv, and Z. Feng, "Wideband Dual-Mode Patch Antenna with Compact CPW Feeding Network for Pattern Diversity Application," IEEE Trans. Ant. Prop., vol. 66, no. 5, pp. 2628-2633, 2018.

[2] J. F. Lin, and Q. X. Chu, "Enhancing Bandwidth of CP Microstrip Antenna by Using Parasitic Patches in Annular Sector Shapes to Control Electric Field Components," IEEE Ant. Wire. Prop. Lett., vol. 17, no. 5, pp. 924-927, 2018.

[3] I. Kharrat, P. Cavier, T.P. Vuong, J. Duchamp, P. Benech, and E. Tourtollet, "Low-Loss Paper Substrate for Printed High Efficiency antennas at 2.4 GHz," IEEE Ant. Wire. Prop. Lett., vol. 14, pp. 1400-1403, 2015.

[4] H. Saghlatoon, L. Sydanheimo, L. Ukkonen and M. Tentzeris, "Optimization of Inkjet Printing of Patch Antennas on Low-Cost Fibrous Substrates," IEEE Ant. Wire. Prop. Lett., vol. 13, pp. 915-918, 2014.

[5] A. Paraskevopoulos, D.S. Fonseca, R.D. Seager, W.G. Whittow, J.C. Vardaxoglou and A.A. Alexandridis, "Higher-mode textile patch antenna with embroidered vias for on-body communication," IET Micro. Ant. Prop., vol. 10, no. 7, pp. 802-807, 2016.

[6] S. Wang, L. Zhu, and W. Wu, "3-D Printed Inhomogeneous Substrate and Superstrate for Application in Dual-Band and Dual-CP Stacked Patch Antenna," IEEE Trans. Ant. Prop., vol. 66, no. 5, pp. 2236-2244, 2018.

[7] N. Yan, K. Ma, and H. Zhang, "A Novel Substrate-Integrated Suspended Line Stacked-Patch Antenna Array for WLAN," IEEE Trans. Ant. Prop., vol. 66, no. 7, pp. 3491-3499, 2018.

[8] D. Sarmah, N. S. Bhattacharyya, and S. Bhattacharyya, "Study of Graded Composite (LDPE/TIO_2) Materials as Substrate for Microstrip Patch Antennas in X-band," IEEE Tran. Dielectr. Electr. Insul., vol. 20, no. 5, pp. 1845-1850, 2013.

[9] E. C. Moreira, A. S. B. Sombra, and G. C. Barroso, "An UHF RFID Reader Antenna made of Recycled and Reutilized Materials from Construction Debris," *IEEE Int. Symp. Indoor and Mobile Radio Comm.,* 2012, pp. 1779-1784.

[10] Uniboard Eco Data Sheet, Dotmar Plastics, 2010. [Online]. Available: http://www.dotmar.co.nz/productmanager/uploads/UNIBOARD%20ECO%20DATA%20SHEET.pdf [Accessed: 11- Feb- 2019]

[11] D. Shimin, "A New Method for Measuring Dielectric Constant Using the Resonant Frequency of a Patch Antenna," IEEE Trans. Microwave Theory and Technique, vol. 34, no. 9, pp. 923-931, 1986.

[12] C. A. Balanis, "Antenna theory: a review," Proc. IEEE, vol. 80, pp. 7-23, 1992.

[13] L-3 Avionics systems, "RF / Microwave PC Board Design and Layout", [Online]. Available: https://www.jlab.org/accel/eecad/pdf/050rfdesign.pdf [Accessed: 27-Feb-2019.

[14] S. A. Sacharias, and S. Suganthi, "Performance Improvement of Triple Band Truncated Spiked Triangular Patch Antenna," *Int. Conf. Emerging Trends in Engg. Tech. and Sci.*, 2016, pp. 1-4.

[15] J. J. Ou, A. S. Andenko, Y. Li, Q. Zhang, and H. Z. Tan, "High-Efficiency and Wide-Frequency-Ratio Dual-Band Slot Patch Antenna Utilizing the Perturbed TM_{02} Modes," IEEE Ant. And Wireless Prop. Lett., vol. 17, no. 4, pp. 579-582, 2018.

[16] W. S. Chen, K. L. Wong, and C. K. Wu, "Inset Microstrip Line-Fed Circularly Polarized Microstrip Antennas," *IEEE Trans. Ant. Prop*. vol. 48, no. 8, pp. 1253-1254, 2000.

[17] N. Liu, L. Zhu, W. Choi and X. Zhang, "A Low-Profile Differential-Fed Patch Antenna With Bandwidth Enhancement and Sidelobe Reduction Under Operation of $TM_{10}$and TM_{12}Modes," *IEEE Trans. Ant. Prop*., vol. 66, no. 9, pp. 4854-4859, 2018.

[18] K. D. Xu, H. Xu, Y. Liu, J. Li and Q. H. Liu, "Microstrip Patch Antennas With Multiple Parasitic Patches and Shorting Vias for Bandwidth Enhancement," *IEEE Access*, vol. 6, pp. 11624-11633, 2018.

[19] M. Sharifian Mazraeh Mollaei, E. Zanganeh and M. Feshki Farahani, "Enhancement of Patch Antenna Gain Using Cylindrical Shell-Shaped Superstrate," IEEE Ant. Wireless Prop. Lett., vol. 16, pp. 2570-2573, 2017.

Chapter 5 reference list:

[1] G. Xiao *et al.*, "Printed UHF RFID Reader Antennas for Potential Retail Applications," *IEEE Journal of Radio Frequency Identification,* vol. 2, no. 1, pp. 31-37, March 2018.

[2] A. Michel, P. Nepa, X. Qing and Z. N. Chen, "Considering High-Performance Near-Field Reader Antennas: Comparisons of Proposed Antenna Layouts for Ultrahigh-Frequency Near-Field Radio-Frequency Identification," *IEEE Antennas and Propagation Magazine*, vol. 60, no. 1, pp. 14-26, February 2018.

[3] P. Parthiban, B. Seet and X. J. Li, "Low-cost low-profile UHF RFID reader antenna with reconfigurable beams and polarizations," *2017 IEEE International Conference on RFID (RFID)*, Phoenix, 2017, pp. 81-87.

[4] J. Lim *et al.*, "A balanced power amplifier utilizing the reflected input power," *2009 IEEE International Symposium on Radio-Frequency Integration Technology (RFIT)*, Singapore, 2009, pp. 88-91.

[5] P. Parthiban, B. Seet and X. J. li, "Scalable Near-field Fed Far-field UHF RFID Reader Antenna for Retail Checkout Counters," *2019 IEEE International Conference on RFID (RFID)*, Phoenix, AZ, USA, 2019, pp. 1-6

[6] Y. Zeng, Z. N. Chen, X. Qing and J. Jin, "A Directional, Closely Spaced Zero-Phase-Shift-Line Loop Array for UHF Near-Field RFID Reader Antennas," *IEEE Transactions on Antennas and Propagation*, vol. 66, no. 10, pp. 5639-5642, October 2018.

[7] C. Huang, C. Wang, J. Zhu and W. Tang, "A Reader Antenna for UHF Near-Field RFID Applications Based on the Segment-Line Oppositely Directed Currents," *IEEE Antennas and Wireless Propagation Letters*, vol. 17, no. 12, pp. 2159-2163, December 2018.

[8] J. Guo, H. Lan and Y. Yin, "A Near-Field UHF RFID Reader Antenna Without Dead Zones," *2018 International Conference on Microwave and Millimeter Wave Technology (ICMMT),* Chengdu, China, 2018, pp. 1-3.

[9] J. Zhang and Z. Shen, "Dual-Band Shared-Aperture UHF/UWB RFID Reader Antenna of Circular Polarization," *IEEE Transactions on Antennas and Propagation*, vol. 66, no. 8, pp. 3886-3893, August 2018.

[10] X. Yi, L. Huitema and H. Wong, "Polarization and Pattern Reconfigurable Cuboid Quadrifilar Helical Antenna," *IEEE Transactions on Antennas and Propagation*, vol. 66, no. 6, pp. 2707-2715, June 2018.

[11] J. Li, H. Liu, S. Zhang, M. Luo, Y. Zhang and S. He, "A Wideband Single-Fed, Circularly-Polarized Patch Antenna With Enhanced Axial Ratio Bandwidth for UHF RFID Reader Applications," *IEEE Access*, vol. 6, pp. 55883-55892, October 2018.

[12] J. Zheng, Y. Yang, X. He, C. Mao, J. Gao and C. Zhou, "Multiple-port reader antenna with three modes for UHF RFID applications," *Electronics Letters*, vol. 54, no. 5, pp. 264-266, March 2018.

[13] D. Ding, J. Xia, L. Yang and X. Ding, "Multiobjective Optimization Design for Electrically Large Coverage: Fragment-Type Near-Field\/Far-Field UHF RFID Reader Antenna Design," *IEEE Antennas and Propagation Magazine*, vol. 60, no. 1, pp. 27-37, February 2018.

[14] J. Yan, C. Liu, X. Liu, J. Li, H. Guo and X. Yang, "A Switchable Near-/Far-Field Reader Antenna for UHF RFID Applications," *IEEE Antennas and Wireless Propagation Letters*, vol. 17, no. 5, pp. 789-793, May 2018.

[15] M. Lalkota, G. Gupta and A. R. Harish, "UHF reader antenna for near and far field RFID operation," *2018 IEEE International Conference on RFID (RFID)*, Orlando, FL, 2018, pp. 1-7.

[16] J. K. Pakkathillam, M. Kanagasabai and M. G. N. Alsath, "Compact Multiservice UHF RFID Reader Antenna for Near-Field and Far-Field Operations," *IEEE Antennas and Wireless Propagation Letters*, vol. 16, pp. 149-152, 2017.

[17] Y. Yao, C. Cui, J. Yu and X. Chen, "A Meander Line UHF RFID Reader Antenna for Near-field Applications," *IEEE Transactions on Antennas and Propagation*, vol. 65, no. 1, pp. 82-91, January 2017.

[18] W.S. Chen, K. L. Wong, and C.K. Wu "Inset microstripline-fed circularly polarized microstrip antennas", IEEE TAP, vol. 48, no. 8, pp. 1253-1254, August 2000.

[19] Speedway r420 reader (2018, December 14). Impinj [Online]. Available: https://www.impinj.com/platform/connectivity/speedway-r420/

[20] Miniweb (2018, December 14). Smartrac-group [Online]. Available: https://www.smartrac-group.com/miniweb.html

[21] Bling (2018, December 14). Smartrac-group [Online]. Available:: https://www.smartrac-group.com/bling.html

Chapter 6 reference list:

[1] Gs1. [Online]. Available: http://www.gs1.org

[2] M. Merenda, S. Pizzi, R. Carotenuto, A. Molinaro, F. Della Corte and A. Iera, “Design Principles of a Fully-Passive RFID-based IoT Sensing Node,” *European Wireless Conf.*, pp. 1-6, 2018.

[3] A. Abdelnour, F. Buchin, D. Kaddour and S. Tedjini, "Improved traceability solution based on UHF RFID for cheese production sector," *IEEE Journal of Radio Frequency Identification, pp. 1-1, 2018.*

[4] A3010 Datasheet. Times-7 Research Ltd. New Zealand [Online]. Available: http://www.times-7.com/assets/files/datasheets/Current%20Datasheets/A3010%20Datasheet_v1.4.pdf

[5] XC-ST900-R1 Datasheet. Invengo. Singapore [Online]. Available: https://channel.invengo.com/wp-content/uploads/2016/06/Invengo_XCST900R1_V21102015.pdf

[6] S8656XR Datasheet. Laird Technologies. UK [Online]. Available: http://rfid.atlasrfidstore.com/hs-fs/hub/300870/file-1486000754-pdf/Tech_Spec_Sheets/Laird/ATLAS_Laird_S9026XRRN.pdf

[7] J. R. Sanford, "A novel RFID reader antenna for extreme environments," *IEEE Antennas and Propagation Society International Sym.*, San Diego, CA, USA, pp. 1-4, 2008.

[8] P. V. Nikitin and K. V. S. Rao, "Compact Yagi antenna for handheld UHF RFID reader," *IEEE Antennas and Propagation Society International Symposium*, Toronto, ON, Canada, pp. 1-4, 2010.

[9] P. V. Nikitin and K. V. S. Rao, "Helical antenna for handheld UHF RFID reader," *2010 IEEE International Conference on RFID (IEEE RFID 2010)*, Orlando, FL, USA, pp. 166-173, 2010.

[10] Z. Esmati, S. Kharkovsky and B. Samali, "Wireless power transmission inside reinforced concrete slab using a resonant antipodal Vivaldi antenna," *IEEE-APS*

Topical Conf. Antennas and Propagation in Wireless Communications (APWC), Cairns, Australia, pp. 118-121, 2016.

[11] G. Castorina, L. Di Donato, A. F. Morabito, T. Isernia and G. Sorbello, "Analysis and Design of a Concrete Embedded Antenna for Wireless Monitoring Applications [Antenna Applications Corner]," *IEEE Antennas and Propagation Magazine*, vol. 58, no. 6, pp. 76-93, 2016.

[12] C. Mariotti, G. Orecchini, M. Virili, F. Alimenti and L. Roselli, "RFID tag antenna embedded in concrete structures for construction industry," *European Conf. Antennas and Propagation (EUCAP)*, Rome, Italy, pp. 3469-3472, 2011.

[13] S. H. Jeong and H. W. Son, "UHF RFID Tag Antenna for Embedded Use in a Concrete Floor," *IEEE Antennas and Wireless Propagation Letters*, vol. 10, pp. 1158-1161, 2011.

[14] Electromagnetic compatibility and Radio spectrum Matters (ERM); Short Range Devices (SRD); Radio equipment to be used in the 25 MHz to 1 000 MHz frequency range with power levels ranging up to 500 mW; Part 1: Technical characteristics and test methods, EN 300 220-1, 2012.

[15] Radio Frequency Identification Equipment operating in the band 865 MHz to 868 MHz with power levels up to 2 W and in the band 915 MHz to 921 MHz with power levels up to 4 W; Harmonised Standard covering the essential requirements of article 3.2 of the Directive 2014/53/EU,EN 302 208, 2016.

[16] N. Chater, T. Mazri and M. Benbrahim, "Array antenna characteristics enhancement for electronic scanning radar application: Parasitic patches and multi-layer substrate techniques," *International Conf. Intelligent Systems and Computer Vision*, Fez, Moroco, pp. 1-5, 2018, 10.1109/ISACV.2018.8354022.

[17] A. M. Chrysler, C. M. Furse, K. L. Hall and Y. Chung, "Effect of Material Properties on a Subdermal UHF RFID Antenna," *IEEE Journal of Radio Frequency Identification*, vol. 1, no. 4, pp. 260-266, 2017.

[18] K. L. Chung, L. Yuan, S. Ji and C. Zhang, "Dielectric constant modelling of Chinese-standard concretes for wireless monitoring of structures," *2017 International Workshop on Electromagnetics: Applications and Student Innovation Competition*, London, UK, 2017, pp. 186-188.

[19] Concrete Standard. [Online]. Available: http://www.mdpi.com/2076-3417/7/2/177/pdf-vor

[20] S. Ji, K. L. Chung and C. Zhang, "Optimal bandwidth of concrete embedded antenna for wireless power transmission," *IEEE International Work. Electromagnetics: Applications and Student Innovation Competition (iWEM),* Nanjing, China, pp. 1-3, 2016, 10.1109/iWEM.2016.7505029.

[21] P. Frojd and P. Ulriksen, "Amplitude and phase measurements of continuous diffuse fields for structural health monitoring of concrete structures," *NDT & E International*, vol. 77, pp. 35-41, 2016, 10.1016/j.ndteint.2015.10.003.

[22] Higgs3 Squiggle Datasheet. Alien Technology. USA [Online]. Available: https://www.alientechnology.com/products/ic/higgs-3/

[23] Speedway-R420. Impinj Inc. USA. [Online]. Available: https://www.impinj.com/platform/connectivity/speedway-r420/

[24] LMR-195. Times Microwave Systems. USA. [Online]. Available: https://www.timesmicrowave.com/documents/resources/LMR-195.pdf

[25] Loading dock size. Orange county convention center. USA. [Online]. Available: https://www.occc.net/Planner-Interactive-Floor-Plans

Chapter 7 reference list:

[1] C.A.Balanis, “Microstrip Antennas,” Antenna Theory: Analysis and Design, 3rd ed. India: Wiley, 2012, pp. 811–872

[2] R. K. Pandey and T. Shanmuganantham, "Miniaturization and bandwidth enhancement of a wideband slotted microstrip patch antenna," *International Conf. Circuit, Power and Computing Technologies (ICCPCT)*, Nagercoil, TN, 2016, pp. 1-4.

[3] J.M.Kovitz and Y.Rahmat-Samii, “Using Thick Substrates and Capacitive Probe Compensation to Enhance the Bandwidth of Traditional CP Patch Antennas,” *IEEE Trans. Antennas and Propagation*, Vol. 62, no. 10, pp. 4970-4979, Oct. 2014.

[4] Y. Liu, L. Shafai and C. Shafai, "Gain and bandwidth enhancement of stacked H-shaped patch-open ring antenna," *International Symp. Antenna Technology and Applied Electromagnetics (ANTEM)*, Montreal, QC, 2016, pp. 1-2.

[5] W. Cao and W. Hong, "Bandwidth and gain enhancement for single-fed compact microstrip antenna by loading with parasitical patches," *IEEE International Conf. Microwave and Millimeter Wave Technology (ICMMT)*, Beijing, 2016, pp. 650-652.

[6] K. Q. da Costa, V. A. Dmitriev and M. N. Kawakatsu, "Enlarging the impedance matching bandwidth of wire and planar antennas using loop parasitic elements," *IEEE International Workshop. Antenna Technology*, Santa Monica, CA, 2009, pp. 1-4.

[7] M. John, M. Ayyappan, B. Manoj and S. Rodrigues, "Bandwidth enhancement of microstrip patch antenna for 5.8GHz by optimized feed offset," *International Conf. Communication and Signal Processing (ICCSP)*, Melmaruvathur, 2016, pp. 2186-2189.

[8] A. G. Koutinos, G. A. Ioannopoulos, M. T. Chryssomallis, G. A. Kyriacou and D. Caratelli, "Bandwidth enhancement of a supershape patch antenna using multiple

feeding technique," *International Workshop. Antenna Technology: Small Antennas, Innovative Structures, and Applications (iWAT)*, Athens, 2017, pp. 211-214.

[9] N. W. Liu, L. Zhu and W. W. Choi, "A Differential-Fed Microstrip Patch Antenna With Bandwidth Enhancement Under Operation of TM_{10} and TM_{30} Modes," *IEEE Trans. Antennas and Propagation*, vol. 65, no. 4, pp. 1607-1614, April 2017.

[10] J. Wang, Q. Liu and L. Zhu, "Bandwidth Enhancement of a Differential-Fed Equilateral Triangular Patch Antenna via Loading of Shorting Posts," *IEEE Trans. Antennas and Propagation*, vol. 65, no. 1, pp. 36-43, Jan. 2017.

[11] M. D. Van Wyk and K. D. Palmer, "Bandwidth enhancement of microstrip patch antennas using coupled lines," *Electronics Letters*, vol. 37, no. 13, pp. 806-807, 21 Jun 2001.

[12] J. C. Dash, G. P. Mishra and B. B. Mangaraj, "Design of dual band patch antenna with bandwidth enhancement using complementary defected ground structure," *2nd International Conf. Contemporary Computing and Informatics (IC3I)*, Noida, 2016, pp. 271-274.

[13] M. Asaadi and A. Sebak, "Gain and Bandwidth Enhancement of 2 × 2 Square Dense Dielectric Patch Antenna Array Using a Holey Superstrate," *IEEE Antennas and Wireless Propagation Letters*, vol. 16, no. , pp. 1808-1811, 2017.

[14] H. F. Pues and A. R. Van de Capelle, "An impedance-matching technique for increasing the bandwidth of microstrip antennas," *IEEE Trans. Antennas and Propagation*, vol. 37, no. 11, pp. 1345-1354, Nov 1989.

[15] R.Przesmycki, M.Wnuk, L.Nowosielski, K.Piwowarczyk and M.Bugaj, "Antenna gain measurement by comparitive method using an anechoic chamber," *PIERS proceedings*, Moscow, Russia, 2012, pp. 1424-1428.

[16] D. Walraven. (2006, November). American Radio Relay League. Newington, CT. [Online]. Available: https://www.arrl.org/files/file/Technology/tis/info/pdf/q1106037.pdf

[17] N. Tahir and G. Brooker, "A novel approach of feeding, impedance matching and frequency tuning of microstrip patch antenna by single microstrip line," *IEEE Symp. Industrial Electronics and Applications*, Langkawi

Chapter 8 reference list:

[1] J. Li, Y. Huang, Y. Wang, Q. Zhang, G. Wen and H. Zhang, "Wideband high gain circularly polarized UHF RFID reader antenna," *2016 IEEE Conference on Antenna Measurements & Applications (CAMA)*, Syracuse, NY, USA, 2016, pp. 1-3.

[2] H. S. Saini, A. Thakur, R. Kumar, G. Chehal and N. Kumar, "A small patch antenna for UHF RFID reader devices," *2016 International Conference on Advances in Computing, Communication, & Automation (ICACCA) (Spring)*, Dehradun, 2016, pp. 1-4.

[3] A. Michel, M. Rodriguez-Pino, and P. Nepa, "Reconfigurable Modular Antenna for Near-Field UHF RFID Smart Point Readers," *IEEE Transactions on Antennas and Propagation* , vol. 65, no. 2, 2017, pp. 498-506.

[4] M. Daiki, and E. Perret, "Near-Field Modular Antenna Concept with Configurable Reading Area for RFID Applications," *IEEE Transactions on Antennas and Propagation* , vol. 65, no. 3, 2017, pp.1015-1025.

[5] Y. Yao, C. Cui, J. Yu and X. Chen, "A Meander Line UHF RFID Reader Antenna for Near-field Applications," *IEEE Transactions on Antennas and Propagation*, vol. 65, no. 1, 2017, pp. 82-91.

[6] A. Kruekaew and C. Phongcharoenpanich, "Linear/circular polarization switchable antenna for UHF RFID reader," *2011 International Symposium on Intelligent Signal Processing and Communications Systems (ISPACS)*, Chiang Mai, pp. 1-4.

[7] Z. Li and X. Zhang, "A shaped beam antenna array for ultra high frequency radio frequency identification reader applications," *Proceedings of 2014 3rd Asia-Pacific Conference on Antennas and Propagation*, Harbin, 2014, pp. 112-115.

[8] PE100 Natural HDPE (2017, January 18). Mulford plastics [Online]. Available: www.mulfordplastics.com/_literature_78466/Ralloy_HDPE_Flye

[9] MT-262006-TRH-A (2017, March 03). MTI Wireless Edge [Online]. Available: http://www.mtiwe.com/?CategoryID=273&ArticleID=299

[10] Keonn advantage p-22 (2017, March 03). Keonn [Online]. Available: https://www.keonn.com/rfid-components/antennas/advantenna-p22.html

[11] 3M 9888T (2017, March 06). 3M (Online). Available: https://multimedia.3m.com/mws/media/765025O/iatd-product-info.pdf

[12] Xrray gateway (2017, March 06). Impinj (Online). Available: http://www.impinj.com/products/gateways/xarray-gateway/

Chapter 9 reference list:

[1] B. T. Malik, V. Doychinov, S. A. R. Zaidi, I. D. Robertson and N. Somjit, "Antenna Gain Enhancement by Using Low-Infill 3D-Printed Dielectric Lens Antennas," *IEEE Access*.

[2] G. Huang, J. Liang, L. Zhao, D. He and C. Sim, "Package-in-Dielectric Liquid Patch Antenna Based on Liquid Metal Alloy," *IEEE Antennas and Wireless Propagation Letters*.

[3] F. Pizarro, R. Salazar, E. Rajo-Iglesias, M. Rodríguez, S. Fingerhuth and G. Hermosilla, "Parametric study of 3D additive printing parameters using conductive filaments on microwave topologies," *IEEE Access*.

[4] M. F. Farooqui and A. Kishk, "3-D-Printed Tunable Circularly Polarized Microstrip Patch Antenna," in *IEEE Antennas and Wireless Propagation Letters*, vol. 18, no. 7, pp. 1429-1432, July 2019.

[5] D. B. BYRNE and D. Nicolas CAPET, "Compact 3D Printed Antenna Technology for Nanosat/Cubesat Applications," *2019 13th European Conference on Antennas and Propagation (EuCAP)*, Krakow, Poland, 2019, pp. 1-3.

[6] Y. Alnaiemy, T. A. Elwi and N. Lajos, "Enhancing the Microstrip Antenna Gain Using a Novel EBG Lens Based on a Single Layer," *2018 11th International Symposium on Communication Systems, Networks & Digital Signal Processing (CSNDSP)*, Budapest, 2018, pp. 1-4.

[7] K. Harshasri, P. V. Babu and P. N. Rao, "Design of Compact C-Band Concave Patch Antenna for Radar Altimeter Applications," *2018 International Conference on Communication and Signal Processing (ICCSP)*, Chennai, 2018, pp. 0542-0546

[8] X. Ren, S. Liao and Q. Xue, "A Circularly Polarized Spaceborne Antenna With Shaped Beam for Earth Coverage Applications," *IEEE Transactions on Antennas and Propagation*, vol. 67, no. 4, pp. 2235-2242, April 2019.

[9] S. Wang, L. Zhu, J. Wang and W. Wu, "Three-dimensional circular patch antenna under TM02 mode with improved impedance matching," *Electronics Letters*, vol. 55, no. 4, pp. 169-170, 21 2 2019.

[10] M. Boyuan, J. Pan, E. Wang and Y. Luo, "Conformal Bent Dielectric Resonator Antennas With Curving Ground Plane," *IEEE Transactions on Antennas and Propagation*, vol. 67, no. 3, pp. 1931-1936, March 2019.

[11] L.F. Chen, C.K. Ong, C.P. Neo, V.V. Varadan and V.K. Varadan. "Reflection methods" *Microwave electronics: measurements and materials characterization*, 1st ed., USA, John Wiley and Sons, 2004, pp. 142-174.

[12] S. Zuo, L. Yang and Z. Zhang, "Dual-Band CP Antenna With a Dual-Ring Cavity for Enhanced Beamwidth," *IEEE Antennas and Wireless Propagation Letters*, vol. 14, pp. 867-870, 2015.

[13] H. Sun and W. Geyi, "A New Rectenna Using Beamwidth-Enhanced Antenna Array for RF Power Harvesting Applications," *IEEE Antennas and Wireless Propagation Letters*, vol. 16, pp. 1451-1454, 2017.

Chapter 10 reference list:

[1] P. Parthiban, "Fixed UHF RFID Reader Antenna Design for Practical Applications: A Guide for Antenna Engineers with Examples," *IEEE Journal of Radio Frequency Identification*, vol. 3, no. 3, pp. 191-204, September 2019.

[2] O. Kazan, O. Memioglu, F. Kocer, A. Gundel and C. Toker, "A Lumped-Element Wideband 3-dB Quadrature Hybrid," *IEEE Microwave and Wireless Components Letters*, vol. 29, no. 6, pp. 385-387, June 2019.

[3] M. M. Mahmoud Ali, S. I. Shams and A. Sebak, "Ultra-wideband printed ridge gap waveguide hybrid directional coupler for millimetre wave applications," *IET Microwaves, Antennas & Propagation*, vol. 13, no. 8, pp. 1181-1187, June 2019.

[4] H. Ahn and M. M. Tentzeris, "Arbitrary Power-Division Branch-Line Hybrids for High-Performance, Wideband, and Selective Harmonic Suppressions From $2f_0$," *IEEE Transactions on Microwave Theory and Techniques*, vol. 67, no. 3, pp. 978-987, March 2019.

[5] M. F. Hagag, R. Zhang and D. Peroulis, "High-Performance Tunable Narrowband SIW Cavity-Based Quadrature Hybrid Coupler," *IEEE Microwave and Wireless Components Letters*, vol. 29, no. 1, pp. 41-43, Jan. 2019.

[6] P. Parthiban, B. Seet and X. J. Li, "Display Frame UHF RFID Antenna for Museums," *2018 IEEE Asia-Pacific Conference on Antennas and Propagation (APCAP)*, Auckland, 2018, pp. 532-533.

[7] X. Gu and W. Geyi, "Design of a Near-Field RFID Antenna Array in Metal Cabinet Environment," *IEEE Antennas and Wireless Propagation Letters*, vol. 18, no. 1, pp. 79-83, Jan. 2019.

[8] A. Hsiao, C. Chao, C. Yang and C. Tsai, "Near-Field Antenna Design for UHF RFID System," *2018 IEEE International Symposium on Antennas and Propagation & USNC/URSI National Radio Science Meeting*, Boston, MA, 2018, pp. 317-318.

[9] Y. Zeng, Z. N. Chen, X. Qing and J. Jin, "A Directional, Closely Spaced Zero-Phase-Shift-Line Loop Array for UHF Near-Field RFID Reader Antennas," *IEEE Transactions on Antennas and Propagation*, vol. 66, no. 10, pp. 5639-5642, Oct. 2018.

[10] W. E. I. Liu, Z. Ning Chen, E. N. Kai Yin, Y. Zeng and X. Qing, "An Inductive Perforated Ground Backed Thin Electrically Large Zero-Phase-Shift Line Loop Antenna for UHF Near-Field RFID Reader," *2018 IEEE International Conference on Service Operations and Logistics, and Informatics (SOLI)*, Singapore, 2018, pp. 123-126.

[11] C. Huang, C. Wang, J. Zhu and W. Tang, "Electrically Large Segmented Dipole Array Antenna With Reflectors for UHF Near-Field RFID Applications," *IEEE Transactions on Antennas and Propagation*, vol. 67, no. 6, pp. 4280-4285, June 2019.

[12] J. Yan, C. Liu, X. Liu, J. Li, H. Guo and X. Yang, "A Switchable Near-/Far-Field Reader Antenna for UHF RFID Applications," *IEEE Antennas and Wireless Propagation Letters*, vol. 17, no. 5, pp. 789-793, May 2018.

[13] P. Parthiban, B. Seet and X. J. Li, "Scalable Near-field Fed Far-field UHF RFID Reader Antenna for Retail Checkout Counters," *2019 IEEE International Conference on RFID (RFID)*, Phoenix, AZ, USA, 2019, pp. 1-6.

[14] G.A. Kouzaev, *Applications of Advance Electromagnetics – Components and Systems*. Heidelberg: Springer, 2013, p. 347-348.

[15] P.Parthiban, "Bandwidth enhancement for thin substrate UHF RFID patch antenna, *International Journal on Smart Sensing and Intelligent Systems*, vol. 12, no. 1, pp. 1-8, May 2019.

[16] Speedway r420 reader (2018, December 14). Impinj [Online]. Available: https://www.impinj.com/platform/connectivity/speedway-r420/

[17] Bling (2019, July 31). Smartrac-group [Online]. Available:: https://www.smartrac-group.com/bling.html

Chapter 11 reference list:

[1] P. V. Nikitin, K. V. S. Rao and S. Lazar, "An Overview of Near Field HF RFID," in *Proc. of IEEE International Conference on RFID*, Grapevine, TX, 2007, pp. 167-174.

[2] B. Shrestha, A. Elsherbeni and L. Ukkonen, "UHF RFID Reader Antenna for Near-Field and Far-Field Operations," *IEEE Antennas and Wireless Propagation Letters*, vol. 10, no. , pp. 1274-1277, 2011.

[3] X. Qing, C. K. Goh and Z. N. Chen, "Segmented loop antenna for UHF near-field RFID applications," *Electronics Letters*, vol. 45, no. 17, pp. 872-873, Aug. 13 2009.

[4] X. Qing, Z. N. Chen and C. K. Goh, "UHF near-field RFID reader antenna with capacitive couplers," *Electronics Letters*, vol. 46, no. 24, pp. 1591-1592, November 25 2010.

[5] P. Yang, Y. Li, L. Jiang and F. Yang, "Near-Field Loop Antenna for the UHF RFID Reader," *Journal of Electronics Science and Technology*, vol.9, No.3, pp.256-260.

[6] C.-H. Chen, C.-T. Liao and H.-M. Chen, "Dual D-loop near-field RFID antenna for water application," in *Proc. of Asia-Pacific Symposium on Electromagnetic Compatibility*, Taipei, 2015, pp. 189-191.

[7] M. J. Chang and H. Ming, "Compact near-field folded-loop antenna for UHF RFID handheld reader," *Antennas and Propagation (ISAP), 2014 International Symposium on*, Kaohsiung, 2014, pp. 107-108.

[8] X. Z. Lai, Z. Xie, and X. Cen, "A Compact RFID Reader Antenna for UHF Near-Field and Far-Field Operations," *International Journal of Antennas and Propagation*, 2013, pp. 1-5.

[9] X. Ding, Q. Wu, K. Zhang and C. Feng, "A Magnetic Coupling Dipole for UHF Near-Field RFID Reader," *IEEE Transactions on Magnetics*, vol. 48, no. 11, pp. 4305-4308, Nov. 2012.

[10] X. Ding, Q. Wu, K. Zhang and C. Feng, "A Magnetic Coupling Dipole for UHF Near-Field RFID Reader," *IEEE Transactions on Magnetics*, vol. 48, no. 11, pp. 4305-4308, Nov. 2012.

[11] Palight (2016, July 04). Palram [Online]. Available: http://www.palram.com/palight

[12] M. Dhaouadi, M. Mabrouk, T. P. Vuong, A. C. de Souza and A. Ghazel, "A capacitively-loaded loop antenna for UHF near-field RFID reader applications," in *Proc. of IEEE Radio and Wireless Symposium (RWS)*, San Diego, CA, 2015, pp. 193-195.

[13] A. Ren, C. Wu, T. Wang and B. Yao, "A novel design for UHF near-field RFID reader antenna based on traveling wave," in *Proc. of 12th IEEE International Conference on Communication Technology (ICCT)*, Nanjing, 2010, pp. 239-242.

[14] A. Michel, R. Caso, A. Buffi, P. Nepa and G. Isola, "Modular antenna for reactive and radiative near-field regions of UHF-RFID desktop readers," in *Proc. of General Assembly and Scientific Symposium (URSI GASS)*, Beijing, 2014, pp. 1-4.

[15] A. Michel, R. Caso, A. Buffi and P. Nepa, "Multifunctional modular antenna for near-field ultra-high frequency radio frequency identification readers," *IET Microwaves, Antennas & Propagation*, vol. 10, no. 8, pp. 843-849, 2016.

[16] W. Choi, J. S. Kim, J. H. Bae, G. Choi and J. S. Chae, "Near-field antenna for RFID smart shelf in UHF," in *Proc. of 2009 IEEE Antennas and Propagation Society International Symposium*, Charleston, SC, 2009, pp. 1-4.

[17] A. C. de Souza, Y. Duroc, T. P. Vuong, A. Luce and J. Perdereau, "A near-field and far-field antenna for UHF RFID applications," in *Proc. of IEEE-APS Topical Conference on Antennas and Propagation in Wireless Communications*, Torino, 2013, pp. 1240-1243

[18] Z.-M. Liu and R. R. Hillegass, "A 3 patch near field antenna for conveyor bottom read in RFID sortation application," in *Proc. of IEEE Antennas and Propagation Society International Symposium*, Albuquerque, NM, 2006, pp. 1043-1046.

[19] Impinj Speedway (2016, July 05). Impinj, Inc [Online]. Available: https://support.impinj.com/hc/en-us/articles/202755278-Speedway-Connect.

[20] Alien SIT Tag (2016, July 05). Alien Technology [Online]. Available: http://www.alientechnology.com/wp-content/uploads/Alien-Technology-Higgs-3-ALN-9613-SIT.pdf

[21] Impinj Monza M5 (2016, July 05). Impinj, Inc [Online]. Available: http://www.impinj.com/products/tag-chips/monza-5/

[22] Impinj Multireader (2016, July 05). Impinj, Inc [Online]. Available: http://www.sbrfid.com/IPJ_SpeedwayR_InstallationOperationsGuide_4-8-0_20110425.pdf

Chapter 12 reference list:

[1] D. J. Sorrell, J. H. Hants, and S. F. Horsham. “Devices and methods related to a display assembly including an antenna.” U.S. Patent 2 010 031 538 9A1, 2010.

[2] D. Huang and Z. Du, "Eight-band antenna with a small ground clearance for LTE metal-frame mobile phone applications," IEEE Antennas and Wireless Propagation Letters, vol. 17, no. 1, pp. 34-37, 2018.

[3] L. Song, Z. Song and S. Liu, "Design and simulation of a kind of conformal microstip patch antenna array with series feed network," in Proc. IEEE 13th International Conference on Signal Processing, Chengdu, China, November 2016.

[4] A. Omar, S. Al-Saif, M. A. Ashraf and S. Alshebeili, "Design and analysis of millimeter wave series fed microstrip patch array for next generation wireless communication systems," in Proc. of 17th International Symposium on Antenna Technology and Applied Electromagnetics, Montreal, Canada, July 2016.

[5] M. K. Ishfaq, T. A. Rahman, Y. Yamada and K. Sakakibara, "8×8 phased series fed patch antenna array at 28 GHz for 5G mobile base station antennas," in Proc. of IEEE-APS Topical Conference on Antennas and Propagation in Wireless Communications, Verona, Italy, September 2017.

[6] R. Sen, A. K. Sarkar, P. C. Sarker, L. C. Paul and M. M. U. Rashid, "RF absorption in biological tissue at varying distances and angles and rapport to tissue impedance," IEEE International Conference on Imaging, Vision & Pattern Recognition (icIVPR), Dhaka, 2017.